SPRAY PYROLYSED ZINC OXIDE THIN FILMS: EFFECTS OF DOPING AND ION BEAM IRRADIATION

Thesis submitted to
Cochin University of Science and Technology
for the award of the Degree of

Doctor of Philosophy

By

Ratheesh Kumar P. M.

Department of Physics
Cochin University of Science and Technology
Cochin – 682 022
India.

January 2007

Dr.K.P.Vijayakumar
Professor

Department of Physics
**Cochin University of Science
and Technology**
COCHIN-682 022
INDIA

Ph:(off):0484-2577404
(res):0484-2577103
Fax:0484-2577595
Email : kpv@cusat.ac.in

CERTIFICATE

Certified that the work presented in this thesis entitled *"Spray pyrolysed zinc oxide thin films: Effects of doping and ion beam irradiation"* is based on the bonafide research work done by Mr. Ratheesh Kumar P. M. under my guidance in the Department of Physics, Cochin University of Science and Technology, Kochi - 682022, and has not been included in any other thesis submitted previously for the award of any degree.

Kochi-22

15-01-2007

Prof. K. P. Vijayakumar

(Supervising Guide)

Contents

List of Publications

Journals

<u>Papers related to thesis work/ZnO films</u>

1) Modifications of ZnO thin films under dense electronic excitation

    P. M. Ratheesh Kumar, C. Sudha Kartha, K. P. Vijayakumar, F. Singh, D. K. Avasthi, Y. Kashiwaba, T. Abe, G. S. Okram, M. Kumar and Sarvesh Kumar

    J. Appl. Phys **97** (2005) 013509

2) On the properties of Indium doped ZnO thin films

    P. M. Ratheesh Kumar, C. Sudha Kartha, K. P. Vijayakumar, Y. Kashiwaba, T. Abe, F. Singh and D. K. Avasthi

    Semicond. Sci. Technol. **20** (2005) 120

3) Effect of fluorine doping on structural electrical and optical properties of ZnO thin films

    P. M. Ratheesh Kumar, C. Sudha Kartha, K. P. Vijayakumar, F. Singh and D. K. Avasthi

    Mat. Sci. Engg. B **117** (2005) 317

4) Doping of spray pyrolysed ZnO thin films through direct diffusion of indium: Structural Optical and Electrical studies

    P. M. Ratheesh Kumar, C. Sudha Kartha and K. P. Vijayakumar

    J. Appl. Phys **98** (2005) 023509

5) On the origin of blue-green luminescence in spray pyrolysed ZnO films.

   P. M. Ratheesh Kumar, K. P. Vijayakumar and C. Sudha Kartha

   J. Mater. Sci. *(Article in Press)*

6) Effects of oxygen ion implantation in spray pyrolysed ZnO thin films

   K. P. Vijayakumar, **P. M. Ratheesh Kumar**, C. Sudha Kartha, K. C. Wilson, F. Singh, K. G. M. Nair and Y. Kashiwaba

   Phys. Stat. Solidi (a) **203** (2006) 820.

7) An investigation on the variations in properties of Ni^+ irradiated ZnO thin films

   P. M. Ratheesh Kumar, C. Sudha Kartha, K. P. Vijayakumar, F. Singh and D. K. Avasthi

   Rad. Effects Def. Sol. (*Accepted*)

Papers related to other materials/techniques not included in the thesis

1) SHI induced modifications in Spray Pyrolysed β-In_2S_3 thin films

   P. M. Ratheesh Kumar, Teny Theresa John, C. Sudha Kartha and K. P. Vijayakumar

   Nucl. Instrs. and Meth. B **244(1)** (2006) 171

2) Effects of thickness and post deposition annealing on the properties of evaporated In_2S_3 thin films

   P. M. Ratheesh Kumar, Teny Theresa John, C. Sudha Kartha, K. P. Vijayakumar, T. Abe and Y. Kashiwaba

J. Mater. Sci **41** (2006) 5519

3) CuInS$_2$ thin films through repeated Chemical Spray Pyrolysis
   Teny Teresa John, K. C. Wilson, **P. M. Ratheesh Kumar**, C. Sudha Kartha,
   K. P. Vijayakumar, Y. Kashiwaba, T. Abe and Y. Yasuhiro
   Phys. Stat. Sol. (a) **202 (1)** (2005) 79

4) Characterization of In$_2$S$_3$ and ZnO for photovoltaic applications using
   Photothermal Deflection technique
   M. Paulraj, S. Ramkumar, P. R. Amjith, Teny Theresa John, **P. M. Ratheesh**
   Kumar, C. Sudha Kartha, K. P. Vijayakumar and K. G. M. Nair
   J. Phys. IV France **125** (2005) 469

5) SHI induced single-phase InSe formation at lower annealing temperature
   R. Sreekumar, **P.M. Ratheesh Kumar**, C. Sudha Kartha, K.P. Vijayakumar,
   D. Kabiraj, S.A. Khan and D.K. Avasthi
   Nucl. Instrs. and Meth. B **244(1)** (2006) 190.

6) Swift heavy ion-induced interface mixing in In/Sb
   R. Sreekumar, **P.M. Ratheesh Kumar**, C. Sudha Kartha, K.P. Vijayakumar,
   D. Kabiraj, S.A.Khan, D.K. Avasthi, Y. Kashiwaba and T. Abe
   Semicond. Sci. Technol. **21** (2006) 382

7) Thermal diffusion of Cu into In$_2$Se$_3$: A better approach to SEL technique in
   the deposition of CuInSe$_2$ thin films
   K. G. Deepa, **P. M. Ratheesh Kumar**, C. Sudha Kartha and K. P.
   Vijayakumar

Sol. Energy Mater. Sol. Cells, **90** (2006) 3481

8) Anomalous behavior of silver doped indium sulphide

    Meril Mathew, R. Jayakrishnan, **P. M. Ratheesh Kumar**, C. Sudha Kartha,

    K. P. Vjayakumar, Y. Kashiwaba and T. Abe

    J. Appl. Phys., **100** (2006) 33504

Conferences

Papers related to thesis work/ZnO films

International/National

1) Studies on structural and optical properties of ZnO thin films prepared using
    spray pyrolysis technique

    P M Ratheesh Kumar, C Sudha Kartha and K P Vijayakumar

    National Conference on Recent Advances in Materials Science (NCMS-
    2002), Nehru Memorial College, Thiruchirappalli, India, 2002

2) Structural and electrical characterisation of swift heavy ion irradiated ZnO
    thin films

    P M Ratheesh Kumar, D K Avasthi, F Singh, C Sudha Kartha and K P
    Vijayakumar

    9th International Symposium on Radiation Physics (ISRP-9), Cape Town,
    South Africa, 2003

3) Photothermal studies on pure and doped ZnO thin films prepared using spray
    pyrolysis

    M Paulraj, S Ramkumar, P R Amjith, **P M Ratheesh Kumar**, C Sudha
    Kartha, K P Vijayakumar and K G M Nair

10th International conference on composites/Nano Engineering. University of New Orleans, 2003

4) Characterization of Indium Doped and Undoped Zinc Oxide Films Deposited by Spray Pyrolysis
   P M Ratheesh Kumar, C Sudha Kartha, K P Vijayakumar, D K Avasthi and F Singh
   14th International Photovoltaic Science and Engineering Conference (PVSEC-14), Bangkok, Thailand, 2004

5) Optical Characterization of 120 MeV Au^+ irradiated ZnO thin films
   P M Ratheesh Kumar, C Sudha Kartha, K P Vijayakumar, D K Avasthi and F Singh
   48th Annual DAE Solid State Physics Symposium, Jiwaji University, Gwalior, India, 2003.

6) XPS and XRD analysis of indium doped ZnO thin films
   P M Ratheesh Kumar, C Sudha Kartha, K P Vijayakumar, Y Kashiwaba and T Abe
   49th Annual DAE Solid State Physics Symposium, GNDU Amritsar, India 2004.

7) Structural and electrical characterization of swift heavy ion irradiated ZnO thin films.
   P.M. Ratheesh Kumar, C. Sudha Kartha K. P. Vijayakumar, D. K. Avasthi and F. Singh
   15th AGM of Materials Research Society of India (MRSI), Banaras Hindu

University,

Varanasi, India, 2004.

9) Photoluminescence studies on ZnO thin films irradiated using 80 Mev Ni^+ ion

P M Ratheesh Kumar, C Sudha Kartha, K P Vijayakumar, F Singh and D K Avasthi (Presented in international conference, OMTAT 2005, Cochin, India)

Papers related to other materials/techniques not included in the thesis

1) SHI induced modifications in Spray Pyrolysed β-In_2S_3 thin films

P M Ratheesh Kumar, Teny Theresa John, C Sudha Kartha, K P Vijayakumar and D K Avasthi

Indo German Work Shop (NANO-05), New Delhi 2005

Preface

In recent years scientists have made rapid and significant advances in the field of semiconductor physics. One of the most important fields of current interest in materials science is the fundamental aspects and applications of conducting transparent oxide thin films (TCO). The characteristic properties of such coatings are low electrical resistivity and high transparency in the visible region. The first semitransparent and electrically conducting CdO film was reported as early as in 1907 [1]. Though early work on these films was performed out of purely scientific interest, substantial technological advances in such films were made after 1940. The technological interest in the study of transparent semiconducting films was generated mainly due to the potential applications of these materials both in industry and research. Such films demonstrated their utility as transparent electrical heaters for windscreens in the aircraft industry. However, during the last decade, these conducting transparent films have been widely used in a variety of other applications such as gas sensors [2], solar cells [3], heat reflectors [4], light emitting devices [5] and laser damage resistant coatings in high power laser technology [6].

Just a few materials dominate the current TCO industry and the two dominant markets for TCO's are in architectural applications and flat panel displays. The architectural use of TCO is for energy efficient windows. Fluorine doped tin oxide (FTO), deposited using a pyrolysis process is the TCO usually finds maximum application. SnO_2 also finds application ad coatings for windows, which are efficient in preventing radiative heat loss, due to low emissivity (0.16). Pyrolitic tin oxide is used in PV modules, touch screens and plasma displays. However indium tin oxide (ITO) is mostly used in the majority of flat panel display (FPD) applications. In FPDs, the basic function of ITO is as transparent electrodes. The volume of FPD's produced, and hence the volume of ITO coatings produced, continues to grow rapidly. But the current increase in the cost of indium and the scarcity of this material created the difficulty in obtaining low cost TCOs. Hence search for alternative TCO materials has been a topic of active research for the last few decades. This resulted in the development of binary materials like ZnO, SnO_2, CdO and ternary materials like

I

Zn_2SnO_4, $CdSb_2O_6$:Y, $ZnSO_3$, $GaInO_3$ etc. The use of multicomponent oxide materials makes it possible to have TCO films suitable for specialized applications because by altering their chemical compositions, one can control the electrical, optical, chemical and physical properties. But the advantages of using binary materials are the easiness to control the chemical compositions and depositions conditions. Recently, there were reports claiming the deposition of CdO:In films with a resistivity of the order of 10^{-5} ohm cm for flat panel displays and solar cells. However they find limited use because of Cd-Toxicity. In this regard, ZnO films developed in 1980s, are very useful as these use Zn, an abundant, inexpensive and nontoxic material. Resistivity of this material is still not very low, but can be reduced through doping with group-III elements like In, Al or Ga or with F [6]. Hence there is a great interest in ZnO as an alternative of ITO.

In the present study, we prepared and characterized transparent and conducting ZnO thin films, using a cost effective technique viz Chemical Spray Pyrolysis (CSP). This technique is also suitable for large area film deposition. It involves spraying a solution, (usually aqueous) containing soluble salts of the constituents of the desired compound, onto a heated substrate. In the present work, several attempts were carried out to modify the structural, electrical and optical properties of ZnO films and results are discussed in the thesis systematically. The thesis is divided into 8 chapters and a brief description of content in each chapter is given below.

CHAPTER 1 is a general introduction to transparent conducting oxides with a specific emphasis on the properties of ZnO material. An exhaustive review on ZnO material is also given in this chapter

CHAPTER 2 gives a general description on the preparation techniques used for the deposition of ZnO films. A brief description of different characterization techniques used in the present work is also given. In the next section, optimization of preparation conditions of spray pyrolysis is given. Zinc acetate dissolved in ethanol and distilled water taken in the ration 1:1 was the precursor. The optimized conditions for obtaining a low resistive transparent ZnO from the present work can be summarized as follows: volume of spray solution is 200 ml, substrate temperature is 400°C and spray rate is 10 ml/min. The molarity of zinc acetate was 0.6 M. Films

prepared with these conditions were used for studying the effects doping and ion beam irradiation and details through which the optimization conditions were reached are included in this chapter.

CHAPTER 3 deals with the results of swift heavy ion irradiation induced modifications in ZnO films. 120 MeV Au ions and 80 MeV Ni ions were used for the irradiation. Structural, compositional, optical and electrical characterizations of the films were carried out using X-Ray Diffraction (XRD), X-ray Photoelectron Spectroscopy (XPS), Photoluminescence, electrical resistivity, optical absorption and transmission. Surface analysis was done using Atomic Force Microscopy (AFM). Crystalline quality of the films was found deteriorated due to Au irradiation while it was slightly affected by the Ni irradiation. Electrical resistivity decreased with the increase in fluence of Au ions while it increased with the fluence of Ni ions. However optical absorption edge remained unaffected in both cases. A reasonable explanation is given for the origin of controversial blue-green emission in ZnO thin films and it was suggested that this emission was assumed to be due to the transition from the conduction band to the acceptor level resulting from the "antisite oxygen". Defect levels were identified using Thermally Stimulated Current (TSC) measurements also.

In order to make the ZnO film low resistive, doping with indium was tried. **CHAPTER 4** describes the effects of indium doping on the structural, electrical and optical properties of ZnO films. Indium was introduced in the film by adding indium chloride in the spray solution and it was observed from XPS analysis that, chlorine was present in the film in elemental form at higher doping concentration. Electrical resistivity decreased with indium, at low concentration. But it increased at higher doping concentration. It was suggested that this increase in resistivity was presumably due to the presence of chlorine in the film. Crystallinity and luminescent properties were also affected adversely due to the doping. In order to avoid unintentional doping of chlorine, indium was doped through thermal diffusion of a thin layer of metallic indium, deposited using thermal evaporation. Electrical resistivity decreased monotonically with increase in mass of indium deposited. Another advantage of this kind of doping was that, both structural and luminescent properties of the film were slightly affected by the indium incorporation. In order to reduce the resistivity further,

III

indium was introduced in the form of indium nitrate and then a thin layer of metallic indium deposited over this. Annealing of this bilayer (ZnO/In) at 673 K resulted the lowest resistivity of 1.45 x 10^{-3} ohm cm. This value was one of the lowest resistivity obtained for the ZnO film prepared by chemical routes. Interestingly absorption edge remained unaffected on doping. Temperature dependent conductivity measurements were performed to identify the defect levels in these films.

Presence of chlorine, in elemental form, was identified as the cause of increase in resistivity in ZnO thin films. In order to confirm this behavior, chlorine was doped separately using ammonium chloride. **CHAPTER 5** illustrates the effects of chlorine and fluorine doping on ZnO films. It was seen that, electrical resistivity increased with increase in doping concentration. Crystallinity also deteriorated considerably due to chlorine doping. Earlier, it was claimed that, chlorine could act as donor in TCO, when it substituted oxygen in its lattice [7-10]. But in those reports, clear evidence of the presence of Cl in the film was not given. In one of the reports [10], a decrease in resistivity was obtained for the ZnO, prepared using MOCVD, when n-butyl chloride was used as precursor. As the ionic radius of Cl is much higher than that of O, it maybe argued that, the substitution of O by Cl might be difficult. We also proposed that chlorine might segregate in grain boundaries and/or occupied in interstitial position. Fluorine, having comparable ionic radius of O, was also used for doping. In this case, interestingly, electrical resistivity decreased at lower doping concentration, while it increased slightly at very high doping level, and this was probably due to the scattering of carriers. From these experiments, it was suggested that, chlorine might be acting as an electron trap, when it segregated in grain boundaries or was in interstitials in elemental form. Optical absorption, Transmission, Photoluminescence, Temperature dependent conductivity measurements were also done.

CHAPTER 6 deals with the effects of 100 keV O^+ ion implantation in ZnO. Crystalline to amorphous phase transition and formation of highly resistive ZnO were the two important results obtained from this work. Creation of high resistive region in semiconductors are most important for inter device isolation in several applications like heterostructure lasers, heterojunction bipolar transistors etc. Sheet resistance of

ZnO films increased to the order of $\sim 10^{10}$ $\Omega/\square$ on O^+ ion implantation. Structural, Optical, TSC and Photoluminescence measurements were also done.

CHAPTER 7 is a summary of the entire work. All the important points are highlighted. The chapter ends with future scope of the present work.

Chapter 1

REVIEW OF EARLIER WORKS ON ZNO

1.1 Introduction

In recent years, scientists have made rapid and significant advances in the field of material science, especially in semiconductor physics. One of the most important fields of current interest in materials science is the fundamental aspects and applications of conducting transparent oxide thin films (TCO). The characteristic properties of such coatings are low electrical resistivity and high transparency in the visible region. First semitransparent and electrically conducting CdO film was reported as early as in 1907 (1). As the early works on these films were performed out of purely scientific interest, substantial technological advances in such films were observed only after 1940. Interest in the study of transparent semiconducting films has been generated mainly by their potential applications in industries related to opto-electronics and photovoltaic device fabrication. Such films have demonstrated their utility as transparent electrical heaters for windscreens in the aircraft industry. However, during the last decade, these conducting transparent films have been widely used in a variety of other interesting applications such as gas sensors, solar cells, heat reflectors, protective coatings, light transparent electrodes and laser damage resistant coatings in high power laser technology. (1)

Just a few materials dominate the current TCO industry and the two dominant markets for TCO's are in architectural applications and flat panel displays. The architectural use of TCO is for energy efficient windows. Fluorine doped tin oxide, deposited through pyrolysis process, is the TCO most often used for this. SnO_2 can also be used as coatings for windows, which are efficient in preventing radiative heat loss due to low emissivity (0.16). Pyrolitic tin oxide is used in PV modules, touch screens and plasma displays. However indium tin oxide (ITO) is the TCO used most

1

often in the majority of flat panel display (FPD) applications. In FPDs, the basic function of ITO is as transparent electrodes. The volume of FPDs produced, [and hence the volume of ITO coatings] continues to grow rapidly. But the enormously high cost of indium and the scarcity of this material create the difficulty in obtaining low cost TCOs. Hence search for other alternative TCO materials has been a topic of research for the last few decades. It includes some binary materials like ZnO, SnO_2, CdO and ternary materials like Zn_2SnO_4, $CdSb_2O_6$:Y, $ZnSO_3$, $GaInO_3$ etc. The introduction of multicomponent oxide materials resulted in the design of TCO films suitable for specialized applications. This is mainly because one can control their electrical, optical, chemical and physical properties by altering the chemical compositions. But the major advantages of using binary materials are that their chemical compositions and depositions conditions can be controlled easily. Even though CdO:In films have been prepared with a resistivity of the order of 10^{-5} ohm cm making them quite useful for flat panel displays and solar cells, currently these are of not much importance because of the toxicity of Cd. Doped ZnO developed in 1980s, uses Zn, an abundant, inexpensive and nontoxic material. Resistivity of this material is still not very low, but can be reduced further by doping it with group-III elements like In, Al or Ga or with F. Hence there is a renewed interest in ZnO as an alternative of ITO.

Important parameters related to the physical properties of ZnO are tabulated in Table 1.1 [2]. It should be noted that still there exists uncertainty in some of these values like hole mobility, thermal conductivity etc.

Property	Value
Lattice parameters at 300 K	
a_0	0.32495 nm
c_0	0.52069 nm
a_0/c_0	1.602
u	0.345
Density	5.606 g/cm3
Stable phase	Wurtzite
Melting point	1975C
Thermal conductivity	1-1.2
Linear expansion coefficient (/C)	a_0: 6.5x10-6
	c_0: 3.0x10-6
Static dielectric constant	8.656
Refractive index	2.008-2.029
Energy band gap	3.4 eV, direct
Exciton binding Energy	60 meV
Electron effective mass	0.24
Electron Hall mobility	200 cm2/Vs
Hole effective mass	0.59
Hole Hall Mobility	5-50 cm2/Vs

Table 1.1 Different parameters of physical properties of ZnO Material

Recently large number of papers is published on this interesting material. A brief review of some of the works is included in the following sections of this chapter.

1.2 Defect Studies in ZnO

Till now, most researchers focused only on the production and optical properties of ZnO and many of the fundamental properties were poorly understood. However some recent interesting reports on the theoretical aspects of intrinsic defects of this material had shed light on these problems. As we know, the defects play very important role in the structural, optical and electrical properties of materials. Hence in the present work, attention was made to include a brief review on theoretical as well as experimental studies on intrinsic defects in ZnO.

Generally there are two types of electrons traps in ZnO varistors; traps located at ZnO-ZnO grain boundaries known as 'interface traps' and traps located within the bulk of the ZnO grains known as 'bulk traps'. Bulk traps can exist throughout the ZnO grains and are located much deeper within the band gap [3]. These traps are accessible to Admittance spectroscopy or deep level transient spectroscopy techniques [4]. Admittance spectroscopy was used to determine the activation energies of the bulk traps in ZnO varistors [5] and the values were found to be 0.17 eV and 0.33 eV below the conduction band edge. These were assigned to be the native defects. Kasai used electron spin resonance to study acceptors and donors in ZnO and showed that oxygen vacancy is a deep donor [6].

Effects of surface point defects [like oxygen vacancies on ZnO (I0$\bar{\text{I}}$0) surface] on Schottky barrier formation were studied. It was found that, with and without surface defect states, ZnO could form almost identical Schottky barrier features, independent of evaporated metal [7]. It was also found that, barrier formation was relatively slow for Au on ZnO, while Al induced pronounced dipole with first half monolayer.

DLTS measurements were done on ZnO single-crystals, grown using hydrothermal technique, to identify the defect levels [8]. An electron trap was

identified at 0.3 eV and this defect level was attributed to singly ionized oxygen vacancies.

In an interesting work on ZnO, using interferometric method [9], Wacogne et al concluded that, in order to increase the accuracy of the optical loss measurements, one has to take care of the variation of refractive index with film thickness. It was also suggested that this method could be used as long as the film was transparent.

Work function of ZnO thin film was determined using temperature dependent I-V measurements of the hetero-junctions ZnO/n-ZnO and ZnO/p-Si [10]. Work function was found to be between 4.45 and 4.5 eV.

Another interesting report was on the band gap of ZnO [11]. The band gap reported for the ZnO at room temperature in the literature was in the range of 3.1 to 3.3 eV. Srikant and Clarke compared the results of different measurements done on same crystal and concluded that room temperature band gap is 3.3 eV and the other values, [3.1 eV or 3.2 eV] were due to the existence of a valence band – donor transition.

Tomlins et al studied the effect of oxygen diffusion in ZnO single crystal for the first time and found that the diffusion was isotropic [12].

Look et al reported the growth of high quality n-type ZnO boules using a new vapor-phase transport method. Electrical properties were studied using temperature dependent Hall measurements [13] and the maximum value of Hall mobility was obtained to be 2000 cm^2/Vs at 50 K. PL measurements were also done which confirmed the high quality of the crystals.

Look et al performed high-energy electron irradiation experiment also on ZnO crystal, which produced shallow donor level at about 30 meV [14]. The production rate of donors was found to be much higher in Zn-face than O-face. This donor was identified as a Zn – sub lattice defect, most likely the interstitials [or Zn_I] related complex. From the values of donor energy of the unirradiated samples discussed in literature, it was clear that the dominant shallow donor in ZnO was Zn interstitials.

Cohen et al used 'first principle pseudopotential method' to determine the electronic structure, atomic geometry and formation energy of native point defects [15]. The result showed that both Zn and O vacancies are the relevant defects in ZnO. A possible transition mechanism and the defect center responsible for the controversial green emission were also discussed. According to their studies, green luminescence was originating due to the transition between conduction band and acceptor level created by vacancy of zinc. First principle 'plane-wave pseudopotential method' was used to investigate the formation energies and electronic structure of native defects in ZnO [16]. It was seen that, when p-type conduction was assumed, the formation energy of donor-type defects could be low; under n-type conditions, vacancy of oxygen had lowest formation energy. However, from electronic structure calculations, zinc interstitials and zinc antisite were found to be responsible for n-type conduction.

To identify the shallow donors in ZnO, Yuming et al performed FP-LMTO method on $ZnO:V_O$, $ZnO:V_{Zn}$ and $ZnO:Zn_I$ and it was seen that V_O formed a deep donor level at ~1.3 eV below from the conduction band [17]. V_{Zn} and Zn_I formed shallow acceptor (~0.3 eV above from the valence band) and shallow donor levels (~0.5 eV below the conduction band) respectively.

Yoshino et al studied the properties of piezoelectric bulk acoustic wave resonators fabricated using ZnO thin films, with negative temperature coefficient of frequency (TCF) and substrates with positive TCF [18]. Two resonators with different frequencies were fabricated.

The effective electromechanical coupling coefficient was studied using thin film bulk acoustic wave resonators and an increase in this coefficient was observed with increase in the ZnO film thickness [19].

Effects of strain [along the c-axis] and grain size on the optical properties of ZnO films were also subjects of study [20]. It was seen that the excitonic transition

energies varied in the presence of strain field. Another important observation was that, strain was relieved and texture improved with larger grain size.

Thermally Stimulated Current [TSC] measurements were done on ZnO varistors to know the degradation properties [21]. This study also revealed that the activation energy was 0.39 eV, which was found to be very close to the reported value for Zn interstitials.

Toumisto et al proved the presence of Zn vacancy, as the dominant acceptors in ZnO, with the help of positron annihilation spectroscopic [PAS] technique [22]. Concentration of Zn vacancy, obtained from PAS studies, was in good agreement with the total acceptor density determined by temperature dependent Hall measurements. In the electron irradiated ZnO samples, the Zn vacancies were dominant; but the 'negative-ion-type' defects, introduced by irradiation also contributed significantly.

In another interesting report, Xu et al studied the electronic structure of ZnO materials and their spectral properties using "Full – potential Muffin – Tin orbital method" [23]. Position of the defect state levels was found to be in the energy band of ZnO. Based on the results, mechanism of absorption and emission spectra were explained.

Sun and Wang reported the *ab initio* calculations of tetrahedrally and octahedrally native interstitials in ZnO, using the full-potential linear muffin – tin orbital method [24]. The results showed that both tetrahedral and octahedral zinc interstitials could contribute to the native n-type conduction while zinc vacancy and octahedral oxygen interstitials might contribute to the p-type conduction. They suggested that 31 meV and 61 meV donors might originate from tetrahedral and octahedral zinc interstitials, and the study was based on temperature dependent Hall measurements.

Electrical and optical properties of defects and impurities in ZnO were discussed in detail, along with the possibility of group V elements converting the ZnO to p-type [25]. It was also observed that Nitrogen might be the best candidate for the

type conversion. Another observation was that, ZnO was highly radiation resistant material [25].

Imai and Watanabe performed band calculations of ZnO doped with different elements [26]. They used 'first principle pseudopotential method' within a framework of local density approximation and compared the results with the resistivities. Main features of the total DOS curves of doped ZnO were the same as that of pure ZnO, except for ZnO: Cr and ZnO: Mn. The Fermi level shifted upward from middle of the energy gap in the case of ZnO: (Al, Ga, In), ZnO: Y, ZnO:Ti. However a downward shift was observed in the case of ZnO: V and ZnO: Fe

The effect of substrate-induced strain in polycrystalline [sol-gel derived] ZnO thin films, on different substrate like GaN, saphire, quartz, Si/SiO_2 and glass was analysed through a detailed study [27]. There was a strong dependence of orientation, crystallite size and electrical resistivity upon the substrate-induced strain along the c-axis. It was seen that electrical resistivity of the films increased with increase in strain while the excitonic peak position shifted to lower energy side increase in strain. The conclusion from the study was that GaN substrate produced ZnO films, with better crystallinity and lower resistivity.

1.3 Deposition techniques

The growth technique played a significant role in controlling the properties of ZnO films, because the same material deposited by two different techniques, usually had different physical properties. This was due to the fact that the electrical and optical properties of the films strongly depended on the structure, morphology and nature of impurities present. Moreover the films grown using any particular technique might have different properties due to the variation of the deposition parameters and hence the properties can be tailored by controlling the deposition parameters. It was, therefore, important and necessary to make a detailed investigation on the different techniques used for the deposition of ZnO films.

1.3.1 Chemical Routes

A fully automatic, Single Ionic Layer Adsorbtion and Reaction [SILAR] technique was used for the deposition of highly photoconductive and transparent ZnO films [28]. Zinc sulfate and ammonia were the starting solutions. Crystalline films with slight preferential orientation along (002) plane were obtained even at room temperature. Band gap was 3.42 eV for very thin films and it reduced to 3.35 eV for thicker films. A very high photocurrent response ($\sim 10^5$) was also reported in these films.

High quality ZnO films were deposited on silica and silicon substrates using 'spin coating technique' in which zinc nitrate solution with glycine was used. Wurtzite structure evolved after the heat treatment at 1000 ºC in air [29]. Raman Studies were used for the first time in this report to identify the wurtzite phase and relatively flat surface was obtained in samples.

ZnO buffer layers were deposited over p-$CuInS_2$ thin films using Chemical Bath Deposition [CBD] technique to improve the light transmission in the blue region [30]. Here, $ZnSO_4$, ammonia and distilled water were used to prepare the starting solution. The 'as prepared film' contained both ZnO and $Zn(OH)_2$ and annealing at higher temperature converted $ZN(OH)_2$ to ZnO. Another technique employed was SILAR and experiment was performed at 97 ºC. In this case, ZnO films exhibited zincite structure with average optical transmittance of 80-90%. The efficiency of the cell fabricated using this film was nearly 4%.

Shimono et al used 'Spin coating technique' for the deposition of transparent and conductive ZnO thin films [31]. They used Zinc acetate mixed with diethanolamine and ethanol for the undoped film and aluminium nitrate and nickel nitrate for doping with aluminium and nickel, along with zinc acetate. As deposited films were amorphous, but annealing at 500°C resulted in wurtzite structure. Sharp absorption edge was obtained at 380 nm. A slight increase in optical band gap was

observed after annealing in hydrogen. As prepared films were highly resistive; but post deposition heat treatment in hydrogen resulted in low resistive films.

ZnO films were grown on plastic substrates using atomic layer controlled growth and these films were highly conducting and transparent [32]. Doping with Ga lowered the resistivity further.

A thin film transistor was fabricated with ZnO deposited using dip-coating technique, in which zinc acetate dissolved in 2-propanaol by adding diethanolamine was the starting solution [33]. Silicon wafers, with a thermally oxidized SiO_2 layer, were used as the substrates. After heat treatment at 600°C, a thin layer of Zn_2SiO_4 was formed at the interface of ZnO and SiO_2. The interface structure was analyzed using TEM.

A simple and a novel method was employed to deposit ZnO films over glass and Si substrates, using two different techniques together viz., (SILAR) and (CBD) [34]. It was seen that when glass was used, films were preferentially oriented along (002) plane. As deposited films were smooth, dense and highly reflecting. More over, the emission property was found to be independent of substrate type.

Structural changes stimulated by UV light irradiation, on sol-gel derived amorphous ZnO thin films, were also subject of investigation [35]. When the samples, kept in air, were exposed to UV light from a low-pressure mercury lamp, a transition from amorphous state to crystalline phase was observed. On irradiation, oxygen ionic species and oxygen atoms, produced from oxygen molecules, oxidized the defective sites, and hence promoted the rearrangement of the Zn-O networks.

Electrical and optical properties of ZnO thin films prepared using sol-gel method was discussed earlier [36]. Drying the as deposited film at 350°C and annealing at 600°C resulted in sharp XRD peak along the (002) plane. As the drying temperature increased, a decrease in resistivity was observed. However the transmittivity was unaffected after the heat treatments.

ZnO films oriented along the (002) plane were grown using sol-gel method in which zinc acetate dihydrate, 2-methoxyethanol and monoethanolamine (MEA) were used as starting solutions [37]. When the as deposited films were dried and then annealed at 600°C, highly oriented films were obtained having an average transmittance of ~80 % in the visible region and a band gap of [nearly] 3.3 eV.

Another study, on sol-gel derived ZnO films, was reported by Ghosh et al [38]. They studied the effect of thermal annealing in different ambient conditions on the properties of ZnO films. Structural properties were almost unaffected in nitrogen and vacuum ambients. But the samples were slightly oriented along (002) when annealed in air. However vacuum annealing resulted in a drastic decrease in resistivity.

Recently Kobayashi et al reported the fabrication of highly oriented (along (002) plane) ZnO thin films using a chemical method with Zn/O ratio 45/55 in the film [39]. Stoichiometry of the films was determined using EPMA and XPS. The presence of $Zn(OH)_2$ was also identified using XPS. Films were showing high resistivity and low optical transmittivity.

1.3.2 Chemical Vapor Deposition (CVD)

Low-pressure metal organic chemical vapor deposition (MOCVD) technique was successfully used for the deposition of ZnO with zinc acetate as precursor solution [40]. Different substrates like InP, GaAs, Si and glass were used and these films were analysed using EDAX and RHEED techniques. Films were polycrystalline with no preferred orientation.

Transparent and conductive ZnO thin films were deposited over Si and InP substrates using CVD and characterized using X-ray diffraction (XRD), AFM, optical measurements etc [41]. The main observation was that the preferred orientation of the ZnO crystallite was along (112) for Si and (002) for InP substrates.

Sallet et al also reported the growth of ZnO on (0001) sapphire substrates using MOCVD [42]. Diethylzinc and tertiarybutanol were used as zinc and oxygen sources respectively. In this paper, the authors had given details of growth conditions such as the substrate temperature and the precursor partial pressures. The influence of the cleanness of the MOCVD silica reactor was also emphasized, since it modified both layer quality and crystalline orientation. More over it also affected the steps in the growth process like sapphire thermal treatment and buffer layer deposition. ZnO epitaxial layers were characterized by scanning electron microscopy (SEM) [to assess the surface orientation and morphology], X-ray diffraction (XRD) and photoluminescence (PL).

Highly conductive polycrystalline ZnO films were grown using MOCVD technique with dimethyl zinc, dimethyl zinc-triethylamine and tertiary butanol as precursors [43]. Films grown using dimethyl zinc-triethylamine were oriented with the c-axis in the growth direction. Resistivity was of the order of $3x10^{-4}$ ohm cm.

Studies were done on high quality ZnO grown using MOCVD, over sapphire substrate [44]. High-resolution TEM and XRD analysess were done on these samples. Films were found to be strain free from low temperature photoluminescence studies.

Another report on ZnO thin films, prepared using plasma assisted MOCVD on sapphire substrate, was using the results of XRD, photoluminescence and optical transmittance studies [45]. Here also the films were preferentially oriented along (002) plane.

Cooray et al discussed two different preparation techniques, viz., sputtering and MOCVD, for the deposition of n-ZnO window layers on CIGS based solar cells [46]. Al doped ZnO films were prepared using DC magnetron sputtering while Boron doped ZnO were prepared using MOCVD technique. Efficiency greater than 14 % was achieved in this solar cell having an active area of 3.2 cm^2.

ZnO films were grown on R plane sapphire substrates for the surface acoustic wave (SAW) filters; an epitaxial relation was also obtained between ZnO and R-plane

sapphire substrates using X-ray diffraction technique [47]. Surface morphology was also studied using SEM and TEM techniques.

Stoichiometric ZnO films were grown on Si substrate using Plasma enhanced CVD with a zinc organic source and carbon dioxide gas mixture [48]. Substrate temperature was kept at 503 K initially with different gas flow rate and then keeping gas flow rate constant, substrate temperature was varied. Films were oriented along (002) plane at higher substrate temperature, while at low temperature, films were polycrystalline with different orientation. Room temperature exciton absorption peak was observed in these films, which vanished at lower substrate temperature. This observation was correlated with the crystalline quality of the film. PL studies were also done at room temperature.

1.3.3 Pulsed Laser Deposition (PLD)

Pulsed Laser Deposition (PLD) technique was one of the sophisticated techniques for the deposition of ZnO thin films. In an interesting report, Myoung et al described the effect of film thickness on the properties of laser deposited ZnO thin films [49]. It was shown that crystallinity was improving with the increase in film thickness. Another interesting observation was the decrease in carrier concentration with increase in the film thickness. PL studies revealed two emissions; one in UV region and the other in visible region.

Effect of laser wavelength and substrate temperature on the properties of PLD films was investigated by Ianno et al [50]. Films were characterized using XRD and optical emission spectroscopy. It was seen that, as the laser wavelength increased to 1064 nm, the films became dull gray in color. High quality film was obtained at 532 nm radiation. As the laser fluence increased, quality of the film became better. Moreover, the increase in the substrate temperature also, enhanced the film quality.

Millon et al reported the deposition of ZnO films on different substrates using femto second pulsed laser [51]. Films were crystalline, smooth, and dense with

13

hexagonal texture. Channeling and rocking curve experiments performed on these films revealed that the film was not as good as that obtained with nanosecond pulses.

ZnO thin films were deposited on Si(1 1 1) substrates, at different substrate temperature, using PLD technique, in oxygen atmosphere [52]. An Nd: YAG pulsed laser, with a wavelength of 1064 nm, was used as the source. Influence of the deposition temperature on the thickness, crystallinity, surface morphology and optical properties of ZnO films were analyzed with the help of X-ray diffraction (XRD), scanning electron microscopy (SEM), selected area electron diffraction (SAED), photoluminescence (PL) spectrum and infrared spectrometer. The results showed that, the ZnO thin films deposited at 400 °C had the best surface morphology and crystalline quality. The PL spectrum with the strongest ultraviolet (UV) peak and blue peak was observed in this condition.

Synthesis and tribological evaluation of alumina doped ZnO films, prepared using PLD technique were also reported [53]. Films were found to be highly crystalline with (002) orientation. The friction coefficient was found to be less for doped films.

Choopun et al discussed the effects of oxygen background pressure on the growth, epitaxy, point defect chemistry, optical and electrical transport properties of Laser deposited epitaxial ZnO thin films [54]. By tuning the oxygen background pressure during the initial and final growth stages, smooth and epitaxial films with high optical quality, high electron mobility and low background carrier concentration were obtained. Highest mobility (70 cm^2/Vs) was observed for the film prepared at a pressure of 10^{-4} Torr.

Transparent conducting thin films of $ZnO-ZrO_2$ were prepared using PLD technique [55] in which KrF excimer laser was the source. The substrate was kept at 673 K. All the films were found to be oriented along (101) plane and average surface roughness [measured using AFM] was 4.4Å. Optical transmittance was about 80% in the visible region.

Studies on Al-, B- and Ga- doped ZnO films [with a low resistivity and high optical transmittivity], deposited using PLD technique for solar cells applications were also done [56]. Among these, Al-doped samples were highly transparent and low resistive. Solar cell was fabricated using ZnO:Al and ZnO:Ga with Cu(In,Ga)Se$_2$ and an efficiency > 10% was obtained.

Studies like Photoluminescence and Raman scattering were done on PLD ZnO films grown on Si substrate and the effects of strain on PL emission and Raman mode were also discussed [57]. ZnO films were also grown on Si substrate with thin buffer layer of AlN and GaN over Si. TEM analysis showed those films deposited on GaN and AlN buffer layers were epitaxial, while films deposited on Si substrate were showing random in-plane orientation [57].

Effect of variation of substrate temperature on the structural and optical properties of ZnO films grown on Si substrate using PLD technique were reported [58]. Substrate temperature was varied from 250ºC to 700ºC and high crystalline quality films were obtained at substrate temperature 650 and 700ºC. PL measurements were also consistent with the XRD analysis.

Heo et al reported the room temperature photoluminescence and ultra violet photoconductivity of epitaxially grown, phosphorous-doped ZnO. These samples were prepared using PLD technique [59]. It was observed that UV emission was shifted to higher energy side for the as prepared, P-doped ZnO films with a reduced intensity. Annealing in oxygen pressure also resulted in the reduction of the intensity of UV emission; however a new emission, related to oxygen defect, was also found.

Duclere et al reported the studies of c-axis oriented ZnO layers, grown on platinum buffer layers using PLD technique [60]. The Pt bottom layer was found good in plane lattice matching with c-ZnO, enabling epitaxial re-growth of ZnO.

Another recent and interesting study was on the optical properties of ZnO thin films deposited on γ-LiAlO2 substrate using again, PLD technique [61]. Films were

found to be highly crystalline with an optical transmittance of ~ 85 %. PL emission at 550 nm was attributed to the oxygen vacancy caused by the Li diffusion from the substrate.

1.3.4 Molecular Beam Epitaxy (MBE)

Plasma assisted Molecular Beam Epitaxy (P-MBE) was used to grow ZnO thin films over Al_2O_3 substrate, under various Zn/O ratios [62]. Highest quality ZnO was obtained when stoichiometric flux conditions were applied. It was seen that, the growth rate increased when Zn flux increased. It was also observed that when the growth temperature increased, Zn flux should be increased to get stoichiometric films. Surface analysis revealed the presence of hexagonal shaped 2D islands. XRD and PL studies were also used on these samples.

An interesting report was on MBE grown ZnO films over lattice matched $ScAlMgO_4$ substrate [63]. To avoid, even the very small (0.09%) lattice mismatch, a buffer layer of ZnO annealed at high temperature was used. On such a surface of annealed ZnO buffer layer, ZnO films were deposited with different laser repetition conditions. Crystallinity of the material was analyzed using high resolution XRD. Flat surface was obtained with low laser repetition, while terrace and step structures were observed at higher repetition. Low temperature PL measurements were also done to identify excitonic emissions.

Electroless chemical deposition of ZnO was reported in which zinc sulphate and tin chloride were used as starting solution [64]. Growth kinetics was studied with Quartz crystal Microbalance in a bath, having thermostat. SEM analysis was done to know the surface morphology.

Highly transparent and conductive ZnO films were grown by atomic layer controlled growth on various substrates including glass, sapphire and polyethylene tetraphthalate (PET) at different temperatures [65]. Effect of doping with Ga was also discussed in this report.

Single crystal ZnO was grown using vapor phase technique and Schottky barrier diodes (with gold; Au/ZnO) were fabricated [66]. Investigations with the help of DLTS could identify four different shallow donor levels. According to this report, crystals grown by this technique were superior to the other single crystals of ZnO reported earlier.

Influence of annealing temperature on the properties of ZnO thin films, deposited using thermal evaporation were studied [67]. It was seen that, oxidation started only after 250ºC and XRD peaks of ZnO appeared only at 300ºC. It was also seen that, high conductive Zn films showed a transition to lower conductive ZnO films, as the annealing temperature increased.

1.3.5 Sputtering

Effects of r.f sputtering power, pressure in the chamber, substrate temperature and deposition rate on the properties of ZnO thin films were subjected to study [68]. It was seen that perpendicularly oriented ZnO films were obtained with lower deposition rate at lower substrate temperature. Size of the grains was also strongly dependent on the sputtering parameters.

Optical properties of ZnO films, grown using r.f sputtering technique on sapphire substrate, were reported by Valentini et al [69]. Films were rather homogeneous and high optical transmittance [~ 85 % in the visible region] wth sharp optical absorption edge at 380 nm. Refractive index was also calculated from reflectance spectra in this paper and values were in the range of 1.9 - 2.1.

In another paper, structural analysis of r.f. sputtered ZnO films were reported [70]. Studies using XRD and SEM were done on these films having different thickness and prepared at different substrate temperature. Grain size increased with increase in the film thickness and also with the increase in substrate temperature.

Properties of sputtered ZnO films were investigated and a junction was fabricated with evaporated CdS film. [71]. A strong interface interactions were observed between CdS and ZnO, which might include interdiffusion and strain.

Gong et al reported the effects of substrate temperature and pressure ratio, K $(P_{O2}/P_{Ar}+P_{O2})$ on the properties of sputtered ZnO thin films [72]. All the films had preferred orientation along c-axis and highly preferred orientation was obtained with K=40%. Crystallinity increased with the increase in the substrate temperature. Carbon was found to be the main impurity in the films, as revealed by the XPS analysis. The average transmission of the films was found to be ~92% in the visible region.

Highly conductive and transparent Al doped zinc oxide thin films were grown using off-axis magnetron sputtering on silica surface and the effects of post deposition annealing were discussed in another paper [73]. Optimized ZnO film was having resistivity of 4.5 x10^{-4} ohm cm and optical transmittance of 85 %.

Electrical characterization of zinc oxide/glass substrate surface acoustic wave [SAW] filters was also reported [74]. It was found that, SAW velocity decreased with increase in the oxygen concentration. Average crystallite size also increased with the increase in film thickness.

Results of Capacitance - Voltage measurements of highly resistive Nickel doped ZnO films, deposited using DC sputtering were reported [75]. ZnO capacitor was fabricated on SiO_2/Si substrate with Al/Ti electrode in the top and bottom. Electron mobility was found to be in the range of $1 - 3$ cm^2/Vs.

Tominaga et al reported the deposition of highly conductive ternary amorphous compound films of ZnO-In$_2$O$_3$ using DC planar magnetron sputtering technique [76]. This was achieved by the simultaneous sputtering of ZnO and In$_2$O$_3$ targets. Effects of impurities like Al and Sn were also studied. Doped films were showing slightly less optical transparency. The best film was having a resistivity of 4x10^{-4} ohm cm.

Kim et al reported the effects of substrates on the structural properties of ZnO films deposited using r.f. sputtering [77]. P-Si and sapphire substrates were used and crystallinity was higher for samples deposited over sapphire substrates. Lattice mismatch was lower in the case of film deposited on sapphire substrates while surface roughness was lower for the Si substrates.

Gupta et al investigated the influence of post deposition annealing on the structural and optical properties of r.f. sputtered insulating ZO thin films [78]. The as grown film, deposited over quartz substrate, was in a state of stress with orientation along c- axis. These films became stress-free after the annealing in air at 673 K for 1hr. Above this temperature, a process of coalescence was observed which caused a major grain growth. This in turn, resulted in the formation of 'microcrack' and surface roughness. Packing density of 99% was observed for the film annealed at 673 K, which indicated almost a void free film.

Effect of post deposition annealing and ion beam bombardment on magnetron sputtered ZnO films was studied in detail with the help of XRD, PL and optical absorption spectroscopy [79]. Average grain was almost the same for both as grown and ion bombarded films, while it increased much for the annealed samples. UV emission shifted towards the high-energy side in the ion-bombarded film, while the green emission was obtained for the annealed samples.

Important physical properties like resistivity, optical absorption of sputtered ZnO films were reported [80]. It was seen that the O/Zn ratio determined the properties of ZnO and this ratio was sensitive to the r.f. power, substrate temperature, oxygen partial pressure etc. Resistivity increased with increase in the oxygen partial pressure while it decreased with increase in substrate temperature. It was also observed that, when ZnO films were exposed to atmosphere for several months, its resistivity increased by 150 %.

A report on the optical and morphological studies of ZnO thin films, prepared using reactive evaporation technique and its application as a transparent window layer

in $CuInSe_2$ based solar cells were published [81]. In this report, bilayer structure of n+-ZnO/i-ZnO and n+-ZnO/ZnSe were used and it revealed that the usage of ZnO increased the spectral range of absorbed radiation in comparison with those using CdS/ZnO as optical window.

Water and Chu reported the physical and structural properties of r.f. sputtered ZnO thin films on Si substrates [82]. Films were characterized as function of deposition temperature, argon-oxygen gas flow rate and r.f. power. Films were oriented along (002) plane and were in a state of stress. Stress increased with increase in the substrate temperature and also with the annealing temperature. Surface roughness decreased with substrate temperature. But at very high temperature, it again increased. Also, roughness increased with increase in the oxygen ratio in the chamber.

Nanocrystalline ZnO thin films were prepared through dc magnetron sputtering in an $Ar + O_2$ gas mixture, using two types of targets; one was commercially available zinc metal (purity 99.99%) and the other was pressed Zn metal powder [83]. Influences of the target conditions as well as the oxygen partial pressure on the structural and optical properties were studied. Microstructure of the films was investigated using XRD and SEM techniques. Optical properties were examined using UV–Visible spectrophotometer. The films deposited from metal target showed better orientation along *c*-axis and exhibited better optical properties compared to the samples prepared using pressed metal powder target.

Brett and Parsons discussed the properties of transparent conducting ZnO film deposited using reactive bias sputtering [84]. Electrical resistivity decreased with increase the substrate bias, while mobility increased with increase in the bias voltage. The lowest resistivity was obtained was $2x10^{-3}$ ohm cm.

Chen et al reported the results of different experiments [XRD, RBS, Positron annihilation, cathodoluminescence and Hall measurements] performed to investigate

the defects of annealed ZnO thin films, prepared using sputtering [85]. Crystallinity of the film improved after the annealing at 1000°C as it was clear from XRD. Electron concentration increased with increasing annealing temperature. From the experimental results, it was seen that the crystal quality, electrical and optical characteristics improved by post deposition annealing.

Lee et al discussed the heat treatment effects on the electrical and optical properties of ternary compound In_2O_3-ZnO films prepared by sputtering the mixture of In_2O_3 and ZnO powders [86]. Comparison of two kinds of films prepared in Ar gas and Ar + O_2 gas were made. Heat treatment was made in vacuum and O_2 atmosphere. Lowest resistivity was obtained after the heat treatment in vacuum at 650 °C.

Valentini et al reported the structural properties of r.f. sputtered ZnO films for optical applications, taking into account of the efficiency and the relative speed of the RHEED analysis process [87]. Optical properties were studied using the analysis of optical wave-guides.

A new compressed magnetic field (CMF) magnetron sputtering was introduced for the deposition of ZnO films with high rate sputtering [88]. The radiation damage undergone by the substrate during the deposition of ZnO films was determined from the CV measurements of metal/ZnO/SiO_2/Si structures.

Gupta et al reported the structural properties of ZnO films prepared using the oxidation of metallic zinc, in which the thin film of metallic zinc was deposited using thermal evaporation [89]. In this report, oxidation was carried out at different temperatures and in different atmospheres of oxygen and ozone. By adjusting oxidation time and temperature, texture and microstructure of the films could be easily changed.

Influence of post deposition annealing of ZnO thin films prepared using electron beam gun evaporation is discussed [90]. It was seen that the as deposited films were colorless and having good crystalline quality. Annealing in air did not

21

modify its optical properties but modified structural properties. These films were having sharp optical band edge at ~3.3 eV.

X-ray photoelectron spectroscopy analysis was performed on ZnO films prepared on glass substrates by DC reactive magnetron sputtering at different substrate temperature [91]. Two resolved peaks obtained in O 1s spectra, in which the lower energy peak at 530 eV could be assigned to O – Zn bonding and the higher energy peak, located at 532 eV, could be assigned to O-H bond. It was also concluded that the decrease in oxygen component at higher energy was an indication of less porous nature of the film and this was confirmed from SEM.

Recently the effects of the injected ambient gas during the temperature elevation and the in-situ thermal annealing after the growth of the low temperature buffer layers on the optical and structural quality were investigated on sputtered ZnO films [92]. The introduction of inert gases such as argon and nitrogen as the ambient gases during the thermal treatments of the buffer layers led simultaneously to the reduction of FWHM value in the XRD rocking curve and the improved emission properties.

ZnO films with deep ultraviolet emission on (006) sapphire substrates were prepared by RF magnetron sputtering by periodically changing the substrate temperature [93]. It was found that the as-prepared ZnO films consisted of multilayered structures as evident from the SEM images of their cross-sections. Room temperature photoluminescence of ZnO films with this multilayered structure showed two emissions centered at 332 and 388 nm, on excitation using source at 260 nm. The strong and deep ultraviolet emission at 332 nm was due to the O $2p$ dangling-bond state in the multilayered structure of ZnO films. Raman scattering spectrum of sample showed that such a structured ZnO film possessed strong compressive stress.

Reflective second harmonic generation (RSHG) was used to analyze the growth condition of poly crystal zinc oxide film having c-axis orientation and grown on the Si substrate using RF magnetron sputtering technique [94]. The relationship

22

between the RSHG intensity and the substrate temperature revealed that the effect of the grain boundaries dominated in the RSHG mechanism. The inclined structures of ZnO films on the Si substrate were explained with reference to these RSHG patterns

Aluminum doped zinc oxide films were prepared with the help of reactive mid frequency magnetron sputtering. Electrical and optical properties as well as the surface morphology were obtained after wet chemical etching [95]. The carrier mobility could be increased up to 42 cm^2/Vs and the transmission between 400 and 1100 nm was enhanced by the reduction of aluminum content in the targets. The working point of the reactive sputtering process strongly influenced the etching behavior and was used to optimize the light scattering properties of the ZnO: Al films after wet chemical etching. Finally, the texture-etched ZnO: Al films were successfully used as substrates for silicon thin film solar cells.

1.3.6 Spray Pyrolysis

ZnO thin films were prepared using spray pyrolysis technique with different precursors such as $ZnCl_2$, $ZnCl_2$ and Zn acetate [96]. By suitably adjusting the deposition parameters, a resistivity of 10^{-3} ohm cm could be achieved. It was seen that, the presence of Cl in the films reduced the resistivity. The photoconductivity of the films was ascribed to desorption of oxygen from the film.

Wu et al reported the properties of ZnO films grown on different substrates by ultrasonic spray pyrolysis method [97]. Single-phase homogeneous uniform films having band gap of 3.27 eV, were obtained by this technique. Particle size was around 5 μm.

Effect of substrate temperature on the properties of ZnO thin films grown on alumina substrate using this technique was investigated in detail [98]. Concentration of starting solution was also varied. The fastest deposition rate occurred between 400 and 450ºC. In this temperature range, the films were uniform, dense and oriented along (002) direction.

In a letter, Goyal et al discussed the effects of concentration of precursors on the various properties of ZnO films [99]. Growth rate and crystalline quality increased with increase in the concentration. Texture coefficient of (002) plane also increased with the increase in molarity of solution.

Goyal et al also discussed the development of transparent and conducting ZnO thin films using spray pyrolysis techniques, in which Zn acetate was used as precursor [100]. Structural and electrical studies were conducted and the stability of the films in hydrogen plasma was also analysed. Highest conductivity was obtained by adding small quantity of indium into the film.

Krunks and Mellikove reported the fabrication of ZnO thin films using spray pyrolysis technique [101]. Zn acetate, dissolved in deionized water and isopropyl alcohol, was used as precursor. Growth temperature was in the range of 625 – 675 K and precursor solution was having concentration in the range of 0.1 – 0.2 mol for obtaining ZnO films with better optical and electrical properties.

The effect of substrate temperature on the structural, electrical and optical properties of ZnO films, prepared using spray pyrolysis technique wase discussed [102]. It was found that there was a critical temperature, Tc = 180 ºC, below which the thermal decomposition to ZnO did not occur or was incomplete. Electrical resistivity was of the order of 10^{-3} ohm cm in dark and it further reduced to 10^{-4} ohm cm after illumination. Band gap was nearly same (3.3 eV) for all samples, prepared at different substrate temperatures.

Influence of substrate temperature on the properties of ZnO thin films was also a subject of study and it has been found that resistivity and optical transmittance of the films were very much dependent on the temperature [103]. Substrate temperature was varied from 573 K to 773 K and spray rate was maintained at 6 mL/min. However films were found to be resistive.

Effects of doping and annealing on the electrical, optical and structural properties of ZnO thin films prepared using this simple technique was also

24

investigated [104]. Annealing in argon or vacuum reduced electrical resistivity substantially. The most pronounced change was observed in argon atmosphere. Highest figure of merit was obtained in the case of indium doped ZnO films.

Lokhande and Uplane discussed the structural, optical and electrical studies on highly oriented (along 100 plane) sprayed ZnO films [105]. The resistivity of the film at room temperature was ~ 10^{-1} ohm cm and the band gap energy was 3.27 eV.

In a very interesting report, Smith had discussed the mechanism of forming ZnO and SnO_2 films by pyrolytical process [106]. A general guideline was established with respect to the growth rate and morphology. When the precursor was in the form of a small and neutral complex, the growth rate increased rapidly

PL studies were performed on sprayed ZnO thin films [107]. Films with the (002) plane with wurtzite structure were formed in the temperature range 250 – 350ºC and post deposition annealing did not affect the crystallinity. Intensity of green emission in these films increased with increase in film thickness. Also, for the films with same thickness, an increase in O/Zn ratio lead to a decrease of the green intensity. Conclusion was that the origin of green luminescence was deeply associated with the oxygen content in the film.

Nunes et al, investigated the influence of various dopants (Al, In and Ga) on the properties of sprayed samples [108]. The most pronounced changes were observed in the electrical properties, where the resistivity decreased two orders of magnitude. Lowest resistivity was obtained for the indium doped ZnO films.

Structural, optical, chemical and electrical properties of sprayed ZnO films deposited over Pt or silica substrates were determined in temperature ranges between 223 and 373 K [109]. These films were found to be oriented along (002) direction. The band bending created barriers at grain boundaries and the mobility of charge carriers was limited by the thermal field emission of electrons at these barriers.

In an interesting report, a comparison of structural properties ZnO films grown by sputtering and spray pyrolysis techniques was also made [110]. All

25

sputtered films exhibited a preferred orientation along the c-axis and increased substrate temperature favored the crystallinity. Sprayed samples also showed a strong c-axis orientation.

Effects of molarity of precursor solution on structural and opto-electrical properties of sprayed ZnO films were discussed in another paper [111]. Film growth rate increased with the increase in molarity. On increasing the molarity of the solution, the preferred orientation changed from (002) to (100) direction. Carrier concentration also increased while electrical resistivity decreased with increase in molarity of the solution.

Effects of annealing on the properties of ZnO films, deposited using ultrasonic spray pyrolysis technique, were analysed in another publication [112]. It was seen that, after the annealing treatment, intensity of (002) plane reduced and electrical conductivity improved. Annealing in hydrogen atmosphere resulted in the formation of lowest resistive films. The average optical transmittance was nearly 80% while the optical band gap was 3.27 eV.

Transparent conducting indium-doped zinc oxide thin films were prepared on soda-lime glass substrates using spray pyrolysis technique [113]. Dependence of electrical, structural, morphological and optical properties on the preparation conditions was discussed in detail in this paper. Two main variables, viz., substrate temperature and molar concentration, were varied in the ranges of 425–525 °C and 0.05–0.5 M, respectively, in order to obtain films with low electrical resistivity and high optical transparency in the visible region. A minimum resistivity value of ~ $3 \times 10^{-3}\,\Omega$ cm was obtained for films deposited from highly concentrated starting solutions, i.e. 0.4 and 0.5 M. Values of the free-carrier concentration and the electronic mobility were estimated by Hall effect measurements. XRD studies proved that the preferential orientation was along the (1 0 1) direction. The surface morphology was clearly affected by the variations in molar concentration, leading to a smoother appearance as the zinc concentration in the starting solution increased.

Typical optical transmittance values in the order of 85% were obtained for all the films.

1.4 Photoluminescence

Recently wide-band semiconductors attracted great interest, because of their future possible applications in areas, such as UV sensors, light-emitting diodes (LEDs), laser diodes (LDs), and other high-speed high-power electronic devices. ZnO being a promising candidate for the next generation electronic devices due to its large band gap easiness of preparation, this material became the center of attraction for several research groups. This is a direct band gap semiconductor, suitable for production of light emitting devices in green, blue or ultraviolet. More over it has some other substantial advantages over currently developed wide-band-gap semiconductor devices (e.g.GaN-based). For example, the high quality bulk single crystals are available now and it has a large exciton binding energy (-60meV) with potential for utilizing the exciton emission at room temperature (RT).

Since these films find great applications in the areas of optics and opto electronics, it is important to investigate the optical properties of ZnO films prepared using different techniques. Not only does it help us to analyze the structure and other properties of ZnO, but also it contributes to the optimization of the growth process so as to make this film suitable for the applications in optical/opto electronic devices. Hence a detailed literature review on the PL measurements of ZnO material is included in the following section.

The luminescence of ZnO films typically has 'near band edge emission' and a 'deep level (blue-green) emission'. Owing to these properties, ZnO can be used to make devices for UV or blue emission. Therefore there are serious efforts to understand the mechanism of these emissions. Researchers have considered that the UV emission could be due to the excitonic transition. But still, controversy exists in explaining the origin of blue-green emission.

Dingle described the role of copper on the origin of green emission in ZnO [114]. The transition was found to be between a highly shielded localized level of copper impurity and a level, which was strongly perturbed by the valence band states of the crystal.

Cathodoluminescence (CL) of deformed ZnO ceramics was studied in SEM based CL measurement system [115]. Mechanical damage of the surface produced the decrease of the CL emission and a shift of the emission peak to higher wavelengths.

Ortiz et al reported the PL spectra of undoped and $TbCl_3$ doped ZnO films. The undoped films had an emission at 510 nm, while doped samples exhibited the emission at 550 nm [116, 117]. However the exact origin of blue green emission (510 nm) was not given. This emission was assumed to be due to the transition within a self-activated center formed by doubly ionized zinc vacancy and ionized zinc interstitials. The emission at 550 nm was probably due to the presence of Tb in the film. Another interesting observation was that, the emission intensity of doped film was decreasing with the time of exposure to the excited light.

Vanheusden et al reported a strong correlation between the green luminescence and oxygen vacancies, by combining electron paramagnetic resonance, optical absorption and PL spectroscopy [118]. It was also demonstrated that the free carrier depletion at the particle surface, and its effect on the ionization state of oxygen vacancies, could strongly affect the green emission.

Another detailed experimental evidence was given to explain the origin of blue green emission in ZnO phosphor powder [119]. It was suggested that the green emission was due to the recombination of electrons in singly occupied oxygen vacancies (V_O^+) with photo-excited holes in the valence band.

Ortiz et al discussed the PL characteristics of lithium doped ZnO films, prepared using spray pyrolysis technique [120]. The emission of these samples was a broad band, composed of four overlapping peaks at 508, 590, 604 and at 810 nm,

while the undoped samples had only the well-known blue green emission. These results indicated that the lithium was giving rise to a donor level in the ZnO

In an interesting report, Studenikin et al discussed the fabrication of green and orange luminescent ZnO films [121]. Green luminescent films possessed a porous structure while orange films possessed a close packed granular morphology. Green luminescence was seen to be due to the oxygen vacancies in layer just below the crystallite surface.

PL spectra of ZnO thin films prepared by oxidation of metallic Zn, exhibited a single exciton peak around 390 nm without any deep-level emission [122]. Zn started transforming into ZnO at 300°C and changed totally to ZnO at 400°C, and this gave very good luminescent properties.

Im et al discussed the ultraviolet emission in ZnO films deposited under various oxygen pressures using PLD technique. The UV emission continuously increased with the increase in oxygen pressure [123]. This was probably due to the improvement in stoichiometry and hence a straight relation was proposed between the stoichiometry and UV emission.

Violet and UV emissions were observed in PLD -ZnO prepared on the sapphire substrate [124]. The violet emission centered at 420 nm, was attributed to the transition from the level due to interface traps existing at the grain boundaries to the valence band. The well-known green emission was also observed in the film, deposited at an oxygen pressure of 200 mTorr. However the origin of this emission was related to the transition from the shallow donor level of oxygen vacancies to deep acceptor level of zinc vacancies.

In an interesting paper, Li et al tried to explain the origin of blue-green emission, in undoped ZnO films [125]. In these samples, two emissions were observed with energies 3.18 eV and 2.38 eV. It was concluded that the green emission was corresponding to the local levels composed by oxygen antisites and the transition was from the conduction band to deep acceptor level of oxygen antisites (O_{Zn}).

In the case of ZnO thin films deposited using photochemical vapor technique, the UV emission exhibited blue shift on decreasing the substrate temperature and this was attributed to the band gap widening [126].

Depth profiling was done on ZnO films using CL spectroscopy [127]. Besides the excitonic and deep level emissions, peaks at 3.13 and 2.57 eV were observed and these were attributed to defects. The emission peaks were examined as a function of electron penetration depth by varying the acceleration voltage. It was seen that the internal absorption strongly affected the near band edge emission, due to pronounced absorption tail.

Temperature dependent CL spectroscopy was used to investigate band edge emission of undoped and Al-doped ZnO single crystals [128]. Free exciton emission was weak throughout the temperature range in the case of doped samples; however bound exciton annihilation emission was intense.

Time resolved and steady state measurements were done on luminescence along with photoconductivity transients in ZnO films [129]. It was observed that, under continuous excitation, the film exhibited green emission while pulsed excitation resulted either blue or green emission, depending upon the excitation intensity. Transient luminescence showed fast and slow components; the fast component was assigned to an inter band exciton recombination, and the slow component was assumed to be due to an electron-hole recombination, which most likely involved oxygen and zinc vacancies.

A strong violet emission, located at 402 nm, and a week violet emission, located at 384 nm, were observed in ZnO films deposited on Si substrates, using ref magnetron sputtering [130]. The former emission was assigned to the transition from conduction band tail to valence band tail and the latter was assumed to be due to electronic transition from conduction band to valence band.

PL of highly oriented ZnO films, annealed in different ambient conditions, was studied in the temperature range −190 to 600°C [131]. The spectra had two

emissions, one in the UV range and the other in visible region. Annealing the as prepared samples in H_2/Ar ambient enhanced UV light emission, while annealing in O_2 atmosphere enhanced the visible emission.

Role of copper in the green emission was investigated using EPR, PL and IR absorption studies [132]. It was suggested that the green emission was caused by donor-acceptor pair recombination, involving the Cu^{2+} ions.

Ozaki et al developed ZnO thin films with strong UV emission at 3.05 eV having smooth surfaces. The films were prepared using ref-sputtering technique [133]. Intensity of UV emission was found to be complementary to that of the red PL, emerging at ~ 2 eV. This was assumed to be from crystal imperfections of the films. It was also observed that, higher substrate temperature and subsequent heat treatment at low temperature reduced the red emission.

A mechanism for the blue emission [446 nm] in ZnO was proposed to be due to the transition from shallow donor level [of oxygen vacancy and zinc interstitials] to the valence band [134].

Agyeman et al investigated the emission properties of undoped ZnO thin films, grown by rf magnetron sputtering on quartz substrates and annealed in various ambient such as in vacuum, reducing gas, oxygen and argon atmosphere etc [135]. There was a strong UV excitonic emission peak [at ~ 3.26 eV] from the samples annealed in the reducing ambient. But the samples annealed in argon and oxygen showed trong emissiosn peaks at 2.4 eV.

Hur et al discussed the variations in PL emissions of ZnO due to different annealing conditions in air and found that the concentration of antisite oxygen increased when ZnO ceramics were in O-rich conditions [136]. It was also seen that, as the concentration of O-antisite increased, the intensity of green emission also increased. Hence in this report, it was proposed that the green emission resulted from the transition from conduction band to the acceptor level of antisite oxygen. However band edge emission intensity reduced when ZnO was in O-rich conditions.

PL of ZnO nanocrystallites, confined in sol-gel silica matrix, was studied [137]. It showed two defect level emissions [in the range, 2.38 – 2.66 eV] and an excitonic emission band [centered at ~4.22 eV]. Annealing the system in oxygen atmosphere reduced the defect level emission, while it increased when annealed in hydrogen atmosphere. Experiments hence proved that the defect emissions were due to the oxygen vacancies.

Different substrates like sapphire, quartz, Si and glass were used to deposit ZnO films using rf sputtering and PL studies were performed [138]. A strong UV luminescence centered at 356 nm, and a weak blue emission located at 446 nm were obtained for the films deposited on sapphire, quartz and Si. But only a strong blue emission at 446 nm was obtained in the case of films deposited over glass substrates. The intensity of UV emission was seen to be increased 7 and 14 times, respectively, for the films on sapphire and quartz, after high temperature annealing in vacuum. Here the blue emission was assumed to be originating from oxygen vacancy to valance band.

Zhang et al discussed in detail, the different PL spectra obtained from rf sputtered ZnO with different excitation wavelengths [139]. When the excitation wavelength was 270 nm, there were emissions at 356 nm [UV peak] and blue peak 446 nm [blue peak] from the films deposited on sapphire, quartz and silicon. But when the excitation wavelength was increased to 300 and 320 nm, the UV emission disappeared and the PL peaks shifted to 480 and 510 nm. Further increase of the excitation wavelength to 340-395 nm range resulted in a broad spectrum.

Wang et al discussed the influence of post – growth annealing on the luminescent properties of ZnO films [140]. Annealing in open ambient resulted in the reduction in intensity of near-band-edge ultraviolet emission. Face to face annealing technique was employed and the intensity increased considerably, while visible luminescence decreased. This was attributed to the reduction in the rate of formation of vacancies (oxygen and zinc) at the surface region.

Peaks due to free- and bound- exciton transitions were observed in the PL spectrum of (0001) ZnO, recorded at 20 K. The temperature dependent free exciton peak energy was fitted using an equation developed by Mangoolian and Woolley [141]. The strongest peak due to the bound exciton transition exhibited thermal activation energy of 14 meV, which was in agreement with the binding energy of the exciton to the defect.

Room temperature PL spectra of ZnO films, prepared by oxidation of Zn metallic films, were showing a strong UV emission [excitonic] and visible emission [142]. The film annealed at 410ºC was showing strongest UV emission. But the visible emission, consisting of two components in the green and yellow range, showed different temperature dependent behavior from that of the UV emission. However exact mechanism of these emissions was not given. It was suggested that yellow emission was probably due to interstitial oxygen.

Jeong et al have discussed the effect of growth conditions on the emission properties of magnetron sputtered ZnO films and reported that intensity of the visible emission was dramatically suppressed on increasing the $O_2/Ar+O_2$ ratio in the growing ambient [143]. It was postulated that the green emission was probably due to the oxygen vacancy or Zn interstitials and exciton related emission was strongly dependent on the size of the micro crystallites forming the film.

The characteristics of impurity bands near the band edge of Al-doped and undoped ZnO ceramics were investigated using PL studies [144]. As the doping concentration increased, Al-impurity bands degenerated from two localized levels to the single localized level. It was also observed that, the green emission intensity got reduced on increasing the Al-concentration.

Strong UV emission was observed in high quality ZnO thin films prepared using 'electrophoretic deposition technique' [145]. TEM and XRD studies revealed that these films had an average grain size of 20 nm. UV emission was attributed to exciton emission.

Shan et al observed a blue shift in near band edge emission of ZnO films doped with Mg and effects of aging of UV and visible emission were also discussed [146]. In this case, the visible emission disappeared as the dopant concentration increased. With aging, the NBE emission enhanced while the green emission disappeared.

Results of PL studies on Cu-doped ZnO nanowire were reported [147]. Copper acted as a catalyst in the nanowire growth and got incorporated during the growth as dopant. A visible emission was observed with a shoulder peak, which was assigned to the electron transfer from the impurity levels in the forbidden gap to the valence band or between the different levels in the forbidden gap.

Structural and luminescent properties of ZnO films deposited using Atmospheric Pressure Chemical Vapor Deposition (APCVD) were studied [148]. It was reported that the crystal quality of the films had strong dependence on the growth temperature, flow rate of carrier gas and the annealing temperature. Luminescence properties were related to the growth and annealing ambience. Intensity of green emission of ZnO films, annealed in O_2 atmosphere, was much stronger than that for the samples, annealed in N_2 atmosphere.

The intensity of UV emission of Ni-doped ZnO films increased with increase in annealing temperature and reached a maximum at 450ºC. Then there was a decrease on further increase in temperature [149]. Also it was found that the annealing of Ni-doped ZnO films resulted in the recovery of microcrystalline defects and homogenization of the film.

The effects of *ex situ* annealing and *in situ* control of the oxygen partial pressure, during the growth of thin films, using UV PL and CL techniques were studied [150]. The intensity of UV emission increased by more than two orders of magnitude, as a result of the annealing. Both defects and strain were found to play important role on the UV emission.

The mechanism of ultraviolet and green emission of ZnO films, deposited over sapphire substrate, was discussed [151]. It was suggested that UV emission was due to the transition from near band edge to valence band and green emission was caused by the transition from deep donor level [due to oxygen vacancies] to valence band.

CL properties of ZnO nano particles at 80 K and 300 K [152] were also reported. It was seen that the near band edge emission significantly increased after heat treatment in H_2. The appearance of strong green emission at 2.4 eV following thermal annealing in Ar gas atmospheres was assumed to be due to formation of bulk oxygen vacancy defects.

Effects of O and Zn implantations in ZnO films on the deep level emission were investigated [153]. It was concluded that, vacancy of zinc (V_{Zn}) was responsible for the observed deep level emission. A novel emission at 3.08 eV appeared at 77K in the O- implanted samples, which was tentatively identified as due to O- antisite.

Heo et al, in an interesting report, discussed the origin of controversial blue-green emission in ZnO [154]. PL and Hall measurements were done and a correlation was established between the deep level emission and carrier density. It was suggested that the green emission was related to the transition between donor - deep acceptor (Vacancy of zinc).

The effects of oxygen partial pressure on the structural and luminescent properties of ZnO films, prepared using DC reactive magnetron sputtering technique, were studied [155]. Films were showing a strong UV emission and a defect related deep level emission in the visible region. The UV emission originated from free excitonic emission. It was seen that, films deposited at higher oxygen pressure showed weaker emission intensities, which might be attributed to the decrease in oxygen vacancies and zinc interstitials related defects.

Effects of CO_2 laser irradiation on the luminescent properties of sputtered ZnO thin films were studied [156]. The irradiated samples exhibited strong visible

luminescence compared to that of the as prepared samples. Optical band edge was also shifted to higher wavelength.

PL studies of ZnO thin films on Si substrate, with and without ITO buffer layers, were studied [157]. Intensity of PL emission in the UV region was found to be strongly dependent on the ITO buffer layer. Thermal annealing could further increase its intensity.

In a very recent paper, Zhang et al discussed the effect of MgO doping on the luminescent properties of ZnO pellets [158]. The emission spectra consisted of two wide bands in green and orange region and the intensity ratio of first emission to the second one decreased when sintering temperature increased. The emission band in the green region was similar to the emission spectrum of ZnO, while that in orange region was related to the long – lasting phosphorescence.

1.5 Role of Hydrogen

In all the semiconductors, interstitial hydrogen was found, theoretically and experimentally, to act as an amphoteric impurity: in p-type material, hydrogen acted as H+ (a donor), and in n-type materials as H- (an acceptor), always counteracting the prevailing conductivity of the material. This amphoteric behavior precluded hydrogen from acting as a dopant, i.e., from being a source of conductivity. But in ZnO, however, it was found that hydrogen occurred exclusively in the positive charge state, always acting as a donor. Experimental indications of hydrogen's behavior as a donor in ZnO, were reported in the 1950s, where an increase in conductivity was observed for ZnO crystals exposed to hydrogen at temperature above 200°C [159].

Thomas and Lander also observed an increase conductivity of ZnO crystals after having the hydrogen diffusion into the material [160]. Quantity of hydrogen diffused was found to be dependent on electrons already in the crystal. It was suggested that hydroxyl group was formed from the hydrogen and oxide ions and a

donor level having ionization energy of 0.04 eV was obtained corresponding to hydrogen.

Those results were, however, remaining unnoticed for about 30 years and now there is an increase in research activity on 'hydrogen in semiconductors'. An et al reported another experimental evidence for the increase in conductivity of ZnO thin films due to the incorporation of hydrogen [161]. Using real time spectroscopic ellipsometry (SE), the interfacial interactions that occur when i- and p-type hydrogenated amorphous silicon-carbon alloys (a-Si$_{1-x}$C$_x$:H), deposited from plasmas containing hydride on to ZnO, was studied. The SE spectra collected during the nucleation of a-Si$_{1-x}$C$_x$:H revealed widening of the near-interface optical gap of ZnO by ~0.1 eV . This effect was attributed to the penetration of atomic H from the plasma. The SE data, along with secondary ion mass spectrometry, revealed that the H diffuses into ZnO to depths ~200 Å. It was suggested that H incorporation in ZnO created point defects like Zn interstitials and O vacancies, which might lead to a shift in the near-interface Fermi level to higher position so as to reach the conduction band of ZnO. There is an estimated enhancement in the electron concentration by ~10^{20} cm^{-3}.

Kohiki et al reported an increase in conductivity of ZnO by introducing hydrogen through ion implantation with protons followed by annealing at 200°C [162].

Sekiguchi et al reported the effect of hydrogenation on the luminescence of ZnO crystals and found that hydrogen treatment strongly reduced the green emission, through the passivation of levels of green emission [163]. It was also seen that, the band edge emission intensity increased considerably after the hydrogen treatment. Another important observation from this study was that, the band edge emission was showing strong temperature dependence after hydrogenation of ZnO samples.

Role of hydrogen on the conductivity of ZnO thin films was discussed with H$_2$ – post treatment using photochemical vapor deposition [164]. Resistivity of the

film decreased from $1x10^{-2}$ to $2x10^{-3}$ ohm cm, after the H_2 treatment. Two possible mechanisms were discussed in this paper to explain this result. First, hydrogen atoms assisted desorption of oxygen from the film and second, it etched the small grains growing among large ones on the surface, resulting in a rough surface.

Van de Walle, based on the first-principles density functional calculations, showed that hydrogen is an excellent candidate for doping in ZnO and showed that H+ is extremely stable and exclusively acted as donors [165, 166]. Hydrogen formed a very strong bond with oxygen, providing a powerful driving force for its incorporation in ZnO and the resulting O-H bonding unit could, in fact, be regarded as a new type of dopant atom, which behaved much like fluorine. Also, the O-H bond reduced the formation energy of H+ to a very low value, which in turn increased the solubility of H in ZnO.

Cox et al experimentally proved that interstitial protium could act as a shallow donor in ZnO, by direct spectroscopic observation of its muonium counterpart [167]. Effects of intentionally doped hydrogen on the electrical properties of ZnO thin films grown using MOCVD technique were studied and free electron concentration increased by nearly a factor of 3 [168]. SIMS analysis, performed on the ZnO films exposed to hydrogen plasma, showed a rapid diffusion of hydrogen in the film. Another interesting aspect observed was that, the plasma exposure did not reveal any measurable oxygen vacancies as observed by Baik et al. Moreover plasma was not responsible for any noticeable etching phenomena.

Kilic and Zunger discussed the n-type doping of certain oxides by hydrogen using 'first-principle total energy calculations' [169]. It was suggested that, hydrogen pinning level existed in oxides at about 3.0±0.4 eV below vacuum level and oxides whose conduction band minimum lie below this level (electron affinity>3.0±0.4 eV), would become conductive, once hydrogen got incorporated into the lattice. But

materials whose conduction band minimum was above this level (electron affinity < 3.0±0.4 eV) remained non conductive, since hydrogen formed a deep donor level.

Infrared (IR) absorption spectroscopy was used for the first time to identify the defect levels related to the hydrogen in ZnO [170]. Three absorption lines were obtained for the two defect levels and one was associated with hydrogen interstitials at bond center site (3611.3 cm^{-1}) and the other is assigned to O-H bond roughly aligned with the c-axis (3349.6 and 3312.2 cm^{-1}).

IR absorption spectroscopy was used by McCluskey et al also to investigate the vibrational modes in ZnO, annealed in hydrogen gas [171]. An O-H stretch mode was observed at 3326.3 cm^{-1} at 8K and they suggested that hydrogen annealing might be a practical method for controlled n-type doping in ZnO materials.

Thermal stability of ion-implanted hydrogen in ZnO single crystal was investigated with the help of SIMS technique [172]. It was seen that the temperature at which implanted hydrogen evolved from the ZnO was considerably lower than that for GaN. PL studies showed that the intensity of near-band-edge emission was considerably reduced in implanted samples, probably due to the nonradiative recombination centers associated with ion-beam induced defects.

Polyakov et al investigated the effect of hydrogen plasma treatment of ZnO crystals and found that shallow donor concentration increased to about the same level as the concentration of hydrogen in the material [173]. Also, hydrogen introduction in the material increased the concentration of existing electron and hole traps. Donor activation energy of 37 meV was attributed to either hydrogen donors or hydrogen donor complexes with native defects.

Shi et al discussed the hidden hydrogen in ZnO wafers on the basis of annealing in different ambient, with the help of IR spectroscopy [174]. An O-H stretching mode at 3326.3 cm^{-1}, previously assigned to a shallow donor level introduced by hydrogen, was absent in as grown sample and it appeared when

annealed at 400ºC without any external source of H.This revealed the fact that substantial concentration of H could be present in as grown ZnO. It was suggested that, interstitial H_2 molecule could be a possible candidate for hidden defect and at higher temperature, H_2 molecule dissociated, giving rise to O-H stretching line at 3326.3 cm^{-1}.

Attenuated Total Reflection Fourier Transform infrared spectroscopy was used to monitor the increase of free carriers in ZnO thin films during the exposure to H from H_2 plasma, proving that the carrier concentration dramatically increased due to room temperature exposure in H_2 plasma [175]. It was also seen that, on exposing it to O2 plasma, density of carriers could be reduced.

Vapor phase grown ZnO samples, treated with hydrogen and/or deuterium plasma, were analysed using photoconductivity (PC) and IR spectroscopy [176]. Three bands at 180, 240 and 310 cm^{-1} were observed in the photoconductivity spectra of hydrogenated ZnO. No PC signal was detected from the virgin samples. These bands were assigned to electronic transitions of three independent hydrogen related shallow donors. Two electronic transitions at 1430 and 1480 cm^{-1} were observed in IR absorption spectra and these were assigned to hydrogen related defects.

Jokela and McClusky discussed the structure and stability of O-H complexes on the basis of high pressure and polarized IR spectroscopy. They could find out that hydrogen occupied an antibonding location, with an O-H bond, oriented at an angle of 110º to the c-axis [177]. By correlating the IR absorbance strength with free electron concentration, it was concluded that the O-H complexes were shallow donors.

In a very recent report, Wang et al discussed the hydrogen-induced 'metallicity' on the ZnO surface [178]. It was found that, the exposure of the mixed-terminated ZnO (1010) surface to atomic hydrogen at room temperature, resulted in a drastic decrease of resistivity and the insulator surface became metallic.

Electron transport properties of high quality MBE grown ZnO thin films were discussed recently [179]. From temperature dependent Hall (TDH) effect

40

measurements, the mobility was found to be strongly depending on the dislocation density [at low temperature region] and polar optical phonon scattering [at high temperature region]. It was concluded from TDH measurements that the n-type conduction in ZnO was due to the hydrogen present in the film and the donor activation energy of ~40 meV was assigned to the shallow level due to the hydrogen.

1.6 Photoconductivity Studies

For the last two decades, it was well known that the photo response of n-type metal oxide semiconductors, such as titanium and zinc oxides showed slow conduction decay process, which was controlled by surface effects such as gas absorption and desorption. In the dark, oxygen gas adsorbed on the oxide surface, as a negatively charged ion by capturing free electrons of the n-type oxide semiconductors, created a depletion layer, with low conductivity near the surface. When this was illuminated, holes, which were produced by light absorption near the surface, migrated to the surface due to the band bending and discharged the negatively charged [adsorbed] oxygen ions. Electrons produced at the same time, by the light, destructed the depletion layer, increasing the conductivity. Thus the photo response in ZnO included adsorption and photo desorption of oxygen on the surface. This is in addition to the very rapid changes in conductivity due to the photo generated hole-electron pairs. Consequently the decay of photoconduction was strongly dependent on the ambient gas conditions, being slow in vacuum or an inert gas atmosphere [such as nitrogen] and fast in air. Some important works on photoconductivity of ZnO materials are discussed in the following paragraph.

Melnick studied the origin of photoconductivity due to desorption of chemically adsorbed oxygen atoms from the surfaces of the ZnO sample [180]. Morrison also discussed the mechanism of oxygen adsorption and its effect on the conductivity of porous ZnO samples [181]. It was explained that, light of wavelength near the fundamental absorption edge created electron-hole pairs from which the hole

was captured by the oxygen, converting the oxygen to physically adsorbed. These physically adsorbed oxygen atoms got easily desorbed and the electron caused an increase in conductivity.

Takahashi et al reported the effect of photoconductivity of ultra thin ZnO films and it was seen that dark conductivity decreased with decrease in film thickness [182]. Photoconductivity was measured in different ambient and found that rate of photoresponse in air or dry oxygen was faster than that in dry nitrogen. Also, the photoresponse in air was faster than in dry oxygen and this effect was attributed to the role of water vapor in air.

The time constant of photo response of [r.f. sputtered] polycrystalline ZnO thin films were studied [183]. The time constant got reduced due to doping the surface layer with nitrogen. The faster photo response was attributed to the elimination of the active layer by incorporated nitrogen. It was observed that, the photo response of the films originated from the changes in barrier heights and when the films were irradiated with UV light, barrier heights of grain boundaries changed. The change in barrier height was assumed to be due to photo desorption of the chemisorbed oxygen on the grain boundaries.

High-quality zinc oxide (ZnO) films were epitaxially grown on R-plane sapphire substrates using MOCVD at temperatures in the range of 350°C to 600°C [184]. In-situ nitrogen compensation doping was performed using NH_3. Microstructural and optical properties of the films, along with the doping effects, were studied in detail. The metal-semiconductor-metal ultraviolet sensitive photo detectors were fabricated on N-doped epitaxial ZnO films. The detector showed fast photo response, with a rise time of 1 ms and a fall time of 1.5 ms. Low-frequency photo response, of the order of 400 A/W at 5 V bias, was also obtained.

Sharma et al studied the ultraviolet photo response of porous ZnO thin films [185]. It was seen that porous ZnO films exhibited a fast ultraviolet photo response with

minimal degradation and the origin of fast response was attributed to oxygen neutrals at the grain boundaries.

Photo response characteristics of polycrystalline ZnO, prepared using the unbalance magnetron sputtering technique, had been analyzed [186]. It was observed that ZnO films with (100) and (101) orientation possessing a small grain size, exhibited a slow response. But porous ZnO films with mixed orientation along (100), (002) and (101) and a larger grain size, exhibited a fast response. Magnitude of the photocurrent and the rise time were found to be decreasing considerably with increasing number of trap levels.

It was also observed that a larger photo response was obtained for the randomly oriented sol-gel ZnO films and it was attributed to the change in barrier height at the grain boundaries due to the embedded oxygen [187]. Faster photo response decay was found in films with smaller crystallite size with porous microstructure.

Using this material, very recently, Xu et al developed photoconductive ultraviolet detector with planar interdigital electrodes having fast response [188]. Linear I-V characteristic curve was obtained at dark and also on illumination using light at 365 nm.

1.7 Ohmic contacts

In a very brief report, annealing effect of different transparent ohmic contacts to the MBE grown epitaxial ZnO thin films over sapphire substrate were discussed [189]. ITO, RuO_2 and TiW ohmic contacts were achieved by r.f. sputtering and annealing treatment. Contact resistances of these electrodes were found to be very low ($\sim 10^{-4}$ ohm) and ITO was the best transparent ohmic contact.

For n-ZnO, specific contact resistances of 7×10^{-3} – 4.3×10^{-5} ohm cm was reported for Ti/ Au on Al-doped epitaxial layers [190-192]

High quality platinum ohmic contacts on unintentionally doped n-type ZnO epitaxial layers grown by pulsed laser deposition on (0 0 0 1) sapphire substrates were reported [193]. The contacts were formed by using Ga focused ion beam and Pt direct-write metal deposition. Contact resistance measurements by the transmission line method, indicated values as low as $3 \times 10^{-4} \ \Omega \ cm^2$ without any annealing. An optimum Ga surface-modification dosage window was determined, within which, the current transport mechanism of these contacts was mainly by tunneling through the Ga-ZnO interface layer.   .

The specific contact resistivity and chemical intermixing of indium-tin-oxide (ITO) / Ti / Au ohmic contacts on n-type bulk ZnO substrates were reported as a function of annealing temperature up to 450°C [194]. A minimum contact resistivity of 4.6×10^{-6} ohm cm^2 was obtained at 50°C and the value remained $<10^{-5}$ ohm cm^2 for all temperatures up to 450°C, suggesting that the Ti is an effective diffusion barrier, which prevented formation of Au–In solid solutions. Optical microscopy of the contacts showed roughening of the morphology after annealing at 450°C. Indium out diffusion to the surface of the contact stack was significant at 350°C, and Zn out diffusion is evident at 450°C. Both the In and underlying Ti became oxidized after these higher temperature treatments.

A review on ohmic and Schottky contacts for n- and p-type ZnO is given in a recent paper[195]. It is relatively straightforward to form high-quality ohmic contacts to n-type ZnO with contacts resistivity in the range $10^{-6} \ \Omega \ cm^2$ even for unannealed contacts. But recent work showed good results (10^{-5}–$10^{-6} \ \Omega \ cm^2$) for Au or Ni/Au annealed at 300–600 °C. Schottky contacts to both n- and p-type ZnO were much lower in number even though one could expect much more, considering the metal work function and the electron affinity of ZnO. This suggested that surface states were more important in determining the effective barrier height. The Schottky contacts also

showed poor thermal stability. For transparent transistors based on ZnO this suggested that oxide gates were more suitable than metal gates.

The role of UV ozone cleaning on the characteristics of Pt contacts on n-type ($n \sim 10^{17}$ cm^{-3}) bulk single-crystal zinc oxide was reported [196]. The contacts were ohmic for samples that were not exposed to ozone prior to Pt deposition, but exhibited excellent rectifying behavior with ozone cleaning. The barrier height of these contacts obtained from current–voltage measurements was 0.70 ± 0.04 eV at 25°C with an ideality factor of 1.49 and a saturation current density of 6.17×10^{-6} A cm^{-2}. A significant decrease in surface carbon concentration was observed after the ozone cleaning (29.5 at.% down to 5.8 at.%, as determined from Auger electron spectroscopy). The measured barrier height for Pt on ZnO was similar to those reported for both Au and Ag rectifying contacts on this material. By sharp contrast, sputter-deposited W contacts were ohmic, independent of the use of ozone cleaning and became rectifying after annealing at 700°C. Probably this might have repaired sputter-induced damages. The barrier height was in the range, 0.45 –0.49 eV, with the ozone cleaning, producing values at the high end of this range.

1.8 Doping Studies

Doping of ZnO not only improved the electrical properties but also enhanced its stability. Generally group III elements like In, Ga, Al and also F were used for doping to increase the electrical conductivity. Detailed literature survey of In and F – doped ZnO thin films would be included in the following chapters. Literature review reported in this chapter is mainly on Al and Ga -doping.

The stability of Al-doped ZnO thin films, deposited using sputtering, was studied and no significant changes were seen on the properties after use in air at room temperature for one year [197]. It was also seen that the stability could be attained for

use in vacuum, inert and nitrogen gases at temperatures as high as 400ºC with Al_2O_3 content above 1.0 at %.

Effects of different deposition conditions on the properties of Al-doped ZnO thin films, prepared using dual target reactive magnetron sputtering technique, were reported [198]. Under optimized conditions, 0.3 mm thick films with 85% thermal IR reflectance were obtained and these films were having a resistivity of $5x10^{-4}$ ohm cm.

Sernelius et al reported the band gap tailoring of ZnO by means of Al doping and band gap widening could be analysed with an effective mass model [199].

The dependence of electrical and optical properties on the temperature of substrate and target had been studied for Al- and Si-doped ZnO films, prepared using r.f. sputtering [200]. The lowest resistivity was obtained for substrate temperature in the range 180 – 220ºC, due to the improvement in crystallinity. Excessive cooling of the target affected the resistivity of the film adversely.

Al-doped ZnO films, for the application as transparent electrode material, were prepared using normal pressure CVD method [201]. Fused quartz substrates were used as substrate and optical transmittance of ~80% was obtained for the films. Band gap of the film could be varied from 3.3 to 3.6 eV by increasing Al-content in the film.

Pushparajah et al studied the physical properties of Li – doped ZnO films, prepared using spray pyrolysis technique [202]. Best film was obtained at substrate temperature of 673 K with resistivity 6.3x10-3 ohm cm. On Li-doping, the sample became amorphous and resistivity also increased.

Thin films of ZnO: Al were deposited using PLD technique, having a resistivity of $1.4x10^{-4}$ ohm cm and an average transmittanceof ~90% [203]. It was seen that, with the increase in substrate temperature, resistivitty of the sample also increased.

Myong et al deposited extremely transparent and conductive ZnO: Al films using photo assisted MOCVD technique with $AlCl_3$. $6H_2O$ as dopant source [204].

Optical transmittance of films [resistivity of 6.22×10^{-4} ohm cm] was ~91 % in visible region.

Optical and electrical properties of Al-doped ZnO thin films, prepared using sol-gel technique were reported [205]. Both ZnO and ZnO: Al films were preferentially oriented along c-axis and showing an optical transmittance of ~90 %. Electrical resistivity was decreasing with increase in the film thickness.

Minami et al reported the origin of electrical property distribution of the substrate surface in Al-doped ZnO films, prepared using magnetron sputtering [206]. It was observed that the ZnO: Al films prepared by DC sputtering, exhibited large increase of resistivity at locations on the substrate, corresponding to the target erosion area. Interestingly the resistivity in these regions was higher than that of the films prepared using rf sputtering.

In an interesting paper, influence of different dopant elements on the structural and electrical properties of spray pyrolysed ZnO thin films was investigated [207]. It was seen that, as the dopant concentration increased, the film growth became non-oriented with poor crystallinity. SEM and TEM micrographs showed that amount of dopant influenced the microstructure of the film to a great extent.

Chen et al reported the structural, electrical and optical properties of ZnO: Al films grown by sputtering [208]. Peak position of (002) plane was shifted to higher angle, as the Al concentration increased. Electrical resistivity decreased initially at lower doping concentration, but again increased at higher Al concentration, probably due to the higher damage in the crystal lattice.

Holmelund et al reported properties of pure and Sn- doped ZnO films [PLD deposited] [209]. Electrical resistivity increased while the transmittance, in the visible region, decreased with increasing Sn concentration.

Low resistivity transparent conducting Al-doped ZnO films were prepared using PLD technique and the effects of variation of Al content in the film was studied

[210]. The lowest resistivity of 8.54×10^{-5} ohm cm and an average transmittance of >88% were obtained for the best film.

Effects of different dopant elements like In, Al and Sn, on the properties of ZnO thin films were investigated [211]. For each dopant, films doped with 1 at % Al, 1 at % In and 2 at % Sn concentration exhibited a stronger c-axis orientation. Effects of the difference in ionic radius of each dopant on the properties were also discussed.

Bougrine et al studied the effect of Sn-doping on the structural, optical and CL properties of ZnO films, prepared using spray pyrolysis technique [212]. Doped samples were showing better crystallinity than the undoped films, probably due to the healing of crystal network. All films were highly transparent in the visible region.

Olvera and Maldonado reported the deposition of high quality ZnO: Ga films using chemical spray pyrolysis technique [213]. Two different precursors were used for the deposition. Lowest resistivity obtained was 4.5×10^{-3} ohm cm and the average optical transmittance in the visible region was about 85 %.

CL of Al doped ZnO thin films was also reported [214]. At room temperature, both doped and undoped films showed a common near-ultra violet band gap peak, while undoped film had an intense blue –green emission (520 nm) and a red emission (672 m). Incorporation of Al rsulted in the shifting of the blue-green emission to 480 nm.

Effects of precursor pulse on the properties of Al-doped ZnO thin films, grown using Atomic Layer Deposition technique, were reported [215]. The preferential orientation was changed from (002) to (101) on Al-doping and overall transmittance was around 80 % in the visible region. Resistivity of the film decreased when the TMA/DEZ pulse ratio increased.

Rapid thermal annealing was performed to achieve high electron concentration and mobility of Al – doped ZnO films, prepared using r.f. magnetron sputtering [216]. PL and Hall measurements showed that both electrical and optical properties of ZnO layers significantly improved when annealing temperature

48

increased to 900ºC. Both, as grown and annealed samples, were showing excellent crystallinity. When annealed at 900ºC, electron concentration of 1.83×10^{20} cm^{-3} and mobility of 65.6 cm^2/Vs were obtained.

Sn-doped ZnO films, prepared using SILAR technique, were used as NO$_2$ gas sensor and the results were reported [217]. Experimental results showed that the sensitivity of ZnO increased on Sn doping.

Bougrene et al have deposited ZnO: Sn films using spray pyrolysis technique on glass substrates and physicochemical properties of these films were studied [218]. Crystallinity and optical transmittance improved on doping. Lowest resistivity obtained was 5×10^{-2} ohm cm.

Influence of hydrogen incorporation in sol-gel derived aluminium doped ZnO thin films were studied [219]. The grain size, crystallinity and conductivity increased after the incorporation of hydrogen. FTIR studies were used to identify the donors-action of hydrogen in ZnO.

Influence of substrate temperature and post deposition treatment on the properties of ZnO: Al thin films, prepared using PLD technique, were reported [220]. The experimental results showed that when deposited at 240C, resistivity of the film was 6.1×10^{-4} ohm cm and it could be further reduced to 4.7×10^{-4} ohm cm, by post deposition annealing at 673 k, for 2 hours in argon atmosphere. As the annealing temperature increased, the optical band gap also increased.

PL studies and SEM imaging were performed on ZnO: Al films deposited using CBD technique [221]. Rapid thermal annealing improved the crystalline quality of the film; UV emission intensity increased, while visible emission was suppressed.

Al-doped zinc oxide and undoped zinc oxide films, for the use as a transparent conductor and buffer layer of solar cell, were prepared using RF magnetron sputtering [222]. Thin films with low resistivity were prepared by using Al-doped ZnO target, while films with high resistivity were obtained by introducing oxygen atmosphere during the deposition. The ZnO: Al thin film having the lowest

resistivity, was prepared with an RF power of 180 W, a sputtering pressure of 10 mTorr; film having thickness of 5000 Å exhibited a resistivity of 1.4×10^{-4} Ω·cm and transmittance of 95% in the visible range. On the other hand, the undoped film deposited using reactive sputtering under in an atmosphere of 10% oxygen content, exhibited the highest resistivity of 6×10^{14} Ω cm.

Electrical conductivity of sol-gel deposited ZnO: Al films was found to be closely related to the parameters of post deposition heat treatment, such as duration, temperature and atmosphere [223]. Grain size reduced after heating in a mixture of H_2 and N_2 atmosphere. Optical transmittance was unaffected by the post annealing treatment.

A dielectric model, comprising of band gap transitions and free electron excitations, was successfully applied to simulated transmittance spectra of ZnO films doped with different Al concentrations [224]. Useful parameters obtained from the fit were electron density, mobility within grains, film thickness, band gap and refractive index.

1.9 P-type ZnO

For the development of optoelectronic devices with ZnO, it is necessary to have high quality materials of both n-type and p-type. However, crystalline ZnO is naturally n-type and is very difficult to dope to make p-type. There have been reports of doping ZnO with group III elements to the point of being a metallic conductor. However, in spite of a number of reports of p-type measurements in ZnO films, there is still no reliable method of producing good quality p-type ZnO consistently.

Despite years of intensive investigations, the origin of this asymmetry in doping is still controversial. Zhang et al theoretically predicted that, in ZnO, the zinc interstitials, a double donor, had low formation energy in both zinc rich and oxygen rich growth conditions [225]. The native defects that could compensate Zn_i [such as oxygen interstitials (O_i) or zinc vacancies (V_{Zn})], had high formation enthalpies in zinc

50

rich conditions. Therefore electrons from Zn_i were the dominant carriers under zinc rich condition. ZnO could not be intrinsically doped to form p-type via shallow native acceptors [O_i and V_{Zn}] in an equilibrium process because those native acceptors could be compensated by defects such as Zn_i , oxygen vacancies (V_O) and Zinc-Oxygen antisite (Zn_O), which had low formation enthalpies under both zinc rich and oxygen rich conditions.

Although the first theoretical report on *p* doping of ZnO came in 1983, serious efforts started to develop p-ZnO in 1996. Sato et al reported nitrogen doping in ZnO using reactive evaporation technique [226]. Nitrogen contained in the film seemed to be acting as acceptor after annealing and carrier density was observed to be decreasing as the N_2 mixing ratio increased. But as the N_2 mixing became larger, ZnO started to be converted as zinc nitrate.

First report on the fabrication of p-ZnO came in 1997 [227]. Minegishi et al has developed p-ZnO using Chemical Vapor Deposition (CVD) technique in which NH_3 was used as the source of nitrogen. These films were showing resistivity of 100-ohm cm. and p-type conduction was obtained when NH_3 and Zn added simultaneously.

Yamamoto and Yoshida theoretically investigated electronic structure of both n and p type ZnO and suggested that codoping of nitrogen and reactive donors like In, Al or Ga would not only enhance the incorporation of nitrogen but also introduce shallow N-acceptor level. This was really the first suggestion put forward for the realization of p-ZnO materials [228].

Joseph et al published first experimental report on the p-ZnO using codoping method in the same year, where they used Ga and N for doping [229]. Pulsed Laser Deposition technique was used for the film preparation, in which NO_2 gas was passed through an electron cyclotron resonance (ECR) plasma source. Resistivity of about 4-ohm cm and mobility of 0.05 cm^2/Vs were obtained for the best film. However the carrier concentration was found to be pretty large for all the p-type films. Another

report on p-ZnO was using Arsenic as the dopant and PLD technique was employed for the film deposition [230]. Best film had a resistivity of 10 ohm cm and mobility of 1 cm^2/Vs, while carrier concentration was low [~ 10^{17} cm^{-3}].

A diode was fabricated with p-ZnO over n-type ZnO substrate using laser doping in which zinc sulphide, used as doping source, deposited over ZnO wafer and subjected to excimer laser pulses [231]. Diode nature was confirmed with I-V characteristics. The electro luminescence spectrum showed a white-violet emission at 110 K.

A theoretical paper was published on nitrogen compensation mechanism in ZnO using real-space multigrid electronic structure calculation within the Local Density-functional Approximation (LDA) [232]. According to this calculation, O-vacancies were the main compensating donors at low N doping level, while at higher doping level, N-acceptors were compensated via the formation of defect complexes with Zn antisites (N-acceptor-zinc-antisite complexes).

Another interesting report on the mechanism of N doping through the theoretical calculations, showed that the use of dilute NO or NO_2 gas, instead of N_2 and N_2O, would resolve the long standing problem of achieving p-type ZnO [233]. They suggested that, when NO and NO_2 were used for doping, these molecules could supply single-N atoms, whereas one had to break N-N bonds, to get single N-defects when N_2 and N_2O are used. It was also seen that N at O site (N_O) contributed shallow acceptor level, while N_2 at O site $(N_2)_O$ is a double shallow donor.

P-type ZnO films [with carrier density 3-6x10^{18} cm^{-3}, resistivity 2-5 Ω cm and Hall Mobility 0.1-0.4 cm^2/Vs] were grown using PLD technique using pure metal Zn target and N_2O plasma [234]. P-type conduction was achieved by optimizing the microwave input power and deposition pressure.

Realization of homo junction was reported with Ga-N codoping of ZnO using Radical Source Molecular Beam Epitaxy [235]. However Hall measurements was

showing n-type conductivity for both codoped and undoped samples. It was also shown that the presence of Ga enhanced the incorporation of N in the film.

Look et al reported another result on p-type conversion of MBE grown ZnO using nitrogen the doping [236]. Li-diffused semi insulating ZnO substrate was used and best film had resistivity of 40 Ω cm and mobility 2 cm^2/Vs. Carrier concentration was about $9x10^{16}$ cm^{-3}.

Park et al theoretically investigated the difficulty of p-type doping using first principles total energy calculations [237]. In this study, they considered the effect of group-I and -V elements and found that substitutional group-I elements were shallow acceptors, while substitutional group-V elements were deep acceptors. Apart from self-compensation effects, the most likely cause for difficulty in doping was the formation of interstitials for group-I elements and antisites for group-V elements. According to this study, N was found to be relatively better candidate for p-type ZnO.

Realization of p-type ZnO by adjusting the oxygen partial pressure in the sputtering plasma was also reported by Xiong et al [238]. The p-n junction was formed by depositing two sequential layers, under oxygen poor (n-type) and oxygen rich (p-type) conditions. Hall effect measurements showed p-type ZnO had resistivity of 3 Ω cm with carrier concentration of $9x10^{17}$ cm^{-3}. The mobility was varying from 2 to 130 cm^2/Vs.

Li et al discussed the deposition of p-type ZnO using MOCVD technique, in which nitric oxide (NO) gas was used for nitrogen doping [239]. P-type conductivity was obtained when doping concentration exceeded 2 at %. Another interesting observation was that, Zn-rich condition favored the incorporation of nitrogen in the film. For the best film, resistivity was 20 Ω cm, mobility was 0.1 cm^2/Vs while carrier concentration was $10x10^{18}$ cm^{-3}.

Ryu et al [240] reported fabrication of homostructural ZnO p-n junction in 2003. The junction was realized with arsenic (As) doping and technique used for the

film deposition was hybrid beam deposition (HBD). In this experiment, initially, undoped ZnO was grown over SiC substrates using PLD of ZnO target. Then p-ZnO was grown using HBD. The turn-on-voltage obtained was in the range of 6-8 V and diode ideality factor was 3 to 5.

In one of the reports, Huang et al described the deposition of p-ZnO using dc reactive sputtering with NH_3 as the dopant source gas [241]. It was seen that, as the deposition temperature was below 400°C, films were n-type and with increase in the temperature, ZnO became p-type. Further increase in temperature (450°C), resulted in very low resistive films (0.97 Ω cm), having carrier concentration of $8x10^{18}$ cm^{-3} and a mobility of 0.8 cm^2/Vs.

Codoping of nitrogen and oxygen yielded p-type conduction in ZnO thin films prepared using r.f. sputtering technique [242]. For the doping, high purity nitrogen and oxygen gases were used. It was observed that, as the oxygen partial pressure increased up to 60%, hole mobility became 60 cm^2/Vs. However, further increase in the oxygen partial pressure, decreased hole mobility. Best film showed a resistivity of 11.8 Ω cm and carrier concentration of $9x10^{16}$ cm^{-3}.

Li et al in another paper, reported the fabrication of p-type ZnO films, using MOCVD technique [243]. In this work also, they discussed the effect of NO concentration on the type of conductivity. Concentration of N was determined using SIMS and AES spectroscopy. It was seen that the N-concentration increased along with an increase in the Zn to O ratio.

The electrical activity of nitrogen as an acceptor was investigated in two ways [244]. It was observed that when nitrogen was introduced during Metalorganic Vapor Phase Epitaxy (MOVPE) growth, no type conversion was observed while diffusion of N in an oxidizing atmosphere led to surface p-type behavior with a hole concentration 10^{17} cm^{-3}.

Kim et al reported the fabrication of p-type ZnO, using phosphorous doping with P_2O_5 as the dopant source, in ref sputtering system [245]. Type conversion was observed by a thermal annealing process at a temperature above 800°C under N_2 ambient. The electrical properties of the p-type ZnO indicated that the hole concentration of 1.0×10^{17}-$1. \times 10^{19}$ cm^{-3}, a mobility of 0.53-3.51 cm2/Vs, and a low resistivity of 0.59 – 4.4 Ω cm.

Another technique used was diffusion of phosphorous into ZnO using phosphorous doping where Zn_3P_2 was used as the dopant source [246]. Initially ZnO films were grown using r.f. sputtering over InP substrate and then doping was done using 'closed ampoule technique'. In order to verify the formation of p-ZnO, a p-n junction was fabricated and turn-on-voltage obtained was ~1.5 V.

PL studies on nitrogen doped ZnO films were carried out and an emission corresponding to acceptor level at ~0.4 eV was obtained; this was believed to be due to the presence of nitrogen [247]. In this work, films were prepared using filtered cathodic vacuum arc technique (FCVA) and these were oriented along (001) plane. Raman studies also proved the presence of nitrogen, since the doped films exhibited nitrogen related local vibrational modes.

Arsenic (As) doped ZnO films also showed p-type conduction when prepared using hybrid beam deposition technique in which (Zn, O) plasma was created using laser ablation. Arsenic molecular beam was supplied with an effusion cell [248]. Temperature dependent Hall effect measurements and PL studies revealed two activation energies corresponding to As acceptor in the range from 110 to 170 meV, above the valence band. It was also concluded that As behaved as hydrogen-like acceptor.

Look and Claflin published a more general report on p-type doping and devices based on ZnO thin films [249]. In this work the Authors had done a detailed investigation on p doping with different elements like phosphorous, nitrogen, arsenic

were done. It was found that nitrogen might be forming shallower acceptor level compared to the other elements. Effects of group-I elements (Li, Na and K) were also discussed. It was predicted that these elements, when substituted on Zn site, might give very shallow acceptor levels. But the probability of forming interstitials (Li_I) was more in ZnO when doped with group-I elements, which was assumed to be donor states. Earlier attempts to fabricate LED were also mentioned in this report.

In another interesting report, Heo et al presented the results of phosphorous doping in (Zn, Mg) O, films prepared using PLD technique [250]. A diode structure, [metal/insulator/p-doped (Zn, Mg) O] was fabricated and C-V measurements were taken. This structure exhibited a polarity consistent with the P-doped (Zn, Mg) O layer. But Hall measurements yielded an indeterminate Hall sign due to small carrier mobility (0.01-0.001 cm^2/Vs). A junction was also fabricated with n-ZnO and P: (Zn, Mg) O and turn-on- voltage was nearly 1 V while the reverse breakdown voltage was in the order of 4.5 V.

Bian et al [251] reported the first result on the deposition of p-ZnO using Ultrasonic Spray Pyrolysis (USP) technique in early 2004. Codoping of N and In was employed in this work. XPS studies identified the presence of N and In in the film. Carrier concentration of 2.44×10^{18} cm^{-3} and mobility 155 cm^2/Vs were obtained for the p-ZnO film. Resistivity was very low (1.7×10^{-2} ohm cm).

In another report, Bian et al described the fabrication of a p-n junction with n and p-type ZnO films, showing a clear rectification behavior with a turn-on-voltage of 3 V [252].

Instead of codoping, Bian et al, also employed monodoping of nitrogen and p-type conduction was realised in ZnO films [253]. A homojunction was also fabricated which exhibited a turn-on-voltage of ~3 V. The p-type ZnO exhibited a resistivity of 3×10^{-2} ohm cm, mobility of 24 cm^2/Vs and a carrier concentration of 8.59×10^{18} cm^{-3}.

First report of hole conduction using ion implantation of N+ ions appeared in the same year, published by Georgobiani et al [254}. They used ion implantation with

the help of 350 keV N+ ions followed by the annealing in oxygen radical atmosphere at high temperature (600°C) for 30 min. Annealing in oxygen atmosphere stimulated transportation of interstitial nitrogen to oxygen sites, resulting hole conduction. However these films were showing high resistivity due to the implantation induced defects. Annealing at very high temperature, [800°C], resulted the out diffusion of nitrogen from the film.

In another report, Chen et al investigated the effect of N+ ion implantation in ZnO single crystals, with different energies ranging from 50 to 380 keV and positron annihilation spectroscopy was used to analyze the defect structure of the film [255]. These films were annealed at 1200°C in nitrogen atmosphere. No p-type conduction was observed in these films and this might be probably due to the out diffusion of nitrogen at this high temperature.

Lee and Chang suggested the possibility of p-type doping using group-I elements such as Li and Na and codoping with hydrogen. It was then observed that, the formation of compensating Li or Na interstitials was severely suppressed and the acceptor solubility was greatly enhanced by forming H-acceptor complexes [256].

P-type conduction was also reported using codoping of nitrogen and aluminium in dc reactive magnetron sputtered ZnO thin films [257]. The lowest resistivity obtained at room temperature was 57.3 ohm cm with a Hall mobility of 0.43 cm^2/Vs and carrier concentration of 2.25×10^{17} cm^{-3}. SIMS analysis was performed for the depth profiling and the presence of N and Al was proved throughout the depth of the sample.

Strongly p-type ZnO was deposited using a two-step process, in which Zn_3As_2 was deposited over glass substrates at 350°C and ZnO was then sputtered on the top of Zn_3As_2 at 450°C [258]. SIMS analysis was performed to identify the presence arsenic in the film. The best film had a resistivity of 0.4 Ω cm and mobility 4 cm^2/Vs while the hole concentration was about 4×10^{18} cm^{-3}.

Results of optical studies on Ga and N implanted ZnO crystals were reported [259]. Implantation was performed using 350 keV implanter and the samples were kept at room temperature during the implantation. Ga was found to be promising for n-type doping. Post-implantation annealing at 800°C restored the optical and structural quality of the film.Even though N implantation produced acceptor levels with E_A between 163 and 196 meV clear p-type conversion was not obtained.

Limpijumnong et al put forward a theoretical model, based on first principle calculations, for large size-mismatched group-V dopants in ZnO [260]. According to this model, the dopants did not occupy the O sites as was widely perceived, but were in the Zn sites. Each formed a complex with two spontaneously induced Zn vacancies in a process that involved five-fold As (Sb) coordination. Moreover, an As_{Zn}-$2V_{Zn}$ (Sb_{Zn}-$2V_{Zn}$) complex might have low formation energy than any of the parent defects.

Lin et al reported the realization of p-type ZnO grown on Si substrate, buffered with Si_3N_4, using nitrogen ion implantation [261]. Si_3N_4 buffer layer could effectively improve the stoichiometry and reduce oxygen vacancies. The electrical properties of ZnO showed hole concentration of 5×10^{16} - 7.3×10^{17} cm^{-3}, hole mobility of 2.51 – 6.02 cm^2/Vs, and resistivity of 10 - 15 Ω cm. The p-type film showed excellent crystallinity and strong UV emission peak near 3.3 eV.

In a review, Look presented brief report on electrical and optical properties of p-type ZnO and also described the recent challenges in the development of p-ZnO [262].

Using ZnO, homojunctions were fabricated on quartz and highly conducting Si substrates by depositing Al-doped n-type ZnO layer on Al-N codoped p-type ZnO layer, through reactive magnetron sputtering [263]. The turn-on-voltage obtained was 2 V. Ohmic contacts were formed by using In/Zn metals. No luminescence was observed from this junction and it was probably due to high contact resistance of the film.

X-ray photoelectron spectroscopy was used to probe the chemical states of N in N-doped ZnO thin films prepared using MOCVD and r.f. sputtering techniques [264]. Four different types of nitrogen were observed in MOCVD-grown ZnO and two different types of N in sputtered ZnO films. The concentration of N_{2O} double donor relative to the N_O acceptor was less in the MOCVD films than in films grown by sputtering.

Vaithianathan et al reported the deposition of p-type ZnO thin films on Al_2O_3 substrate with phosphorous doping by pulsed laser deposition using Zn_3P_2 as the dopant source material [265]. Hall measurements showed that 3-mol% phosphorous doped ZnO films, thermally annealed at temperature between 600 and 800°C under O_2 atmosphere, exhibited p-type behavior [hole concentration of 5.1×10^{14} - 1.5×10^{17} cm^{-3}, a hole mobility of 2.38 – 39.3 cm^2/Vs, and a resistivity of 17 - 330 Ω cm]. Low temperature PL measurements revealed neutral acceptor bound exciton emission at 3.358 eV.

Another report on p-type ZnO dealt with nitrogen and manganese doping using MOCVD technique [266]. Hall measurements in these samples showed resistivity of 34 Ω cm, Hall mobility of 0.8 cm^2/Vs and carrier concentration of 2.3×10^{17} cm^{-3}.

Zhang et al reported p-type conduction in ZnO by N-Al codoping method using DC reactive magnetron sputtering technique, at various substrate temperatures in pure N_2O ambient [267]. When the substrate temperature increased from 300°C to 550°C, resistivity and hall mobility decreased while carrier density increased. When the substrate temperature increased beyond 550°C, the films showed n-type conduction. The optimum temperature was found to be 500°C for getting better results.

Effect of Al content on p-type conduction was studied in N-Al codoped ZnO thin films, deposited using DC reactive magnetron sputtering [268]. Best codoping effect was observed for Al concentration of 0.4 at % in Al target.

Wardle et al, using Local density functional calculations, discussed the theory of p-doping in ZnO using Li atoms [269]. Even though Li was found to be highly soluble in ZnO, it was seen that Li_{Zn}, as an acceptor, was less stable than the Li interstitial donors. Another interesting point was that, the Li_{Zn}-H bond was found to be relatively strong. If the presence of H increased the intake of Li, then such a codoping might have resulted in a super saturation of Li_{Zn} which could be activated by a similar annealing stage to that proposed for the dissociation of Li_{Zn}-Li_I pairs.

Recently ion beam assisted deposition was used to deposit p-type ZnO thin films and electrical, optical properties were studied in detail [270]. 1.8 keV O+ ion beam was used for sputtering of In doped Zn target, in the atmosphere of pure NH_3 and keeping the substrate at 200°C. Hall measurements indicated a carrier concentration of 2.2×10^{17} cm^{-3} and mobility of 3.51 cm^2/Vs. Annealing at higher temperature resulted in good transmittance of the film. Films were oriented along the (102) plane.

MOCVD technique was used for the deposition ZnO thin films showing hole conduction [271] where nitrogen was doped using NO gas in oxygen- poor ambient. P-type conversion was observed in the temperature range of 400 – 440°C. Hall measurements showed a carrier concentration of 8.36×10^{17} cm^{-3} and mobility of 4.55 cm^2/Vs. Resistivity of the film was 1.6 Ω cm. C-V measurement also confirmed the p-type conversion. SIMS analysis was performed to identify the presence of N in the film.

A novel deposition technique (repeated temperature modulation epitaxy) was reported recently for the fabrication of p-type ZnO and diode [272]. In this technique, Laser MBE with N as dopant, produced films on lattice matched $ScAlMgO_4$ (SCAM)

substrate. Single crystal ZnO and (Zn, Mg) O targets were ablated using Kref excimer laser and the substrate was heated with a semiconductor laser which enabled to heat it up to ~1000°C. Room temperature Hall mobility was 8 cm^2/Vs while the carrier concentration was $2x10^{20}$ cm^{-3}. Violet electroluminescence from a homostructural p-i-n junction was also reported in this paper. Fairly good rectification was obtained with a threshold voltage of about 7 V.

Yang et al fabricated ZnMgO/ZnO p-n junctions on bulk ZnO substrates using pulsed laser deposition through phosphorous doping [273]. Without any post deposition annealing, films were showing p-type conduction and the junction was showing a turn – on – voltage of 6.5 V at room temperature. It was also seen that the turn – on- voltage decreased with increase in the temperature. Ni/Au served as ohmic contact to p-ZnO and Ti/Au for n-ZnO.

Reproducible, high mobility, antimony (Sb) doped ZnO films were grown on silicon substrates by electron cyclotron assisted molecular beam epitaxy (ECRAMBE) technique [274]. Temperature dependent Hall measurements and low temperature PL measurements showed existence of Sb in ZnO films. At room temperature, sample exhibited a low resistivity of 0.2 Ω cm, high hole concentration of $1.7x10^{18}$ cm^{-3} and high mobility of 20 cm^2/Vs.

Chen et al reported deposition of p-ZnO film employing codoping of N and In by DC reactive sputtering technique [275]. The lowest reliable resistivity was found to be 3.12 Ω cm with a carrier concentration of $2.04x10^{18}$ cm^{-3} and a Hall mobility of 0.98 cm^2/Vs. Depth profile analysis was done using SIMS and presence of N and In in the film was confirmed. Another interesting experiment was the fabrication of two-layered structure, in which one layer was of codoped ZnO and the other was N-doped film. It was clearly seen from SIMS analysis that concentration of N decreased drastically in the N-doped film. Hence it was concluded from this study that, the presence of In might have enhanced the incorporation of N in the film.

Recently, Zeng et al reported the realization of p-ZnO with Lithium (Li) doping by DC reactive magnetron sputtering [276]. Samples were prepared at different substrates and the optimized result was realized at the substrate temperature of 550°C with a resistivity of 16.4 ohm cm, Hall mobility of 2.65 cm^2/Vs, and hole concentration of 1.44×10^{17} cm^{-3}. It was experimentally verified that these p-type samples were stable for more than one month. Junction was also fabricated using n- and p-type Zno thin films over glass substrates.

Very recently, Fons et al had studied the effect of nitrogen in MBE grown ZnO films [277]. It was believed earlier that, when plasma source was used for N-doping, nitrogen was incorporated into ZnO lattice in the form of N_2- molecule at O-site, leading to compensation rather than p-type doping, since N_2 (O) was double donor. But in this study, they observed that, N got incorporated substitutionally at O sites, where it was expected to be an acceptor [This was proved using x-ray absorption spectra studies]. It was also suggested that, the effective p-type doping of ZnO with N might be possible only for low temperature growth process.

A low resistive p-ZnO thin film was deposited using DC reactive magnetron sputtering with pure zinc metal target and Ar-N_2-O_2 mixture of sputter gas [278]. Effects of N_2/O_2 as well as the annealing treatments on structural and electrical properties were investigated. Optimized preparation conditions (N2 to O_2 ratio of 20:10 and annealing at 450°C for 3 hours) resulted in the lowest resistivity to be 8.34 ohm cm and highest hole concentration to be 7.47×10^{18} cm^{-3}.

A very interesting review on "the future of ZnO light emitters" was published in 2004 by Look et al [279]. In this review, some general problems related to the measurement of electrical properties of p-type ZnO were discussed. It was clearly stated that, sometimes, Hall effect determination of type of carriers might give fake information. Mainly two reasons were put forward in this paper. The Hall effect requires $p\mu_p^2 > n\mu_n^2$ for p-type indication. But unfortunately, the Hall voltage measured

was often very low due to the low mobility. In order to eliminate the effect of this difficulty, the Hall measurements must be averaged over current and magnetic field polarities. In addition, if the Hall voltage was obtained using the Van der Pauw method, then two switching configurations must be used, so that eight different measurements must be taken to determine single Hall voltage. A large noise spike during one of the eight measurements could affect the final result. Another problem was that the persistent photoconductivity (PPC) of ZnO. If the sample was irradiated using UV light, electrons and holes were created, and sometimes the holes could be trapped, making them unavailable for recombination after the light was turned off. Since the electron mobility was much higher than the hole mobility the non-equilibrium electrons would turn the Hall voltage negative. Even the UV content in normal room light was sometimes enough to switch a weakly p-type sample to n-type. Some of the earlier reports on the light emitting devices using ZnO were also discussed in the paper.

Liu et al discussed the realization of light emitting diode, using ZnO thin films, deposited over bulk ZnO substrate and it was seen that it emitted blue and yellow colours [280]. The turn on voltage was found to be 30 V for the junction fabricated.

ZnO based p-n homojunctions were grown using molecular beam epitaxy, in which Sb and Ga were used as dopants, to achieve p- and n- type films [281]. The turn-on-voltage of the diode was found to be 2 V and diode was showing very good response to UV light; this was further studied using photoconductivity measurements. Possibility of using photodiodes for ultraviolet detection was also discussed in this report.

Another recent report on the fabrication of p-type ZnO dealt with ion beam enhanced deposition method [282]. N and In were used for doping and as deposited films were showing p-type conduction with a resistivity of 2.4 ohm cm. Annealing in nitrogen atmosphere below 600ºC reduced resistivity further and lowest resistivity

obtained was 0.8 ohm cm. When annealing was done at temperature greater than 600ºC, films became n-type.

The following table gives some of the details of different dopants and method of preparation for the realization of p-type ZnO from previous reports. From this table it can be seen that lowest resisitivity and reasonable mobility was obtained with the N-In codoping using ultrasonic spray pyrolysis technique.

First Author	Technique	Dopant	Resistivity (Ohm cm)	Year
Minegishi	CVD	N	34	1997
Joseph	PLD	N	4	1999
Joseph	PLD	N, Ga	0.5	2001
Look	MBE	N	40	2002
Bang	Sputtering	P	20	2003
Ryu	Hybrid Beam	As	2	2003
Ye	Mag. Sputering	N, Al	160	2004
Look	Evaporation	As	0.4	2004
Bian	Ultrasonic Spray Pyrolysis	N, In	0.03	2004
Chen	Reactive sputtering	N, In	22.4	2005
Zhuge	Mag. Sputtering	N, Al	0.074	2005
Zeng	Mag. Sputtering	Li	16.4	2006
Mandalapu	MBE	Sb	6	2006

1.10 Summary of best results

Different groups tried to deposit ZnO films using Sol Gel technique and Musat et al reported reasonably superior properties with a resistivity of 2.9×10^{-3} ohm

cm, mobility 14 $cm^2(Vs)^{-1}$and optical transmittance of 85 % [223]. Hahn et al deposited highly conductive polycrystalline ZnO films using MOCVD technique with resistivity of the order of $3x10^{-4}$ ohm cm and mobility of 60 $cm^2(Vs)^{-1}$. Average optical transmittance was nearly 85% [43]. Several groups could achieve very low resistive ZnO films with reasonable good optical transmittance. The minimum resistivity was $1.4x10^{-4}$ ohm cm was obtained with Al doping [222] by Jeong et al. These films exhibited an average transmittance of 95% in the visible region. Chen et al developed the lowest resistivity ZnO films, using PLD technique was $8.54x10^{-5}$ ohm cm, which showed an average optical transmittance of 88%[208].Chemical spray pyrolysis technique generally resulted resistive films compared to the physical methods like sputtering or PLD. Studenikin et al reported the lowest resistivity value for the spray pyrolysed ZnO film and it was 10^{-3} ohm cm. [102]. In the present study the lowest resistivity value obtained is $1.45x10^{-3}$ ohm cm and an average optical transmittance in the visible region is 83%. Highest resistivity obtained in our case was $9.74x10^{4}$ ohm cm when it implanted with oxygen ions. When doped with chlorine, the average optical transmittance was about 94%.

References

[1] Transparent Semiconducting Oxides, H. L. Hartnagel, C. Jagdish, IOP Publishing House, 1995.

[2] S. J. Pearton, D. P. Norton, K. Ip, Y. W. Heo and T. Steiner, Prog. Mater. Sci., **50(3),** (2005) 293.

[3] M. Rossinelli, G. Blatter and C. Greuter, Electrical Ceramics, British Ceramic Society p 1 (1985)

[4] D. V. Lang, J. Appl. Phys. **45,** (1974)3023.

[5] J. F. Cordaro, Y. Shim and J. E. May, J. Appl. Phys. **60,** (1986) 4186.

[6] P. H. Kasai, Phys. Rev. **130,** 989 (1963)

[7] W. Gopel, L. J. Brillson and C. F. Brucker J. Vac. Sci. Technol. **17(5),** (1980) 894.

[8] J. C. Simpson and J. F. Cordaro, J. Appl. Phys. **63,** (1988) 1781.

[9] B. Wacogne, C. N. Pannell, M. P. Roe and T. J. Pattinson, Appl. Phys. Lett. **67,** (1995) 161.

[10] K. B. Sundaram and A. Khan J. Vac. Sci. Technol. A **15(2),** (1997) 428.

[11] V. Srikant and D. R Clarke, J. Appl. Phys. **83,** (1998) 5447.

[12] G. W. Tomlins, J. L. Routbort and T. O. Mason J. Am. Ceram. Soc. **81 (4),** (1998) 869.

[13] D. C. Look, D. C. Reynolds, J. R. Sizelove, R. L. Jones, C. W. Litton, G. Cantwell and W. C. Harsch, Sol. State Commun. **105,** (1998) 399.

[14] D. C. Look, J. W. Hemsky and J. R. Sizelove, Phys. Rev. Lett. **82,** (1999) 2552.

[15] A. F. Cohen, G. Ceder, D. Morgan and C. G. Van de Walle, Phys. Rev. B **61,** (2000) 15019.

[16] F. Obe, S. R. Nishitani, S. Isotani and H. Adachi, J. Appl. Phys. **90,** (2001) 824.

[17] S. Yuming, X. Pengshou, X. Faqiang, P. Haibin and L. Erdong, J. Electron. Spectrosc. Relat. Phenom. **114-116,** (2001) 1123.

[18] Y. Yoshino, M. Takeuchi, K. Inoue, T. Makino, S. Arai and T. Hata, Vacuum **66,** (2002) 467.

[19] M. Takeuchi, H. Yamada, Y. Yoshino, T. Makino and S. Arai, Vacuum **66,** (2002) 463.

[20] H. C. Ong, A. X. E. Zhu and G. T. Du, Appl. Phys. Lett., **80,** (2002) 941.

[21] W. Mielcarek, D. N. Wozny, K. Prociow and A. Gubanski, Rad. Effects Def. Sol. **157,** (2002) 1051.

[22] F. Toumisto, V. Ranki, K. Saarinen and D. C. Look, Phys. Rev. Lett. **91,** (2003) 205502.

[23] P. S. Xu, Y. M. Sun, C. S. Shi, F. Q. Xu and H. B. Pan, Nucl. Instr. and Meth. B **199,** (2003) 286.

[24] Y. Sun and H. Wang, Physica B **325,** (2003) 157.

[25] D. C. Look, C. Coskun, B. Claflin and G. C. Farlow, Physica B **342,** (2003) 32.

[26] Y. Imai and A. Watanabe, J. Mater. Sci: Mater Electron. **15,** (2004) 743.

[27]R Ghosh, D. Basak and S. Fujihara, J. Appl. Phys., **96,** (2004) 2689.

[28] A. E. Jimenez-Gonzailez and P. K. Nair, Semicond. Sci. Technol. **10,** (1995) 1277.

[29] G. J. Exarhos and S. K. Sharma, Thin Solid Films **270,** (1995) 27.

[30] E. Ennaoui, M. Weber, R. Scheer and H. J. Lewerenz, Sol. Energy Mater. Sol. Cells **54,** (1998) 277.

[31] D. Shimono, S. Torikai, T. Watari and M. Murano, J. Cer. Proc. Res. **2(4),** (2001) 184.

[32] A. W. Ott and R. P. H. Chang, Mater. Chem. Phys., **58,** (1999) 132.

[33] Y. Ohya, T. Niwa, T. Ban and Y. Takahashi, Jpn. J. Appl. Phys. **40,** (2001) 297

[34] X. D. Gao, X. M. Li and W. D. Yu, Mater. Res. Bull. **40,** (2005) 1104.

[35] N. Asakuma, H. Hirashima, H. Imai, T. Fukuki, A. Maruta, M. Toki and K. Awazu J. Appl. Phys. **92,** (2002) 5707.

[36] J. -H. Lee, K. –H Ko, B.-O. Park, J. Cryst. Growth **247,** (2003) 119.

[37] H. Li, J. Wang, H. Liu, C. Yang, H. Xu, X. Li and H. Cui, Vacuum **77,** (2004) 57.

[38] R. Ghosh, G. K. Paul and D Basak, Mater. Res. Bull. **40**, (2005) 1905.

[39] S. Kobayashi, K. Oshima, T. Sasaki, N. Tsuboi and F. Kaneko, Jpn. J. Appl. Phys. **44**, (2005) 1372.

[40] O. F. Z. Khan and P. O'Brien, Thin Solid Films **173,** (1989) 95.

[41] M. Purica, E. Budianu, E. Rusu, M. Danila and R. Gavrila, Thin Solid Films **403-404,** (2002) 485.

[42] V. Sallet, C. Thiandoume, J. F. Rommeluere, A. Lusson, A. Rivière, J. P. Rivière, O. Gorochov, R. Triboulet and V. Muñoz-Sanjosé, Mater. Lett**., 53,** (2002) 126.

[43] B. Hahn, G. heindel, E. P. Schoberer and W. Gebhaardt, Semicond. Sci. Technol., **13,** (1998) 788.

[44] H. Shen, M. Wraback, J. Pamulapati, S. Liang, C. Gorla and Y. Lu Proc. Symposium, Boston, MA, USA, 1998 (www.nsr.mij.mrs.org)

[45] G. Du, J. Wang, X. Wang, X. Jiang, S. Yang, Y. Ma, W. Yan, D. Gao, X. Liu, H. Cao, J. Xu and R. P. H. Chang, Vacuum **69**, (2003) 473.

[46] N. F. Cooray, K. Kushiya, A. Fujimakaki, I. Sugiyama, T. Miura, D. Okumura, M. Sato, M. Ooshita and O. Yamase, Solar. Energy Mater. Sol. Cells **49,** (1997) 291.

[47] N. W. Emanetoglu, C. Gorla, Y. Liu, S. Liang and Y. Lu, Mater. Sci. Semicond. Proc. **2,** (1999) 247

[48] B. S. Li, Y. C. Liu, Z. Z. Zhi, D. Z. Shen, J. Y. Zhang, Y. M. Lu, X. W. Fan and X. G. Kong, J. Vac. Sci. Technolo. A **20(5),** (2002) 1779.

[49] J. –M. Myoung, W. –H. Yoon, D. –H. Lee, H. Yun, S. –H. Bae and S. –Y. Lee, Jpn. J. Appl. Phys. **41**, (2002) 28.

[50] N. J. Ianno, L. McConville, N. Shaikh, S. Pattil and P. G. Snynder, Thin Solid Films **220,** (1992) 92.

[51] E. Millon, O. Albert, J. C. Loulergue, J. Etchepare, D. Hulin and J. Perrie` re, Appl. Phys. Lett. **88,** (2000) 6937.

[52] M. Liu, X.Q. Wei, Z.G. Zhang, G. Sun, C.S. Chen, C.S. Xue, H.Z. Zhuang and B.Y. Man, Appl. Surf. Sci., **252,** (2006) 4321.

[53] S. V. Prasad, J. J. Nainaparampil and J. S. Zabinski, J. Vac. Sci. Technolol, A **20(5),** (2002) 1738.

[54] S. Choopun, R. D. Vispute, W. Nouch, A. Balsamo, R. P. Sharma, T. Venkatesan, A. Iliadis and D. C. Look, Appl. Phys. Lett. **75,** (1999) 3947.

[55] S. B. Qadri, H. Kim, J. S. Horwitz and D. B. Chrisey J. Appl. Phys. **88,** (2000) 6564.

[56] K. Matsubara, P. Fons, K. Iwata, A. Yamada, K. Sakurai, H. Tampo and S. Niki Thin Solid Films **431**-**432,** (2003) 369.

[57] A. Tiwari, M. Park, C. Jin, H. Wang, D. Kumar and J. Narayan, J. Mater. Res **17(10)**, (2002) 2480.

[58] W. Z. Yang, H. L. Zhong, Z. Jie, S. Jie and W. Z. Jun Vacuum **78,** (2005) 53.

[59] Y. W. Heo, K. Ip, S. J. Pearton and D. P. Norton Phys. Stat. Sol. (a) **201(7),** (2004) 1500.

[60] J. R. Duclere, C. M. Loughlin, J. Fryar, R. O. Haire, M. G. Viry, A. Meany, A. Perrin, E. McGlynn, M. O. Henry and J. P. Mosnier, Thin Solid Films **500**, (2006) 78.

[61] J. Zou, S. Zhou, C. Xia, X. Zhang, F. Su, G. Peng, X. Li and J. Xu, Thin Solid Films **496,** (2006) 2005.

[62] H. –J. Ko, T. Yao, Y. M. Chen and S. –K. Hong, J. Appl. Phys. **92,** (2002) 4354.

[63] A. Tsukazaki, A. Ohtomo, S. Yoshida, M. Kawasaki, C. H. Chia, T. Makino, Y. Segawa, T. Koida, S. F. Chichibu and H. Koinuma, Appl. Phys. Lett. **83,** (2003) 2784.

[64] A. M. Chaparro, C. Maffiote, M. T. Gutirrez and J. Herrero, Thin Solid Films **431-432,** (2003) 373.

[65] A. W. Ott and R. P. H. Chang, Mater. Chem Phys. **58,** (1999) 132.

[66] F. D. Auret, S. A. Goodman, M. J. Legodi, W. E. Meyer and D. C. Look, Appl. Phys. Lett. **80,** (2002) 1340.

[67] N. Bouhsirra, S. Abed, E. Tomasella, J. Cellier, A. Mosbah, M. S. Aida and M. Jacquet, Appl. Surf. Sci., (article in Press)

[68] A. Krzesinski, Thin Solid Films **138,** (1986) 111.

[69] A. Valentini, A. Quirini and L. Vasanelli, Thin Solid Films **176,** (1989) L167.

[70] S. Sen, D. J. Leary and C. L. Bauer, Thin Solid Films **94,** (1982) 7.

[71] F. Sauberlisch, J. Fritsche, R. Hunger and A. Klein, Thin Solid Films **431-432,** (2003) 378.

[72] H. Gong, Y. Wang, Z. Yan and Y. Yang, Mater. Sci. Semicond. Process. **5,** (2002) 31.

[73] M. K. Jayaraj, A. Antony and M. Ramachandran, Bull. Mater. Sci. **25,** (2002) 227.

[74] Y. Yoshino, T. Makino, Y. Katayama and T. Hata, Vacuum **59,** (2000) 538.

[75] H. Kawamura, H. Yamada, M. Takeuchi, Y. Yoshino, T. Makino and S. Arai, Vacuum **74,** (2004) 567.

[76] K. Tominaga, T. Takao, A. Fukushima, T. Moriga and I. Nakabayashi, Vacuum **66,** (2002) 505.

[77] H. W. Kim and N. H. Kim, Phys. Stat. Sol. (a) **201(2),** (2004) 235.

[78] V. Gupta and A. Mansingh, J. Appl. Phys **80(2),** (1996) 1063.

[79] R. Hong, J Huang, H. He, Z. Fan and J. Shao, Appl. Surf. Sci. **242,** (2005) 346.

[80] N. Croitoru, A. Seidman and K. Yassin, Thin Solid Films **150,** (1987) 291.

[81] C. Calderon, H. Infante and G. Gordillo, Surf. Rev. Lett. **9,** (2002) 1617.

[82] W. Water and S. –Y. Chu, Mater. Lett. **55,** (2002) 67.

[83] A. K. Chawla, D. Kaur and R. Chandra, Opt. Mater. (Article in Press)

[84] M. J. Brett and R. R. Parsons, Sol. State Commun. **54 (7),** (1985) 603.

[85] Z. Q. Chen, S. Yamamoto, M. Maekawa, A. Kawasuso, X. L. Yuan and T. Sekiguchi, J. Appl. Phys. **94,** (2003) 4807.

[86] J. –K. Lee, H. –M. Kim, S. –H. Park, J. –J. Kim and B. –R. Rhee, J. Appl. Phys. **92,** (2002) 5761.

[87] A. Valentini, P. M. Quaranta, M. Rossi and R. Vasanelli, Thin Solid Films **175,** (1989) 255.

[88] T. Hata, K. Toriyama, J. Kawahara and M. Ozaki, Thin Solid Films **108,** (1983) 325.

[89] R. K. Gupta, N. Sridhar and M. Katiyar, Mater. Sci. Semicond. Process. **5,** (2002) 11.

[90] N. R. Aghamalyan, I. A. gambaryan, E. K. oulaninan, R. K. Hovsepyan, R. B. Kostanyan, S. I. Petrosyan, E. S. Vardanyan and A. F. Zerrouk, Semicond. Sci. Technol. **18,** (2003) 525.

[91] L. –J. Meng, C. P. Moreira de Sá and M. P. dos Santos, Appl. Surf. Sci. **78,** (1994) 57.

[92] T. E. Park, B. H. Kong, H. K. Cho, D. J. Park and J. Y. Lee, Physica B (Article in Press)

[93] Z. Zhang, Y. Zhang, L. Duan, B. Lin and Z. Fu, J. Cryst. Growth **290,** (2006) 341

[94] K. –Y. Lo, S. –C. Lo, S. –Y. Chu, R. –C. Chang and C. –F. Yu, J. Cryst. Growth **290**, (2006) 532.

[95] J. Hüpkes, B. Rech, S. Calnan, O. Kluth, U. Zastrow, H. Siekmann and M. Wuttig, Thin Solid Films **502,** (2006) 286.

[96] J. Aranovich, A. Ortiz and R. H. Bube, J. Vac. Sci. Technol. **16,** (1979) 994.

[97] P. Wu, Y. –M. Gao, J. Baglio, R. Kershaw, K. Dwight and A. Wold, Mat. Res. Bull. **24,** (1989) 905.

[98] F. Caillaud, A. Smith and J. –F. Baumard, J. Europ. Cer. Soc. **6,** (1990) 313.

[99] D. J. Goyal, C. M. Agashe, B. R. Marathe, M. G. Takwale and V. G. Bhide, J. Mater. Sci. Lett. **11,** (1992) 708.

[100] D. J. Goyal, C. Agashe, M. G. Takwale, B. R. Marathe and V. G. Bhide, J. Mater. Sci. **27,** (1992) 4705.

[101] M. Krunks and E. Mellikov, Thin Solid Films **270,** (1995) 33.

[102] S. A. Studenikin, N. Golego and M. Cocivera, J. Appl. Phys. **83,** (1998) 2104.

[103] B. Joseph, K. G. Gopchandran, P. K. Manoj, P. Koshy and V. K. Vaidyan, Bull. Mat. Sci. (1999) 921.

[104] P. Nunes, A. Malik, B. Fernandes, E. Fortunato, P. Vilarinho and R. Martins, Vacuum **52,** (1999) 45.

[105] B. J. Lohkhnade and M. D. Uplane, Appl. Surf. Sci., **167,** (2000) 243.

[106] A. Smith Thin Solid Films, **376,** (2000) 47.

[107] K. H. Yoon and J. Y. Cho, Mat. Res. Bull., **35,** (2000) 39.

[108] P. Nunes, E. Fortunato, P. Tonello, F. B. Fernandes, P. Vilarinho and R. Martins, Vacuum **64,** (2002) 281.

[109] R. Ayouchi, D. Leinen, F. Martin, M. Gabas, E. Dalchiele and J. R. R. Barrado, Thin Solid Films, **426,** (2003) 68.

[110] A. Mosbah, A. Moustaghfir, S. Abed, N. Bouhassira, M. S. Aida, E. Tomasella and M. Jacquet, Surf. Coat. Technol., **200,** (2005) 293.

[111] B. N. Pawar, S. R. Jadkar, M. G. Takwale, Sol. Energy Mater. Sol. Cells. (article in press)

[112] J. –H. Lee, W. Yeo and B. –O. Park, Thin Solid Films, **457,** (2004) 333.

[113] M.A.Lucio-López, M.A. Luna-Arias, A. Maldonado, M. de la L. Olvera and D.R. Acosta, Sol. Energy Mater. Sol. Cells, **90,** (2006) 733.

[114] R. Dingle, Phys. Rev. Lett., **23,** (1969) 579.

[115] J. Piqueras and E. Kubalek, Sol. Stat. Commun., **54,** (1985) 745.

[116] A. Ortiz, C. Falcony, M. Garcia and A. Sanchez, J. Phys. D: Appl. Phys., **20,** (1987) 670.

[117] C. Falcony, A. Ortiz, M. Garcia and J. S. Helman, J. Appl. Phys. **63,** (1988) 2378.

[118] K. Vanheusden, C. H. Seager, W. L. Warren, D.R. Tallant and J. A. Voigt, Appl. Phys. Lett., **68,** (1996) 403.

[119] K. Vanheusden, W. L. Warron, C. H. Seager, W. L. Warren, D.R. Tallant, J. A. Voigt and B. E. Gnade, J. Appl. Phys., **79,** (1996) 7983.

[120] A. Ortiz, C. Falcony, J. Hernandez, M. Garcia and J. C. Alonso, Thin Solid Films, **293,** (1997)103.

[121] S. A. Studenikin, N. Golego and M. Cocivera, J. Appl. Phys., **84,** (1998) 2287.

[122] S. Cho, J. Ma, Y. Kim, G. K. L. Wong and J. B. Ketterson, Appl. Phys. Lett. **75,** (1999) 2761.

[123] S. Im, B. J. Jin and S. Yi, J. Appl. Phys. **87,** (2000) 4558.

[124] B. J. Jin, S. Im and S. Y. Lee, Thin Solid Films, **366,** (2000) 107.

[125] B. Lin, Z. Fu and Y. Jia, Appl. Phys. Lett. **79,** (2001) 943.

[126] G. H. Lee, Y. Yamamoto, M. Kourogi and M. Ohtsu, Thin Solid Films, **386,** (2001) 117.

[127] H. C. Ong, A. S. K. Li and G. T. Du, Appl. Phys. Lett., **78,** (2001) 2667.

[128] N. Ohashi, T. Sekiguchi, K. Aoyama, T. Ohgaki, Y. Terada, I. Sakaguchi, T. Tsurumi and H. Haneda, J. Appl. Phys., **91,** (2002) 3658.

[129] S. A. Studenikin and M. Cocivera, J. Appl. Phys., **91,** (2002) 5060.

[130] Q. P. Wang, D. H. Zhnag, Z. Y. Xue, X. T. Hao, Appl. Surf. Sci., **201,** (2002) 123.

[131] W. S. Shi, O. Agyeman and C. N. Xu, J. Appl. Phys. **91,** (2002) 5640.

[132] N. Y. Garces, L. Wang, L. Bai, N. C. Giles, L. E. Halliburton and G. Cantwell Appl. Phys. Lett., **81,** (2002) 622.

[133] K. Ozaki and M. Gomi Jpn. J. Appl. Phys., **41,** (2002) 5614.

[134] D. H. Zhang, Z. Y. Xue and Q. P. Wang J. Phys. D: Appl. Phys. **35,** (2002) 2837.

[135] O. Agyeman, C. N. Xu, W. Shi, X. G. Zheng and M. Suzuki, Jpn. J. Appl. Phys., **41,** (2002) 666.

[136] T. –B. Hur, G. S. Jeen, Y. –H. Hwang and H. –K. Kim, J. Appl. Phys., **94,** (2003) 5787.

[137] S. Chakrabarthi, D. Gangli and S. Choudhari, J. Phys. D: Appl. Phys., **36,** (2003) 146

[138] Q. P. Wang, D. H. Zhang, H. L. Ma, X. H. Zhang and X. J. Zhang, Appl. Surf. Sci., **220**, (2003) 12.

[139] D. H. Zhang, Q. P. Wang and Z. Y. Xue, Appl. Surf. Sci., **207,** (2003) 20.

[140] Y. G. Wang, S. P. Lau, X. H. Zhang, H. H. Hng, H. W. Lee, S. F. Yu, B. K. Tay, J. Cryst. Growth **259,** (2003) 335.

[141] D. W. Hamby, D. A. Lucca, M. J. Klopfstein and G. Cantwell, J. Appl. Phys., **93,** (2003) 3214.

[142] Y. G. Wang, S. P. Lau, H. W. Lee, S. F. Yu, B. K. Tay, X. H. Zhang and H. H. Hng, J. Appl. Phys., **94,** (2003) 354.

[143] S. H. Jeong, J. K. Kim and B. T. Lee, J. Phys. D: Appl. Phys., **36,** (2003) 2017.

[144] T. –B. Hur, Y. –H. Hwang and H. –K. Kim, J. Appl. Phys., **96,** (2004) 1507.

[145] W. Z. Jun, W. Z. Jian, L. S. Chun, W. Z. Heng, L. Y. Ming and Y. J. Shan, Chin. Phys., **13,** (2004) 750.

[146] F. K. Shan, B. I. Kim, G. X. Liu, Z. F. Liu, J. Y. Sohn, W. J. Lee, B. C. Shin and Y. S. Yu, J. Appl. Phys., **95,** (2004) 4772.

[147] C. X. Xu, X. W. Sun, X. H. Zhang, L. Ke and S. J. Chua, Nanotechnology **15,** (2004) 856.

[148] Z. G Liang, L. B. Xia, H. Liang, M. X. Dong and F. Z. Xi, Chin. Phys. Lett., **21,** (2004) 1381.

[149] D. J. Qiu, H. Z. Wu, A. M. Feng, Y. F. Lao, N. B. Chen and T. N. Xu, Appl. Surf. Sci., **222,** (2004) 263

[150] G. Wang, G. Zhang, J. B. Ketterson and R. Gatt, Thin Solid Films **460,** (2004) 232.

[151] H. S. Kang, J. S Kang, J. W. Kim and S. Y. Lee, J. Appl. Phys., **95,** (2004) 1246.

[152] M. R. Phillips, O. Gelhausen, and E. M. Goldys, **201,** (2004) 229.

[153] Q. X. Zhao, P. Klason, M. Willander, H. M. Zhong, W. Lu and J. H. Yang, Appl. Phys. Lett., **87,** (2005) 211912.

[154] Y. W. Heo, D. P. Norton and S. J. Pearton, J. Appl. Phys., **98,** (2005) 073502.

[155] R. Hong, H. Qi, J. Huang, H. He, Z. Fan and J. Shao, Thin Solid Films **473,** (2005) 58.

[156] R. Hong, C. Wei, H. He, Z. Fan and J. Shao, Thin Solid Films, **485,** (2005) 262.

[157] X. M. Teng, H. T. Fan, S. S. Pan, C. Ye and G. H. Li, J. Phys. D: Appl. Phys., **39,** (2006) 471.

[158] J. Zhang, F. Pan, W. Hao and T. Wang, Mater. Sci. Engg. B **129,** (2006) 93.

[159] E. Mollwo Z. Phys **138,** (1954) 478.

[160] D. G. Thomas and J. J. Lander, J. Chem. Phys. **25,** (1956) 1136.

[161] I. An, Y. Lu, C. R. Wronski, and R. W. Collins, Appl. Phys. Lett. **64,** (1994) 3317.

[162] S. Kohiki, M. Nishitani, T. Wada and T. Hirao, Appl. Phys. Lett. **64**, 2876 (1994).

[163] T. Sekiguchi, N. Ohashi and Y. Terada, Jpn. J. Appl. Phys. **36,** (1997) L289.

[164] S. J. Baik, J. H. Jang, C. H. Lee, W. Y. Cho and K. S. Lim, Appl. Phys. Lett. **70,** (1997) 3516.

[165] C. G. Van de Walle, Phys. Rev. Lett. **85,** (2000) 1012.

[166] C. G. Van de Walle, Physica B **308-310**, (2001) 899.

[167] S. F. J. Cox, E. A. Davis, S. P. Cotterll, P. J. C. King, J. S. Lord, J. M. Gil, H. V. Alberto, R. C. Vilao, J. P. Duarte, N. A. de Wales, R. L. Lichi and S. J. C. Irvine, Phys. Rev. Lett. **86,** (2001) 2601.

[168] B. Theys, V. Sallet, F. Jomard, A. Lusson, J. Rommeluere and Z. Teukam J. Appl. Phys. **61,** (2002) 3922

[169] C. Kilic and A. Zunger Appl. Phys. Lett. **81,** (2002) 73.

[170] E. V. Lavrov, J. Weber, F. Börrnert, C. G. Van de Walle and R. Helbig Phys. Rev. B **66,** (2002) 165205.

[171] M. D. McCluskey, S. J. Jokela, K. K. Zhuravlev, P. J. Simpson and K. G. Lynn Appl. Phys. Lett. **81,** (2002) 3807.

[172] K. Ip, M. E. Overberg, Y. W. Heo, D. P. Norton, S. J. Pearton, S. O. Kucheyev, C. Jagadish, J. S. Williams, R. G. Wilson and J. M. Zavada Appl. Phys. Lett. **81,** (2002) 3996.

[173] A. Y. Polyakov, N. B. Smirnov, A. V. Govorkov, K. Ip, M.E. Overberg, Y. W. Heo, D. P. Norton, S. J. Pearton, B. Luo, F. Ren and J. M. Zavada, J. Appl. Phys. **94,** (2003) 400.

[174] G. A. Shi, M. Saboktakin, M. Stavola and S. J. Pearton Appl. Phys. Lett. **85,** (2004) 5601.

[175] C. A. Wolden, T. M. Barnes, J. B. Baxter and E. S. Aydi J. Appl. Phys. **97,** (2005) 43522.

[176] E. V. Lavrov, F. Borrnert and J. Weber Phys. Rev. B **72,** (2005) 85212.

[177] S. J. Jokela and M. D. McCluskey Phys. Rev. B **72,** (2005)113201.

[178] Y. Wang, B. Meyer, X. Yin, M. Kunat, D. Langenberg, F. Traeger, A. Birkner and C. Woll, Phys. Rev. Lett. **95,** (2005) 266104.

[179] Y. S. Jung, O. V. Kononenko and W. –K. Choi Sol. Stat. Commun. **137,** (2006) 474.

[180] D. A. Melnick J. Chem. Phys. **26,** (1957) 1136.

[181] E. E. Hahn, J. Appl. Phys. **22,** (1951) 855.

[182] Y. Takahashi, M. Kanamori, A. Kondoh, H. Minoura and Y. Ohya, Jpn. J. Appl. Phys. **33,** (1994) 6611.

[183] D. H. Zhang J. Phys. D: Appl. Phys. **28,** (1995) 1273.

[184] Y. Liu, C. R. Gorla, S. Liang, N. Emanetoglu, Y . Lu, H. Shen, and M. Wraback, J. Electron. Mater. **29,** (2000) 69.

[185] P. Sharma, A. Mansingh and K. Sreenivas Appl. Phys. Lett. **80**, (2002) 553.

[186] P. Sharma, K. Sreenivas and K. V.Rao J. Appl. Phys. **93,** (2003) 3963.

[187] R. Ghosh, B. Mallik and D. Basak, Apl. Phys. A **81,** (2005) 1281.

[188] Q. A. Xu, J. W. Zhang, K. R. Ju, X. D. Yang and X. Hou, J. Cryst. Growth **289,** (2006) 44.

[189] Y. –Z. Chiou and K. –W. Lin, J. Electrochem. Soc. **153,** (2006) G141.

[190] H. -K. Kim, J. W. Bae, K.-K. Kim, S.-J. Park, T.-Y. Seong, and I. Adesida, Thin Solid Films **447,** (2004) 90.

[191] A. A. Iliadis, R. D. Vispute, T. Venkatesan, and K. A. Jones, Thin Solid Films **420**, (2002) 478.

[192] H.-K. Kim, S.-H. Han, T.-Y. Seong, and W.-K. Choi, J. Electrochem. Soc. **148,** (2001) G114.

[193] A. Inumpudi, A. A. Iliadis, S. Krishnamoorthy, S. Choopun, R. D. Vispute and T. Venkatesan, Sol. Stat. Electron., **46**, (2002) 1665.

[194] B. S. Kang, J. J. Chen, and F. Ren, Y. Li, H.-S. Kim, D. P. Norton, and S. J. Pearton, J. Appl. Physics, **88,** (2006) 182101.

[195] K. Ip, G.T. Thaler, H. Yang, Sang Youn Han, Yuanjie Li, D.P. Norton, S.J. Pearton, S. Jang and F. Ren, J. Cryst. Growth, **287,** (2006) 149.

[196] K. Ip, B. P. Gila, A. H. Onstine, E. S. Lambers, Y. W. Heo, K. H. Baik, D. P. Norton, S. J. Pearton, S. Kim, J. R. LaRoche and F. Ren, Appl. Surf. Sci., **236,** (2004) 387.

[197] S. Takata, T. Minami and H. Nanto, Thin Solid Films **135,** (1986) 183

[198] Z. –C. Jin, I. Hamberg and C. G. Grnaqvist, Thin Solid Films **164,** (1988) 381.

[199] B. E. Sernelius, K. F. Bergrren, Z. -C. Jin, I. Hamberg and C. G. Grnaqvist, Phys. Rev. B **37,** (1988) 10244.

[200] T. Minami, H. Sato, T. Sonoda, H. nanto and S. Takata, hin Solid Films **171,** (1989) 307.

[201] J. Nishino, S, Ohshio and K. Kamata, J. Am. Ceram. Soc. **75,** (1992) 3469.

[202] K. Pushparajah, A. Kariem and S. Radhakrishna, J. Phys. D: Appl. Phys. **27,** (1994) 1518.

[203] A. Suzuki, T. Matsushita, N. Wada, Y. Sakamoto and M. Okunda, Jpn. J. Apl. Phys. **35,** (1996) L56.

[204] S. Y. Myong, S. J. Baik, C H. Lee, W. Y. Cho and K. S. Lim, Jpn. J. Appl. Phys. **36,** (1997) L1078.

[205] A. E. J. Gonzalez, J. A. S. Urueta and R. S. Parra, J. Cryst. Growth **192,** (1998) 430

[206] T. Minami, T. Miyata, T. Yamamoto and H. Toda, J. Vac. Sci. Tecnol. A **18,** (2000) 1584.

[207] F. Paraguay, J. Morales, W. Estrada L, E. Andrade and M. Miki Yoshida, Thin Solid Films **366,** (2000) 16.

[208] M. Chen, Z. L. Pei, X. Wang, C. Sun and L. S Wen, J. Vac. Sci. Technol. A, **19,** (2001) 963.

[209] E. Holmelund, J. Schou, S. Tougaard and N. B. Larsen, Appl. Surf. Sci. **197-198,** (2002) 467.

[210] H. Agura, A. Suzuki, T. Matsushita, T. Aoki and M. Okuda, Thin Solid Films **445,** (2003) 263.

[211] J. –H. Lee and B. –O. Park, Thin Solid Films **426,** (2003) 94.

[212] A. Bougrine, A. E. Hichou, M. Addou, J. Ebothe, A. Kachouane and M. Troyon, Mate. Chem. Phys. **80,** (2003) 438.

[213] M. de la L. Olvera and A. Maldonado, Phys. Stat. Sol. (a) **196,** (2003) 400.

[214] A. E. Hichou, M. Addou, A. Bougrine, R. Dounia, J. Ebothe, M. Troyon and M. Amrani, Mater. Chem. Phys. **83,** (2004) 43.

[215] S. J. Kwon, Jpn. J. Appl. Phys. **44(2),** (2005) 1062.

[216] K. –K. Kim, S. Niki, J. –Y. Oh, J. O. Song, T. –Y. Seong, S. J. Park, S. Fujita and S. W. Kim. J. Appl. Phys. **97,** (2005) 66103.

[217] S. T. Shishiyanu, T. S. Shishiyanu and O. I. Lupan, Sensors and Actuators **107,** (2005) 379.

[218] A. Bougrene, M. Addou, A. Kachouane, J. C. Bernede and M. Morsli, Mater. Chem. Phys. **91,** (2005) 247.

[219] P. Sagar, M. Kumar and R. M. Mehra, Thin Solid Films **489,** (2005) 94.

[220] X. Chen, W. Guan, G. Fang and X. Z. Zhao, Apl. Surf. Sci. **252,** (2005) 1561.

[221] S. T. Shishiyanu, O. I. Lupan, E. V. Monaico, V. V. Ursaki, T. S. Shishiyanu and I. M. Tiginyanu, Thin Solid Films, **488,** (2005) 15.

[222] W.J. Jeong, S.K. Kim and G.C. Park, Thin Slid Films, **506-507,** (2006) 180.

[223] V. Musat, B. Teixeira, E. Fortunato and R. C. C. Monteiro, Thin Solid Films, **502,** (2006) 219.

[224] Z. Qiao, C. Agashe and D. Mergel, Thin Solid Films **496,** (2006) 520.

[225] S. B. Zhang, S. –H. Wei and A. Zunger, Phys. Rev. B **63**, (2001) 75205.

[226] Y. Sato and S Sato Thin Solid Films **281-282,** (1996) 445.

[227] K. Minegishi, Y. Koiwai, Y. Kikuchi, K. Yano, M. Kasuga and A. Shimizu, Jpn. J. Appl Phys. **36**, (1997) L1453.

[228] T. Yamamoto and K. Yoshida Jpn. J. Appl. Phys. **38,** (1999) L166.

[229] M. Joseph, H. Tabata and T. Kawai, Jpn. J. Appl. Phys. **38,** (1999) L1205.

[230] Y. R. Ryu, S. Zhu, D. C. Look, J. M. Wrobel, H. M. Jeong and H. M. White, J. Cryst. Growth **216**, (2000) 330.

[231] T. Aoki, Y. Hatanaka and D. C. Look, Appl. Phys. Lett. **76,** (2000) 3257.

[232] E –C. Lee, Y. –S Kim, Y. 0G. Jin and K. J. Chang, Phys. Rev. B **64,** (2001) 85120

[233] Y. Yan, S. B. Zhang and S. T. Pantelides, Phys. Rev. Lett. **86,** (2001) 5723.

[234] X. –L. Guo, H. Tabata and T. Kawai. J. Cryst. Growth **223**, (2001) 135.

[235] K. Nakahara, H. Takasu, P. Fons, A. Yamada, K. Iwata, K. Matsubara, R. Hunger and S. Niki Appl. Phys. Lett. **79,** (2001) 4139.

[236] D. C. Look, D. C. Reynolds, C. W. Litton, R. L. Jones, D. B. Eason and G. Cantwell. Appl. Phys. Lett. **81**, (2002) 1830

[237] C. H. Park, S. B. Park and S. –H. Wei Phys. Rev. B **66**, (2002) 73202.

[238] G. Xiong, J. Wilkinson, B. Mischuk, S. Tuzemen, K. B. Ucer and R. T. Wiliams Appl. Phys. Lett. **80,** (2002) 1195.

[239] X. Li, Y. Yan, T. A. Gessert, C. DeHart, C. L. Perkins, D. Young and T. J. Coutts, Electrochem. Sol. Stat. Lett. **6(4),** (2003) C56.

[240] Y. R. Ryu, T. S. Lee, J. H. Leem and H. W. White, Appl. Phys. Lett. **83,** (2003) 4032.

[241] J. Huang, Z. Ye, H. Chen, B. Zhao and L. Wang, J. Mater. Sci. Lett. **22**, (2003) 249.

[242] A. V. Singh, R. M. Mehra, A. Wakahara and A. Yoshida, J. Appl. Phys. **93**, (2003) 396.

[243] X. Li, Y. Yan, T. A. Gessert, C. L. Perkins, D. Young, C. DeHart, M. Young and T. J. Coutts, J. Vac. Sci. Technol. A **21(4)**, (2003) 1342.

[244] J. F. Rommeluère, L. Svob, F. Jomard, J. Mimila-Arroyo, A. Lusson, V. Sallet and Y. Marefaing, Appl. Phys. Lett. **83,** (2003) 287.

[245] K. –K. Kim, H. –S. Kim, D. –K. Hwang, J. –H. Lim and S. –J. Park, Appl. Phys. Lett. **83**, (2003) 63.

[246] K. –H. Bang, D. –K. Hwang, M. –C. Park, Y. –D. Ko, I. Yun and J. –M. Myoung, Appl. Surf. Sci. **210,** (2003) 177.

[247] Y. G. Wang, S. P. Lau, X. H. Zhang, H. W. Lee, H. H. Hng and B. K. Tay, J. Cryst. Growth, **252**, (2003) 265.

[248] Y. R. Ryu, T. S. Lee and H. W. White, Appl. Phys. Lett. **83**, (2003) 87.

[249] D. C. Look and B. Claflin, Phys. Stat. Sol. (a) **241,** (2004) 624.

[250] Y. W. Heo, Y. W. Kwon, Y. Li, S. J. Pearton and D. P. Norton, Appl. Phys. Lett. **84,** (2004) 3474.

[251] J. M. Bian, X. M. Li, X. D. Gao, W. D. Yu and L. D. Chen, Appl. Phys. Lett. **84**, (2004) 541.

[252] J. M. Bian, X. M. Li, C. Y. Zhang, L. D. Chen and Q. Yao, Appl. Phys. Lett. **84,** (2004) 3783.

[253] J. M. Bian, X. M. Li, C. Y. Zhang, W. D. Yu and X. D. Gao, Appl. Phys. Lett. **85**, (2004) 4070.

[254] A. N. Georgobiani, A. N. Gruzintsev, V. T. Volkov, M. O. Vorobev and V. A. Dravin, Russian Microelectronics, **33(3)**, (2004) 204.

[255] Z. Q. Chen, T. Sekiguchi, X. L. Yuan, M. Maekawa and A. Kawasuso, J. Phys: Condens. Matter 16 (2004) S293

[256] E. –C. Lee and K. J. Chang Phys. Rev. B **70,** (2004) 115210

[257] J. G. Lu, Z. Z. Ye, F. Zhuge, Y. J. Zeng, B. H. Zhao and L. P. Zhu, Appl. Phys. Lett. **85,** (2004) 3134.

[258] D. C. Look, G. M. Renlund, R. H. Burgener II, J. R. Sizelove, Appl. Phys. Lett. **85,** (2004) 5269.

[259] F. Reuss, C. Kirchner, Th. Gruber, R. Kling, S. Maschek, W. Limmer, A. Waag and P. Zeimann, J. Appl. Phys. **95,** (2004) 3385.

[260] S. Limpijumnong, S. B. Zhang, S. –H. Wei and C. H. Park, Phys. Rev. Lett. **92**, (2004) 155504.

[261] C. –C. Lin, S. –Y. Chen, S. –Y. Cheng and H. –Y. Lee, Appl. Phys. Lett. **84**, (2004) 5040.

[262] D. C. Look, Semicond. Sci. Technol. **20**, (2005) S55.

[263] F. Zhuge, L. P. Zhu, Z. Z. Ye, D. W. Ma, J. G. Lu, J. Y. Huang, F. Z. Wang, Z. G. Ji and S. B. Zhang, Appl. Phys. Lett. **87,** (2005) 92103.

[264] C. L. Perkins, S. –H. Lee, X. Li, S. E. Asher and T. J. Coutts, J. Appl. Phys. **97,** (2005) 34907.

[265] V. Vaithianathan, B. –T. lee and S. S. Kim, J. Appl. Phys. **98**, (2005) 43519.

[266] E. J. Egerton, A.K. Sood, R. Singh, Y. R. Puri, R. F. Davis, J. Pierce, D. C. Look and T. Steiner, J. Electron. Mater. **34,** (2005) 949.

[267] Z. –H. Zhang, Z. –Z. Ye, D. –W. Ma, L. –P. Zhu, T. Zhou, B. –H. Zhao and Z. –G. Fei, Mater. Lett. **59**, (2005) 2732.

[268] Y. –J. Zeng, Z. –Z. Ye, J. –G. Lu, L. –P. Zhu, D. –Y. Li, B. –H. Zhao and J. –Y. Huang, Appl. Surf. Sci. **249**, (2005) 203.

[269] M. G. Wardle, J. P. Goss and P. R. Briddon, Phys. Rev. B **71,** (2005) 155205.

[270] Z. Yan, Z. T. Song, W. L. Liu, Q. Wan, F. M. Zhang and S. L. Feng, Thin Solid Films, **492,** (2005) 203.

[271] X. Li, S. E. Asher, B. M. Keyes, H. R. Moutinho, J. Luther and T. J. Coutts, *Proc. of 23rd IEEE Photovoltaic Specialists Conference and Exhibition*, Florida, Jan 3-7, 2005

[272] A. Tsukazaki, A. Ohtomo, T. Onuma, M. Ohtani, T. Makino, M. Sumiya, K. Ohtani, S. F. Chichibu, S. Fuke, Y. Segawa, H. Ohno, H. Koinuma and M. Kawasaki, Nat. Mater. **4**, (2005) 42.

[273] H. Yang, Y. Li, D. P. Norton, S. J. Pearton, S. Jung, F. Ren and L. A. Boatner, Appl. Phys. Lett. **86,** (2005) 172103.

[274] F. X. Xiu, Z. Yang, L. J. Mandalapu, D. T. Zhao, J. L. Liu and W. P. Beyermann, Appl. Phys. Lett. **87**, (2005) 152101.

[275] L. L. Chen, J. G. Lu, Z. Z. Ye, Y. M. Lin, B. H. Zhao, Y. M. Ye, J. S. Li and L. P. Zhu, Apl. Phys. Lett. **87,** (2005) 252106.

[276] Y. J. Zeng, Z. Z. Ye, W. Z. Xu, D. Y. Li, J. G. Lu, L. P. Zhu and B. H. Zhao, Apl. Phys. Lett. **88,** (2006) 62107.

[277] P. Fons, H. Tampo, A. V. Kolobov, M. hkubo, S. Niki and J. Tominaga, Phys. Rev. Lett. **96,** (2006) 45504.

[278] C. Wang, Z. Ji, J. Xi, J. Du and Z. Ye Mater. Lett. **60,** (2006) 912.

[279] D. C. Look, B. Calflin, Y. I. Aliov and S. J. Park, Phys. Stat. Sol. (a) **201 (10),** (2004) 2203.

[280] W. Liu, S. L. Gu, J. D. Ye, S. M. Zhu, S. M. Liu, X. Zhou, R. Zhang, Y. Shi, Y. D. Zheng, Y. Hang and C. L. Zhang Apl. Phys. Lett. **88,** (2006) 92101.

[281] L. J. Mandalapu, Z. Yang, F. X. Xiu, D. T. Zhao and J. L. Liu Appl. Phys. Lett. **88,** (2006) 92103.

[282] N. Yuan, J. Li, L. Fan, X. Wang and Y. Zhou J. Cryst. Growth (Article in Press)

EXPERIMENTAL DETAILS

2.1 Modern Techniques available for ZnO Films Preparation

The growth techniques play a significant role in governing the properties of transparent semi conducting oxides. This may be due to the fact that the electrical and optical properties of these films strongly depend on the structure, morphology and the nature of impurities in the film [1]. However different technologies for depositing thin films of ZnO, ranging from the very simple Chemical Spray Pyrolysis [CSP] to the highly sophisticated molecular Beam Epitaxy (MBE), exhibit similar stages of growth. The film is first discontinuous, followed by the formation of a network and finally continuous. In this chapter, a very brief description of some of the preparation techniques, widely used for the deposition of ZnO thin films is given.

2. 1. 1 Sputtering

Sputtering is one of the versatile techniques used for the deposition ZnO thin films. Compared to the chemical methods, sputtering produces films with higher purity and is capable of having better control over composition, homogeneity and film thickness. Sputtering process involves the creation of gas plasma by applying voltage between cathode and anode. Cathode is used as the target holder while anode is used as the substrate holder. Target is subjected to intense bombardment by ions and particles are ejected from the surface of cathode/target. These diffuse away from the target and are deposited on the substrate. Sputtering is normally performed at a pressure of 10^{-2} to 10^{-3} Torr. For conducting targets, DC voltage is applied between cathode and anode (DC Sputtering). But for non-conducting samples and insulators, a high frequency generator is connected between the electrodes (RF Sputtering). Magnetron sputtering is useful where high deposition rate and low substrate temperature are required. In magnetron sputtering, a magnetic field is applied to enhance the sputtering rate, which in turn, enhances the deposition rate also.

Non-stoichiometric ZnO thin films can be prepared by sputtering either a metallic zinc target in the presence of an oxygen-argon atmosphere, or an oxide target (99.999% purity), usually in a gas mixture of hydrogen and argon [2]. Generally crystallinity gets improved with increase in the substrate temperature [3]. If the distance between the substrate and the target is less than the mean free path of zinc atoms, films of better texture are obtained. Growth rate of ZnO depends markedly on oxygen concentration, substrate temperature and sputtering rate.

2. 1 .2 Pulsed Laser Deposition (PLD)

Pulsed laser deposition (PLD) is a sophisticated technique used for depositing transparent semi conducting oxides. This technique attained importance recently. This involves evaporation of a solid target in a High Vacuum/Ultra High Vacuum chamber, by means of short and high-energy laser pulses. A pulsed laser beam vaporizes the surface of the target; this condenses on the substrate, producing a film, with the same composition as the target. This is the result of the extremely high heating rate of the target surface (10^8 K/s) due to pulsed laser irradiation. It leads to the congruent evaporation of the target irrespective of the evaporating point of the constituent elements or compounds of the target. Because of the high heating rate involved,this technique demands a much lower substrate temperature than the other techniques. Due to this reason, the semiconductor and the underlying integrated circuit are not damaged.

The main components required are a laser, optics, and a vacuum system. It not only involves the physical process of the laser-material interaction of the impact of high-power pulsed radiation on solid target, but also the formation of the plasma plume with high energetic species and transfer of the ablated material, through the plasma plume, onto the substrate surface. The targets used in PLD are small compared with the large size required for sputtering techniques. It is quite easy to produce multi-layered films of different materials by sequential ablation of assorted targets. Besides,

by controlling the number of pulses, a fine control of film thickness, down to atomic monolayer, can be achieved.

2. 1. 3 Chemical Vapor Deposition (CVD)

Chemical Vapor deposition technique involves reaction of one or more gaseous reacting species on a solid surface (Substrate). In this process, metallic oxides are generally grown by the vaporization of a suitable 'organometallic' compound. A vapor, containing the condensate material, is transported to the substrate, where it gets decomposed, usually by a heterogeneous process. The decomposition condition should be such that the reaction occurs only at or near the substrate surface and not in the gaseous phase. This is to avoid formation of powdery deposits, which may lead to haziness in the film.

2. 1. 4 Chemical Spray Pyrolysis (CSP)

Chemical Spray Pyrolysis (CSP) technique, one of the chemical methods for the preparation of thin films, is widely used to deposit variety of thin films. It involves spraying a solution, usually aqueous, containing soluble salts of the constituents of the desired compound, onto a heated substrate. It is quite suitable for depositing large area thin films, with good reproducibility. In CSP, doping process is rather simple and by varying the concentration of the dopant in the solution, one can vary the percentage of doping in the sample. A major drawback of this technique is that it cannot use for the deposition of very thin films. Another shortcoming lies in the selection of substrate since it is a high temperature process. In the present work, we have chosen this technique for the deposition of ZnO films. Details of the experimental conditions will be discussed later in this chapter.

In order to deposit ZnO thin films using CSP technique, a salt solution of zinc is to be used as the precursor. It can be acetate, nitrate or chloride. Oxygen, air or nitrogen can be used as carrier gas. Nitrate solution requires lower substrate temperature to decompose while chloride needs higher temperature.

2. 1. 5 Sol Gel techniques

Sol gel dip coating technique is a simple and cost effective method, which can be used for depositing films of complex shapes and large surfaces. 'Sol gel' is a colloidal suspension of particles that is gelled to form a solid. The substrate is first inserted into the solution, containing the organometallic compounds, and then pulled out at a constant speed, into an atmosphere containing water vapor. In this atmosphere, hydrolysis and condensation process take place. Water and carbon groups are removed by baking at high temperature.

The reaction stages leading to oxide formation are

$$M(OR)_n + nH_2O \xrightarrow{heat} M(OH)_n + nROH$$
$$2M(OH)_n \longrightarrow M_2O_n + nH_2O$$

Where M and R represent the metal and the alkyl groups respectively. Advantages of this method are its versatility and the possibility to obtain high purity materials. More over, the composition of the sample can be perfectly controlled.

2. 2 Ion beam Irradiation Set up

The 15 UD pelletron of Nuclear Science Centre, New Delhi was used for the ion beam irradiation experiment in the present study. It is a versatile, heavy ion tandem type electrostatic accelerator. In this machine, negative ions are produced and preaccelerated to ~300KeV in Ion Source. SNICS (Source of negative ions by Cesium sputtering) is the widely used source for the ion accelerator. The sputter source uses accelerated cesium ions, striking a cold cathode, to produce a negative ion beam of cathode material (provided the material could form negative ions) A tantalum ionizer immersed in cesium weaper produces cesium ions. A thin layer of cesium, condensed on the cathode surface, enhances negative ion production. Almost all beams can be produced by SNICS source.

These negative ions are then injected into the strong electrical field inside an accelerator tank filled with SF_6 insulating gas. At the centre of the tank there is a

terminal shell, which is maintained at a high voltage (~15 MV). The negative ions on traversing through the accelerating tubes from the top of the tank to the positive terminal, get accelerated. On reaching the terminal, they pass through a stripper, which removes some electrons from the negative ions, thus transforming the negative ions into positive ions. These positive ions are then repelled away from the positively charged terminal and are accelerated to ground potential to the bottom of the tank. In this manner, same terminal potential is used twice to accelerate the ions. After coming out from the tank, the ions are bent into horizontal plane by analyzing magnet, which also selects a particular beam of ion. The switching magnet diverts the high-energy ion beams into various beam lines for the different experimental areas of the beam hall. The entire machine is computer controlled and is operated from the control room.

These ions are accelerated to a high vacuum chamber in the Materials Science beam Hall, where the samples are loaded in the sample holder, made of thick block of copper. The pressure in the chamber is maintained at 1×10^{-6} Torr during the irradiation.

2.3 Ion implantation set up

Ion implantation is a technique used to introduce impurities into solids in a uniform and reliable manner. The technique makes use of ions with energy in the range of keV to a few MeV, which collide with the target. In the present work, implantation was carried out using a J-15 Sames, 150 kV accelerator of Indira Gandhi Centre for Atomic Research (IGCAR), Kalpakkam, India. The accelerated ion beam is mass analysed using an H shaped magnet. This mass analysed beam is allowed to enter the implantation chamber, which is made compatible with ultra high vacuum (UHV).

2.4 Characterization Tools

For the development of a device quality film, the main objective is the optimization of preparation conditions. This can be done on the basis of suitable structural, morphological, compositional optical and electrical characterization of the films obtained in each condition. In this chapter, the techniques used in the present studies are described briefly. Optimization of preparation condition of ZnO thin films is also discussed in this chapter.

2.4. 1 X-ray Diffraction technique (XRD)

Many researchers, to explore the structural characterization, have extensively used XRD, which is a non-destructive technique. This technique can be used to determine the crystal structure of metals and alloys, minerals, inorganic compounds, polymers and organic materials. Also, this technique is applied to derive information on fine structure of materials like crystallite structure, lattice strain, chemical composition etc. Typical XRD pattern consists of a series of peaks, in which peak intensity is plotted on the Y-axis and diffraction angle (2θ) along X-axis. These peaks are called "reflections". Each peak in the diffraction pattern corresponds to x-rays diffracted from a specific set of planes in the material; these peaks are of different heights (intensities). The positions of the peaks in XRD pattern depend on the crystal structure of the material while intensities depend on many factors like atomic structure factors, incident intensity, slit width, number of grains etc. Experimentally obtained diffraction pattern of the material is compared with Joint Council Powder Diffraction (JCPDS) data for standards. This gives information of different crystallographic phases, relative abundance and preferred orientation. From the width of the diffraction peak, average grain size can also be estimated.

Average crystallite size can be calculated using Debye Scherrer's formulae,

$$D = \frac{k\lambda}{\beta \cos\theta} \ldots\ldots\ldots\ldots(2.1)$$

Where k is a constant ~1 and β, the Full Width at Half Maximum (FWHM) measured in radian and θ is the diffraction angle. λ is the wavelength of x-rays used.

Lattice constants for hexagonal systems can be calculated using the relation

$$\frac{1}{d^2} = \frac{4}{3}\frac{(h^2 + hk + k^2)}{a^2} + \frac{1}{c^2} \ldots\ldots\ldots\ldots(2.2)$$

where 'a' and 'c' are lattice parameters and 'd' is the lattice spacing.

In this work, XRD measurements were taken using Rigaku (D.Max.C) X-ray diffractometer employing CuK$_\alpha$ line (λ= 1.5404 Å) radiation and Ni filter operated at 30 kV and 20 mA.

2. 4. 2 Glancing Angle X-ray Diffraction Studies. (GAXRD)

The basic idea of the glancing angle X-ray geometry is to reduce the penetration of X-rays into a surface and hence to limit the depth from which information will be gathered. This can be achieved by simply reducing the angle of incidence of the beam on the sample surface. In standard XRD geometry, the incident angle on the sample surface is maintained at the same angle as the detector. Thus any crystalline planes detected will lie parallel to the surface of the sample. This is not true for the two main glancing angle geometries - the grazing incidence angle asymmetric Bragg (GIAB) geometry and the grazing incidence X-ray scattering (GIXS) geometry. GIAB geometry is the most widely available and it is more suitable for studying polycrystalline surfaces than for studying single crystal surfaces. GIXS geometry is ideal for studying sets of crystalline planes that are perpendicular to the sample surface.

In the present work, GXRD measurements were taken on few samples at Centre de Spectrometrie Nucleaire et de Spectrometrie de Masses (CSNSM), Orsay Campus, Paris, using Siemens D5000 X-Ray Diffractometer.

2. 4. 3 X-ray Photoelectron Spectroscopy (XPS)

X-ray photoelectron spectroscopy (XPS; also called 'electron spectroscopy for chemical analysis'- ESCA) is electron spectroscopic method that uses x-rays to knock electrons out of inner shell orbitals. The kinetic energy (E_K) of these photoelectrons is determined by the energy of the x-ray radiation ($h\nu$) and the electron binding energy (E_b)

$$E_K = h\nu - E_b \ldots\ldots\ldots..(2.3)$$

The electron binding energies are dependent on the chemical environment of the atom. XPS is therefore useful to identify the oxidation state of an atom. Binding energy of the core electrons are affected by the valance electrons and therefore by the chemical environment of the atom. When atomic environment of an atom changes, it alters the local charge surrounding the atom. This charge, in turn, reflects itself as a variation in the binding energy of all the valence electrons of the atom. Thus binding energies of valence electrons experience a characteristic shift. Hence the shift in the binding energy can give important information regarding the valence states/compound formation of the atom in the sample and one can use this technique to find out whether an element present in a sample is in pure or in compound form. XPS technique is generally a surface analysis technique. However, with facility for physically etching using sputtering technique, depth profile is also achieved. In XPS spectra, 'intensity' of the emitted photoelectron signal is plotted as a spectrum of binding energies

In the present study, XPS spectra were recorded using an ULVAC – PHI unit (Model: ESCA- 5600 CIM) employing Argon ion sputtering.

2. 4. 4 Scanning Electron Microscopy (SEM)

The scanning electron microscope is one of the most useful and versatile instruments for the investigation of surface topography, microstructutral features, etc. The principle involved in imaging is to make use of the scattered secondary electrons

when a finely focused electron beam impinges on the surface of the specimen. The electrons are produced by a thermal emission source, such as heated tungsten filament, or by using field emission cathode. To create SEM image, the incident electron beam is scanned in a raster pattern across the sample surface. Secondary electrons are produced due to the interaction of the primary electron beam. The emitted electrons are detected at each position in the scanned area by an electron detector. Intensity of the emitted electron signal is displayed as brightness on a cathode ray tube. There are two modes of imaging: one is by using Secondary Electrons and the other is by using Backscattering Electrons. Secondary electron imaging provides high resolution imaging of fine surface morphology and for this, the samples must be electrically conductive.

Cambridge Model 7060 Scanning electron Microscope was used for recording surface image of ZnO thin films in the present work. A very thin layer of gold was coated over the ZnO samples to obtain conductivity without significantly affecting surface morphology.

2. 4. 5 Atomic Force Microscopy (AFM)

Atomic force Microscopy (AFM) is a form of scanning probe microscopy (SPM) where a small probe is scanned across the sample to obtain information about the sample's surface. The information, gathered from the probe's interaction with the surface, could be as simple as the physical topography. These data are collected, as the probe is scanned in a raster pattern across the samples to form a map of the measured property relative to X-Y position. Thus the AFM image shows the variation in the measured property (height or magnetic domains) over the area imaged. The AFM probe has a very sharp tip, often less than 100Å diameter, at the end of a small cantilever beam. The interatomic forces between the probe tip and the sample surface cause the cantilever to deflect as the sample's surface topography changes. A laser light, reflected from the back of the cantilever, measures the deflection of the

91

cantilever. This information is fed back to a computer, which generates a map of topography and/or other properties of interest.

In the present work, AFM studies were performed on few samples using Digital Instrument's Multimode Scanning Probe Microscope (SPM) with Nanoscope IIIa controller.

2. 4. 6 UV- Vis- NIR Spectroscopy

The most direct and simplest method for determining the band structure of semi conductors is by measuring the absorption spectrum. Absorption is expressed in terms of a coefficient $\alpha(h\nu)$, which is related to the energy gap E_g according to the equation,

$$\alpha h\nu = A\left(h\nu - E_g\right)^n ....(2.4)$$

where A is a constant, h is the Plank's constant, ν the frequency of the incident beam and n is equal to ½ for a direct gap and 2 for an indirect gap.

Absorption and transmission spectra of all the samples were recorded using UV-Vis -NIR spectrophotometer (Hitachi U-3410) model. Optical band gap was determined using the $(\alpha h\nu)^2$ versus hν plot by extrapolating the linear portion of the curve to the 'hν−axis'.

2. 4. 7 Photoluminescence (PL) Studies

Photoluminescence (PL) is contactless, non-destructive technique, for the determination of certain impurities in semiconductors. It is particularly suitable for the detection of shallow level impurities, provided the radiative recombination events dominate non-radiative recombination. Identification of impurities is easy with PL; but measurements of the concentration of impurities are more difficult. PL can provide simultaneous information on different types of impurities.

Photoluminescence in solids can be classified in terms of the nature of the electronic transitions producing it. Mainly we can have intrinsic and extrinsic

emission. There are three kinds of intrinsic luminescence, i) band to band luminescence, ii) exciton luminescence and iii) cross luminescence. In band-to-band luminescence, emission occurs when an electron in conduction band recombine with hole in valence band. This emission can be observed in very pure crystal at higher temperature and at lower temperature this emission is transformed into exciton luminescence. If there are some impurities having their level in the forbidden gap, electron or holes are trapped by them and recombine with each other via such level, either radiatively or non radiatively. 'Cross luminescence' is usually observed in alkaline and alkaline earth halides. Luminescence caused by intentionally incorporated impurities, in most cases metallic impurities, is classified as "extrinsic luminescence". In semiconductors, most important impurities are donors and acceptors that dominate semiconductor property and these act as luminescence activators.

Photoluminescence studies were performed in the present work, on ZnO thin films, using excitation with 325-nm line from Kimmon He-Cd laser and the emission spectrum was recorded using Michelle 900 spectrograph. Photoluminescence studies were also taken using Jobin Yvon Fluorolog Spectrofluorimeter with the same excitation of 325 nm.

2. 4. 8 Electrical Characterization Technique

Resistivity and photosensitivity measurements were done with the help of Keithley 236 Source Measure Unit, interfaced by GPIB card and ICS software. Electrical contacts were given using silver paint, in the form of two end contacts, having a distance of 5 mm between them. The sample was illuminated with a tungsten halogen lamp, having a power of 100 mW/cm^2. Photosensitivity was calculated using the equation,

$$\Phi = \frac{(I_L - I_D)}{I_D} \ \ldots\ldots\ldots \ (2.5)$$

where I_L is the illuminate current and I_D is the dark current.

Resistivity measurements of few samples were also done using Schlumberger SI 7071 computing multimeter, employing four-probe method. Values of resistivity obtained with these two methods were more or less the same.

Dark conductivity was measured as a function of temperature in the range 100 K-300 K. For this, samples were placed in a liquid helium cryostat having auto tuning temperature controller (Lakeshore 321 Model). Output was measured across two magnanin wire leads pasted on the silver electrodes coated on the samples. Arrhenius plot, $\ln(\sigma)\, vs\, \dfrac{1000}{T}$ was used to evaluate activation energies of defect levels present in the ZnO thin films.

Hall effect measurements were done using Van der Pauw DC method (Toyo Corporation, Resitest 8300) with a current, 0.04 mA and a magnetic field 0.45 T.

2. 4. 9 Thermally Stimulated Current (TSC) Measurements

Measurement of "thermally stimulated current" has been used extensively as a defect characterization technique. It is one among the several photo-electronic techniques used to analyze and characterize crystalline, polycrystalline and amorphous materials. This technique also helps to identify the traps or defects present in the material and determine trap parameters [like activation energy and capture cross section]. A TSC spectrum usually consists of a number of [more or less resolved] peaks in current *versus* temperature graph called "glow curve". These peaks, in most cases, are related to a species of traps. Measured curve is then analyzed to obtain such characteristics as the location of the peak on the temperature scale, its width etc. These data are then utilized to compute trapping parameters by applying appropriate theoretical models.

In the present study, TSC measurements were taken using Lab Equip (IMS 2000) in the temperature range of 100 – 400 K. TSC spectrum was analyzed using

Microcal Origin 6.0 software. The defect level associated with this peak was determined using Half-width method, in which activation energy of the defect is directly related to the square of the peak temperature by the relation,

$$E_a = \frac{\left(2kT_m^2\right)}{T_2 - T_1} \ldots\ldots\ldots(2.6)$$

where $(T_2 - T_1)$ is the width of peak at half maximum, which was obtained by fitting the TSC curve using 'Gaussian fittings' and T_m is the temperature of the maximum peak and k is Boltzmann constant.

2.4.10 Rutherford Backscattering (RBS) Spectroscopy

RBS is based on bombarding a sample with energetic ions - typically He ions of 1 to 3 MeV energy - measuring the energy of the backscattered He ions. It allows the determination of atomic masses of the elements in sample, their depth distribution and crystalline structure etc.

Rutherford Backscattering analysis was done in the present work, using 3 MV Tandem Pelletron Accelerator of Institute of Physics, Bhubaneswar (National Eletcrostatic Corporation, USA; Model 9SDH2). 3 MeV He2+ ions were incident on the sample at an angle 10º and signals were collected using a silicon detector placed at 160º in back scattering geometry. Detailed investigations on the results using GISA or RUMP software could not be done because of the unknown composition of glass substrate.

2.5 Chemical Spray Pyrolysis set up

Experimental set-up for the CSP technique is schematically shown in Fig. 2.1. Cleaned glass slides (37x12x1.4 mm³) were placed on a thick iron block, which could be heated to the required temperature with a controlled heater. Temperature of substrate holder was measured using a digital thermometer (Thermis, series 4000) and was controlled using a variable transformer. Spray head and the base plate with the

heater, were kept inside a chamber, and provided with an exhaust fan for removing gaseous by-products and vapors of the solvent. During spray, temperature of the substrate was kept constant with an accuracy of ±5° C. Pressure of carrier gas was noted using a nanometer and was kept at 90±0.5 cm of Hg. Spray rate was 10 ml/min, and the distance between spray head and the substrate was ~ 15 cm.

1. Air Compressor
2. Gas flow control valve
3. Manometer
4. Solution reservoir   8. Temperature Controller
5. Solution flow control valve 9. Substrate Heater
6. Spray Head   10. Dimmerstat
7. Substrate   11. Exhaust Fan
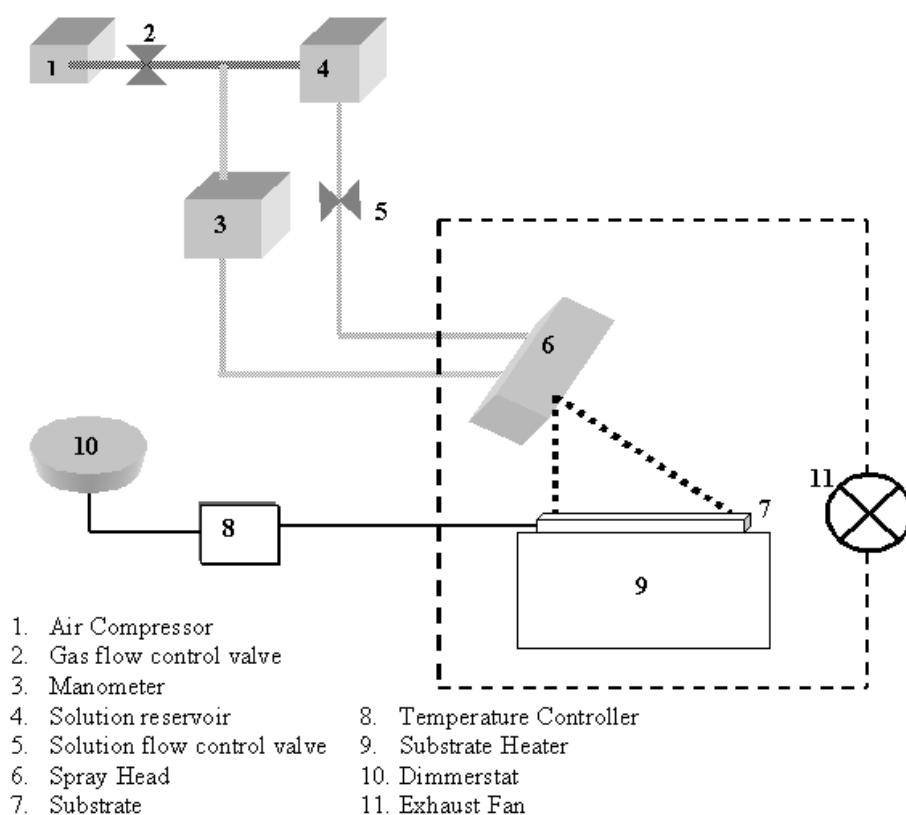
FIG. 2.1 Schematic Diagram of Chemical Spray Unit

In this work, ZnO thin films were deposited by spraying aqueous solution of zinc acetate using compressed air as carrier gas. Zinc acetate was used as the precursor to obtain the films without chlorine contamination. The additional advantage of zinc acetate was its high vapor pressure. Temperature of the substrate

was kept at $400 \pm 5°C$. Initially volume of the precursor solution was fixed at 50 ml and varied the molarity from 0.2 M to 1 M.

Samples prepared were named as ZnO_0.2M, ZnO_0.4M etc, implying that the films were prepared with 0.2 M and 0.4 M of $Zn(Ac)_2$ solution respectively. Then the molarity of the solution was fixed at 0.6 M and the volume of the sprayed solution was varied from 50 ml to 300 ml. In aqueous media, Zn could precipitate in the form of zinc hydroxide ($Zn(OH)_2$. Acetic acid was added (5ml) to the solution in order to prevent the formation of milky $Zn(OH)_2$. Quantity of acetic acid added to the solution was also a key parameter for the film deposition. Depending upon the pH of the solution, Zn^{2+} was progressively converted into complexes, which were $Zn(Ac)^+$ and $Zn(Ac)_2$. Concentration of these species played crucial role in the film formation. It is preferable to have neutral zinc acetate ($Zn(Ac)_2$) in solution in order to get film deposition. But addition of acetic acid locks the pH in the range of 4-5, resulting $Zn(Ac)_2$ as dominating species in the solution, enhancing the film deposition. In the present study pH was kept nearly at 4.5, which in turn increased the $Zn(Ac)_2$ and hence expected high deposition rate. Possible reaction proposed by Paraguay et al [4] on the formation of ZnO thin film is given by

$$Zn(CH_3COO)_2 \text{ (Solid near substrate)} \xrightarrow{Heat} 4Zn(CH_3COO)_2 + H_2O \text{ (Gas near substrate)} \xrightarrow{Adsorption}$$

$$Zn_4O(CH_3COO)_6 + 2CH_3COOH, \text{ (Adsorb/sub)} \quad \text{Solid near substrate}$$

$$Zn_4O(CH_3COO)_6 \text{ (Adsorb/sub)} \longrightarrow 4ZnO \text{ (Film)} + 6CH_3COOH \text{ (Gas)}$$
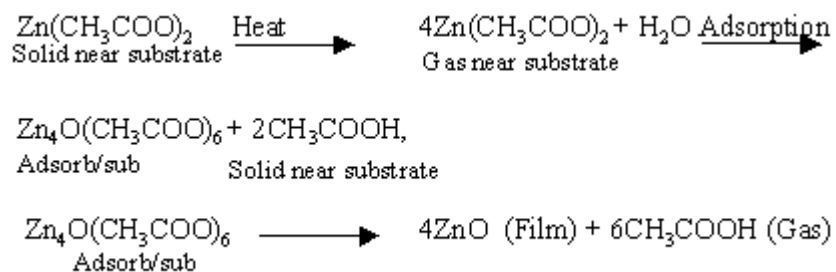
Details of the effects of variation of molarity and volume of the precursor solution will be discussed in the following section. Films formed were uniform, transparent and having good adhesion with the substrate.

2. 6 Results and Discussion

2. 6. 1 Effect of variation of molarity

Samples were prepared at different molarities of zinc acetate by varying it from 0.2 M to 1 M and keeping the volume of the solution at 50 ml; substrate temperature at 400ºC in all cases. These films were characterized using XRD and electrical resistance measurements.

2. 6. 1. 1 Structural Analysis

Figure. 2.2 show the diffraction pattern of ZnO thin film with different molar concentration of zinc acetate solution. All the films were showing preferential orientation along (002) plane. Film with 1M zinc acetate exhibited two additional peaks, corresponding to the planes (100) and (101). Intensity of the (002) plane was drastically reduced for this sample. At low molarity, the Zn concentration in the starting solution was low and hence Zn might have been present only at the regular lattice sites in ZnO. Therefore only (002) preferred orientation could be observed at low molarity. But at higher Zn concentration, the excess Zn would occupy the interstitial sites in the ZnO lattice, which altered the growth pattern [5]. Grain size was calculated and tabulated [Table 2.1]. It was seen that grain size decreased with molarity at lower concentration but remained nearly a constant at higher concentration.

Crystallinity was getting improved with increase in the molarity upto 0.6M; after that there was a reduction in crystallinity. This reduction might be due to the decrease in growth rate at higher molar concentration. Growth of ZnO films was governed by two growth mechanisms viz. Rideal-Eley mechanism and Langmuir-Hinshelwood mechanism [6]. According to Rideal-Eley mechanism, ZnO films grew continuously with the molarity of Zn-containing species by the reaction with the adsorbed water molecules. In spray pyrolysis it was difficult to control the incorporation of O_2 into the film during the growth process because the film was

deposited in atmospheric conditions. Hence in addition to growth rate, the stoichiometry was also controlled by Zn-concentration. At higher molar concentration, the availability of O_2 from the water molecule was insufficient for further increase in the growth rate and consequently the growth rate got saturated or started decreasing (Langmuir-Hinshelwood mechanism). Thus the growth rate of ZnO films was controlled by both these mechanisms. The molarity of 0.5 M appeared to be the optimum molarity of the precursor solution.
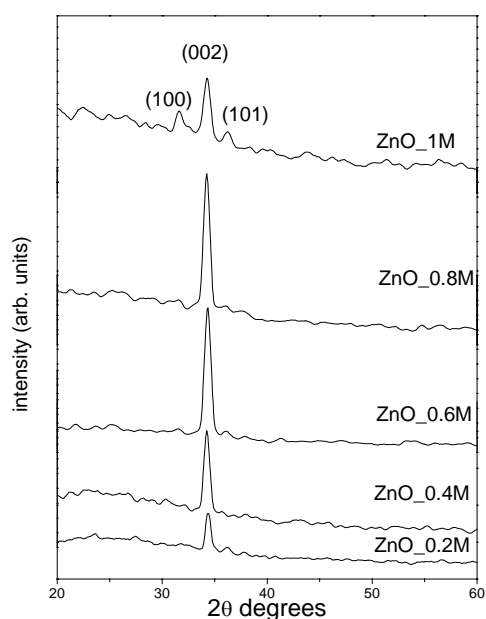
FIG. 2.2 XRD pattern of ZnO deposited with different molar concentration of zinc acetate.

2. 6. 1. 2 Electrical Resistance Measurements

Electrical resistance measurements were done in all samples using two-probe method. Electrical resistance was found to be decreasing with the increase of molarity of zinc acetate. Values are tabulated [Table 2.1]. The decrease in resistance was

probably due to the increase in regular lattice sites available for Zn atoms [2]. With the increase in molarity of the precursor solution, the Zn content in the solution increased, leading to the formation of Zn interstitial atoms in the film. Therefore oxygen vacancy in the film increased and consequently electrical resistance decreased.

Sample	Grain Size (Å)	Sheet Resistance (MΩ/□)
ZnO_0.2M	182.8	158.6
ZnO_0.4M	185.7	59.06
ZnO_0.6M	158.7	25.55
ZnO_0.8M	162.3	24.1
ZnO_1M	158.3	30.83

Table 2.1. Grain size and resistance variation of ZnO with molarity

2. 6. 2 Effects of Volume of precursor solution

Molarity of zinc acetate was fixed at 0.6M, since it was showing comparatively low resistance and better crystallinity. Volume of the precursor solution was varied from 50 ml to 300 ml. Here samples were named as ZnO_50, ZnO_100 etc, representing samples, prepared with 50 and 100ml volume of $Zn(Ac)_2$. Substrate temperature was kept at constant temperature of 400ºC.

2. 6. 2.1 Structural Studies

XRD pattern of ZnO with different precursor solution volume is shown in figure 3.3. Films showed preferential orientation along (002) plane. Small peak corresponding to the plane (101) was also observed for higher volume. Crystallinity was getting much improved with increase in the volume of zinc acetate. But for the sample ZnO_300, intensity of the peak corresponding to the plane (002) decreased while intensity corresponding to the plane (101) increased. The preferred orientation along (002) plane in sprayed ZnO sample was explained earlier and this might be

attributed to the chemical purity of the film [7]. Also the chemical purity of the film was controlled by the level of thermal decomposition of compound in the starting solution [7]. Grain size was calculated [Table 3.2] and was found to be increasing with volume of the precursor solution initially and then decreased at higher volume.
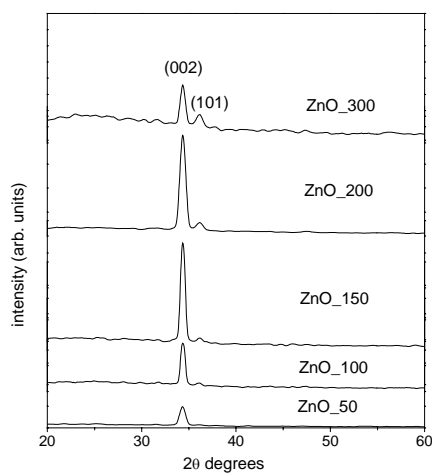
FIG.2. 3 XRD pattern of ZnO deposited with different volume of zinc acetate.

2. 6. 2. 2 Electrical Resistance Measurements

Electrical resistance measurements were done in all the samples and this was found to be decreasing with increase in the volume of the precursor solution. This might be due to the enhancement of the thickness of the film and also due to improved crystallinity. But for the sample ZnO_300, resistance again increased, probably due to smaller grain size. Resistance values are given in the table 2.2.

Sample	Grain Size (Å)	Sheet Resistance (MΩ/□)
ZnO_ 50	158.7	25.55.
ZnO_100	323.8	16.67
ZnO_150	274.6	6.72
ZnO_200	254.1	1.44
ZnO_300	182.3	3.76

Table 2.2. Grain size and resistance variation of ZnO with volume of zinc acetate.

2. 6. 2. 3 Optical Absorption and Transmission Studies

Optical absorption spectra were recorded in the wavelength range 350 – 900 nm. Absorption edge remained nearly constant for all samples [Fig. 2.4]. Band gap was determined from $(\alpha h\nu)^2$ vs hν plot and it was equal to 3.3 eV for all samples. Figure 2.5 shows the typical $(\alpha h\nu)^2$ vs. hν plot of ZnO.
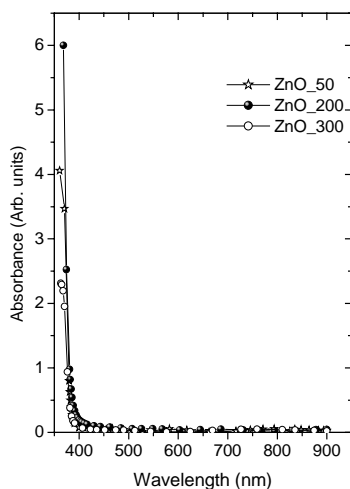
FIG 2.4 Absorption spectra of ZnO prepared with different Volume
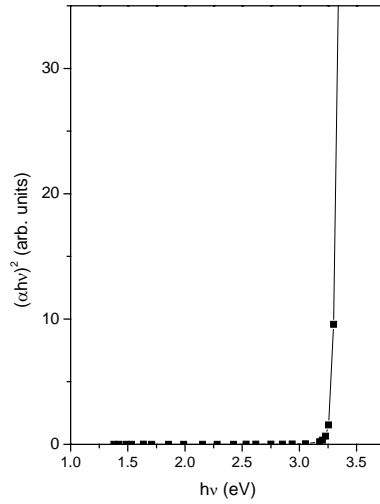
FIG. 2.5. $(\alpha h\nu)^2$ vs. $h\nu$ plot of ZnO

Optical transmission spectra were recorded for all samples in the wavelength range 350-1500 nm [Fig. 2.6]. Samples were showing good transparency. Interference fringe-like pattern of the transmittance curves established the smooth, reflecting nature of the films. Interestingly percentage of transmission decreased with increase in the volume of the solution.
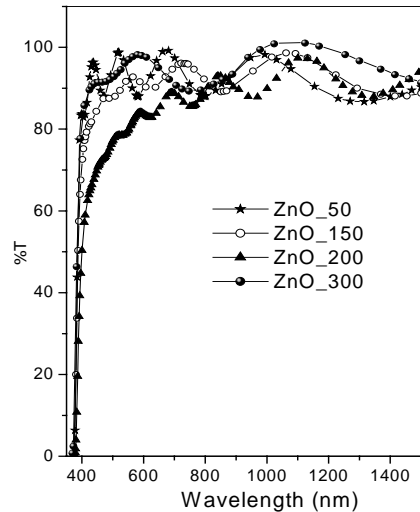
FIG. 2.6 Transmission curves for ZnO with various volume of the precursor solution.

2.7 Conclusion

We optimized the preparation conditions of ZnO thin film, to get good quality films using CSP technique. Molarity was fixed at 0.6 M and volume of the spray solution, at 200 ml. Substrate temperature was fixed at 400ºC. we used these conditions for the preparation of ZnO thin film for further studies presented in the thesis. Thickness of this film was 0.54 μm and this was determined using Stylus surface profiler.

References

[1] H. L. Hartnagel, A. L. Dawar, A. K. Jain and C. Jagadish, Semiconducting transparent thin films, IOP Publishing Ltd (Bristol and Philadelphia) 1995.

[2] N. Tsuji, H. Komiyama and K Tanaka, Jpn. J. Appl. Phys. **29,** (1990) 835.

[3] K. B. Sundaram and B. K. Garside, J. Phys. D: Appl. Phys. **17,** (1984) 147.

[4] D. F. Paraguay, L. W. Estrada, D. R. Acosta, M. E. Andrade and Miki Yoshida, Thin Solid Films **350,** (1999) 192.

[5] B. N. Pawar, S. R. Jadkar, M. G. Takwale, Sol. Energy Mat. Sol. Cells (article in press)

[6] R. N. Ghostagore, J. Electrochem. Soc. **125,** (1978) 110.

[7] M. Krunks and E. Mellikov, Thin Solid Films **270,** (1995) 33.

EFFECTS OF SWIFT HEAVY IONS IRRADIATION

3.1 Introduction

Swift heavy ion irradiation is a unique post deposition treatment, used to modify structural, optical and optoelectronic properties of thin film samples through the intense interaction of incident ions with the target atoms. There are several reports on structural and micro structural phase transformation due to irradiation using high-energy heavy ion, in poly crystalline and single crystal materials [1-10]. Ion irradiation can create new defects in some materials and anneal out pre-existing defects in some others. Only very few studies were done in ZnO with ion beam irradiation.

Thomas and Walsh reported the effects of annealing of Li-doped ZnO single crystals, implanted with different ions of different energies [11]. Also attempts were made to produce p-type ZnO, employing ion implantation with group V elements like vanadium and phosphorous. However the results were discouraging. Hall effect measurements were done as a function of annealing temperature.

Kohiki et al reported the conductivity enhancement in ZnO thin films due to hydrogen ion implantation [12]. 100 keV H+ ions were used for the implantation with different fluences in the samples kept at 373 K. The conductivity increased form 10^{-7} Ω^{-1} cm^{-1} to 10^{2} Ω^{-1} cm^{-1}, after post- ion implantation annealing at 473 K for 4 h in N$_2$ atmosphere. They concluded that doped hydrogen atoms formed OH ions, which acted as donors in the ZnO crystal and improved the conductivity.

Recently, Kucheyev et al demonstrated the isolation of different portions of ZnO single crystals as result of ion implantation with lighter elements like ^{1}H, ^{7}Li, ^{16}O and ^{28}Si at room temperature [13]. They confirmed that the sheet resistance of ZnO samples could be increased by ~7 orders of magnitude, as result of implantation using

lighter ions, having energy of ~ MeV. It was also shown that the ion doses, necessary for electrical isolation, had an inverse dependence on the number of lattice displacements produced by the ion beam.

A detailed investigation of evolution of lattice defects in single crystal ZnO, bombarded with 60 keV ^{28}Si and 300 keV ^{197}Au ions at 77 K and 300 K, was also done [14]. Rutherford Backscattering/channeling (RBS/C) spectrometry, cross sectional transmission electron microscopy (XTEM), XPS and AFM techniques were used for the studies. Crystalline to amorphous phase transition was observed due to ^{28}Si ion implantation.

Sakaguchi et al studied the effects of annealing on indium implanted ZnO single crystal [15]. 170 keV In was used for the implantation and these samples were subjected to annealing at ~1000K in air atmosphere. They showed that post implantation annealing could recover the emission properties of ZnO.

Photoluminescence studies on optically active Erbium (Er) implanted ZnO thin films were reported [16] earlier. As prepared samples gave single emission at 375 nm, while the Er-implanted samples exhibited an additional emission at 1540 nm. This additional emission was related to Er-O complexes formed in the film.

Recently there was a report on the formation of nano particles of Cu in ZnO single crystals as a result of negative ion implantation with 60 keV Cu ions [17]. The surface plasmon resonace peak in the absorption spectra proved the existence of nano particles and the damages produced in ZnO were analyzed using XRD and RBS.

In another paper, Sakaguchi et al reported the recovery of luminescence property of sulfur- implanted ZnO thin films, after annealing at 1073 K for 15 min [18]. They showed that, the near band edge emission was completely lost after the implantation with 50 keV S ions and the post implantation annealing at 1073 K retained the emission properties.

In an interesting paper, Schattat and Bolse reported the interface mixing studies of various systems [1]. One of the systems was ZnO/SiO$_2$, where they used Ar,

Kr, Xe and Au ions with very high energy (90-350 MeV). They concluded that 'thermal spike model' dominated 'Coulomb explosion model' in the present systems.

Very recently, Matsunami et al reported modifications of electrical and optical properties of ZnO and Al doped ZnO thin films, due to ion implantation with 100 keV Ne and Ar ions [19]. They observed a drastic reduction in resistivity and grain growth by annealing irradiated Al -doped ZnO films.

Another interesting paper was on irradiation effects using 1.6 MeV electrons in single crystal ZnO [20]. In this paper, D C Look et al predicted that high energy electrons could produce both acceptors and donors in ZnO and the damage was more in the (000I) direction (Zn face) than in the (000Í) direction (O face). They also confirmed that ZnO was more radiation resistant than Si, GaAs or GaN.

Swift heavy ions could produce point defects like vacancies, interstitials in a material. These defects changed the properties of materials to a very large extent. Another point was that it avoided the effects due to implantation since the range of the ion in the material was quite larger than the film thickness. Hence this technique could be effectively used for tuning different properties of materials as well as for material analysis.

3.2 Effects of 120 MeV Au ions

In the present work, thin film samples of ZnO were prepared for the irradiation using Au ions of 120 MeV energy. These samples were cut in to pieces of area 1 cm^2 and were irradiated using 120 MeV Au ion with fluences $1x10^{12}$, $3x10^{12}$, $1x10^{13}$ and $3x10^{13}$ ions/cm^2 . In this range of energy, modifications were expected mainly due to electronic excitation. These samples were named as ZnO_F1, ZnO_F2, ZnO_F3 and ZnO_F4, indicating that samples were irradiated with fluences $1x10^{12}$, $3x10^{12}$, $1x10^{13}$ and $3x10^{13}$ respectively. Stopping powers of 120 MeV Au ions in ZnO thin film was calculated (using TRIM-Transport of Ions in Matter) to be $2.466x10^3$ eV/Å, while nuclear stopping power was 44.9 eV/ Å. Figure 3.6 depicts the variation

of electronic and nuclear stopping power of 120 MeV au ions in ZnO thin films with ion energy. From this figure, it was clear that the electronic stopping power mechanism dominated the nuclear stopping power. Hence one could assume that the modification, induced in ZnO thin film due to 120 MeV Au ions, might be due to the electronic excitation rather than nuclear movement. Beam current was kept constant during experiments and it was around 1 particle nano ampere. Ion beam was focused to a spot of 1 mm diameter and then scanned over 1 cm × 1 cm area using a magnetic scanner. This high energy was selected to have the range of the ions few microns (9.86 μm) with a lateral straggling of 761.5 nm, so that no ions were implanted in the film. But there would be only defects due to the irradiation.
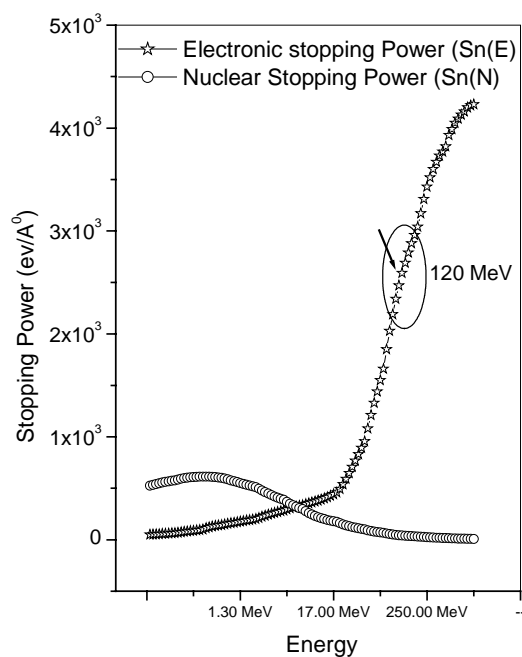
FIG. 3.1. Variation of electronic and nuclear stopping power with ion energies. Encircled portion indicates the energy used in the present study.

109

3.2.1 Structural Characterization

Crystallinity of pristine and irradiated samples was analyzed using XRD technique This is shown in Fig. 3.2. Pristine samples were preferably oriented along (002) plane at $2\theta = 34.7°$. The 'd' values were compared with standard JCPDS data card (79-0207). A weak X-ray diffractogram peak was also observed at $2\theta = 36.55°$, d $= 2.4565$ as depicted in Fig.3.7; this was corresponding to the plane (101)) of ZnO respectively.
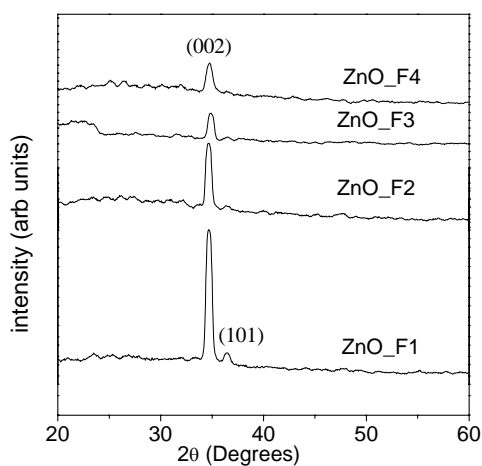
FIG. 3.2 XRD pattern of irradiated films

Intensity of the peak corresponding to the plane (002) decreased with ion fluence. The small peak corresponding to the plane (101) decreased with ion fluence and this vanished completely at the ion fluence of 1×10^{13} ions/cm^2. Grain size of the films, calculated from the peak at $2\theta = 34.7°$, was found to be decreasing with the ion fluence as seen from Table 3.1. Due to irradiation, only grain size was affected. From these observations, it might be concluded that the grain size of ZnO film was getting

110

smaller due to heavy ion irradiation. Lattice strain along c-axis was also calculated and it was nearly same for all the samples. Interestingly, there was no shift in the peak position in the XRD pattern, due to ion beam irradiation. Variation of integrated intensity of the peaks is shown in figure. It was decreasing with increase in the ion fluence.
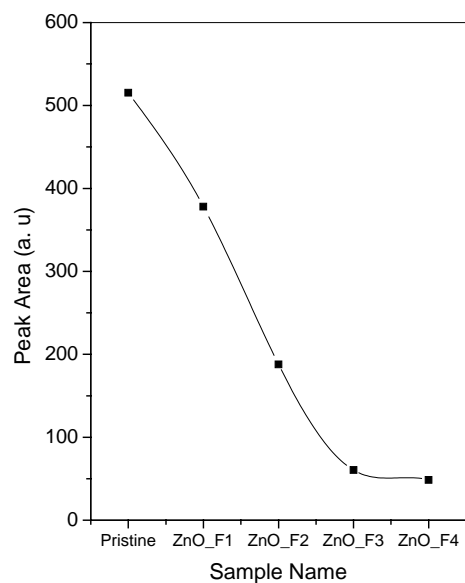
FIG. 3. 3 Peak area versus ion fluences of ZnO thin films

Table 3.1 Variation in Grain Size and FWHM with ion fluences

Sample Name	FWHM (degrees)	Grain Size (Å)
Pristine	0.320	260.19
ZnO_F1	0.331	251.52
ZnO_F2	0.327	254.60
ZnO_F3	0.384	216.96
ZnO_F4	0.488	170.64

3. 2. 2 Glancing Angle XRD (GAXRD) studies

Three samples were analysed using Glancing angle XRD-one pristine and two irradiated samples. The intensities of the peaks corresponding to the planes (100), (002) and (101) decreased with the increase of the fluence. However the other peaks remained without any change in the intensity, except the one, that was corresponding to the plane (103), and this was increasing [Fig. 3. 4]. The plane (002) was having a straight relation with the oxygen content in the film. Hence we could make a conclusion that oxygen diffused out from the film, making the crystallinity also worsened.
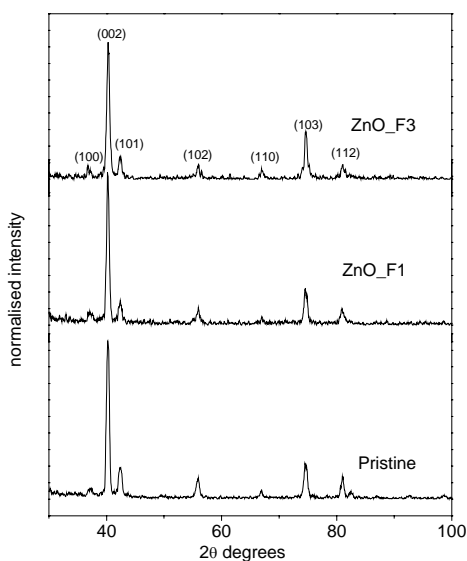
FIG. 3.4 GAXRD spectrum of pristine and irradiated samples

Structural factors were calculated which are listed in the table 3.2. These values were compared with natural structural ratio in the powder.

Table 3.2. Structural factors calculated from GXRD graph.

Line	(100)	(002)	(101)	(102)	(110)	(103)	(112)
Natural structural factor	57%	44%	100%	23%	32%	29%	23%
Measured	12-17	100	16-30	14-19	8-10	21-38	10-15

3. 2. 3 Optical Studies

Optical absorption of the samples was recorded in the wavelength range 350 to 900 nm. A sharp optical absorption edge was observed for all samples. Band gap was found to be 3.3 eV for all the samples. Another point worth mentioning here is that there was no observable change in the values of band gap due to irradiation, implying that the basic crystal lattice of ZnO was not modified. This was in agreement with the structural results as in the Fig. 3.1.
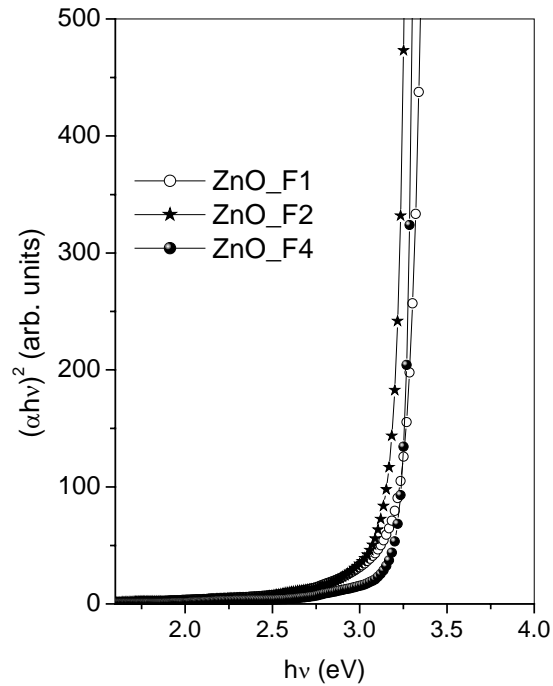
FIG. 3.5 $(\alpha h\nu)^2$ vs $h\nu$ plot for the irradiated ZnO thin films. Inset shows the same plot for the pristine sample for a comparison

Optical transmission spectra of the pristine and irradiated samples were also recorded in the wavelength range 350-900 nm [Fig. 3.6]. For the pristine sample, interference fringe- like pattern was observed in the transmission spectrum and this fringe pattern revealed that the surface of the film was fairly smooth and highly reflecting. As a result of ion beam irradiation, the interference fringe pattern became flat. Pristine sample had 80-90 % transmittance in the visible region and above 90 % in near IR region. But this reduced to 70-80% in the visible and IR region due to irradiation. The reduction in optical transmittance due to irradiation might be resulting from the increase in metal to oxygen ratio (Zn/O) in irradiated films, causing increase in carrier density. Another reason for the observed reduction in percentage

transmission might be the scattering loss, caused by the rough surface formed as a result of swift heavy ion irradiation.
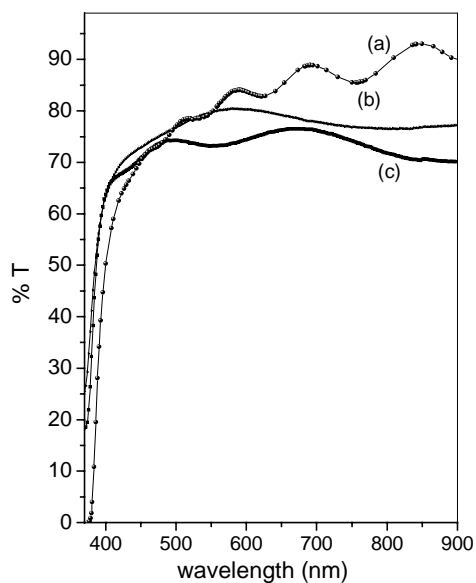
FIG. 3.6 Transmission spectra of ZnO thin films, irradiated with a fluence of   (a) Pristine (b) ZnO_F1 (c) ZnO_F4

3. 2. 4 Electrical Studies

Electrical resistivity of all the samples was measured using four-probe method and interestingly it was found to be decreasing with increase in the ion fluence. Resistivity values are given in Table 3.3. ZnO has donor levels due to oxygen vacancies (V_o) and interstitial zinc (Zn_i) atoms. Hence one could assume that the decrease in resistivity might be due to the creation of oxygen vacancies (V_O) and zinc interstitial (Zn_i), during the irradiation with swift heavy ions.

Table 3.3 Variation in resistivity, carrier concentration and mobility of ZnO thin films with ion fluences

Sample Name	Resistivity (Ω cm)	Carrier Density (cm^{-3})	Mobility ($cm^2V^{-1}sec^{-1}$)
Pristine	78.08	$1.3x\ 10^{15}$	61.57
ZnO_F1	48.22	$1.50x10^{16}$	8.65
ZnO_F2	32.21	$2.41x10^{16}$	8.05
ZnO_F3	2.86	$1.03x10^{17}$	21.23
ZnO_F4	0.71	$1.20x10^{17}$	73.22

Generally it was expected that resistivity should increase due to the decrease in grain size and also due to the increase in the grain boundary scattering. But the increase of Zn/O ratio was observed here which competed with earlier described phenomena. Hence we could say that increase in the Zn/O ratio was dominating the grain boundary scattering effects and this enhanced the conductivity. Carrier concentrations against ion fluence are given in table 3.2. This was found to be increasing with the ion fluence. Carrier density of pristine sample was $1.3x10^{15}$ cm^{-3} and that of irradiated sample (irradiated with a fluence of $3x10^{13}$ ions/cm^2) was $1.2x10^{17}$ cm^{-3}. A graph is plotted to show the variation of carrier concentration, mobility and electrical resisivity with ion fluences [Fig. 3.7]. The increase in carrier concentration was also resulting from the increase in Zn/O ratio due to irradiation. Mobility was determined using Hall measurements and for the pristine sample, it was equal to 60. For the irradiated films, initially mobility decreased at lower fluences and then increased at higher fluence. This was pretty interesting that even at large carrier concentration and low grain size, ZnO was showing higher mobility. Initial decrease might be due to the formation of defects and decrease in grain size. But at very high ion fluences, defect-annealing might have occurred, which increased the mobility.
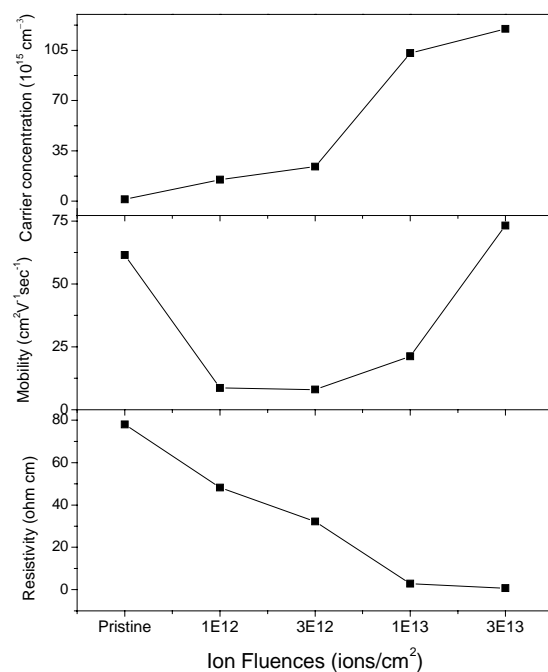
FIG. 3.7 Variation in resistivity, carrier concentration and mobility of ZnO thin films with ion fluences

3. 2. 5 Photoluminescence Studies

PL measurements were done at room temperature and results are depicted in Fig. 3.8. All samples showed the characteristic peak at 517 nm, which was corresponding to the blue-green emission. These emissions were found to be extremely broad due to phonon-assisted transition [21]. Intensity of PL spectra decreased with ion fluence. The center responsible for the blue green emission in ZnO was not been completely understood. It had been suggested that this peak was associated with copper impurities at a substitutional positions [22] oxygen vacancies, and porosity of the films [23]. However more recently it has been proposed that blue-green emission in this material might be related to a transition within a self-activated

center, formed by doubly ionized zinc vacancy (V_{Zn}^{-2}) and the ionized interstitial Zn_i or two nearest interstitial [24]. It has also been reported that the origin of green emission was due to the electronic transition from the bottom of the conduction band to the antisite defect O_{Zn} level [25]. In the case of our undoped ZnO samples, no intentional copper doping was done. Moreover presence of copper could not be detected from XPS analysis. Thus the green emission could not be related to the Cu impurity. Using full-potential linear muffin –tin orbital method, the energy levels of intrinsic defects were calculated [26]. It was found that the energy interval from the bottom of conduction band to the O_{Zn} level was 2.38 eV, which was in good agreement with the energy of green emission of PL observed in our experiment (2.40 eV). So we could suggest that the characteristic blue-green emission in ZnO film might be due to the antisite oxygen. As the ion fluence increased, we observed a decrease in the integral intensity of the PL spectra. It may be due to the fact that as the ion fluence increased, this level due to the antisite oxygen was getting depleted from the sample.
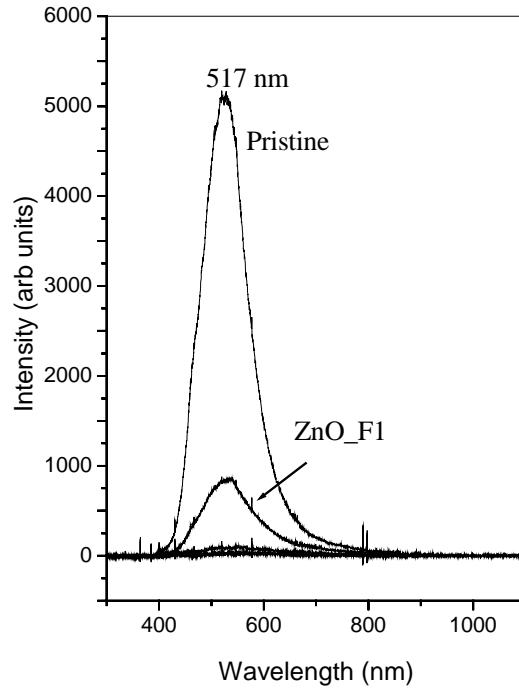
FIG. 3.8 PL spectra of both undoped and doped ZnO thin films. Intensity of the emission at 517 nm was decreasing with ion fluences.

PL emission intensity was plotted against ion fluence [Fig. 3.9]. This curve followed an exponential behavior. An equation, $P(\phi) = P(o)e^{-\sigma\phi}$ could be fitted with this graph to find out the ion interaction radius. Ion interaction radius was found to be 5.86 nm and this was in very good agreement with the earlier reported values of interaction size. Also from the nature of this curve, one could conclude that the type of interaction was single ion irradiation.
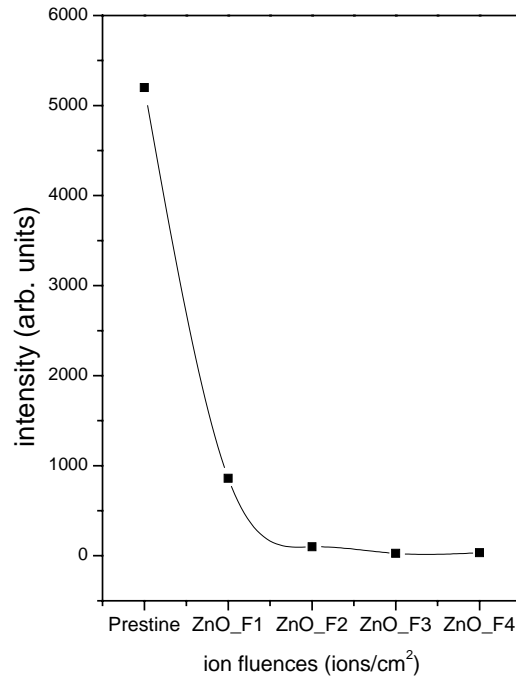
FIG. 3.9 PL intensity versus ion fluences

3.2.5.1 On the origin of blue-green emission in ZnO

Luminescence of ZnO films typically consisted of near band edge emission and a deep level (blue-green) emission. Owing to these properties, ZnO could be used to make devices for UV or blue emission. Therefore there were serious efforts to understand the mechanism of these emissions. Researchers had considered that the UV emission could be due to the excitonic transition. But still, controversy existed in explaining the origin of blue-green emission. Hence special emphasis was given to the origin of this controversial blue-green emission in this chapter. An acceptable explanation on the origin of blue - green emission was given on the basis of our experimental results and the existing theoretical works on the defect levels of ZnO thin films. Further support to this argument will be discussed in the next chapter also.

120

In order to see the effect of PL emission, ZnO samples were annealed at 673 K in vacuum for one hour and PL analysis was done. Fig. 3.10 shows the PL spectrum of annealed ZnO film. It was clear from the graphs (comparing the intensities from Fig. 3.8 and Fig. 3.10) that, annealing caused a decrease in intensity of blue-green emission. It was generally seen that, ZnO film, when annealed in vacuum, out diffusion of oxygen took place from the film. Here it was assumed that concentration of oxygen decreased on annealing and hence the decrease in intensity could be attributed to the depletion of oxygen. It could be either oxygen antisite (O_{Zn}) or oxygen interstitials (O_I) from theoretical calculation. The values of energy levels obtained theoretically were 2.38 and 2.28 eV respectively for O_{Zn} and O_I. But, it was already proved that the acceptor levels due to oxygen interstitials were the origin for red emission in ZnO [27]. The energy value corresponding to the PL emission at 517 nm in the present study was 2.4 eV. Hence it was presumed that, from the irradiation experiment and the annealing effect, the emission at 517 nm was due to the oxygen antisite. Transition was from conduction band to the acceptor level of $O_{Zn.}$

In addition to the emission at 517 nm, another emission at 640 nm (orange) also appeared in annealed ZnO. Earlier it was shown that both green and orange emissions related to the amount of oxygen [23]. It was also suggested that, strong green and orange emissions could not be observed simultaneously and orange emission increased at the expense of orange emission or vice versa.
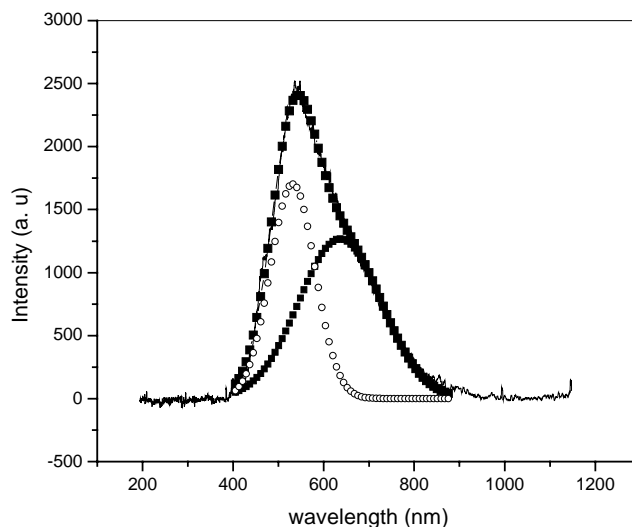
FIG. 3.10 PL spectra of vacuum annealed ZnO film. Intensity of the blue-green
emission was reduced on annealing.

3. 2. 6 XPS Analysis

Depth profile analysis was done using XPS on pristine and one irradiated (irradiated with 3×10^{13} ions/cm^2) sample as showed in Fig. 3.11 and 3.12 respectively. Bottom portion of the spectra represents the surface of the film and at the top it is the substrate. The results indicated that zinc and oxygen were uniformly distributed throughout the depth in both pristine and irradiated sample. The binding energy values were in agreement with the reported values. The binding energies of zinc and oxygen clearly indicated the formation of zinc oxide (1022.95 eV for Zn3P$_{3/2}$ and 531.02 eV for O1s). In the irradiated sample, we observed a shift in binding energy of oxygen (533.75 eV) present at the surface of the film and we suspected that it might be associated with silicate formation at the surface.

122
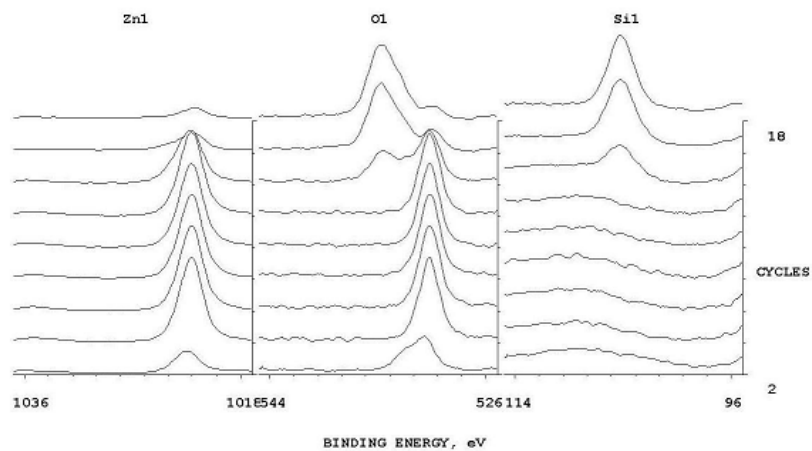
FIG. 3.11 XPS depth profile of Pristine ZnO thin films
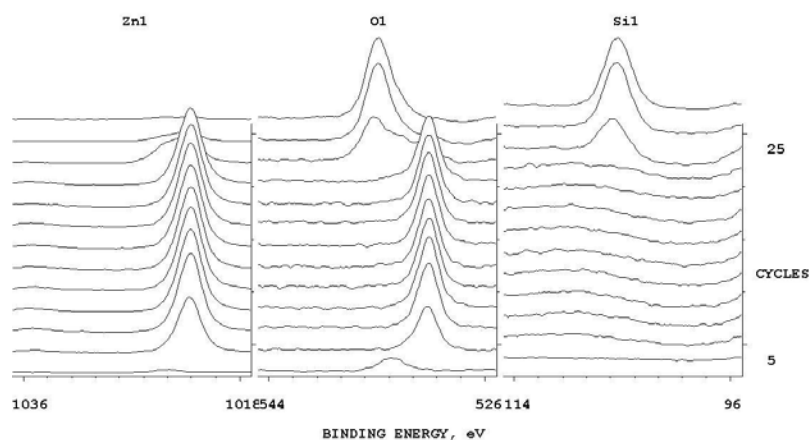
FIG. 3.12 XPS depth profile of irradiated ZnO thin films

The atomic concentration of zinc and oxygen was determined for the pristine and irradiated ($3x\ 10^{13}$ ions/cm^2) films [Fig. 3.13 and 3.14]. For the pristine sample, atomic concentration of zinc was found to be 62.33% and that of oxygen was 35.18% (Zn/O ratio is 1.77) and in irradiated sample atomic concentration of zinc was 64.22% and that of oxygen is 32.76% (Zn/O ratio is 1.96). Thus we observed a 10.6% increase in the Zn/O ratio after irradiation and this change in Zn/O ratio in the film resulted in

the decrease in resistivity and optical transmittance. Moreover the reduction in peak height of PL spectra due ion irradiation also suggested reduction in oxygen. XPS spectra showed an interface mixing between ZnO and SiO$_2$ substrate.
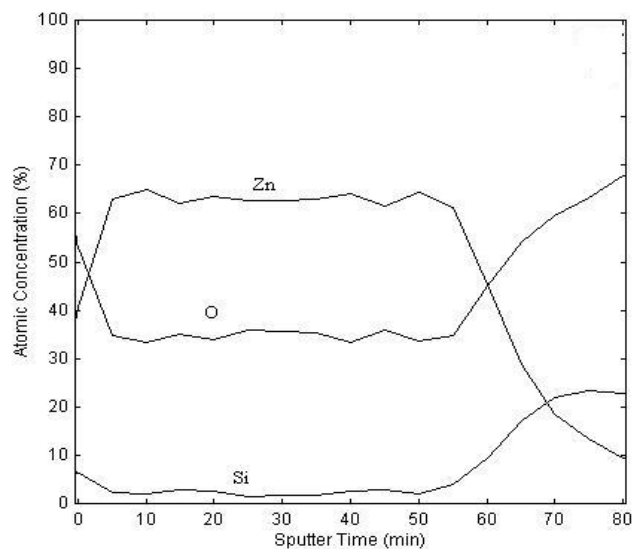
FIG. 3.13 Atomic concentration profile of Pristine ZnO
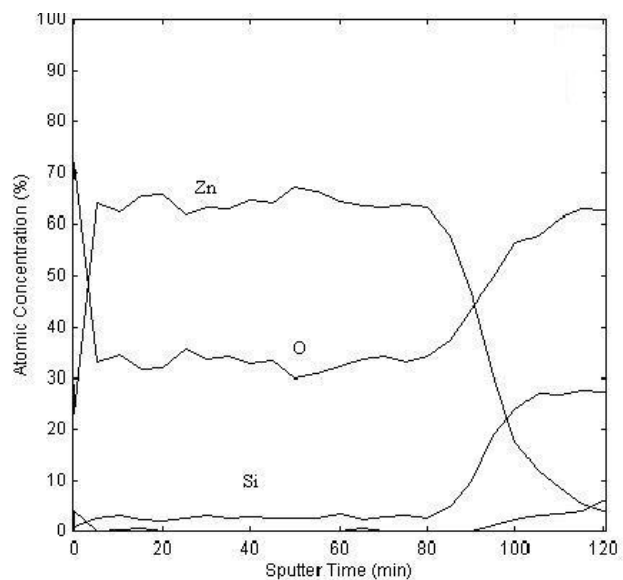
FIG. 3.14 Atomic concentration profile of 120 MeV Au$^+$ ions irradiated ZnO thin film

3. 2. 7 AFM Studies

2D and 3D AFM images of both pristine [Fig 3.15] and irradiated [Fig. 3.16] samples clearly depicted the change in surface morphology due to the swift heavy ion beam irradiation. AFM image of pristine sample showed a typical three dimensional growth structure with irregular grains of nearly same sizes and a surface roughness (RMS) of 17 nm. Irradiation with a fluence of 5×10^{11} ions/cm^2, resulted a substantial increase in RMS roughness of ZnO thin films (81 nm). This change in the film morphology was due to the damage created by the Au ions.
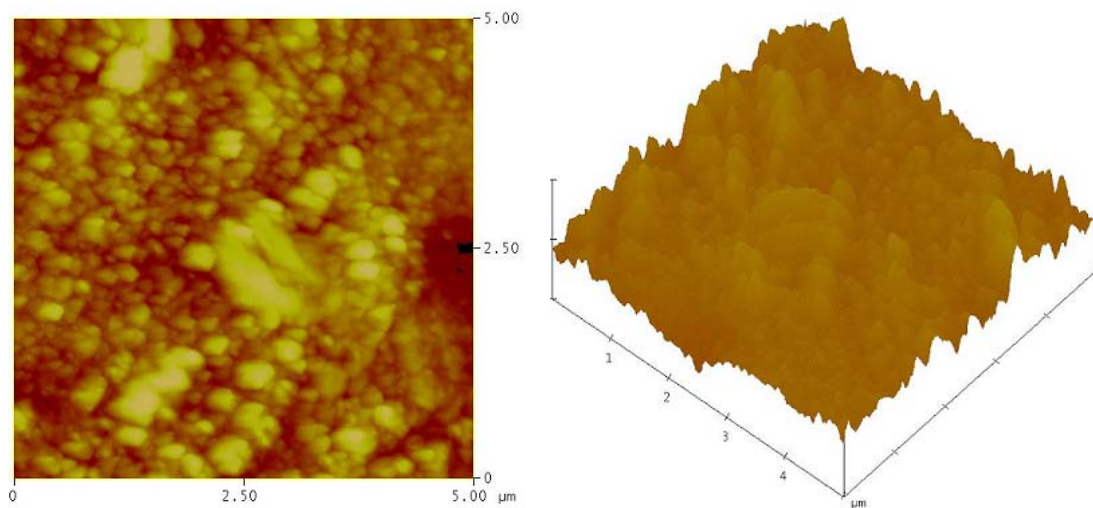
FIG. 3.15 AFM pictures (2D and 3D) of pristine ZnO thin films
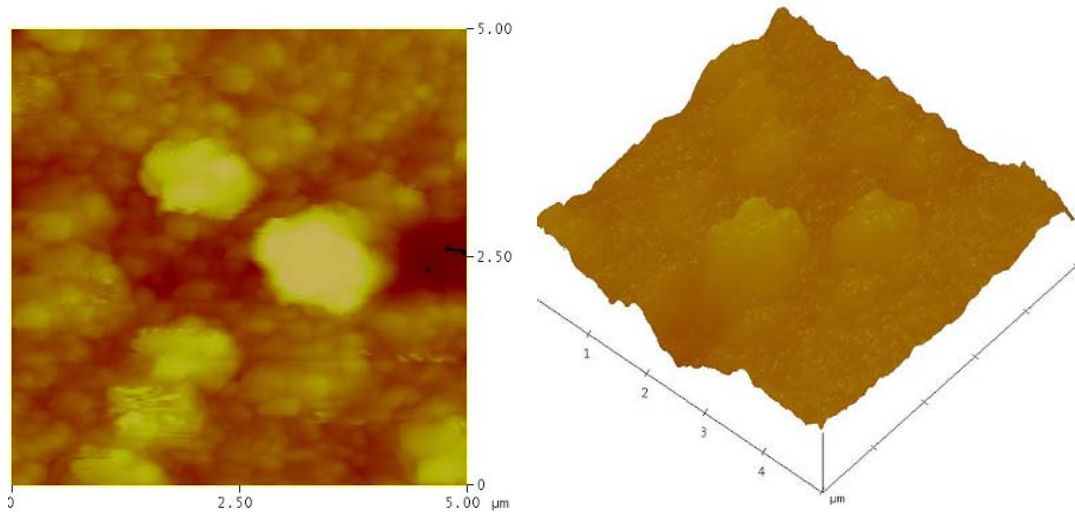
FIG. 3.16 AFM pictures (2D and 3D) of irradiated ZnO thin films

3. 3 Effects of 80 MeV Nickel ions

80 MeV Nickel (Ni) ions with different ion fluences, 5×10^{11}, 1×10^{12}, 3×10^{12}, 1×10^{13} and 3×10^{13} ions/cm^2 were also used for irradiation studies. Since Ni was lighter element than Au, and also the energy used was less than that of Au ions, we expected the damages produced to be small. The projected range was calculated using TRIM 2003 (~ 10.09 μm) with a lateral straggling of 795 nm. The values of electronic stopping power and nuclear stopping power were calculated to be 1.349 x10^3 eV/Å and 3.346 eV/Å. The electronic excitation could thus induce extended structural defects in ZnO thin films. Thickness of all the samples was same (540 nm), so that all the ions passed through the film, finally residing in substrate. Ion-substrate interaction was not a subject of the present study. Names of the samples were ZnO_NF1, ZnO_NF2, ZnO_NF3, ZnO_NF4 and ZnO_F5 in which N represented Ni ions and F1, F2 are the different fluence (F1=5×10^{11}, F2= 1×10^{12} ions/cm^2)

3. 3. 1 Structural Characterization

X-Ray diffraction studies on all samples showed preferential orientation along (002) plane. In addition to this plane, one could clearly see the other diffraction peak corresponding to the plane (101) [Fig. 3.17].
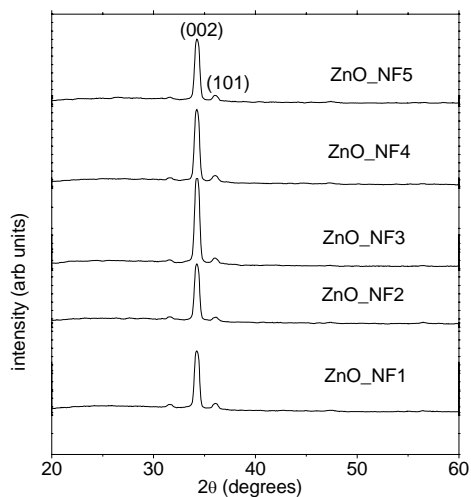
FIG. 3.17 XRD diagram of Ni irradiated ZnO thin films

Initially at lower fluences, crystallinity decreased with the increase in fluence. However for the sample ZnO_NF3, crystallinity increased first and then started decreasing with further increase in the fluence. Interestingly, average crystallite size remained same for all samples (~260 Å). It was also interesting to see that, the peak height corresponding to the plane (101) was almost unaffected by the swift heavy ion irradiation.

Normalized peak area of the plane (002) was plotted against ion fluences for the Au and Ni irradiated samples. It was seen that for the higher Se(E) (with Au ions), peak area was decreasing exponentially with the increase in the ion fluence, while it remained more or less constant for smaller Se(E) [Fig.3.18]. Hence from the structural

127

analysis one could conclude that, the threshold value of electronic stopping power was in between 1.35 and 2.45 keV/Å. Peak position corresponding to the (002) plane was remaining same even after the irradiation using very high fluence. This implied that the strain developed in the film was extremely feeble.
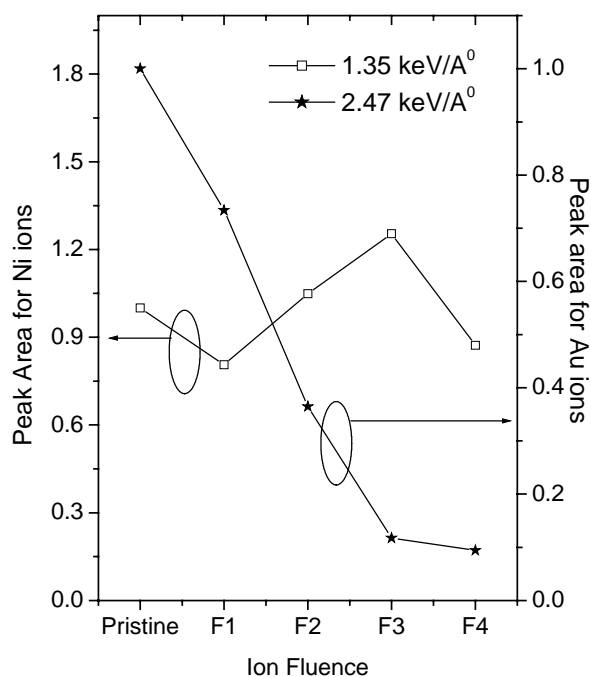
FIG. 3.18. Variation of Peak area versus Ion Fluence. Here F1, F2 represents ion fluences 1×10^{12}, 3×10^{12} ions/cm^2 etc

3. 3. 2 Optical absorption and transmission

Optical absorption spectra were recorded in the visible region (350 – 700 nm). Absorption edge at the UV region was sharp for all samples. It supported the XRD results that the basic crystal structure was not affected by the swift heavy ion irradiation. Band gap was determined from the $(\alpha h\nu)^2$ vs $h\nu$ graph (3.3 eV) for all samples [Fig. 3.19].
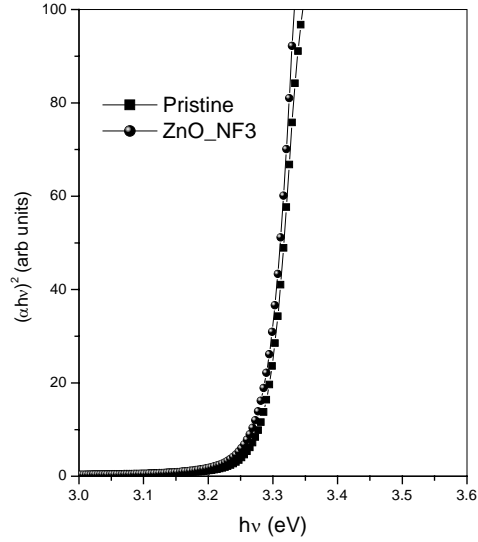
FIG. 3.19 $(\alpha h\nu)^2$ vs hν graph of Pristine and irradiated ZnO (with a fluence of 3×10^{12} ions/cm^2) thin films

Optical transmittance curve showed interference fringe like pattern and this was not affected by the swift heavy ion irradiation [Fig. 3.20]. Interference fringe like pattern proved the reasonably smooth surface of the film. There was a slight decrease in percentage of transmission, probably resulting from the scattering loss of light at the surface of ZnO, due to roughness caused by the ion beam irradiation. Transmittance spectra also revealed the steady nature of band edge.
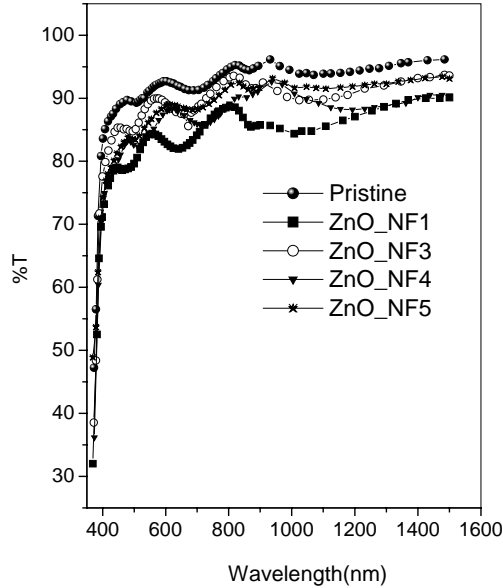
FIG. 3.20 Optical Transmittance spectra of Ni irradiated ZnO thin films

3. 3. 3 Electrical Resistivity and Photosensitivity Measurements

Electrical resistivity measurements were carried out in all samples using two-probe method. In general, resistivity increased with swift ion irradiation. But at very high fluence (sample F5) resistivity decreased. Variation of resistivity of ZnO was rather slow up to sample F2 and then it increased [Fig. 3.21]. This could be explained on the basis of single ion impact. Generally the size of ion interaction was few nm (5-8 nm) and hence up to the ion fluence of $1x10^{12}$ ions/cm^2 (Region I), irradiation could be realized as 'the single ion irradiation' process. As a result, resistivity variation was not significant. Above this fluence, the overlapping of ions might have come into action, leading to multi ion impact. This resulted in the large increase ion beam induced defects, which in turn, increased the resistivity (Region II). However at a fluence of $3x10^{13}$ (Region III), a decrease in resistvity was observed, which could be attributed to the commencement of hopping conduction of ion beam-

produced defects. When these films were irradiated with 120 MeV Au ions, a continuous decrease in resistivity was observed due to the out-diffusion of oxygen from the film. But in this case, there was no such decrease in resistivity and this might probably due to the predominance of defects created in the film by swift ions.

Photosensitivity of irradiated samples was low in comparison with that of pristine sample. Swift heavy ion irradiation might have produced lot of defects in the ZnO thin films. These defects might be acting as traps for light generated carriers and hence showing lower photosensitivity. Figure 3.21 depicts the variation of photosensitivity of ZnO thin films with different nickel ion fluences.
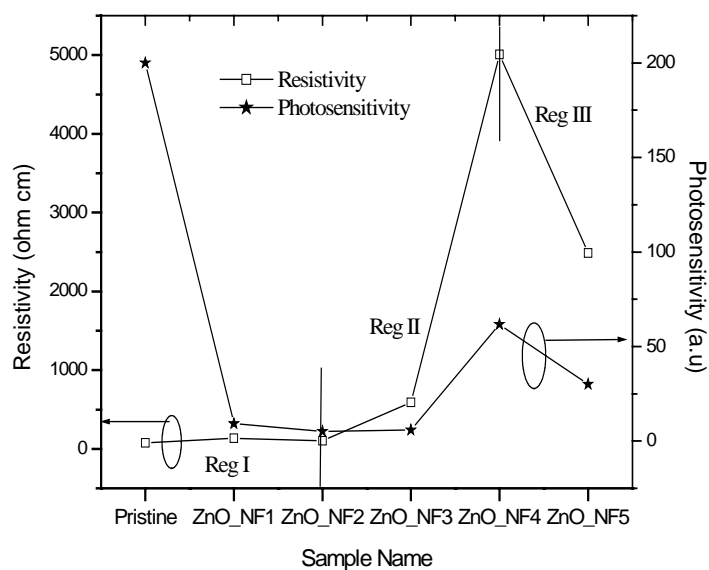
FIG. 3.21 Variation in resistivity and photosensitivity of ZnO films with Ni ion fluences.

3. 3. 4 TSC measurements

TSC measurements were done on pristine and two irradiated samples [Fig. 3.22]. TSC spectra obtained for pristine sample exhibited one peak. The defect level associated with this peak was determined

TSC glow curve of the pristine sample exhibited only one peak having an activation energy of 0.6 eV, which might be due to the defect level of Zinc interstitials (Zn_I) [25, 26]. Sample irradiated with a fluence of $3x10^{12}$ ions/cm^2 showed three peaks having activation energies 0.36 eV, 0.56 eV and 0.75 eV. Divalent zinc vacancy (V^{2-}_{Zn}) could provide donor states 0.4 to 0.7 eV below the conduction band [28]. Hence the activation energy of 0.36 eV from our study might be attributed to the donor state due to V^{2-}_{Zn}. The activation energy of 0.56 eV was attributed to zinc interstitials (neutral) that was present in the pristine sample also. A donor level was reported at 0.7 eV below the conduction band due to monovalent zinc interstitial (Zn^+_I) [28, 29]. Hence the level at 0.75 eV in the present study could be ascribed to the monovalent zinc interstitials.

When the sample was irradiated with a fluence of $3x10^{13}$ ions/cm^2, one peak was obtained corresponding to an activation energy of 1.28 eV, which was due to the oxygen vacancy, acting as donor level.

132
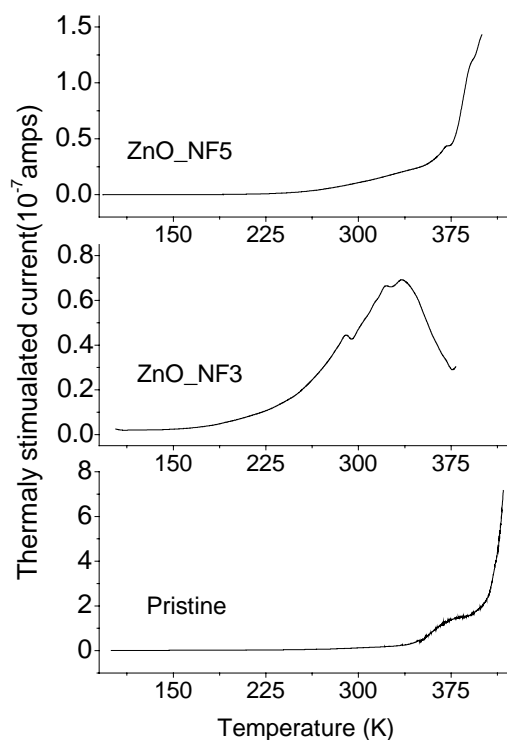
FIG. 3.22 TSC Glow curves of pristine and irradiated ZnO films.

3. 3. 5 Photoluminescence Studies

Photoluminescence measurements of irradiated samples were recorded [Fig. 3.23] and it depicted two emissions at 517 nm and 590 nm. The emission at 517 nm was due to oxygen antisite (O_{Zn}). The additional peak at 590 nm was having energy of 2.1 eV. A deep donor level was reported at 1.3 eV for ZnO. Earlier Xu et al theoretically predicted a level at 1.3 eV below the conduction band, corresponding to vacancy of oxygen [30]. Kasai had reported the defect state due to oxygen vacancy as a deep donor level [31]. Ortiz et al had also reported the level at 590 nm due to oxygen vacancy, in their spray pyrolysed ZnO thin films [32]. Hence we concluded

133

that the emission at 590 nm might be due to the transition from the level resulting from oxygen vacancy to the valence band.
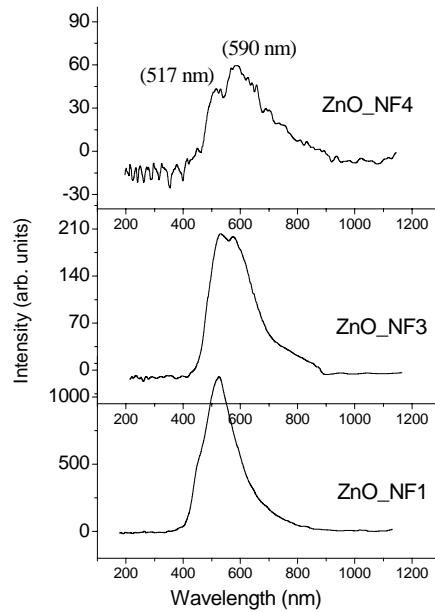
FIG. 3.23 Photoluminescence spectra of Ni irradiated ZnO

When the ion fluence increased, the intensity of the emission at 517 nm decreased while at 590 nm increased. At higher fluences, the intensity of the emission at 590 nm was greater than that of the emission at 517 nm. Finally for the sample ZnO_NF5, the emission at 517 nm completely vanished and the only emission was at 590 nm [Fig. 3.24]. The reduction in intensity of emission at 517 nm was also observed in the case of 120 MeV Au irradiated ZnO film. But the emission at 590 nm was totally absent in those samples. This might be due to the loss of emission property of ZnO due to the large defect density. According to SRIM calculation, 80 MeV Ni ions could create nearly 100 vacancies per ion during the irradiation. According to Van Vechten [33], for a compound to form a vacancy, the atom with the larger

134

covalent radius needed larger energy than that having the smaller radius. Covalent radii of Zn and O atoms were 1.25 Å and 0.73 Å in ZnO, and calculation showed that the energy to form zinc vacancy (5.41 eV) was greater than that of oxygen vacancy (3 e V). Thus, in the present study, the possibilities of forming oxygen vacancies were more during the nickel ion beam irradiation and this supported our arguments on the origin of emission at 590 nm.
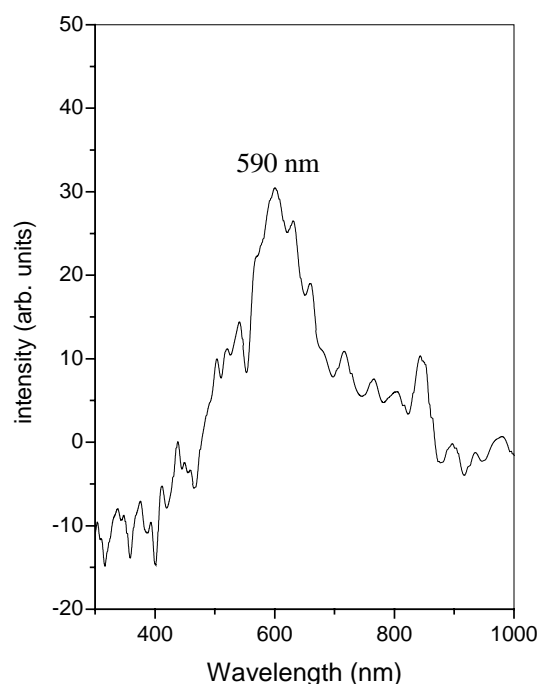
FIG. 3.24 PL spectrum of ZnO film irradiated with a fluence of 3×10^{13} ions/cm^2

3.4 Conclusion

ZnO thin films, prepared using CSP technique, were irradiated with 120 MeV Au ions and 80 MeV Ni ions. Both pristine and irradiated films were characterized using different techniques. It was observed that the impact on ZnO was more when irradiated with Au ions, probably due to higher energy and mass. When irradiated

with Au ions, crystalline quality of ZnO films got deteriorated very much while the crystallinity was slightly affected on Ni irradiation. Optical band gap remained at 3.3 eV even after the irradiation with both Au and Ni ions. However, the percentage of transmission was reduced with ion fluence in the case of Au ion irradiation while it was unaffected by Ni irradiation. Another interesting observation was related to the interference fringe like pattern of the transmittance curves. The fringe like pattern was completely lost when irradiated with Au ions. But it was almost unaffected by Ni irradiation. Interestingly electrical resistivity decreased drastically with ion fluence of Au ions, while it increased on Ni irradiation. XPS analysis performed on Au irradiated ZnO films, showed an increase in Zn/O ratio and this increase might be the reason for the enhanced conductivity of the film.

Pl emission of the pristine sample gave single emission at 517 nm, which was probably due to the transition from conduction band to the acceptor level due to antisite oxygen. This level was getting depleted on Au irradiation. However, when irradiated with Ni ions, the intensity of this emission decreased with increase in the ion fluence and another emission at 590 nm was also observed. This emission might be due to the transition from the deep donor level of oxygen vacancy to the valence band. TSC measurements, performed on the Ni irradiated samples, could also identify this level due to oxygen vacancy.

References

[1] B. Schattat and W. Bolse, Nucl. Instrum. Methods. Phys. Res. B **225**, (2004) 105.

[2] P. Sathyavathi, S. T. Chavan, D. Kanjilal and V. N. Bhoraskar, Nucl. Instrum. Methods. Phys. Res. B **156**, (1999) 72.

[3] D. C. Ingram and A. W. McCormick, Nucl. Instrum. Methods. Phys. Res. B **34**, (1988) 68.

[4] A. Benyagoub, F. Couvreur, S. Bouffard, F. Levesque, C. Dufour and E. Paumier, Nucl. Instrum. Methods. Phys. Res. B **175**, (2001) 417.

[5] C. Gilbert- Mougel, F. Couvreur, J. M. Costantini, S. Bouffard, F. Levesque, S. Hemon, E. Paumier and C. Dufour, J. Nucl. Mater. **295**, (2001) 121.

[6] S. Nakao, K. Saitosh, M. Ikeyama, H. Niwa, S. Tanemura, Y. Miyagawa and S. Miyagawa, Thin Solid Films **281**, (1996) 10.

[7] S. Balamurugan, B. R. Mehta, D. K. Avasthi, F. Singh, Akhilesh. K. Arora, M. Rajalakshmi, G. Raghavan, A. K. Tyagi and S. M. Shivaprasad, J. Appl. Phys. **92**, (2002) 3304.

[8] M. S. Kamboj, G. Kaur, R. Thangaraj and D. K. Avasthi, J. Phys. D; Appl. Phys. **35**, (2002) 477.

[9] P. Shah, S. Kumar, A. Gupta and D. K. Avasthi, Nucl. Instrum. Methods. Phys. Res. B **156**, (1999) 222.

[10] M. Levalois and D. Marie, Nucl. Instrum. Methods. Phys. Res. B **156**, (1999) 64.

[11] B. W. Thomas and D. Walsh, J. Phys. D: Appl. Phys., **6,** (1973) 612.

[12] S. Kohiki, M. Nishitani, T. Wada and T. Hirao, Appl. Phys. Lett., **64,** (1994) 2876.

[13] I. Sakaguchi, D. Park, Y. Takata, S. Hishita, N. Ohashi, H. Haneda and T. Mitsuhashi, Nucl. Instr. and Meth. B **206,** (2003) 153.

[14] T. Fukudome, A. Kaminaka, H. Isshiki, R. Saito, S. Yugo and T. Kimura, Nucl. Instr. and Meth. B **206,** (2003) 287.

[15] K. Kono, S. K. Arora and N. Kishimoto, Nucl. Instr. and Meth. B **206,** (2003) 291.

[16] E. Alves, E. Rita, U. Wahl, J. G. Correia, T. Monteiro, J. Soares and C. Boemare, Nucl. Instr. and Meth. B **206,** (2003) 1047.

[17] S. O. Kucheyev, C. Jagadish, J. S. Williams, P. n K. Deenapanray, M. Yano, K. Koike, S. Sasa, M. Inoue and K. Ogata, J. Appl. Phys., **93,** (2003) 2972.

[18] I. Sakaguchi, Y. Sato, D. Park, N. Ohashi, H. Haneda and S. Hishita, Nucl. Instr. and Meth. B **217,** (2004) 417.

[19] N. Matsunami, O. Fukuoka, M. Tazawa and M. Sataka, Surf. Coat. Technol., **196,** (2005) 50.

[20] D C Look, D C Reynolds, J W Hemsky, R L Jones and J R Sizelove, Appl. Phys. Lett., **75,** (1999) 811.

[21] D. C. Reynolds, D. C. Look, B. Jogai and H. Mokoc, Solid State Commun. **101**, (1997) 643.

[22] N. Y. Garces, L. Wang, L. Bai, N. C. Giles, L. E. Halliburton and G. Cantwell, Appl. Phys. Lett. **81**, (2001) 2285.

[23] S. A. Studenikin, N. Golego and M. Cocivera, J. Appl. Phys. **84**, 2287 (1998).

[24] P. S. Xu, Y. M. Sun, C. S. Shi, F, Q, Xu and H. B. Pan, Nucl. Instrum. Methods.Phys. Res. B, **199**, (2003) 286.

[25] B. Lin, Z. Fu and Y. Jia, Appl. Phys. Lett. **79**, (2001) 943.

[26] Y. M. Sun, Ph.D thesis, University of Science and Technology of China, July 2000.

[27] Y. G. Wang, S. P. Lau, X. H. Zhang, H. W. Lee, H. H. Hng, B. K. Tay, J. Crystal Growth **252,** (2003) 265.

[28] C. X. Xu, X. W. Sun, X. H. Zhang, L. Ke and S. J. Chua, Nanotechnology**, 15**, (2004) 856.

[29] S. A. M. Lima, F. A. Sigoli, M. Jr. Jafelicci and M. R. Davolos, Int. J. Inorg. Mater. **3,** (2001) 749.

[30] P. S. Xu, Y. M. Sun, C. S. Shi, F. Q. Xu and H. B. Pan, Nucl. Instru. Meth. B **199,** (2003) 286.

[31] P. H. Kasai, Phys. Rev. **130,** (1963) 989.

[32] A. Ortiz, C. Falcony, A. J. Hernandez, M. Garcia and J. C. Alonso, Thin Solid Films **293,** (1997) 103.

[33] J. A. Van Vechten, J. Electrochem. Soc. **122,** (1975) 419.

ON THE PROPERTIES OF INDIUM DOPED ZnO THIN FILMS

4.1 Introduction

Addition of 'impurities' to a wide band gap semiconductor often induces dramatic changes in electrical and optical properties. Doping of ZnO is achieved by replacing Zn^{2+} atoms with the atoms of elements of higher valency, in order to improve the electrical conductivity. Efficiency of the dopant elements depends on its electro negativity and the difference between ionic radius. A precise study on the properties of doped film is essential to control the doping parameters, and this is indispensable for optoelectronic device applications. Again the technique we used for film preparation is very simple viz CSP technique. It is rather easy to vary the doping concentrations in this technique and hence to adjust the properties of the films. Several reports are available on the properties of indium doped ZnO thin films. Indium was proved to be one of the best candidates for making ZnO low resistive. When ZnO is doped with group III elements, such as Al, Ga or In, it is expected that the dopants act as singly charged donors by substituting Zn. The excess carriers supplied by the impurities to the conduction band contribute to the increase of the electrical conductivity of ZnO.

Major et al investigated the optical and electronic properties of Indium doped ZnO thin films, prepared using chemical spray pyrolysis in detail and optical constants were calculated using specular reflectance and transmittance data [1]. They found that these values were well correlated with those obtained for single crystal ZnO. Drude model was used to explain the optical behavior in the IR region. Films doped with 3 at % In was found to be thermally stable up to 650K in vacuum and 450 K in oxygen ambient. Lowest resistivity ($1.1x10^{-3}$ ohm cm) was obtained for the film doped with 3 at % indium. Dependence of resistivity (ρ), carrier concentration (N) and mobility (μ) on the film thickness was also subjected to the study and they concluded that both N

and µ were increasing with film thickness up to 400 nm, beyond which, both tend to saturate.

Major et al has reported the deposition of low resistive ZnO films with indium doping [2]. Spray pyrolysis technique has been used for the deposition and they could attain a resistivity of (8-9) $\times 10^{-4}$ ohm cm without any post deposition heat treatment. Zinc acetate dissolved in isopropyl alcohol and water and indium chloride were used as precursors. Both undoped and doped films were characterized using different techniques like XRD, Electron diffraction, optical transmission and Hall Effect measurements etc. These films exhibited an average visible transmittance of about 85%. Indium concentration was found to be the most critical parameter to affect the electrical properties of the films. Carrier concentration was increased with Indium concentration up to 2 at % In and beyond this, it saturated at ~ 4×10^{20} cm^{-3}. However mobility initially decreased with indium concentration, passed through a minimum and then increased sharply to saturate at about 15 cm^{2}V^{-1}s^{-1}. The electron transport properties were also discussed and were consistent with the 'grain boundary trapping model'. They suggested that that the samples were degenerate.

Major et al also investigated the thickness dependent properties of indium doped ZnO thin films [3]. It was found that, the density of trap states, due to chemisorbed oxygen at the grain boundaries, depended on the orientation of grains, which in turn, depended on the film thickness. The changes in the electrical parameters of vacuum annealed films were attributed to the decrease in grain size while the shift in optical band gap was attributed to the changes in carrier concentration.

In a short communication, Shih et al reported the successful deposition of low resistive indium doped ZnO film, using rf sputtering for the first time [4]. 'Electron probe microanlysis' was carried out to determine the indium concentration in the film.

Another report on the indium doped ZnO films was given by Qiu et al [5]. RF sputtering technique was used for the deposition of the film having resistivity as low as 3×10^{-4} ohm cm. ZnO containing 2 wt % In_2O_3 was used as the target material and glass substrates were held in vertical position. Substrate temperature was between 200 and 350°C. They found that, when substrates were held in horizontal position, the resisitivity was $\sim 3 \times 10^{-3}$ ohm cm. However these low resistive films were found to be unstable in air even at 200°C.

Wang et al prepared Indium doped ZnO powder, having conductivity of 30 (ohm cm)$^{-1}$ [6]. Using 'Time differential perturbed angular correlation (TDPAC)' spectroscopy, they showed that indium was at normal zinc sites. Another conclusion from this study was that, zinc interstitial were not ionized and therefore did not contribute significantly to the conductivity.

Structural and electrical characterization of indium doped ZnO thin films prepared using spray pyrolysis technique were reported by Maldonado et al [7]. They used zinc acetate and indium nitrate as precursors and substrate temperature was varied from 675 to 800 K. By using indium nitrate instead of indium chloride for doping, the unintentional doping of chlorine in the film was avoided. The lowest resistiviy value of 6×10^{-3} ohm cm was obtained for the sample prepared at 775 K and these films showed an average transmittance of around 85% in the visible region. Both doped and undoped films were polycrystalline with preferential orientation along (101) plane except at lower substrate temperature [<700 K]. At those temperatures, there was significant contribution in the (002) direction.

Optical and electrical characterization of indium and Aluminum doped ZnO thin films, prepared using dc reactive magnetron sputtering, were reported [8]. Substrate temperature was kept at 573 K. Here the lowest resistivity obtained was 4.0×10^{-4} ohm cm for the Al-doped films. In-doped films were having a resistivity of 8.7×10^{-4} ohm cm. Average optical transmittance was above 85% in the visible range.

Zironi et al reported the deposition of low resistive In-doped ZnO using spray pyrolysis technique, in which zinc acetate and different salt solutions of indium were used as the precursor solutions [9]. Indium acetate, indium sulfate and indium nitrate were used with different concentrations. Al the films were polycrystalline with preferential growth along (101) plane. Lowest resistivity ($2x10^{-3}$ ohm cm) was obtained when indium acetate was used as the precursor at 3 at % concentration of Indium.

Maldonado et al also investigated the effects of pH on the physical properties of indium doped ZnO films using spray pyrolysis deposited over glass substrates at 500°C [10]. pH was varied by varying the concentration of acetic acid in the solution. Electrical resistivity decreased with decrease in the pH while surface texturing increased on increasing the pH. X-ray diffraction pattern showed (002) to be the preferential orientation for pH = 3.2, while it showed (002) and (101) to be the preferential orientation at pH= 3.8. The results were discussed on the basis of the chemical species involved in the solution.

Yoshida et al reported the structural and morphological properties of indium doped ZnO thin films prepared using spray pyrolysis technique [11]. Zinc acetate and indium acetate were used as the precursors. Different substrates like alumina, soda lime glass and sodium chloride crystal were used for the film deposition. Scanning Electron Microscopy (SEM) and Transmission electron Microscopy (TEM) were used to study the microstructure of the film. Energy dispersive spectroscopy and Rutherford backscattering technique were used to determine the film composition. Reitveld refinement methods were used to analyze X-ray diffraction pattern. Films doped with lower indium concentration showed a preferential orientation along (002) plane, while higher doping concentration changed the preferential orientation to the (101) plane.

Kim et al reported the variations in the optical absorption properties of In-doped ZnO films due to the changes made in the carrier concentration, analysed using 'spectroscopic ellipsometry' [12]. In this work, the films were deposited over Al_2O_3 (0001) substrates, kept at 500°C, using rf magnetron sputtering technique. Optical band gap of doped film shifted to higher energies for $N < 5 \times 10^{19}$ cm^{-3} and to lower energies for $N = 1.2 \times 10^{20}$ cm^{-3}. Band gap shift to higher energy side was explained in terms of the 'Burstein-Moss band filling effect' and the abrupt jump of the band edge from blue to red, was attributed to 'impurity induced potential fluctuations'.

Another interesting result was obtained when zinc acetyl acetonate and indium chloride were used as precursors for the spray pyrolysis [13]. Effects of substrate temperature, dopant concentration and the solvent alcohols were analysed in the study and the optimum deposition conditions (ethanol as solvent alcohol, substrate temperature 475°C and indium concentration 2.5 at %) for getting film of resistivity of 2.8×10^{-3} ohm cm, mobility of 5 $cm^2/V\text{-}s$ and carrier concentration of 10^{20} cm^{-3} were identified. Effect of solvent alcohol on surface roughness was also studied and found that smooth film with small grains was obtained when methanol was used as the solvent. Use of isopropyl alcohol resulted in a rough surface and this kind of variation was explained in terms of the boiling point (B.P.) of alcohols. The reported B.P of methanol, ethanol and isopropyl alcohol were 65, 78.5 and 82°C, respectively and hence methanol evaporated more rapidly than the others.

Effect of substrate temperature on the structural, electrical and optical properties of indium doped ZnO thin films, prepared by the pyrosol process was given by Tokumoto et al [14]. At a substrate temperature of 450°C, these films showed the lowest resistivty of 6×10^{-3} ohm cm and a blue shift in optical band gap (3.29 to 3.33 eV) was observed with the increase in the substrate temperature.

In another similar report, Maldonado et al presented the morphological and optical properties of In:ZnO prepared using Spray Pyrolysis technique; here also zinc

acetyl acetonate was used as the precursor for zinc [15]. Effect of solvent alcohol was also a subject of this study and they found that films had better transmittance when methanol was used as the solvent. Films deposited using methanol and isopropyl alcohol showed preferential growth along (101) planes, while ethanolic solution showed a significant contribution of the (002) plane along with (100) planes. Resisitivity of 3×10^{-3} ohm cm, mobility of 6 cm^2/Vs and carrier concentration of 10^{21}cm^{-3} were obtained for the best film. Optical transmittance was about 85% for all the samples and band gap was remained at 3.3 eV.

In an unpublished work, Rahman et al investigated the electrical and optical properties of indium doped zinc oxide thin films [16], deposited using magnetron sputtering. Both undoped and doped films were showing preferential orientation along (002) plane. An optical band gap of 3.63 eV and a lowest resistivity of 10^{-2} ohm cm were obtained, when doped with 1.8 at % In. The observed large band gap was explained in terms of Burstein Moss shift.

Recently, Eliwa et al discussed the effect of indium doping on the physical properties of spray pyrolysed zinc oxide films. InCl$_3$ and zinc acetate were used as the precursors for the deposition of the film [17]. Undoped films showed preferential growth along (002) plane while doping reduced the intensity of this peak; three additional peaks corresponding to the planes (100), (101) and (110) also appeared. Band gap remained unaffected (3.26 eV) and lowest value of resistivity (2.2×10^{-2} ohm cm) was obtained at 2 % In. Film composition was obtained using EDX technique. Refractive index was determined from the optical transmission curve and it varied in the range 1.7 – 2, which was suitable for antireflection coating materials.

Very recently, Savchuk et al deposited indium doped ZnO thin films using pulsed laser deposition [18]. They studied the influence of deposition parameters like substrate temperature and oxygen partial pressure on the electrical and optical parameters of both doped and undoped films. Amorphous films were obtained when

deposited at room temperature and showed polycrystalline nature at 400°C. Films were showing an average optical transmittance of about 85% in the visible region when substrate temperature was 480°C and oxygen pressure, (4-8) x10^{-2} Torr. Lowest resistivity value obtained was 10^{-1} ohm cm, when substrate temperature kept at 480°C and oxygen pressure at 10^{-3} Torr. With increase in oxygen pressure, resistivity increased. Doped films showed green luminescence and the intensity of the emission exhibited dependence on the concentration of the doping atoms. The maximum emission occurred at 3.5 mol% concentration of In atoms in the film.

In another recent report, Machado et al reported the deposition of indium doped films by electro deposition over Cu substrates, using $Zn(NO_3)_2$ and $InCl_3$ as the electrolytes [19],and keeping the pH of the solution at 2.5 and deposition temperature at 80°C. Compositional analysis was done using EDS and XPS techniques to confirm the presence of indium in the film. Undoped film was showing a preferential orientation along (002) plane and it diminished with increase in the indium concentration. Grain size of all the samples was greater than 50 nm and the presence of indium improved the grain size. Optical band gap was in the range of 3.27 to 3.42 eV and absorption edge was sharper in the case of undoped samples. Widening of the band gap was attributed to Burstein- Moss shift.

In another recent paper from Lopez et al, reported the preparation of indium doped ZnO thin films using Chemical Spray technique [20]. Substrate temperature and molar concentration of precursor solution were varied and films were characterized structurally, electrically and optically. Lowest resistivity obtained was 3x10^{-3} ohm cm with high molar concentration of the solution (>0.4M). All the films had the preferential orientation along (101) plane.

In this chapter, effects of indium doping on structural, electrical and optical properties of spray pyrolysed ZnO thin films are described. We doped the ZnO films using indium in two different ways. First, indium chloride solution was added to the

zinc acetate solution and in next process, indium was thermally diffused in to the ZnO thin films. This was to avoid the presence of chlorine. Unintentional doping of chlorine occurred when indium was doped in the form of indium chloride.

4.2.Experimental Details

Indium was introduced in the film through indium chloride solution. Indium chloride solution (0.6 M) was added to the zinc acetate solution with different concentration to see the effects of variation of indium in ZnO films. All other preparation conditions were kept the same. Samples were named as ZnO_0.5In, ZnO_1In, ZnO_3In and ZnO_5In, implying different doping percentage 0.5 at %, 1 at %, 3 at % and 5 at % respectively.

Indium was also doped using thermal diffusion of evaporated indium into the ZnO thin films. For this, thin layer of indium was deposited using vacuum evaporation technique (pressure during evaporation was ~2×10^{-5} Torr) and subsequent annealing at 100˚C in vacuum, resulted in the diffusion of whole indium into the film. Four different masses of indium (3, 5, 8 and 10 mg) were evaporated for doping different sets of ZnO films. These doped samples were named as ZnO:3In, ZnO:5In, ZnO:8In and ZnO:10In respectively. Thickness of the ZnO film used was measured using Stylus thickness profiler and it was equal to 540 nm. It was assumed that evaporation of indium and successive annealing did not modify the thickness of ZnO films considerably.

Inorder to reduce the resistivity further, indium was introduced in the form of indium nitrate and followed by the diffusion of metallic layer of indium. For this, indium nitrate was added to the zinc acetate solution with two different concentrations (1 and 1.5 at %) and sprayed at 673 K. All other preparation conditions were kept as the same for pristine samples. Over these samples, thin layer of metallic indium was deposited and then annealed at 673 K to diffuse indium (In) into ZnO. Two different quantities of In (5 mg and 8 mg) were evaporated. Samples were named as

ZnO_1InN, for the samples doped with 1 at % indium nitrate, while ZnO_1InN:A represents the annealed samples. ZnO_1InN:5In stands for the samples diffused (at 673 K) with 5 mg of indium. The effect of vacuum annealing of as-prepared (without indium diffusion) sample on the electrical resistivity was also studied. These samples were named as ZnO_1InN:A and ZnO_1.5InN:A, implies ZnO films with 1 at % In and 1.5 at % respectively. Characterization techniques used, were XRD, XPS, optical studies and electrical resistivity measurements.

4.3 Results and discussions

4.3.1. Indium Doping through indium chloride

4.3.1.1 Structural Analysis

Incorporation of indium, through the solution used for deposition, changed the structural properties of the films (Fig. 4.1). Undoped ZnO film showed a preferential orientation along (002) plane at $2\theta = 34.7°$. The'd' values were compared with standard JCPDS data card (79-0207). A weak XRD peak was observed at $2\theta = 36.55°$, d = 2.457 corresponding to the plane (101). When indium was incorporated in the film, the intensity of the peak corresponding to the plane (002) decreased and that of (101) increased. When doped with 3 at % In, an additional peak at $2\theta = 31.60°$, d = 2.825 corresponding to the plane (100) appeared and very small preferential growth along (101) plane was also observed. Peak position of the plane (002) remained the same even after the heavy doping, which implied that the lattice strain along c axis was unaffected by the indium doping. But crystallinity reduced enormously.

Grain size of the films decreased with doping concentration as depicted in Table 4.1
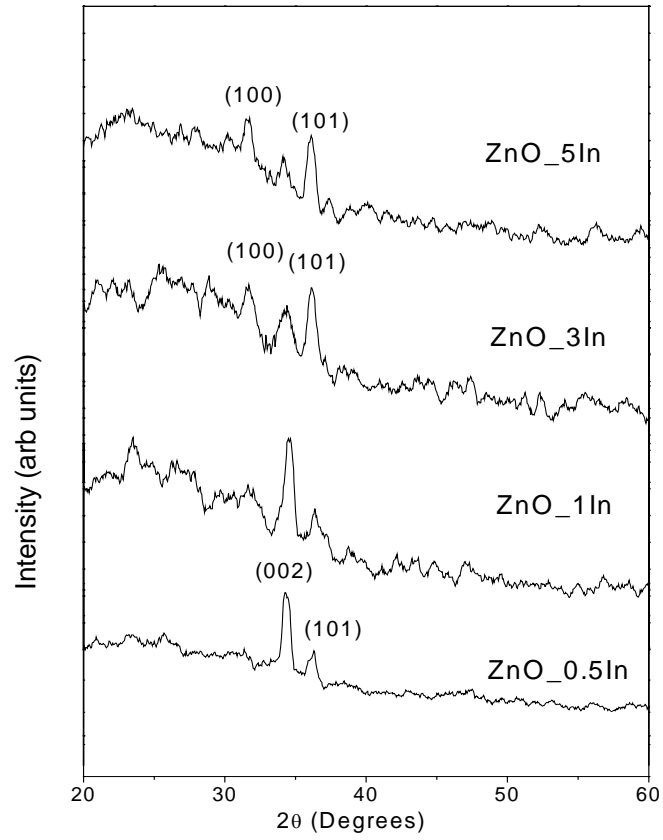
FIG. 4.1 XRD pattern of indium doped ZnO thin films

Table 4.1 Variation in structural parameters with indium concentration

Sample Name	Preferential Orientation	FWHM (degrees)	Grain size (Å)
Undoped	(002)	0.323	261.0
ZnO_0.5In	(002)	0.392	212.3
ZnO_1In	(002)	0.434	191.7
ZnO_3In	(101)	0.494	169.2
ZnO_5In	(101)	0.542	154.2

Scanning Electron Micrographs showed a close packed morphology for both undoped and In-doped films; decrease in grain size with doping was clearly seen in micrographs (Fig. 4.2 and 4.3). SEM micrograph of undoped sample showed plaquet-like grains with textured surface for undoped ZnO film. It was been reported that the textured morphology was a consequence of the nucleation of oriented c- axis grains that grew geometrically and impinge laterally [21]. ZnO thin films prepared using r.f. Sputtering also exhibited preferential c-axis orientation and textured surface morphology [22] as we observed in our spray pyrolysed sample. Hence one can observe a good similarity (through XRD studies and SEM studies) between ZnO samples prepared using CSP and r f sputtering.
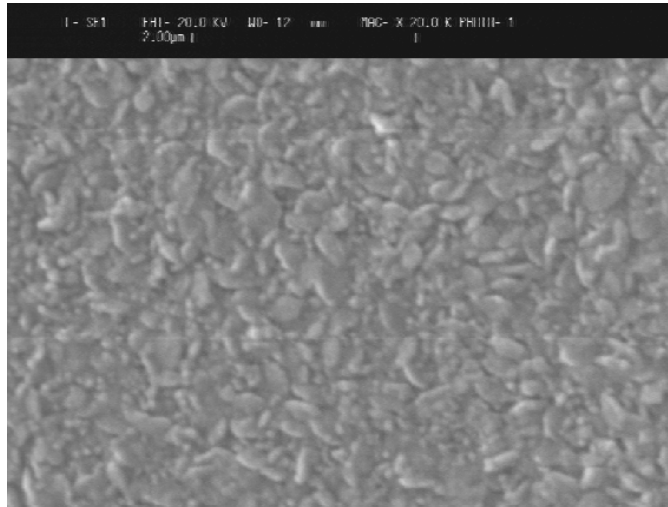
FIG. 4.2 SEM micrograph of undoped ZnO
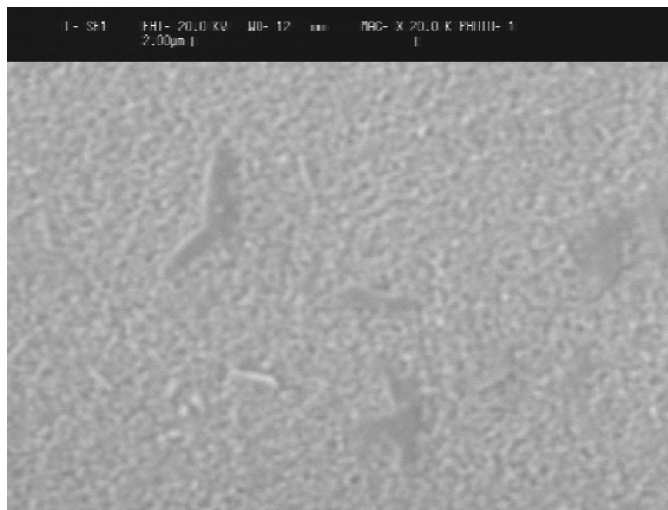
FIG. 4.3 SEM image of ZnO_3In

4.3.1.2 Optical Studies

Figure 4.4 depicts the absorbance in the UV-Vis regions of ZnO films and it was clear that there was almost no optical absorption in the visible region. Here thickness did not affect the optical absorption significantly. The band to band excitation for ZnO corresponded with the charge transfer from O^{2-} to Zn^{2+}, because

the valence and conduction bands mainly consisted of the orbital of oxygen and zinc atoms, respectively. It could be observed that UV region of the absorbance versus wavelength graph showed a 'split peak'. This might be due to the presence of metallic zinc as interstitial atoms in the lattice of ZnO crystallites and resulted in distortion of crystallites Therefore, the Zn^{2+} with d electron energy level could be split by the effect of crystal field, resulting in the split peak in the UV spectrum [21]. Beyond the absorption edge at the UV end of absorption graph, transmittance was reduced to zero for both undoped and doped films. The energy, at which oxygen and metal transfer occurred, had dependence on the cation and the symmetry of its coordination site [21]. Figure was not symmetric for the undoped film, [indicating less transfer of charge between oxygen and zinc] and symmetric for lightly doped (ZnO_1In) film [indicating charge transfer between oxygen and zinc]. The symmetric nature was again decreasing for higher doping levels, indicating the decrease in the charge transfer. The symmetry of absorbance spectrum could be related to the transfer of electrons to conduction band and hence with the variation in resistivity.
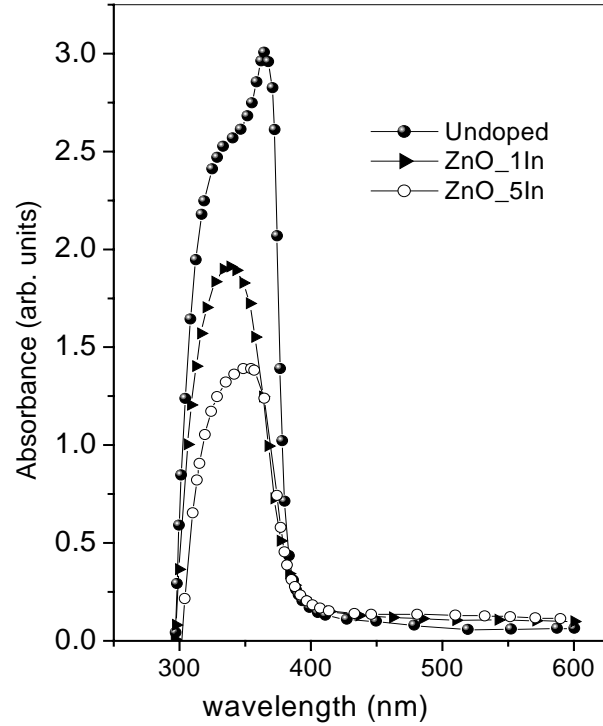
FIG. 4.4 Absorption spectra of undoped and doped ZnO thin films

Optical transmittance spectra of doped and undoped ZnO films were recorded in the wavelength region 350 - 1500 nm (Fig. 4.5). Undoped and lightly doped samples showed interference fringe pattern in transmission spectrum. It was very clear from the transmittance spectra that the indium doped ZnO films had better transparency than pure ZnO films (80% at 540 nm for undoped ZnO and 91% at 540 nm for ZnO_0.5In), except at high doping levels. Interference fringes of transmittance curve revealed that the film surface was highly reflecting without much scattering or absorption loss in the films. When the doping concentration increased, the amplitude of the fringe pattern became smaller and finally flat for the sample having 5 at % indium concentration. This might be due to the formation of grainy surface leading to large scattering loss. Film thickness and refractive index could be calculated using the

152

procedure developed by Swanepol from transmission spectra, which was described elsewhere in detail [23]. Thickness, measured using Stylus thickness profile was in very good agreement with the calculated value from the transmittance spectra. Refractive index was in the range of 1.7-1.85. Band gap was determined from the $(\alpha h\nu)^2$ versus $h\nu$ graph [Fig. 4.6] and also from the transmission curve. The band gap was slightly higher than that of the undoped samples (3.3 eV) and itincreased with the increase in the doping concentrations. This small widening might be due to low crystallinity and also due to increase in carrier concentration.
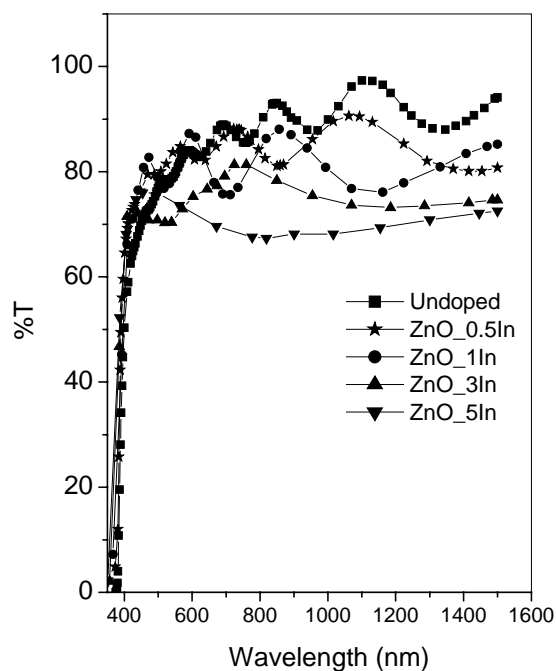
FIG. 4.5 Transmission spectra of ZnO (doped and pure) thin films
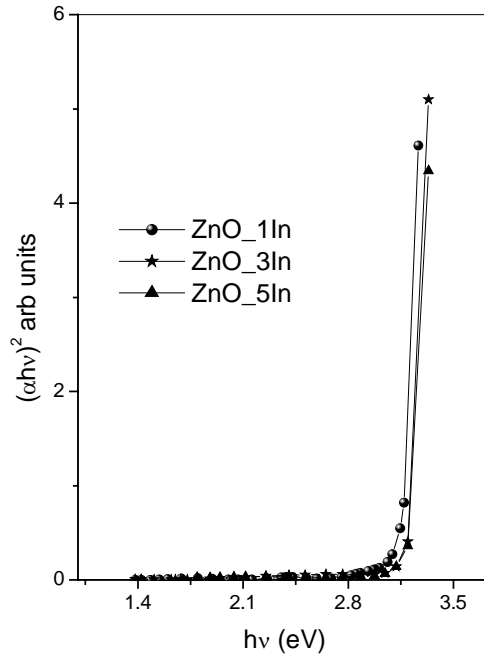
FIG. 4.6 $(\alpha h\nu)^2$ versus $h\nu$ graph for the indium ZnO doped thin films

4.3.1.3 XPS Analysis

XPS analysis was done on In-doped ZnO films [Fig. 4.7]. Here bottom portion of the figure represented the surface of the film and at the top, it was the substrate. Results indicated that zinc and oxygen were uniformly distributed throughout the depth in both doped and undoped samples. Both Zn and O atoms diffused a little into the glass substrate at lower indium concentration, while diffusion of Zn was large at higher doping concentrations. But O and In did not at all diffused into the substrate. Binding energies of zinc and oxygen clearly indicated formation of zinc oxide (1022.95 eV for $Zn3P_{3/2}$ and 531.02 eV for O1s). Atomic concentration of zinc and oxygen was determined and Zn/O ratio in the undoped sample was equal to 1.77. From the XPS spectra of lightly doped ZnO films, no obvious peaks for Indium oxides or $In(OH)_3$ were observed [Fig. 4.8].

154
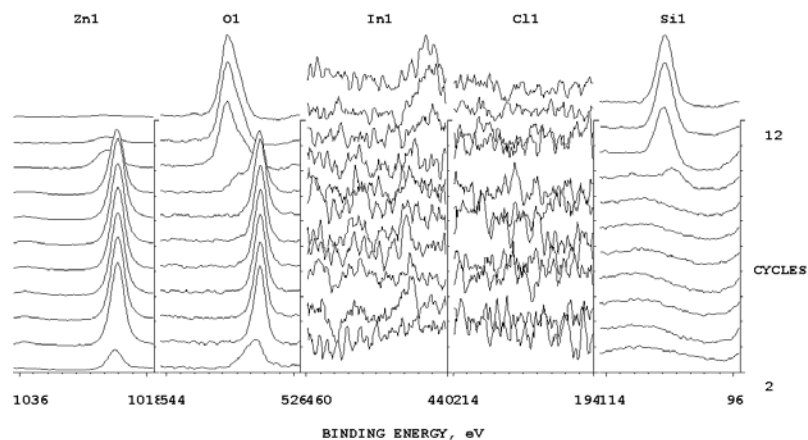
FIG. 4.7 XPS depth profile of ZnO_0.5In

But for the heavily doped (ZnO_3In and ZnO_5In) films indium was present in both elemental (452.7 eV) and in $In(OH)_3$ (445.38 eV) form and moreover chlorine was also present (200 eV) in elemental form. Atomic concentration profile of a typical indium doped (ZnO_3In) sample is given in a separate figure [Fig.5.9]. In/Zn ratio was calculated for the sample ZnO_3In and ZnO_5In and it was nearly equal to 0.026 and 0.034 respectively.
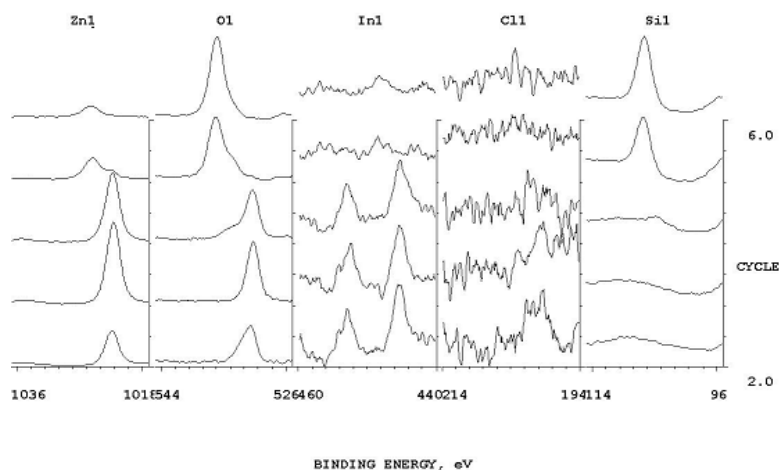
FIG. 4.8 XPS depth profile of ZnO_3In.

155
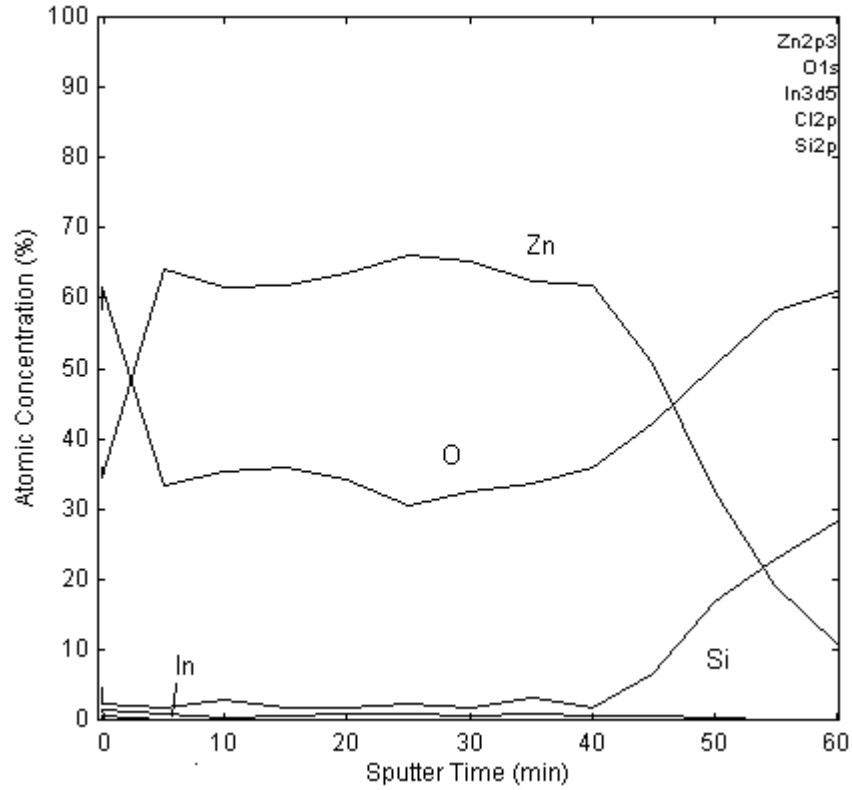
FIG. 4.9 Atomic concentration graph of ZnO_3In

4.3.1.4 Electrical Resistivity Measurements

Electrical resistivity measurements were carried out using four-probe method and values are tabulated [Table 4.2]. Undoped sample had resistivity of 78 Ω-cm. This low value of resistivity may be due to the formation of metal rich films (Zn/O ratio was 1.77).

Table 4.2 Electrical and opto electronic parameters of ZnO:In thin films

Sample Name	Resistivity (ohm cm)	Photosensitivity $((I_L-I_D)/I_D)$	Figure of Merit (Ω^{-1})
Undoped	78.1	200.9	8.4×10^{-5}
ZnO_0.5In	22.9	1.53	2.14×10^{-4}
ZnO_1In	19.4	5.65	2.42×10^{-4}
ZnO_3In	29.9	6.23	1.45×10^{-4}
ZnO_5In	85.8	2.68	5.74×10^{-5}

An initial decrease in the value of resistivity was observed with doping concentration and then the value increased. With doping concentration, grain size was decreasing. Hence grain boundary scattering might have increased. But an initial decrease in resistivity was also observed. Initially doped indium ions (In^{3+}) might have substituted Zn^{2+} sites or gone to the interstitial positions leading to the release of free carriers. However at higher doping concentration, the availability of chlorine atoms in the sample was also increasing, which was observed in XPS spectra of heavily doped films [Fig.4.8]. This chlorine could very well act as a trap for electrons or even as recombination centre, leading to an increase the resistivity. We observed a similar increase in resistivity due to the presence of Cl in In_2S_3 thin films, prepared using spray pyrolysis with indium chloride as precursor solution. In comparison, the samples prepared using indium nitrate (avoiding Cl), were less resistive [24].

In the case of a transparent conducting oxide film, both optical transmission and electrical conductivity should be as large as possible for applications in optoelectronic devices. A way for evaluating this is through the 'figure of merit' defined as $\Phi_{TC} = T/R_s$, where R_s is the sheet resistance of the film and T is optical transmittance [25]. Figure of merit was calculated for all samples at $\lambda = 543$ nm and it

is given in Table 2. The highest value of $\Phi_{TC} = 2.42 \times 10^{-4} \Omega^{-1}$ was obtained for ZnO_1In.

4.3.1.5 Photosensitivity Measurements

Photosensitivity (defined as I_L-I_D)/I_D where I_L is illuminated current and I_D is the dark current) measurements were done and the results are depicted in Table 2. Maximum photosensitivity was obtained for the undoped sample (200.9) and this decreased with indium concentration. Photosensitivity of doped sample, (even when having its resistance was greater than the undoped sample), was still lower than that of undoped sample. This may be due to the loss of photo generated minority carriers at grain boundaries [as result of bulk recombination; as the grain size decreased after the introduction of $InCl_3$, this might have increased] or through the chlorine atoms acting as recombination centres.

4.3.1.6 Photoluminescence Measurements

PL spectra of undoped and doped ZnO films were recorded at room temperature (Excitation wavelength - 325 nm). Undoped sample exhibited a very broad high intensity peak, centered at 517 nm, corresponding to the well known 'blue-green emission'. Three additional emissions at 408, 590 and 688 nm were also observed in the In-doped samples [Fig. 4.10]. When indium was doped in the film, it was assumed that, some of the indium atoms occupied the zinc lattice site, reducing the probability of oxygen occupying the zinc sites. Hence the density of oxygen antisites would be less in the film. This might be the reason for the decrease in intensity of the blue-green emission due to doping. Resistivity of the film decreased with the indium doping at low concentration, which proved the occupancy of indium at zinc site. [Our suggestion on the origin of emission at 517 nm was already given in chapter 3] This observation might be a support to the argument on the origin of blue-green emission.
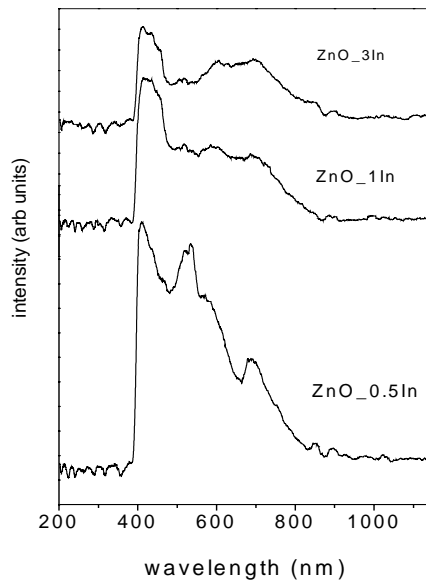
FIG. 4.10 PL spectra of indium doped ZnO with different indium concentration.

The violet emission was probably due to the radiative defects related to the interface traps existing at the grain boundaries and emitted from the radiative transition between this level and valence band [26]. Sample ZnO_0.5In, had smaller grain size and larger grain boundary area, and therefore this sample was emitting the violet luminescence with intensity. But the emission from the sample having higher indium concentrations might not be detected effectively, since the grains were not preferentially oriented [26]. Hence a decrease in the intensity of violet emission was observed for heavily doped film (ZnO_3In). Emission corresponding to 590 nm might be due to the localized state introduced by the indium impurities [27]. Peak at 688 nm was corresponding to the oxygen -interstitial related visible emission [28]. Even though doping did not create this level, we could not observe this emission in undoped film. This might be due to the very high intensity of blue green emission. Doping

caused the weakening of blue green emission making the emission at 688 nm more evident.

4.3.1.7 Temperature dependent Conductivity measurements

Temperature dependence of electrical conductivity of the samples was measured in the range 100 – 300 K. [Fig 4.11]. Sample was placed on cold finger of liquid helium cryostat using thermal grease to avoid any thermal gradient along or across the sample. Cryostat was evacuated to a pressure of 10^{-5} mbar. We obtained two activation energies 148 meV and 65 meV for the undoped samples. The existence of an intrinsic donor level, in the range150 to 170 meV, below the conduction band was reported earlier [29]. There were also reports on theoretical calculations of another native donor, with activation energy 61 meV, that originated from octahedral zinc interstitials [30]. These values were in good agreement with our experimental data. When ZnO was doped with indium, two activation energies (~ 30 meV and ~ 15 meV) were obtained for 0.5 at % and 5 at % indium. The activation energy of 30 meV was identified as due to tetrahedral zinc interstitials and we suspect that the shallow donor level at 15 meV might be due to indium at interstitial position. For moderately doped samples, the level at 30 meV disappeared, while the level at 15 meV was remaining.
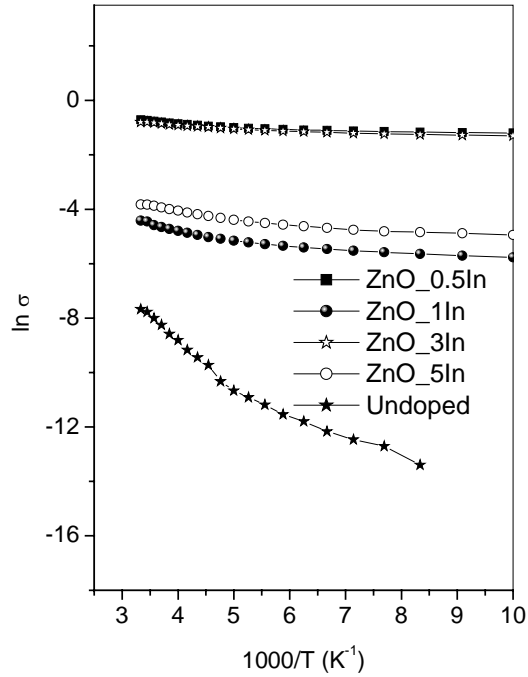
FIG. 4.11 Arrehenius plot of In-doped ZnO thin films.

4.3.1.8 *Effect of Vacuum Annealing*

In order to reduce the resistivity of the doped films further, the lowest resistive film, ZnO_1In was annealed at 673 K. Crystallinity improved after annealing [Fig. 4.12]. Grain size was 191.7 Å for the unannealed sample while it was 284Å for the annealed sample. Electrical resistivity also reduced drastically after annealing and it was equal to 1.5×10^{-2} Ω cm. The reason for this drastic decrease in resistivity might be due to the increase in grain size and hence the reduction in grain boundary scattering. Another reason may be attributed to desorption of oxygen leading to the annihilation of oxygen acceptor states at the grain boundaries [31].

161
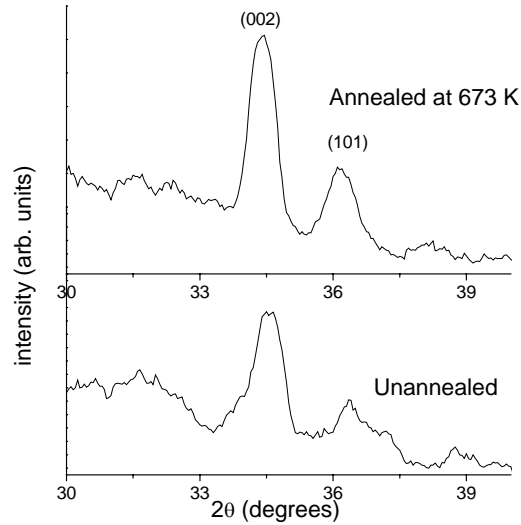
FIG. 4.12 XRD Pattern of ZnO_1In before and after annealing

4.3.2 Effects of In Diffusion

4.3.2.1 Structural Properties

Fig. 4.13 shows X-ray diffraction (XRD) pattern of the doped ZnO thin films with different indium concentrations. It was found that all films showed preferential orientation along (002) plane and intensity of peak corresponding to this orientation did not vary much with indium concentration. It was shown that the intensity of the peak corresponding to (002) plane had a strong dependence on oxygen content in the sample [32]. Hence one could state that, due to indium diffusion, oxygen concentration was also not varying much in the sample. Again, intensity of (002) peak was much stronger than that of (101) orientation. This indicated that the c -axis of the grains became uniformly perpendicular to the substrate surface, suggesting that the surface energy of (002) plane was the lowest in ZnO crystals [33]. No new phases were observed, even when the mass of evaporated In was increased upto 10 mg,

162

indicating that incorporation of indium neither could change wurtzite structure of ZnO nor resulted in the formation of In_2O_3.
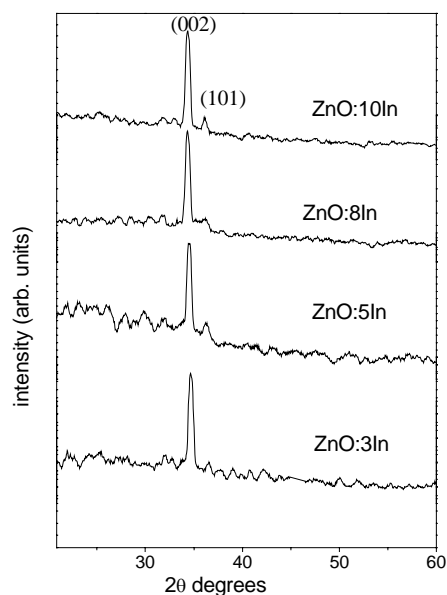
FIG. 4.13 XRD spectra of indium diffused ZnO thin films with different indium concentrations.

From the figure 4.13, it was also clear that the peak positions corresponding to the planes (002) and (101) were shifted to lower values of 2θ, when indium was incorporated. The value of lattice spacing (d) was correspondingly increased and these values are tabulated in Table 4.2. Lattice constants were calculated for hexagonal ZnO and it was found that, with the increase of the doping concentration, lattice constant (a) increased linearly from 3.224 Å to 3.265 Å and c increased from 5.166 Å to 5.217 Å. Therefore the ratio c/a was nearly constant for all samples. There was a slight decrease for the sample ZnO:10In. Similar results had been observed by Miki-Yoshida *et al* [34] in indium doped spray pyrolyzed ZnO thin films. Moreover it was

known that the difference in lattice parameter *c* could be related to the micro strains produced by the residual stress in the film [35]. Grain size was calculated using Debye Scherrer formula. It was found that grain size reduced on indium doping. But after an initial decrease, the grain size remained practically constant for all higher indium concentrations [Table 4.3].

The strain along the c axis (ε_{zz}) is given by the equation

$$\varepsilon_{zz} = (c_0\text{-}c)/c_0 \text{ X } 100 \text{ \%}$$

where c is the lattice parameter of the strained ZnO thin films calculated from x-ray diffraction data and c_0 is the unstrained lattice parameter of ZnO. Strain could be positive (tensile) or negative (compressive) according to the above equation. Lowest strain value was for the undoped ZnO while it increased with indium concentration. Strain might be probably due to the incorporation of indium at zinc site, since the ionic radius of In is higher than that of Zn.

Table 4.3. Variation in grain size, lattice strain and lattice parameters with indium concentration

Sample Name	Grain size (Å)	a (Å)	c (Å)	Lattice strain (%)
Undoped	251.4	3.224	5.166	-0.745
ZnO:3In	189.8	3.224	5.166	-0.745
ZnO:5In	187.6	3.240	5.195	-0.188
ZnO:8In	182.7	3.253	5.217	0.234
ZnO:10In	181.4	3.265	5.217	0.234

4.3.2.2 Optical Studies

Optical absorption spectra were recorded in the wavelength region 350 -900 nm. In order to determine the optical band gap, $(\alpha h\nu)^2$ against $h\nu$ graph was plotted [Fig. 4.14].
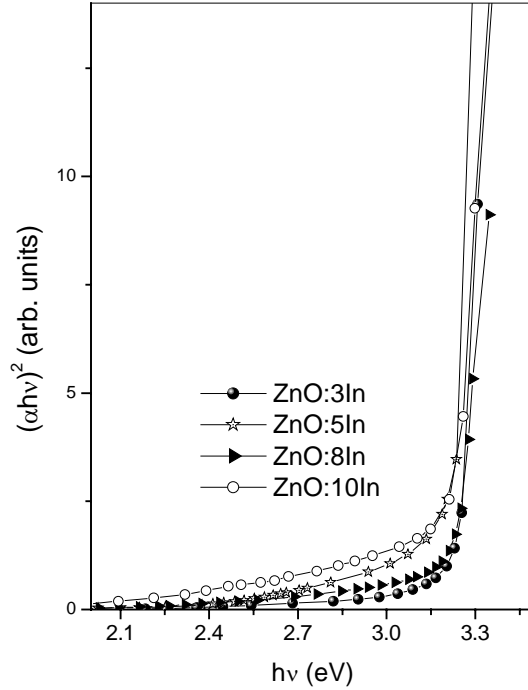
FIG. 4.14 $(\alpha h\nu)^2$ vs hν graph for indium diffused ZnO thin films

Sharp optical band gap was determined from this plot for all films by the linear fit in the straight portion of the graph. Band gap of undoped sample was 3.3 eV. This decreased slightly with doping concentration and became 3.2 eV for ZnO:10In. But it could be seen that, variation of band gap with indium concentration was not regular, and it remained around 3.2 eV. This slight decrease in band gap might be due to merging of donor levels just below the conduction band. However there could be the possibility of having small error while calculating the band gap from $(\alpha h\nu)^2$ vs. hν plot using curve fitting method. From the absorption spectra of undoped sample, it was clear that there was almost no absorption in the visible region. But for the doped samples, absorption edge was not sharp and there was absorption in this region [Fig. 4.15]. This might be due to the introduction of shallow donor level due to doping of

indium. Slight shift in absorption edge towards the higher wavelength for the doped sample was also clear from the absorption spectra.
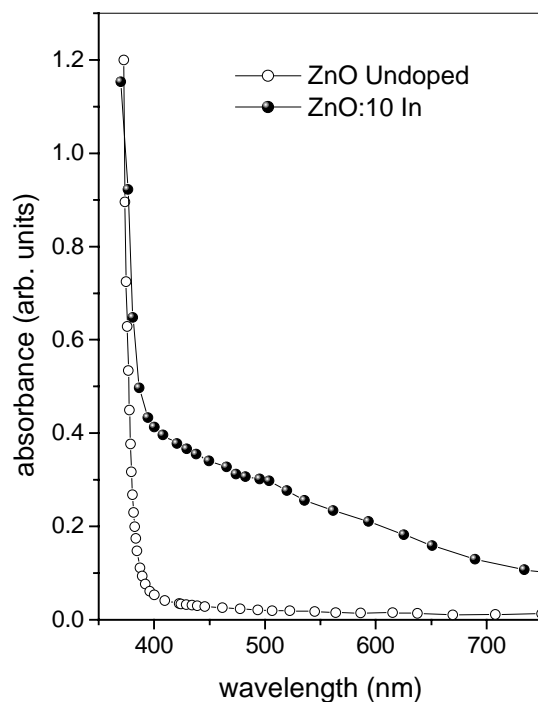
FIG. 4.15 Optical absorption spectra of ZnO and ZnO:In.

Optical transmission spectra were also recorded in the wavelength region 350 – 1500 nm. From the Fig. 4.16, it was clear that percentage of transmittance was decreasing with increase in indium concentration. In this regard, it has to be specifically noted that there was no appreciable decrease in transmittance, for samples ZnO:3In and ZnO:5In. Transmittance was affected considerably for ZnO:10In only. In transparent metal oxides, metal to oxygen ratio decided the percentage of transmittance. A metal rich film usually exhibited less transparency. Hence the decrease in optical transmittance in doped samples might be due to the increase in metal to oxygen ratio, (Zn+In)/O. The large decrease in transmittance in the IR region

might be due to the free carrier absorption, since the doped samples were showing high electrical conductivity.
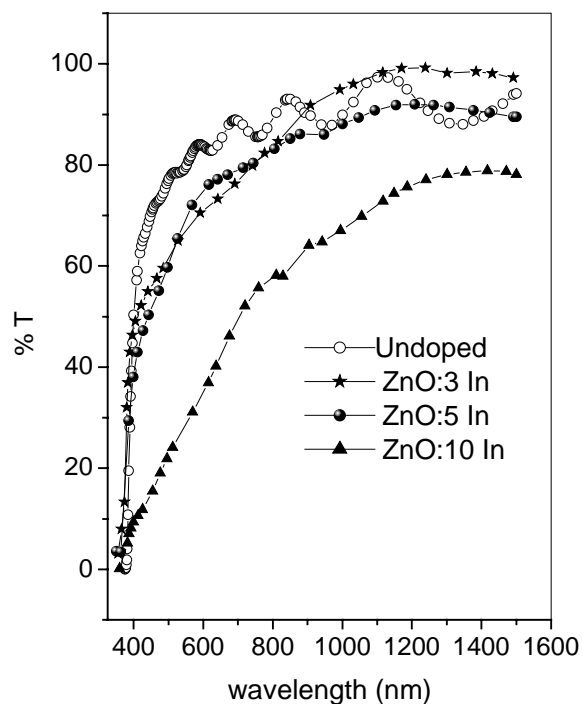
FIG. 4.16 Transmittance spectra of Indium diffused ZnO thin films

4.3.2.3 Photoluminescence measurements

Photoluminescence (PL) spectra, at room temperature, were recorded in the range 350-600 nm. Both undoped and doped samples showed two emission peaks centered at 377 nm and 500 nm [Fig. 4.17], in which the peak at 377 nm was corresponding to Near Band Edge (NBE) emission while the one at 500 nm was corresponding the to characteristic blue green emission. NBE emission at low temperature was well understood owing to sharp and intense emission peaks [36]. Broadening of the emission peak at higher temperature made it difficult to identify the emission mechanism. In majority of the published works, NBE emission had been

attributed to free-exciton annihilation from the position of peak energy [37, 38]. Some attempts were made to correlate crystallinity with the intensity of NBE emission [32, 39, 40]. In the present work, it was clear from the PL spectra that, the intensity of NBE emission was almost constant with doping concentration. Also from XRD analysis, one could see that, degree of crystallinity was almost same for all samples. Hence intensity of the emission might have dependence on crystallinity of the films. From Fig. 4.17, it was clear that peak position of NBE emission shifted to higher wavelength region as doping concentration increased and blue green emission shifted to lower wavelength region. It was shown from the optical absorption spectra that, on indium doping, the band edge shifted slightly to higher wavelength. Hence the shift in NBE emission to higher wavelength side might be related to the nature of variation of band gap. The peak position of NBE emission from PL measurements, was coinciding with the value of absorption edge, calculated from $(\alpha h\nu)^2$ against $h\nu$ graph [Fig 4.18].
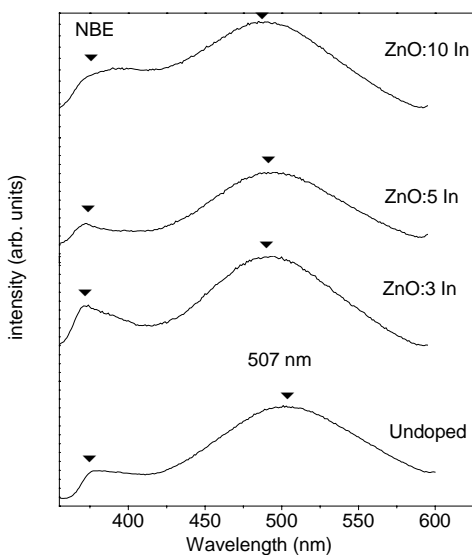
FIG. 4.17 PL spectra of In diffused ZnO thin films

Generally one could see that NBE was always less than band gap due to the exciton binding energy. Here, the similarity in the value of NBE and absorption edge, was probably due to the measurement error in the value of the band gap obtained by fitting the $(\alpha h\nu)^2$ versus $h\nu$ graph.

PL emission centered at 507 nm was characteristic emission of ZnO thin films. The emission was extremely broad and this might be due to phonon-assisted transition [41]. It was suggested that this emission was due to the transition form the conduction from conduction band to an acceptor level created by antisite oxygen. The possible reasons of this emission, previously reported, were discussed in detail in chapter 3.
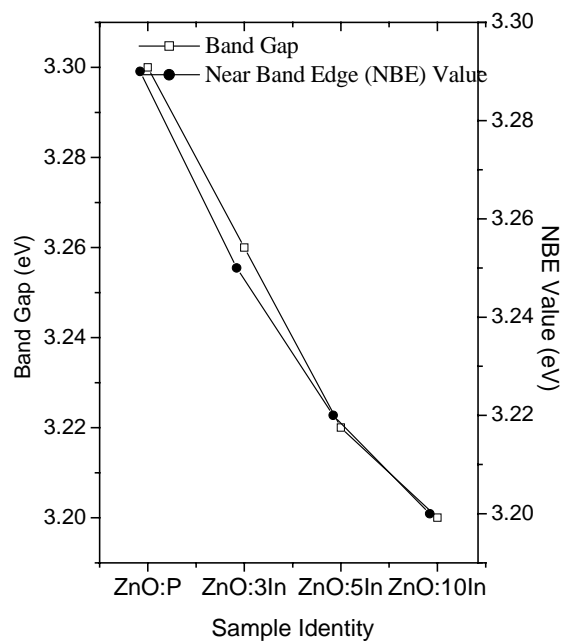
Fig. 4.18 Variation in Band gap and NBE with indium concentrations

PL emission peak, centered at 507 nm, was shifted to lower wavelength, as the doping concentration increased. Since the emission was extremely broad, the small shift in peak position was insignificant. There were reports on peak shift of blue green emission towards higher wavelength region due to doping with terbium chloride [42]. But the exact reason for this shift was not explained. A red shift in peak position of blue-green emission with annealing temperature was also reported which was consistent with band gap variation [43]. They had also reported some anomalous annealing temperature, at which UV peaks were shifted to higher wavelength while green emission shifted to lower wavelength. The reason for this odd behavior was also not clear.

Emission near UV region for the sample ZnO:10 In could be fitted well by two peaks located at 387 nm and 407 nm. The violet emission (~410 nm) was probably due to the radiative defects related to the interface traps existing at the grain boundaries and emitted due to the radiative transition between this level and valence band [44]. In the present work it was observed that the grain size of ZnO decreased at the initial level of doping and there was not much change as doping percentage was increased. Hence we avoided this explanation for the emission at 407 nm. Using full-potential linear muffin –tin orbital method, the energy levels of undoped ZnO were calculated [45]. A level at 3.06 eV below the conduction band was identified corresponding to the acceptor level V_{Zn}. So the emission at 407 nm might be due to the transition from the conduction band to the level due to V_{Zn}. The emission at 387 nm might be NBE in ZnO:10In. Appearance of two peaks in the UV emission was observed only in heavily doped ZnO:10In sample. Here the possibility of formation of a defect level due to zinc vacancy was more due to indium diffusion.

4.3.2.4 Photosensitivity measurements

Photosensitivity $(I_L-I_D)/I_D$ (I_L is illuminated current and I_D is the dark current) measurements were taken and the results are depicted in Table 4. 4. Two-probe method was employed to measure the dark and photocurrent. A potential difference of

1-2 volts was applied across the two silver electrodes. For the photocurrent measurement, the sample was illuminated with a tungsten halogen lamp (100 mW/cm^2) and the photocurrent was measured simultaneously. Maximum photosensitivity was obtained for the undoped sample (200.9) and decreased with the increase of indium concentration. This might be due to the increasing in the number of majority carriers on doping with indium, leading to huge dark current (I$_D$).

Table 4.4 Variations in electrical resistivity and photosensitivity with indium mass

Sample Identity	Resistivity (ohm cm)	Photosensitivity	Figure of Merit (Ω^{-1})
ZnO:3In	19.1	1.23	2.028x10^{-4}
ZnO:5In	2.7	0.53	1.52x10^{-3}
ZnO:8In	1.3	0.11	1.85x10^{-3}
ZnO:10In	0.9	0.07	2.13x10^{-3}

4.3.2.5 Rutherford Backscattering (RBS) Analysis

RBS analysis was done using 3 MeV Helium ions in undoped ZnO and ZnO:5In samples to identify the presence of indium in the film. The ratio of In/Zn was calculated and it was equal to 0.043. Fig 4.19 shows the RBS spectrum of both undoped and doped ZnO samples. The exact compositional analysis of oxygen [using software like GISA or RUMP] was difficult for ZnO in RBS studies, since the composition of glass substrate was not exactly known.
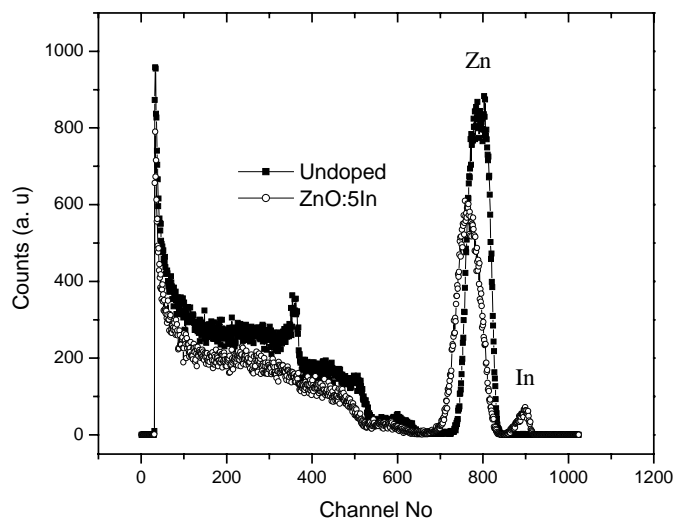
FIG. 4.19 RBS spectrum of ZnO samples

4.3.2.6 Electrical Resistivity Measurements

Electrical resistivity measurement was done on doped samples and was found to be decreasing with indium concentration. Figure 4.20 depicts the variation of resistivity with indium concentration and values were tabulated [Table 4.4]. It is very clear from the figure that ZnO:5In had practically lowest resistivity and there was no further significant decrease of resistivity due to the further increase in doping concentration. Undoped sample had a resistivity 78.1 Ω cm. Resistivity of ZnO: 10In was 0.9 Ω cm. The decrease in resistivity might be naturally due to the donor action of indium. On doping, zinc at lattice sites might be progressively replaced by indium atom and/or indium could occupy interstitial position, promoting the conductivity. Moreover the grain boundary scattering effect might be less, since there was no

appreciable decrease in grain size with indium doping. The values of figure of merit was calculated and tabulated in table 4.4
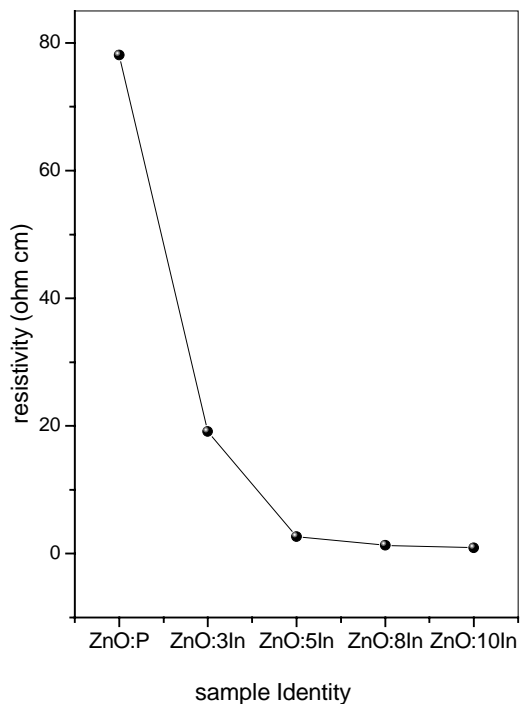
FIG. 4.20 Resistivity variations with indium concentration of indium doped ZnO

When indium (5 mg) was diffused into ZnO sample by annealing at 673 K, electrical resistivity again decreased drastically to 8.9 x10^{-3} ohm cm. Here another factor also may be contributing to the enhancement of conductivity; ie., the destruction of oxygen acceptor states. Interestingly the film was showing better crystallinity than the sample, ZnO:5In. Grain size was found equal to 46.4 nm. This may be also contributing to the decrease in the resistivity. XRD pattern is given in the figure 4.21.
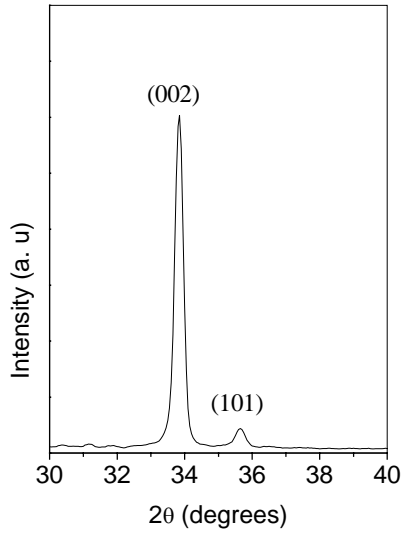
FIG. 4.21 XRD pattern of ZnO:5In annealed at 673 K

Optical band gap remained at 3.3 eV [Fig. 4.22]. Optical transmittance spectra revealed that, when indium diffused by annealing at 673 K, the interference fringe like pattern of transmission curve was retained. Moreover, percentage of transmission was slightly getting improved [Fig 4.23]. This may be probably due to the reduction in the scattering centers in the film. Indium at interstitials might be acting as scattering centers and this may also support the enhancement of conductivity.
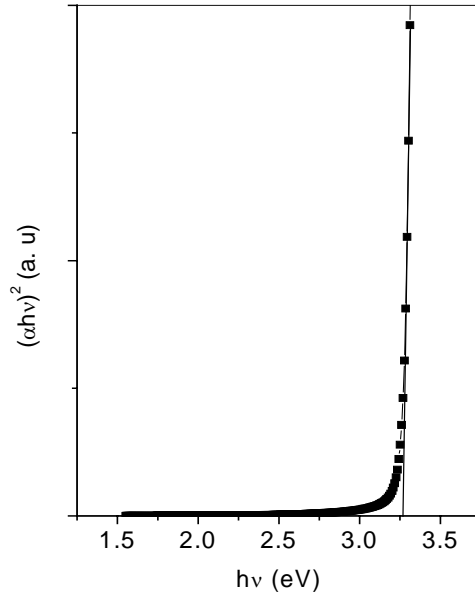
FIG. 4.22 $(\alpha h\nu)^2$ vs hν plot of ZnO:5In annealed at 673 K
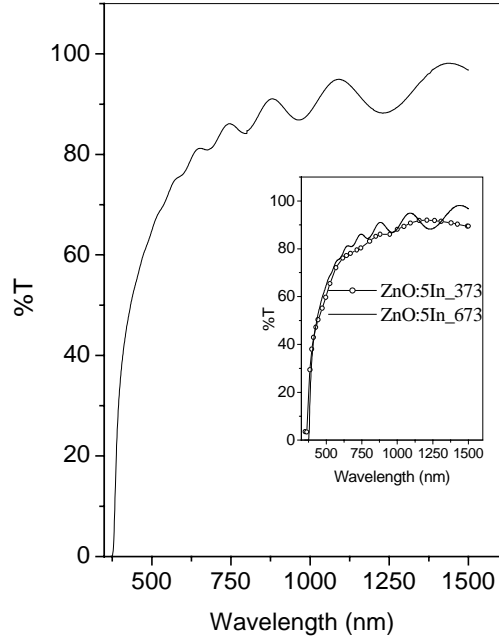
FIG. 4. 23 Optical Transmission spectra of ZnO:5In annealed at 673 K. Inset shows the comparison with ZnO:5In annealed at 373 K.

Carrier concentration of 1.3×10^{15} cm^{-3} and mobility of 60 cm^2/Vs were obtained for the undoped sample while a carrier concentration of 2.8×10^{17} cm^{-3} and 4.4×10^{17} cm^{-3} were obtained for ZnO:5In and ZnO:10In, respectively. Mobility decreased to 22.7 cm^2/Vs and 14 cm^2/Vs for ZnO:5In and ZnO:10In respectively. The decrease in mobility might be due to the scattering of charge carriers by neutral impurities.

4.3.2.7 Temperature Dependent Conductivity Measurements

When ZnO was doped with indium, both 148 meV and 65 meV levels got suppressed. Instead, activation energies ~30 meV and ~15 meV were obtained [Fig 4.24].
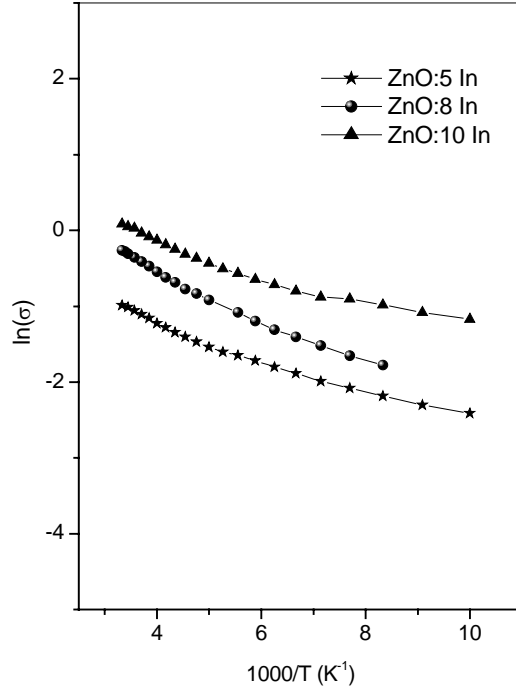
FIG. 4.24 Arrehenius plot of Pure and doped ZnO thin films

Donor ionization energy was calculated using hydrogen atom approximation for ZnO using the expression,

$$E_{id}/E_{iH} = m_e/m\epsilon^2 \,,$$

where ϵ is the dielectric constant of the ZnO and m_e is effective mass of electron, m is mass of electron and E_{iH} is ionization energy of H_2 atom. The value was found equal to ~ 40 meV. However the level at 30 meV might be related to the donor level due to tetrahedral Zn interstitials [46]. Hence in the present study we are not able to assign this level exactly. We suspect that the shallow donor level at 15 meV might be due to indium at interstitial position. These levels might be the reason for absorption in the visible region for the doped films.

4.3.3 Towards a Low Resistive ZnO Films

4.3.3.1 XRD Studies

XRD analysis was done in all the samples. Figure 4.25 showed the XRD pattern of the ZnO samples doped with 1 at % indium. When it annealed in vacuum (ZnO_1InN:A) at 673 K, the peak position corresponding to the plane (002) was shifted to lower 2θ values, subsequently the 'd' values increased, which indicated the increase in the lattice strain. Annealing in vacuum might have caused the desorption of oxygen from ZnO samples, which in turn resulted a disorder in crystal network. This disorder might be the reason for increased lattice strain. Also, when In was introduced into the film by thermal diffusion, the strain might have again increased.
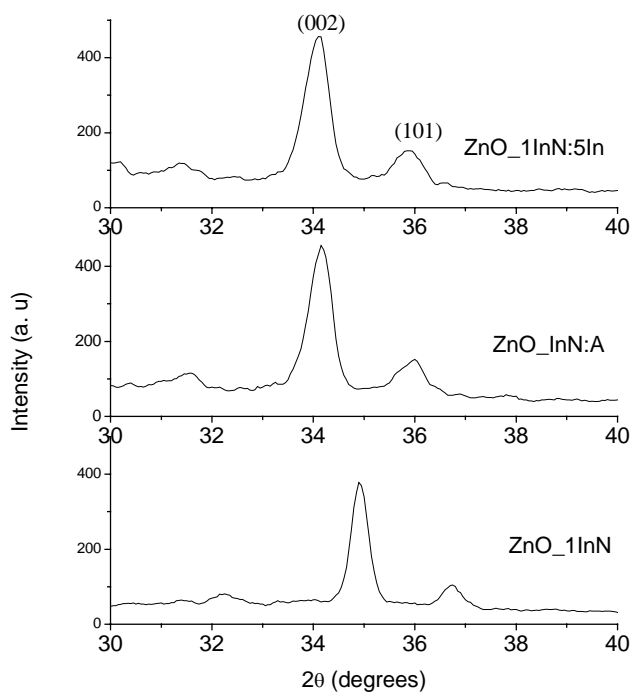
FIG. 4.25 XRD Pattern of ZnO samples doped with 1 at % In

Grain size was calculated and it was found that grain size reduced on annealing and due to   In diffusion. The values are tabulated (Table 4.5). It was seen that the grain size decreased on indium diffusion. It was also observed that, as the lattice strain increased, the grain size decreased.

Figure 4.26, shows the XRD pattern of ZnO samples doped with 1.5 at % indium nitrate and followed by the indium diffusion at different concentration. Here also, for the sample ZnO_1.5InN:5In, the peak position corresponding to the plane, (002) was shifted to lower 2θ values which indicated an increase in lattice strain. But interestingly, lattice strain was again (as the shift in 2θ values towards the higher value). Lattice strain values are tabulated in table 4.5. Here grain size also initially decreased and then increased. The initial decrease in grain size may be attributed to the lattice strain in the film.
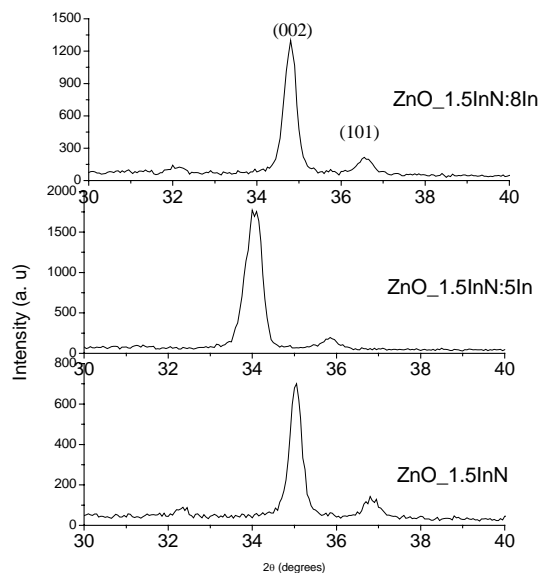
FIG. 4.26 XRD Pattern of ZnO films doped with 1.5 at % Indium.

4.3.3.2 XPS Analysis

XPS analysis was done on two samples viz., ZnO_1.5InN and ZnO_1.5InN:8In. Both Zn and O were found have diffused into the substrate, while In did not diffused much. From the depth profile analysis, it was clear that, the concentration of indium increased throughout the layer depth of ZnO. This might be the reason for decreased resistivity. Another interesting observation was that, when the samples were annealed at higher temperature, the concentration of oxygen diffused into the substrate decreased. In the earlier experiment of indium doping, in the form of indium chloride, similar results were observed at higher doping concentrations. The exact reason for this kind of behavior is not understood clearly.
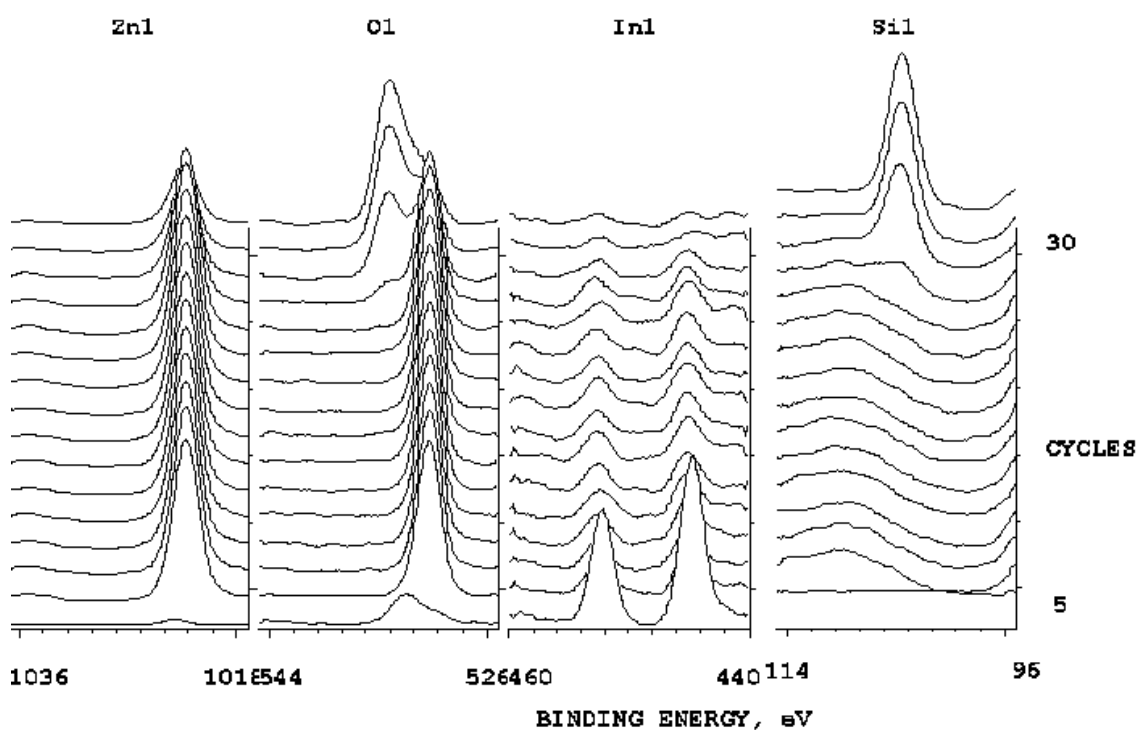
FIG. 4.27 XPS depth profile of as prepared ZnO_1.5InN
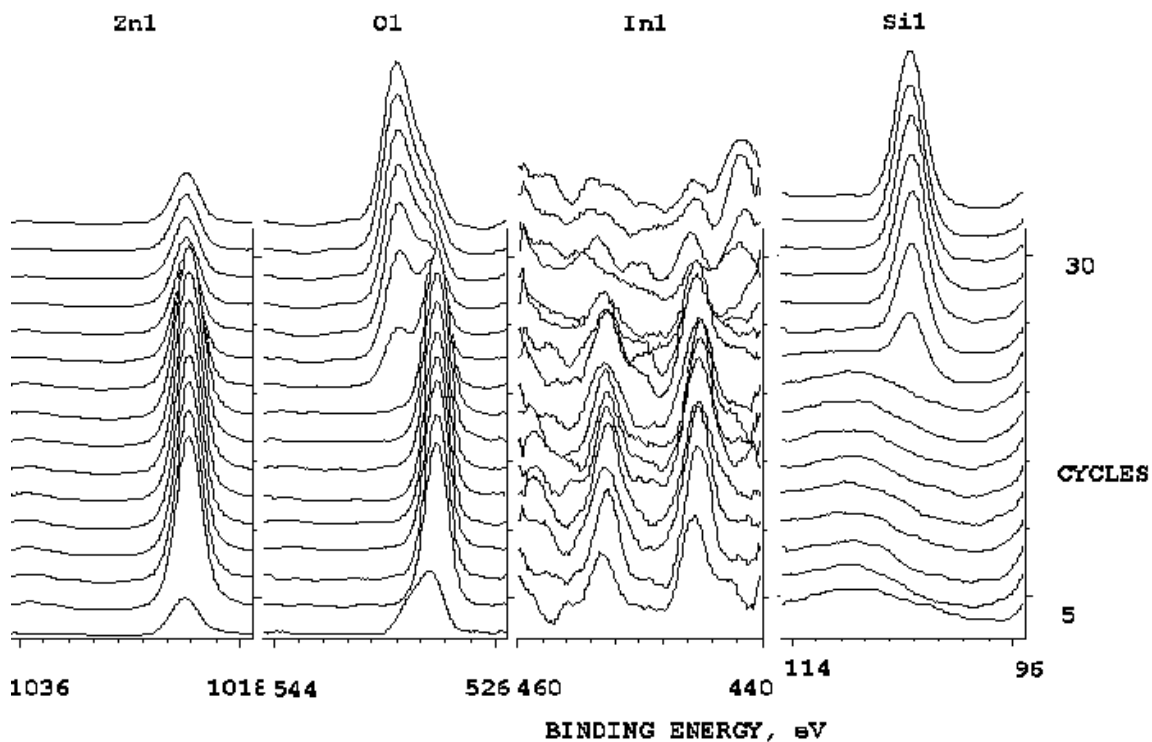
FIG. 4.28 XPS depth profile of ZnO_1.5InN:8In annealed in vacuum with a thin layer
of indium (8 mg)

4.3.3.3 Optical Absorption and Transmission Studies

Optical absorption studies proved that the absorption edge remained unaffected on indium doping, even if its resistivity value decreased by three orders of magnitude. Band gap also remained at 3.3 eV for all the films. Optical transmission spectra showed that, the percentage of transmission got slightly affected by the indium doping. The as-prepared-doped samples showed better transmittance than the pristine in the visible region, while a slight reduction was observed in the IR region. But when annealed at higher temperature with and without a thin layer of indium, there was a slight reduction in transmission in visible region. A large decrease of transmittance in

181

the IR region might be attributed to the free carrier absorption. It was also interesting to see from the optical transmittance spectra that, the sample ZnO_1.5InN was showing better transmittance than ZnO_1InN. Also it is clear that, the transmission started at the same wavelength for all the samples.

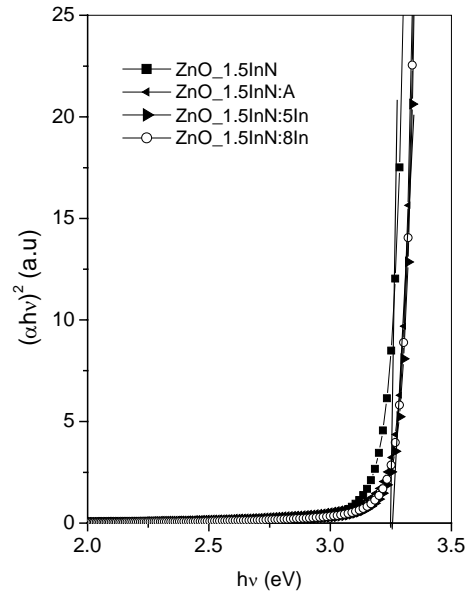FIG. 4.30 $(\alpha h\nu)^2$ vs hν plot of ZnO: In (1 at %) films
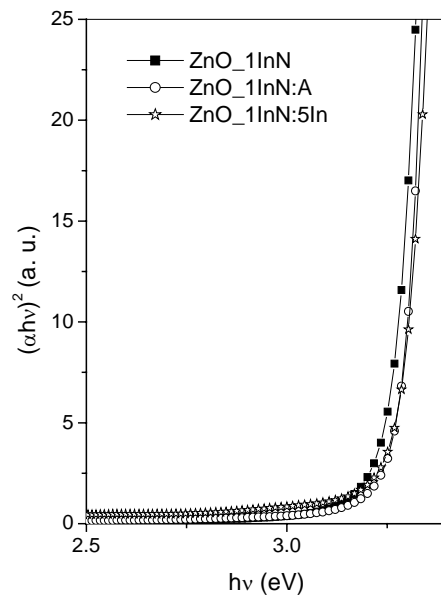
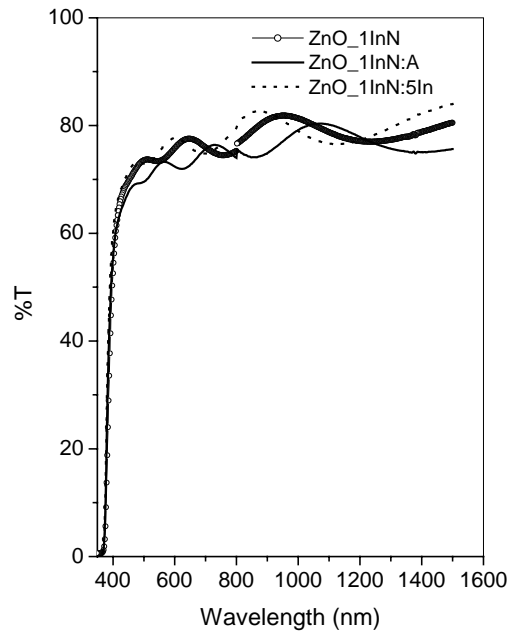FIG. 4.30 $(\alpha h\nu)^2$ vs $h\nu$ plot of ZnO: In (1.5 at %) films

FIG. 4.31 Optical Transmittance spectra of ZnO:In (1 at %)
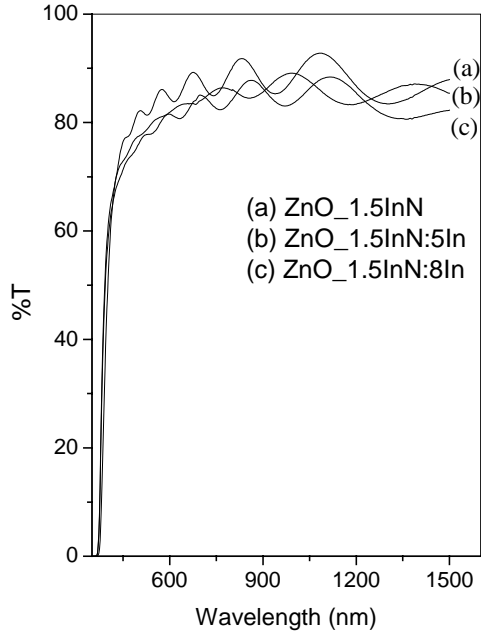
FIG. 4.32 Optical Transmittance spectra of ZnO:In (1.5 at %)

4.3.3.4 Electrical Resistivity Measurements

Electrical resistivity of all samples was measured and results are given in table 4.5. It was interesting to see that the resistivity of the sample doped with 1 at % In using indium nitrate solution was less than that of the film doped with 1 at % In using indium chloride solution. Hence the effect of chlorine as an electron trap was again verified. The electrical resistivity decreased with the increase in the indium concentration in the spray solution and also with the increase in mass of indium diffused. Lowest resistivity was obtained for the sample prepared with 1.5 at % In in the solution and followed by the annealing at 673 K with 8 mg of indium (ZnO_1.5InN:8In). The value obtained was 1.45×10^{-3} ohm cm and this is one of the lowest resistivity values obtained for indium doped ZnO thin films using spray pyrolysis technique. Figure of merit is calculated at the wavelength of 544 nm and

185

values are tabulated in Table 4.5. The highest value was obtained for the sample ZnO_1.5InN:8In. Hence form the studies, it was concluded that, this film could be used as transparent conducting electrode for the devices like solar cells, flat panel displays etc.

Table 4.5 Grain Size, Resistivity and Figure of Merit values of indium doped films

Sample Name	Grain Size (nm)	Lattice Strain (%)	Resistivity (ohm cm)	Figure of Merit (Ω^{-1})
ZnO_1InN	24.8	-1.32	9.73	4.09×10^{-4}
ZnO_1.5InN	25.4	-1.63	3.24	1.39×10^{-2}
ZnO_1InN:A	18.7	+0.6	7.9×10^{-3}	0.5
ZnO_1InN:5In	17.7	+1.2	5.1×10^{-3}	0.8
ZnO_1.5InN:A			3.73×10^{-3}	0.97
ZnO_1.5InN:5In	20.5	+1.21	2.71×10^{-3}	1.59
ZnO_1.5InN:8In	26.9	-1.06	1.45×10^{-3}	2.91

4.4 Conclusion

Indium doping reduced the resisitivity of ZnO thin films. It could be done either by mixing solution of indium with zinc precursor or by thermally diffusing indium into the film. Undoped films showed a preferential orientation along (002) plane, while high percentage of indium doping resulted in preferred orientation along (101) direction. But when indium was doped via thermal diffusion, no change in the preferential orientation was observed. Luminescence property was also preserved on indium diffusion, while it reduced drastically on indium doping using indium chloride. Optical band gap remained almost the same in both cases while percentage of optical transmission decreased on indium diffusion at higher percentage. When indium was doped in the form of indium chloride, electrical resistivity decreased at initial doping

concentration and increased at higher doping concentration. Lowest resistivity obtained in this case was 1.5×10^{-2} ohm cm. When indium chloride was used as precursor for indium, at higher doping concentration, chlorine was present in the film unintentionally. It might have caused the increase of the resistivity of the film at higher indium concentration. But when indium was thermally diffused, a monotonic decrease in resistivity was observed. Lowest resistivity (8.9×10^{-3} ohm cm) was obtained when indium (5 mg) was diffused at 673 K. Annealing at higher temperature improved the grain size significantly. Considering all these factors, in order to achieve a low resistive ZnO films, indium was doped in the form of indium nitrate and then it annealed at 673 K with a thin layer of indium deposited over it using thermal evaporation. By using indium nitrate, instead of indium chloride we could avoid the unintentional doping of chlorine in the film. The lowest resistivity value obtained was 1.45×10^{-3} ohm cm for the film doped with 1.5 at % indium nitrate followed by the annealing in vacuum with 8 mg of indium deposited over this. From the analysis based on these experiments, we can state that, chlorine, when occupied at inertial position/grain boundaries could capture electrons, which in turn reduced the conductivity of the film. In order to give supplementary proof to this statement, we have done chlorine doping separately and the results of this experiment will be discussed in the next chapter.

References

[1] S. Major, A. Banerjee and K. L. Chopra, Thin Solid Films **125,** (1985) 179.

[2] S. Major, A. Banerjee and K. L. Chopra, Thin Solid Films, **108**, (1983) 333.

[3] S. Major, A. Banerjee, K. L. Chopra and K. C. Nagpal, Thin Solid Films, **143**, (1986) 19.

[4] I. Shih and C. U. Qiu, J. Appl. Phys. **58** (1985) 2400.

[5] S. N. Qiu, C. X. Qiu and I. Shih, Sol. Energy Mater. **15** (1987) 261.

[6] R. Wang, A. W. Sleight, R. Platzer and J. A. Garden, J. Sol. State Chem. **122,** (1996) 166.

[7] A. Maldonado, M. de la Luz Olvera, R. Asomoza,E. P. Zironi, J. Canetas-Ortega and J. Palacios-Gomez, J. Vac. Sci. Technol. A **15**, (1997) 2905.

[8] B. Szyszka and S. Jager, J. Non. Cryst. Solids **218,** (1997) 74.

[9] E. P. Zironi, L. Canetas-Ortega, H. Gomez, A. Maldonado R. Asomoza and J. Palacios-Gomez, Thin Solid Films **293,** (1997) 117.

[10] A. Maldonado, R. Asomoza, J. Canetas-Ortega, E. P. Zironi, R. Hernanndez, R. Patino and O. Solorza-Feria, Sol. Energy Mater. Sol. Cells **57,** (1999) 331.

[11] M. Miki-Yoshida, F. Paraguay-Delgado, W. Estrada-Lopez and E. Andrade, Thin Solid Films **376,** (2000) 99.

[12] K. J. Kim and Y. R. Park, Appl. Phys. Lett. **78,** (2001) 475.

[13] A. Maldonado, M. de la Luz Olvera,R.. Asomoza and S. T. Guerra, J. Mater. Sci: Mater. Electron. **12,** (2001) 623.

[14] M. S. Tokumoto, A. Smith, C. V. Santilli, S. H. Pulcinelli, A. F. Craievich, A. Traverse and V. Briois Thin Solid Films **416,** (2002) 284.

[15] A. Maldonado, M. de la Luz Olvera, S. T. Guerra and R. Asomoza, Sol. Energy Mater. Sol. Cells **82,** (2004) 75.

[16] S. N. A. Rahman, A. Shafii, A. F. Md Nor and B. Kamaluddin (upublished)

[17] A. Eliwa, H. Afifi, S. El-Hefnawi, M. Abdel-Naby and N. Ahmed WCPEC Conference proc. (2004)

[18] V. Savchuk, B. Kotlyarchuk and M. Oszwaldowski (unpublished; ArXiv reference)

[19] G. Machado, D. N. Guerra, D. Leinen, J. R. Ramos-Barrado, R. E. Marotti and E. A. Dalchiele Thin Solid Films **490**, (2005) 124.

[20] M. A. Lucio-Lopez, M. A. Luna-Arias, A. Maldonado, M. de la L. Olvera and D. R. Acosta, Sol. Energy Mater. Sol. Cells (Article in Press)

[21] S. –S. Lin, J. –L. Huang and D. –F. Lii, Surf. Coat. Technol. **176,** (004) 173.

[22] P. M. Verghese and D. R. Clarke, J. Mater. Res. **14,** (1991) 1039.

[23] R. Swanepoel, J. Phys. E: Sci. Instrum **16,** (1983) 1214.

[24] Teny Theresa John , C. Sudha Kartha, K. P. Vijayakumar, T. Abe and Y. Kashiwaba, Appl. Surf. Sci. **252,** (2005) 1360.

[25] H. L. Hartnagel, A. L. Dawar, A. K. Jain and C. Jagadish, 1995 Semiconducting transparent thin films. (Bristol and Philadelphia, Inst. Phys. Pub), p 306

[26] B. J. Jin, S. Im and S. Y. Lee, Thin Solid Films **366,** (2000) 107.

[27] A. Ortiz, C. Falcony, A. J. Hernandez, M. Garcia and J. C. Alonso, Thin Solid Films **293,** (1997) 103.

[28] Y. G. Wang,, S. P. Lau, X. H. Zhang, H. W. Lee, H. H. Hng and B. K. J. Tay, Crystal Growth **252,** (2003) 265.

[29] V. Srikant and D. R. Clarke, J. Appl. Phys. **83,** (1998) 5447.

[30] Y. Sun and H. Wang, Physica B **325,** (2003) 157.

[31] P. Nunes, A. Malik, B. Frnandes, E. Fortunato, P. Vilarinho and R. Martins, Vacuum **52,** (1999) 45.

[32] S. Im, B.J. Jin and S.Yi, J. Appl. Phys. **87,** (2000) 4558.

[33] K.L Chopra, S. Major and D. K. Pandya, Thin Solid Films **102,** (1983) 1.

[34] M. Miki-Yoshida, F. Paraguay-Delgado, W. Estrada-Lopez and E. Andrade Thin Solid Films **376,** (2000) 99.

[35] K. Ellmer, R. Cebulla and R. Wendt, Thin Solid Films **317,** (1998) 413.

[36] C. Klingshirn, Phys. Status. Sol. B **71,** (1975) 547.

[37] P. Zu, Z. K. Tang, G. K. L. Wong, M. Kawasaki, A. Ohtomo, H. Koinuma and Y. Segawa, Solid State Commun. **103,** (1997) 459.

[38] S. Cho, J. Ma, Y. Kim, Y. Sun, G. K. L. Wong and J. B. Ketterson, Appl. Phys. Lett. **75,** (1999) 2761.

[39] K. Ozaki and M. Gomi, Jpn. J. Appl. Phys. **41,** (2002) 5614.

[40] F. K. Shan, B. I. Kim, G. X. Liu, Z. F. Liu, J. Y. Sohn, W. J. Lee and B. C. Shin, J. Appl. Phys. **95,** (2004) 4772.

[41] D. C. Reynolds, D. C. Look, B. Jogai and H. Mokoc, Solid state. Commun. **101**, (1997) 643.

[42] C. Falcony, A. Ortiz, M. Garcia and J. S. Helman, J. Appl. Phys. **63(7),** (1988) 2378.

[43] Y. G. Wang, S. P. Lau, H. W. Lee, S. F. Yu, B. K. Tay, X. H. Zhang and H. H. Hng, J. Appl. Phys. **94,** (2003) 354.

[44] J. B. Jin, S. Im and S. Y. Lee, Thin Solid Films **366,** (2000) 107.

[45] Y. M. Sun, Ph.D thesis, University of Science and Technology of China, 2000

[46] Y. Sun and H. Wang, Physica B **325**, (2003) 157.

PROPERTIES OF CHLORINE AND FLUORINE DOPED ZnO

FILMS

5.1 Introduction

When ZnO films were doped with indium using indium chloride, unintentional doping with chlorine also occurred. Moreover the presence of chlorine in the film had considerable effects on different properties of the film. Hence to investigate the exact effect of chlorine on the different properties of ZnO, chlorine was doped separately. Probably this may be the first report on the chlorine doping in ZnO thin films, prepared using CSP technique. It was known that halogen group elements are good candidates as donors in ZnO, when these occupy the Oxygen cite [1]. Hence it was quite appropriate that doping with fluorine also has significance in the present studies. Moreover the atomic size of fluorine is more comparable with oxygen than chlorine. Hence in the present study, thin films of ZnO was doped with chlorine and fluorine separately and a detailed comparison of the properties was made.

Generally it was believed that halogen group elements increase the conductivity of transparent conductors like SnO_2 [2]. Previously effect of chlorine doping in SnO_2 thin films was demonstrated and it was believed that Cl would partially fill the oxygen cites. However there was no clear evidence for this. There were contradictory arguments, stating that when Cl occupied the vacant oxygen site, it was really decreasing the donor states and hence one could not expect a reduction in resistivity of the films. But if it replaced oxygen, it would be beneficial for the conductivity, since chlorine required only one electron to complete the outer most orbit.

Jousse at al carried out a detailed investigation to see the effect of Cl in SnO2 earlier [3]. Here SnO_2 was prepared using spray pyrolysis technique and the precursor

solution was SnCl$_4$. It was observed that, samples prepared at lower substrate temperature contained more Cl than those prepared at higher temperature. Also the films prepared at lower substrate temperature had high conductivity. Hence they correlated the effect of Cl to the conductivity. But in the paper itself, a three-order increase in conductivity was observed, when the substrate temperature was increased from 280 to 320°C. However this behavior was explained on the basis of amorphous to crystalline phase transition and effect of thickness on resistivity was not taken care of in the paper. They also mentioned that, at higher substrate temperature (>400°C), the doping efficiency of the Cl decreased due to the compensating effects of Li and Na in substitution sites.

In another paper, Jousse described the effect of Cl in SnO$_2$ in more detail, where he classified the material into three sections, depending upon the substrate temperature [4]. He demonstrated that all the Cl atoms introduced in the lattice behaved as active donors (350 ≤ Ts ≤ 500°C) and when clustered or segregated at grain boundaries, the doping efficiency decreased (300≤Ts<350°C). In short, he demonstrated that Cl could not act as donors, when segregated in grain boundaries or when it was incorporated in amorphous region.

Aranovich et al reported the effects of precursor solution on the properties of Spray Pyrolysed ZnO thin films [5]. They used ZnCl$_2$, ZnCl$_2$ with H$_2$O$_2$ and Zn(Ac)$_2$ as the source materials for zinc. In this report, they described the donor action of Cl, where they found that, as the Cl concentration decreased due to the increase in the substrate temperature, resistivity of the films increased. They found that, when substrate temperature was greater than 420°C, resistivity increased and this was probably due to the low concentration of Cl in the film. However they did not consider the effect of film thickness, [which decreased with increase in the substrate temperature] on the resisitivty variation. They also observed that when Zn(Ac)$_2$ was

used as precursor, resistivity value was higher than that of the sample prepared with ZnCl2. They attributed this difference as due to the absence of Cl in the film.

Hence it becomes clear from the references cited here that the studies were only on the effects due to 'unintentional chlorine doping' on the transparent conducting oxides like SnO_2 and ZnO. We found that the interpretation of the results are not totally convincing with the experimental observations. In all these papers, authors were just considering the variations of Cl concentration alone in the films and other effects (like thickness dependence, zinc concentration etc) were also to be discussed in order to get the correct picture. More over, there was no report on doping ZnO or SnO_2 using chlorine alone. Hence we felt that it was more appropriate to do the Cl doping in TCO's for the academic as well as device application interest. In order to demonstrate the effect of chlorine in ZnO, chlorine was introduced separately using ammonium chloride (NH_4Cl).

5.2 Experimental Details

In order to dope ZnO with chlorine, chlorine was added to the solution by dissolving required quantity of ammonium chloride (NH_4Cl). Other preparation conditions were kept at the same as in the case of undoped films. Samples were named as ZnO:0.5Cl, ZnO:1Cl, ZnO:3Cl etc for 0.5 at % , 1 at % and 3 at % chlorine respectively. These samples were characterized with different analysis such as XRD, optical absorption, optical transmission, PL measurements, temperature dependent conductivity measurements and electrical resistivity measurements.

Required quantity of ammonium fluoride was dissolved in this solution for doping with fluorine. In order to vary the doping concentration, volume of NH_4F was varied, keeping the molarity as constant. Volume of total sprayed solution was also kept at 200 ml. Temperature of the substrate (673 K) and spray rate (10 ml/min) were fixed. F-doped films were characterized structurally, electrically and optically. Samples were named as ZnO:0.5F, ZnO:1F, ZnO:2F and ZnO:5F implying different

concentrations (0.5 at %, 1 at %, 2 at % and 5 at % respectively) of fluorine in the precursor solution. In order to reduce the resistivity further, F-doped samples were annealed at 673 K in vacuum (10^{-5} mbar) for one hour. A tremendous decrease in resistivity was observed for the annealed samples. Annealed samples were characterized using XRD and electrical resistance measurements.

5.3 Results and Discussion

5.3.1 Effects of Chlorine

5.3.1.1. Structural Analysis

Fig 5.1 depicts XRD patterns of chlorine-doped samples. All the samples were showing polycrystalline nature, with hexagonal wurtzite structure, having preferred orientation along (002) plane. Even though ZnO:Cl samples were still showing preferential orientation along (002), incorporation of chlorine reduced the crystallinity considerably. Also it was clear from the figure that ratio of the intensity of the peaks, corresponding to (002) plane to (101) plane, decreased drastically at initial level of chlorine doping and then it remained practically a constant for higher chlorine concentrations. It was shown earlier that HCl vapor acted as a surfactant during the growth process of ZnO, inhibiting the growth of specific planes and favoring some others [6]. In the present study, we suspect that HCl vapor might have formed during the pyrolytic reaction and this might be the reason for reduced intensity of the diffraction peak corresponding to the (002) plane. Interestingly in the previous chapter, dealing with doping using $InCl_3$, a preferential orientation change from (002) to (101) planes at higher doping concentration was observed.
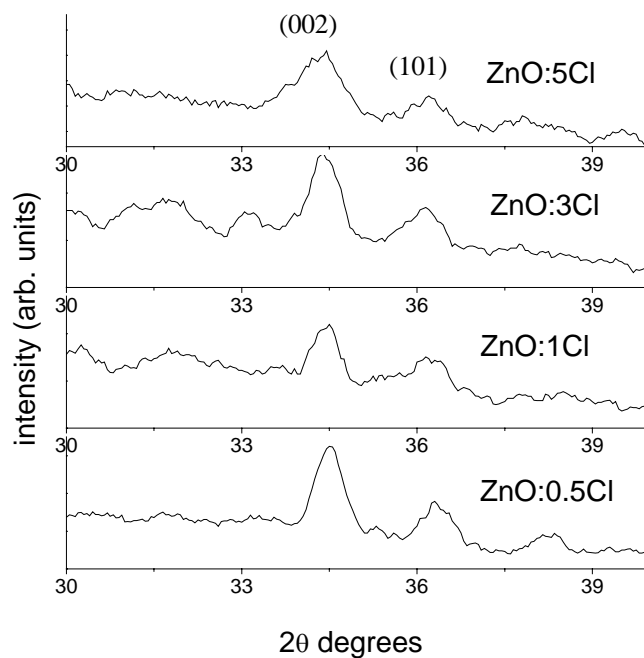
FIG. 5.1 XRD pattern of Cl doped ZnO thin films

It was also revealed from the structural analysis that the basic crystal structure of ZnO film was not modified due to chlorine doping. After an initial decrease, intensity remained practically a constant for all higher doping concentration. But the peak width increased to a high value (0.92 degrees) for ZnO:5Cl, making grain size (calculated using Debye Scherrer formula) very much low on higher percentage of doping. It reduced to < 10 nm for the sample ZnO:5Cl. Values of grain size at different doping concentrations are tabulated [Table 5.1].

Table 5.1 Grain size, resistivity, lattice strain and photosensitivity variation with chlorine concentration

Sample Name	Grain size (Å)	Resistivity (ohm cm)	Photosensitivity	Lattice strain (%)
ZnO:0.5Cl	166	451.6	103.1	-0.48
ZnO:1Cl	170	463.5	51.2	-0.48
ZnO:3Cl	158	749.93	112.6	-0.077
ZnO:5Cl	91	881.66	9.8	0.37

The strain along the c axis (ε_{zz}) of Cl-doped ZnO thin films was calculated from x-ray diffraction data. Strain increased with chlorine concentration [Table 5.1]. and was found to be inversely proportional to the grain size, which implied that strain was relieved at larger grain size. Similar results were reported earlier [7].

5.3.1.2 X-ray Photoelectron Spectroscopy Aanalysis

Compositional analysis of doped samples was done using XPS measurements. Results of the analysis are shown in Fig 5.2. From this it was clear that both Zn and O were uniformly distributed along the depth of the films. Surprisingly very small quantity of Si was observed throughout the depth, which might have diffused from the glass substrate during the spray pyrolysis as the temperature of the process was rather high (400˚C). But this was never observed in the case films like In_2S_3 [8] or $CuInS_2$ [9], which were also prepared using CSP technique.
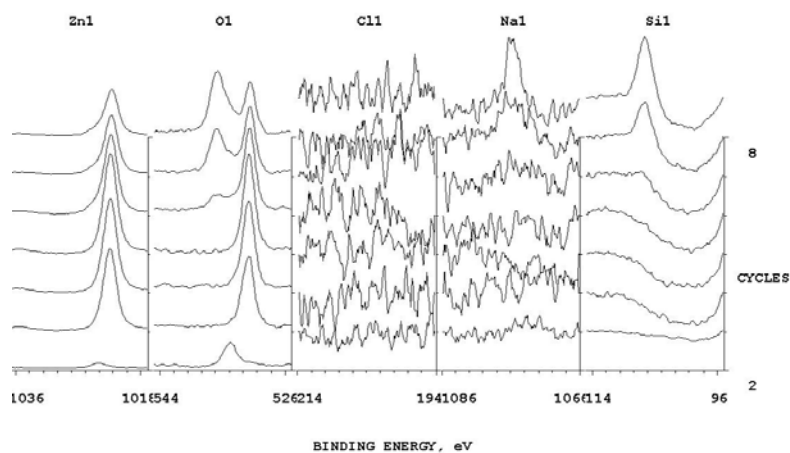
FIG. 5.2 XPS depth profile of ZnO:3Cl

Binding energies of Zn and O clearly indicated the formation of ZnO (1022.95 eV for $Zn3P_{3/2}$ and 531.02 eV for O1s). Variation of atomic concentration of constituent elements in the doped ZnO films along the depth is shown in Fig. 5.3. At the surface of the film, one could see that binding energies were higher for both zinc (1025.8 eV) and oxygen (533.6 eV). Binding energy of oxygen indicated the presence of SiO_2 at the surface and this might be resulting from the oxidation of diffused silicon. Atomic concentrations of Zn, O, Si and Cl in the doped samples were calculated from the XPS measurements. It was found that zinc and oxygen were 61.6% and 33.33% respectively so that the Zn/O ratio was 1.85 in this case. Concentrations of Zinc and oxygen were less compared to those of undoped samples. [Atomic concentration of zinc was found to be 62.33% and that of oxygen was 35.18% (along with a small quantity of silicon ~2%) making Zn/O ratio 1.77 in undoped sample. But silicon content got increased (~4%). For lower doping concentration, percentage of chlorine present in the sample was very small and could not be even determined from the graph. As the concentration of chlorine in the solution was 5%, the concentration in the sample became nearly 1%. It was surprising that the presence of elemental chlorine was clearly detected in the XPS analysis in the

197

ZnO samples doped with indium chloride, while it was not so evident in the present study. It might be due to the fact that the presence of indium might have been enhancing the incorporation of chlorine in the film.
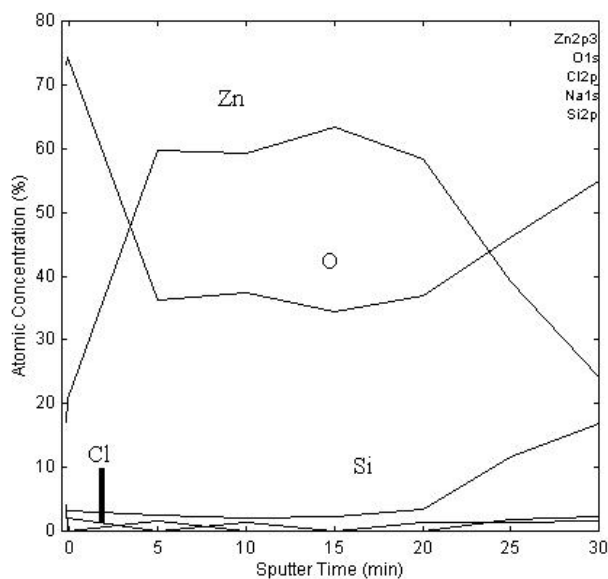

FIG. 5.3 Atomic concentration of Zn, O, Cl and Si along the layer depth of ZnO:3Cl

5.3.1.3 Optical Absorption and Transmission

Optical absorption studies were carried out in the wavelength range 350 – 900 nm. Optical band gap was determined by extrapolating the linear part of the curve $(\alpha h\nu)^2$ vs. $h\nu$ to intercept the energy axis (at $\alpha =0$) [Fig 5.4]. Band gap values were nearly same as that of undoped films. This was in good agreement with earlier observations from the structural analysis that chlorine doping did not modify the basic crystal structure of ZnO.
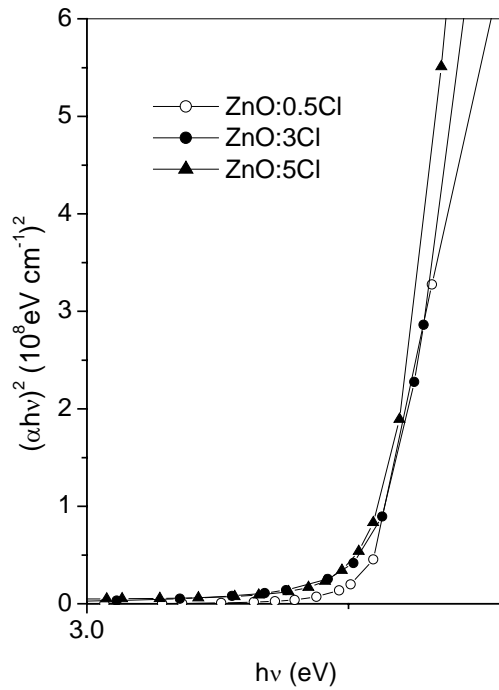
FIG. 5.4 $(\alpha h\nu)^2$ vs. $h\nu$ curve of Cl-doped ZnO thin films

Optical transmittance spectra were also recorded in the wavelength range 350 nm to 1500 nm [Fig. 5.5]. It was clear from the figure that percentage of transmission in the visible range increased due to chlorine doping, probably because of the decrease in the concentration of zinc in the film, after the incorporation of chlorine.

199
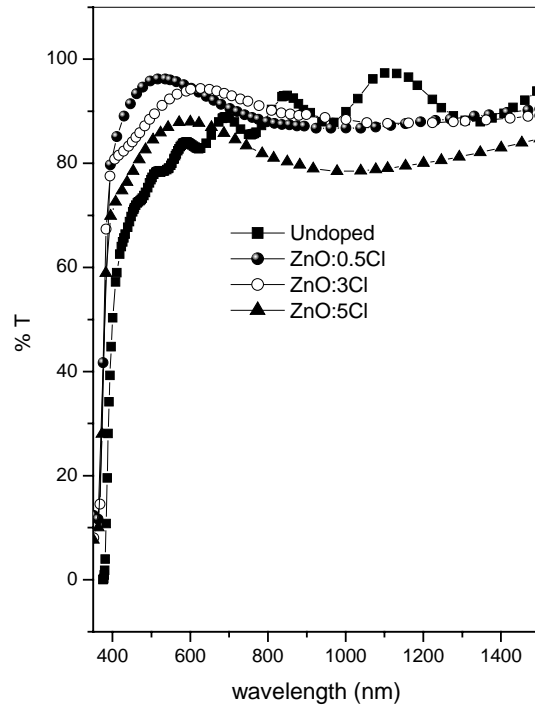
FIG. 5.5 Optical Transmittance spectra of ZnO doped with Chlorine.

Wavy nature of transmission spectra of the undoped sample was lost after the chlorine addition. This might be due to the reduction in quality of surface of the film. Since the transmission percentage was still higher than that of undoped sample, one could say that, scattering loss in the film was less.

5.3.1.4 Photoluminescence Studies

Photoluminescence [PL] studies were carried out in some of the doped samples [Fig. 5.6 (a-c)]. PL spectra could be fitted with three Gaussian curves and peak positions were identified. PL spectrum of ZnO:1Cl exhibited three peaks at 415, 517 and 640 nm. But for the samples, ZnO:5Cl and ZnO:8Cl, the emission at 640 nm was shifted to 680 nm. This emission was probably due to the oxygen interstitials [acceptor level] and transition was from conduction band to the acceptor level. The

emission at 415 nm was probably due to the defect level related to the interface traps existing at the grain boundaries and emision was due to the transition between this level and valence band. The emission at 517 nm was due to the transition from the conduction band to the acceptor level of oxygen antisite (O_{Zn}). Details are already demonstrated in the previous chapter. However, the shift in peak position of the emission at 640 nm to 680 nm was not clearly known from the present study.

Relative intensities of emissions at 415 nm and 680 nm with respect to the emission at 517 nm were determined; this value was increasing with increase in the doping concentration. Values are tabulated in Table 5.2. Earlier, it was assigned that the violet emission at ~ 415 nm was probably due to the defect level related to the interface traps existing at the grain boundaries. From structural analysis, it was found that the grain size was drastically reduced with the increase in doping percentage of chlorine, which in turn, increased the grain boundary area, causing an increase in density of the interface traps. These traps might have been originated from the segregation of chlorine in the grain boundaries, which also reduced the electrical conductivity of the film. The variation of electrical conductivity with chlorine concentration will be discussed in the following sections.

Table 5.2 Relative intensity values of PL emission at 415 nm and 680 nm with respect to the emission at 517 nm

Sample Name	I_{415}/I_{517}	I_{680}/I_{517}
ZnO:1Cl	0.28	0.31
ZnO:5Cl	0.64	0.44
ZnO:8Cl	1.06	1.52

It was interesting to note that emission and crystallinity were strongly affected/decreased by the chlorine present in the film. One could see that, when

indium was doped in the form of InCl$_3$ solution, these properties of ZnO were affected very much while it was almost unaffected when indium was doped by thermal diffusion of metallic indium. Hence as the conclusion, one could say that the presence of chlorine degraded both crystallinity and PL emission properties of ZnO thin films.
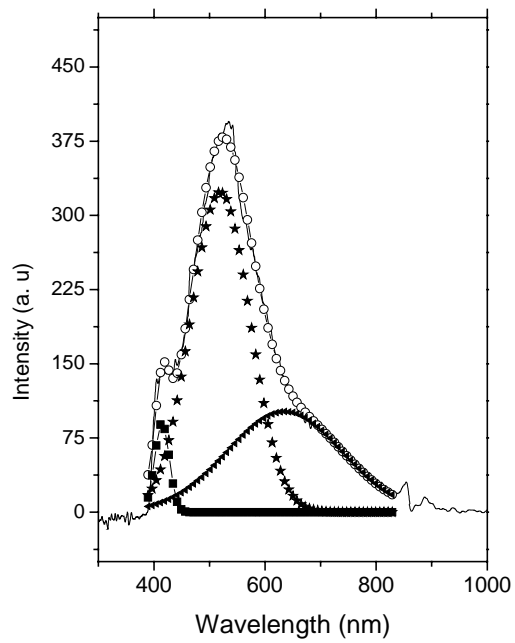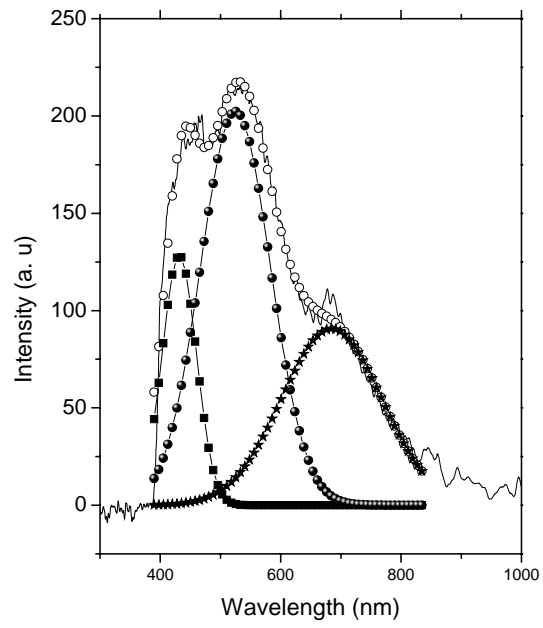

PL. 5.6a PL spectrum of ZnO:1Cl

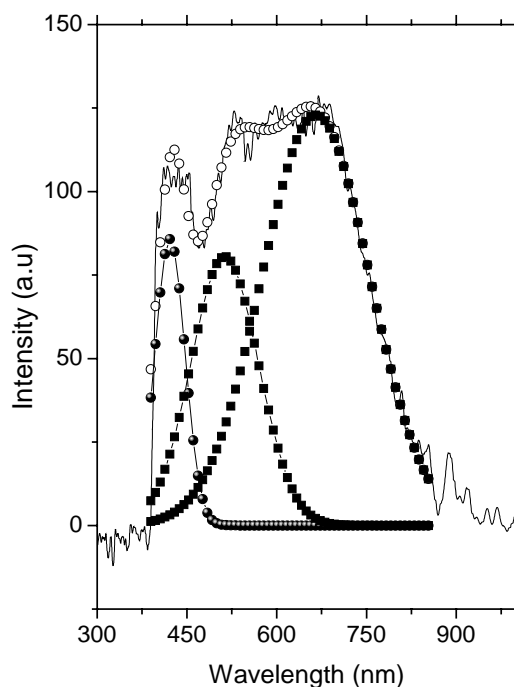FIG. 5.6b PL spectrum of ZnO:5Cl samples.

FIG. 5.6c PL spectrum of ZnO:8Cl samples

5.3.1.5 Electrical Resistivity Measurements

All films were n-type and it was realized using hot probe method. Electrical resistivity measurements were done, at room temperature, using two-probe method. Variation of electrical resistivity with doping concentration is given in Fig. 6. Undoped sample was having a resistivity of 78 Ω cm. As the doping concentration increased, resistivity also increased (Table 5.1). Generally in transparent semi conducting oxides, halogen doping resulted in the reduction of resistivity, if it substituted oxygen [10,11]. But the ionic radius of chlorine (167 pm) was much greater than oxygen (126 pm) and hence it seemed very difficult for chlorine to occupy oxygen sites. At higher doping concentrations, naturally the chlorine content also increased, resulting in high resistivity of the sample. This might be probably due

204

to the clustering or segregation of Cl atoms in the grain boundaries/sitting in the interstitial positions in the films [4]. As the grain size of the film decreased with Cl concentration (which in turn increased grain boundary area), more and more Cl occupied in the grain boundaries (which increased the resistivity). The atomic concentration versus depth profile graph [Fig.5.3], revealed that there is significant amount of Cl present in the film. Earlier, we had seen that the sprayed In_2S_3 films, [when indium chloride was the precursor solution], were showing higher resistivity than those obtained with indium nitrate precursor [12]. Significant amount of Cl was present in those films prepared using chloride-based precursors, which might be the cause of higher resistivity. Grain size was more or less same for both types of films. It was also found that the resistivity of Cl-doped ZnO, increased linearly with strain and this might be due to the higher density of grain boundaries associated with the smaller grains of chlorine-doped films [Fig. 5.7]. Hence we suggest that these two effects were contributing to the increase in resistivity.
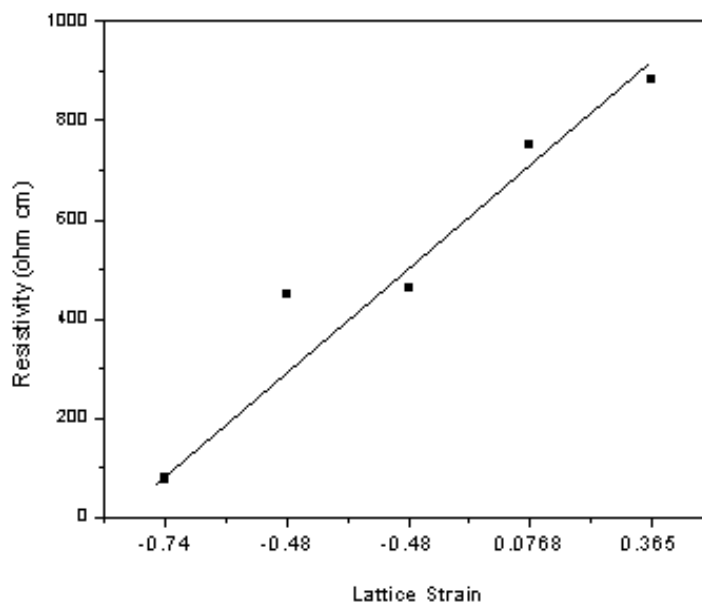

FIG. 5.7 Resistivity versus lattice strain of ZnO:Cl films

5.3.1.6 Photosensitivity Measurements

Results of photosensitivity measurements are depicted in Fig. 5.8. Samples were showing much low photosensitivity than the undoped samples, even though the resistivity was higher. Usually higher photosensitivity was associated with higher resistivity, as majority carrier density would be low in such samples. But here doped samples, in spite of having higher resistivity, were showing lower photosensitivity. This odd behavior in the present study, could be due to the decrease in both majority and minority carriers resulting from the recombination through chlorine atoms. Hence it is assumed that the photo-generated carriers might be lost as result of the increased recombination.
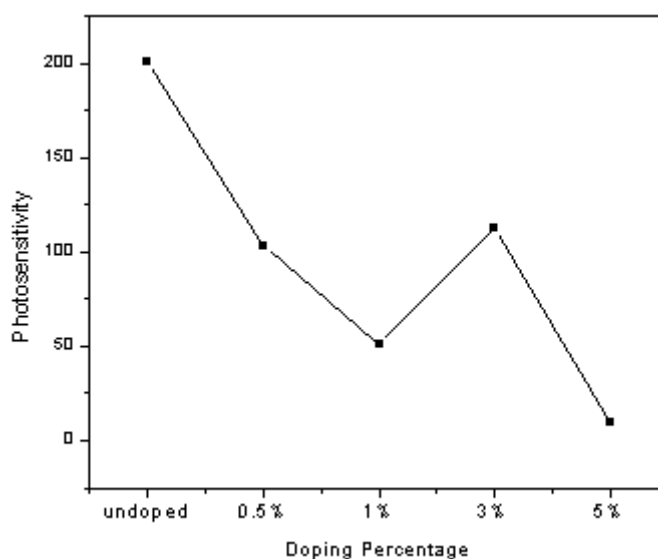

FIG. 5.8 Variation in photosensitivity of In-doped ZnO with indium concentrations

5.3.1.7 Temperature Dependent Conductivity Measurements

Temperature dependence of electrical conductivity exhibited by the samples was measured in the range 100 – 300 K [Fig. 5.9]. When doped with chlorine, level at 148 meV of the undoped sample got suppressed and a new level was created around 30 meV, in addition to the level at 65 meV. Theoretical calculations also showed the

206

existence of a level due to tetrahedral zinc interstitials at 31 meV [13]. The values obtained were matching well with the theoretically obtained values. Slight variations were within the limit of errors.
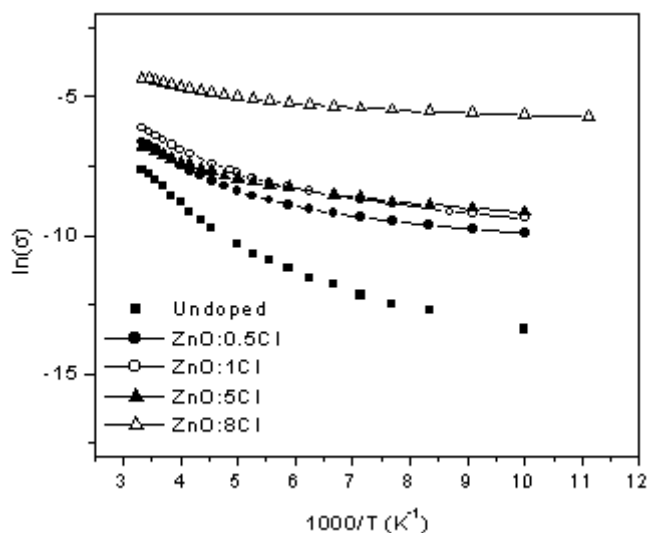

FIG. 5.9 Arrehenius Plot of Cl-doped ZnO thin films

5.3.2 Effects of Fluorine doping

A renewed interest in the study of zinc oxide thin films exists due to the simultaneous properties of low resistivity and high transmittance besides chemical stability under strong reducing environments. Despite the extensive investigations on this material, there are still some unknown points related with the effect of some dopants in the transport properties. The case of fluorine doped ZnO thin films is an example for this.

Apart from the academic interest, the fluorine doping has several potential advantages over the well-known and successful In-doping, such as low cost and abundance. More over fluorine does not introduce significant perturbation into the conduction band, due to the size compatibility of the oxygen and fluorine atoms

[14]. Fluorine was expected to occupy the oxygen site in ZnO and hence promoting the conductivity of the film. We describe the effect of fluorine on the properties of ZnO thin films in this chapter. Structural, electrical and optical characterization techniques were used for the present study.

Sanchez et al reported the role of F/Zn ratio in the starting solution and substrate temperature, on the structural and optical properties of ZnO thin films prepared using chemical spray pyrolysis technique [15]. Ammonium fluoride (NH$_4$F) was used as precursor for fluorine. Films were polycrystalline with preferred orientation along (002) plane at substrate temperature above 400°C. It was also shown that grain size decreased with the increase in the F/Zn ratio in the starting solution. Doped films were showing optical transmission above 85% in the visible range. A critical substrate temperature of 425°C, was observed at which these films showed [n-type] electrical dark conductivity of 9 (ohm cm)$^{-1}$ when using a solution spray rate of 16 ml/min and a gas flow rate of 10 l/min.

The same group reported electrical and optical characterization on the F-doped ZnO thin films. Resistivtiy as low as 1x10^{-1} ohm cm, Hall mobility of 10 cm^2/V-s and effective carrier concentration of 4x10^{19} cm^{-3} were obtained. The refractive index was also calculated; its value increased with fluorine concentration [16]. Widening of the optical band gap was also observed for the F-doped ZnO films.

Olvera et al studied effects of fluorine concentration, substrate temperature and acidity of the spray solution on structural, electrical and optical properties of ZnO films [17,18]. Here starting solution was zinc acetyl acetonate and ammonium fluoride. They also observed that the aging of the solution had remarkable effect on resistivity of the film. Under the optimum conditions, samples having resistivity of 1.5x10^{-2} ohm cm, mobility of 6 cm^2/V-s and carrier concentration of 2x10^{19} cm^{-3} were prepared. All the films showed preferential

orientation along the (002) plane irrespective of substrate temperature or acidity of the solution. AFM and SEM studies revealed that grain size of the films decreased with the increase in the acidity of the solution, while homogeneity increased.

Very recently, Maldonado et al studied the effect of aged and fresh solution of precursors on the physical properties of the ZnO:F films [19]. In this interesting experiment, two different precursor solutions, zinc acetate and zinc pentanedionate were used. It was observed that, the aged solutions could give low resistive films. The lowest resistivity values of as grown films deposited at 500°C using a two-day aged starting solution of zinc acetate and zinc pentaedinate, were 1.4×10^{-2} and 1.8×10^{-2} ohm cm, respectively. After vacuum annealing (films prepared with aged solution of zinc acetate) at 400°C for 30 minutes the resistivity further decreased to 6.5×10^{-3} ohm cm. Films were polycrystalline with strong preferential orientation along (002) direction and SEM images showed a uniform surface with rounded grains.

Santiago et al reported effect of ageing time of starting solution and substrate temperature on the properties of F-doped ZnO films [14]. The precursor solution contained zinc acetate, dissolved in alcohol and water; here hydrofluoric acid was used for fluorine doping. The pH of the solution was locked at 4, which avoided the early precipitation of the solution. Substrate temperature was varied from 450 to 500°C. Electrical resistivity decreased with the aging of the solution and lowest resistivity obtained was 7×10^{-3} ohm cm, when nine-days aged solution was used. Optimum substrate temperature was 500°C. All the films were polycrystalline in nature with preferred orientation along (002) plane for the 'nine-days aged' solution, while it showed the preferred growth along (101) direction when 'twenty-days aged' solution was used. Optical transmittance increased with the aging of the solution.

209

Altamirano developed a low resistive ZnO thin film using sol-gel technique by doping it with fluorine and aluminium [20]. NH_4F and aluminium nitrate were used as the precursors for fluorine and aluminium, respectively. All the films were thermally pre-treated at 100°C and then subjected to an annealing process at 450°C in two different atmospheres; open air and H_2/N_2 (96:4) gas mixture. The advantage of doping both Al and F was that, it maintained good transparency since only very small quantities were present in these films. In this study, initially Al and F were doped individually and then simultaneously. When doped individually, films were showing a slight preferred orientation along (002) plane. Grain size was less for Al-doped films than the F-doped one. These films showed good adherence to the glass substrate and exhibited an optical transmittance higher than 90% for wavelength > 430 nm. The lowest resistivity obtained was 8.6×10^{-3} ohm cm for annealed co doped films in H_2/N_2 atmosphere. The carrier concentration and mobility for the best film were 3×10^{19} cm^{-3}, 27 $cm^2/V\text{-s}$, respectively.

A El Hichou et al reported the cathodoluminescence (CL) characteristics of spray pyrolysed, F-doped ZnO thin film, using $ZnCl_2$ as starting solution [21]. Optical band gap and transmission were found to be unaffected by the F-doping. CL spectra of undoped sample showed two peaks at 382 and 520 nm, while doped films showed an additional emission at 454 nm. The additional emission at 454 nm was attributed to the lattice modification of the Zn^{2+} environment in the crystal.

Recently Kityk et al reported a giant linear electro-optic (Pockels) effect in ZnO doped with fluorine.They interpreted the effect as due to substantial non-centro-symmetric charge density distribution between the ZnO [wurtzite like] films and the bare glass substrate as well as by additional charge density polarization caused by fluorine atoms [22].

Effective doping of fluorine can be performed with many fluorine compounds, which are highly soluble in aqueous solvents. Earlier, it was shown that hydrofluoric acid, [HF], could be used for highly conducting tin oxide or indium oxide thin films. But only very few reports were available regarding the usage of HF acid as dopant solution. One of the reasons for not using HF was the early precipitation of the solution, which occurred as soon as the HF was added to the starting solution.The corrosive character of HF might have been another important reason. Hence ammonium fluoride (NH_4F) was chosen as the doping solution for fluorine in the present study.

5.3.2.1 Structural Characterization

Fig. 5.10 depicts XRD pattern of F-doped samples. All samples showed preferential orientation along (002) plane. The intensity of the peak corresponding to the plane (002) reduced on fluorine incorporation; but it was almost unaffected by the variation in fluorine concentration. The (002) direction corresponds to the c-axis of the crystal lattice, normal to the substrate plane. A weak XRD peak corresponding to the plane (101) was also observed for the undoped and ZnO:0.5F samples. But this peak completely vanished for the sample ZnO:1F. One can assume the substitution process of O by F species and this process could only be partial leading to the formation of a specific configuration like ZnF_xO_{1-x} [21]. Probably this could be the reason for reduced intensity of XRD peak of F:ZnO.
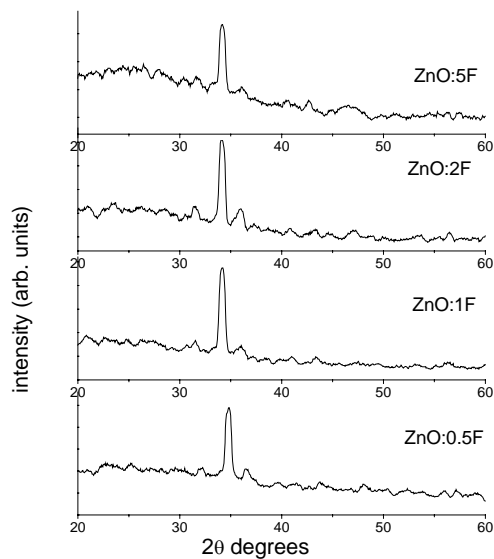
FIG. 5.10 XRD diagram of F-doped ZnO thin films

Mean crystallite size was calculated for the (002) diffraction peak, using Scherrer formula and found that the value is getting decreased slightly with increase in fluorine percentage. These values are tabulated [Table 5.2].

Table 5.2 Variation in grain size, resistivity and photosensitivity with fluorine doped samples

Sample	Grain Size (nm)	Resistivity (ohm cm)	Photosensitivity
ZnO:0.5F	25.4	59.9	4.2
ZnO:1F	23.9	43.0	2.8
ZnO:2F	23.3	41.3	4.5
ZnO:5F	21.8	151.8	11.2

Another interesting point was that the peak position corresponding to the plane (002) was slightly shifted to lower 2θ values, 34.7 to 34.2 at very high

212

doping concentrations, while it remained unaffected at lower concentration. Lattice constant [c] increased from 5.166 to 5.238 and a corresponding increase of lattice strain, ⁻0.75 to 0.63 %, along c-axis was also observed. The increase in lattice strain may be due to the increase in interstitial fluorine atoms at higher doping concentrations.

It is interesting to compare the crystalline quality of ZnO doped with F and Cl. Crystallinity was not much affected by the F doping but it deteriorated drastically on Cl doping. One of the possible reasons for this sort of behavior might be the difference in ionic radius of Cl and F. Fluorine has comparable ionic radius with O but ionic radius of Cl was much greater than that of oxygen. Hence chance of getting Cl into O lattice might be difficult and Cl might have moved to the interstitial position, which in turn, reduced the crystalline quality of the films.

5.3.2.2 Optical Absorption and Transmission Studies

Optical Absorption spectra of doped and undoped samples were recorded in the wavelength range 350-900 nm. Optical band gap was determined from the plot of $(\alpha h\nu)^2$ vs $h\nu$ graph [Fig. 5.11].
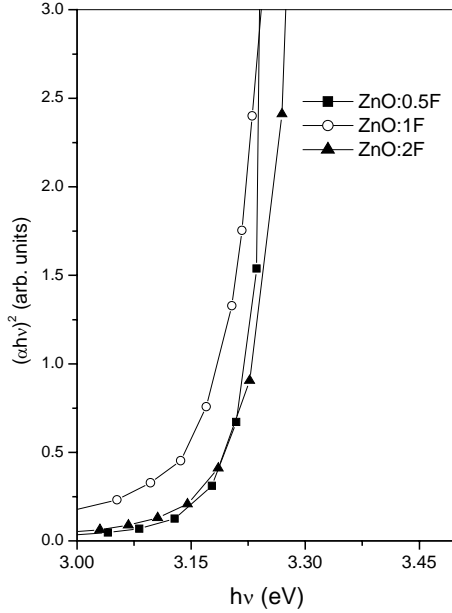
FIG. 5.11 $(\alpha h\nu)^2$ vs hν graph of F:ZnO

Undoped sample had band gap of 3.3 eV. We observed band-gap narrowing (BGN) for the F:ZnO samples. Band gap was reduced to 3.19 eV for the sample ZnO:0.5F and 3.1 eV for the ZnO:1F. Again it increased to 3.18 eV for ZnO:2F and then decreased to 3.09 eV for ZnO:5F (not shown in figure). There were two broad peaks corresponding to two defect levels in absorption spectrum of fluorine-doped samples [Fig 5.12]. For the sample ZnO:0.5F. these levels were at 476 nm and 646 nm, while for ZnO:1F these peaks are at 455 nm and 586 nm. The blue shift observed for the ZnO:1F sample was not clearly understood. The appearance of two broad absorption peaks, centered at 455 and 476nm, might be related to the presence of large number of defect levels just below conduction band. Probably these defect levels, near the conduction band, might be the reason for the small reduction in band gap. Absorption peak at 650 nm was observed for the sample ZnO:2F. Photoluminescence measurements also showed two

214

emissions at 455 nm and 670 nm for the doped sample, which will be discussed later in the section 5.3.2.4
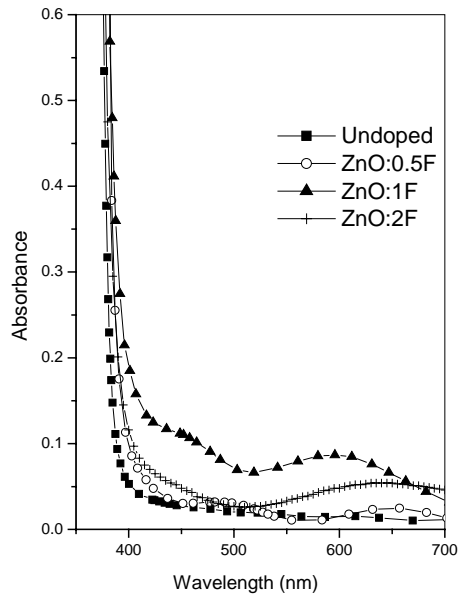

FIG. 5.12 Absorption spectra of undoped and doped ZnO samples

Optical transmission spectra were recorded in the wavelength range 350-1500 nm [Fig. 5.13]. Both undoped and doped films showed interference fringe pattern in transmission spectrum. This revealed the smooth reflecting surfaces of the film and there was not much scattering loss at the surface. Interestingly, doped sample exhibited increased optical transmission in the visible and NIR region and this was good for device fabrication. In transparent metal oxides, metal to oxygen ratio decides the percentage of transmittance. A metal rich film usually exhibits less transparency [1].
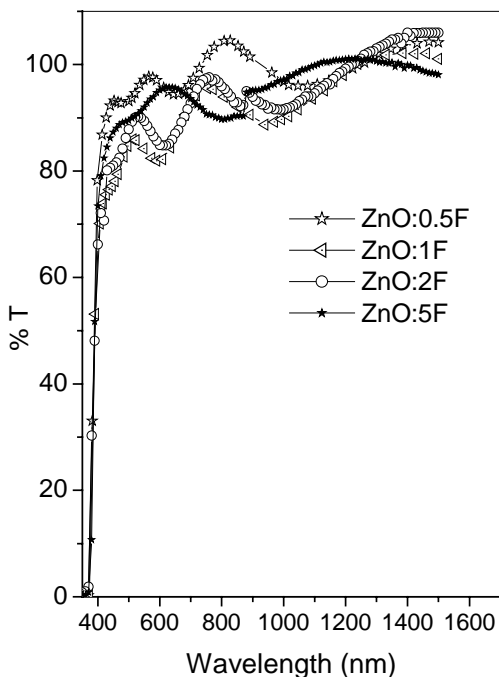
FIG. 5.13 Optical Transmission spectra of doped ZnO thin films

Fluorine doped samples were showing higher transmittance than the undoped samples. This may be due to the decrease in the Zn/[O+F] ratio in the film. Amplitude of interference fringes decreased at higher doping concentration and this indicated the loss surface smoothness leading to a slight scattering loss.

5.3.2.3 Electrical Resistivity and Photosensitivity Measurements

Electrical resistivity was measured using two-probe method. It was found that resistivity decreased considerably with fluorine doping (10^3 to 10^1 Ωcm) [Table 5.2]. This might be due to the fact that fluorine was occupying oxygen site. Variations in resistivity and photosensitivity are plotted [Fig. 5.14]. This was also clear from the XRD results that the intensity of the peak corresponding to the plane (002) was decreasing slightly with the increase in F concentration in the solution. Fluorine required only one electron for making covalent bond with zinc

and the other electron was set free which enhanced the conductivity. Higher doping concentration (ZnO:5F) resulted an increase in the resistivity. When doping concentration increased, fluorine turned into interstitials and since fluorine had more electro negativity than oxygen, it might cause an increase in the electrical resistivity, by capturing the free electrons. Another reason might be due to the decrease in grain size of the film, which might have reduced the mobility of the majority carriers because of the scattering process [15]. Also increased concentration of fluorine might have caused scattering of charge carriers, which also reduced the mobility and hence the conductivity.

Interestingly, when Cl was doped in ZnO, the resistivity increased while F doping decreased the resistivity at lower concentration and increased at higher concentrations. Hence, one can conclude that halogen atoms, when occupied in interstitials, acted as electron trap, which in turn, reduced the conductivity. When these atoms replace the oxygen in ZnO, the conductivity of ZnO enhanced.

Another point is that a doping limit was existing in materials because the intentional doping by donors (acceptors), moves the Fermi Energy, E_F towards the Conduction Band Minimum (Valance Band Maximum), thus lowering the formation energy of spontaneously formed acceptors (donors) which compensates the intentional donor (acceptor) dopants [23]. This can be demonstrated by noticing that the formation energy [24] of a defect α of charge q is

$$\Delta H\left(\alpha, q\right) = Constant + qE_F \ldots\ldots\ldots(5.1)$$

Usually constant term is of the order of a few eV. For acceptor like defects, q is negative and for donor type defects, q is positive. When we introduce donors, E_F moved towards the Conduction Band Minimum, and consequently, the formation energy for acceptors was lowered by an amount often comparable to the respective constant term in the above equation. Lower formation energy resulted

in higher acceptor concentrations, compensating the intentionally introduced donors. This was true for the F-doped ZnO thin films, as we observed an emission due to oxygen interstitials, which is an acceptor level in ZnO. Hence one could also attribute this compensation effects, to the increase in resistivity, at higher doping concentration.

Photosensitivity was calculated and there was significant decrease in photosensitivity on fluorine doping, which might be due to the increase in majority carrier concentration.
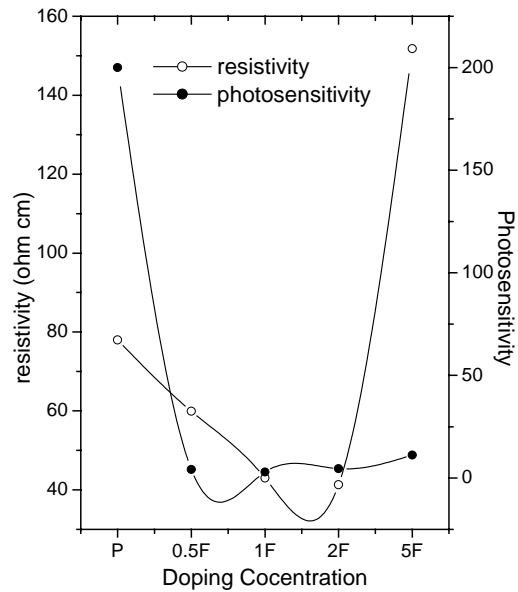
FIG. 5.14 Variation in resistivity and photosensitivity of ZnO with fluorine concentration

5.3.2.4 Photoluminescence Measurements

Photoluminescence (PL) measurements were done on both doped and undoped samples at room temperature [Fig.5.15].
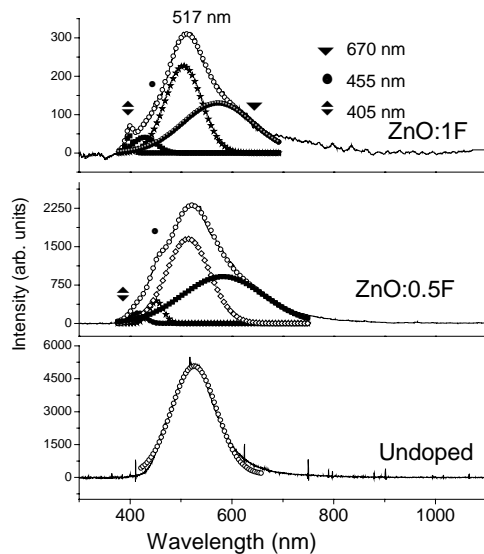
FIG. 5.15 Photoluminescence spectra of doped ZnO thin films. PL
spectrum of Undoped film is also given for a comparison. Graph is
fitted with Gaussian function to get the defect levels.

Undoped ZnO film gave single broad emission peak centered at 517 nm (2.4
eV). It was the characteristic blue-green emission. Exact mechanism responsible
for blue-green emission is still not clearly understood. All possible mechanisms
responsible for this emission were already discussed in previous chapters and it
was concluded that this emission was probably due to the transition from the
bottom of conduction band to the antisite oxygen (O_{Zn}) level [25]. PL emission
spectrum of F:ZnO exhibited four emissions at λ = 405, 455, 517 and 670 nm.
With the increase in fluorine concentration, intensity of the peak at 517 nm was
getting decreased and this might be due to the fact that, when fluorine was
incorporated, the level due to antisite oxygen might be getting depleted. Ionic
radii of oxygen and fluorine were comparable and there might be a possibility of
replacing oxygen by fluorine. Electrical resistivity measurements were also

219

supporting this argument. Hence one could assume that the level corresponding to the antisite oxygen (O_{Zn}) was also getting depleted on fluorine doping. Fluorine doping had only an insignificant effect on the crystallinity of the film. Hence one could expect emission property of doped samples similar to that of the undoped one. But intensity of emission at 517 nm decreased drastically, even for low fluorine concentration. Hence it was reasonable to assume that depletion of level due to antisite oxygen on fluorine doping was causing this.

The violet emission at 405 nm (3.07 eV) might be due to the radiative transitions from defect levels, related to interface traps existing at the grain boundaries, to valence band [26]. It was found that relative intensity of emission at 405 nm, increased slightly with fluorine doping. This might be due to the fact that grain size of the films was getting reduced with increase in fluorine doping, making grain boundary area larger. Hence the intensity was higher for higher doping concentration. Another emission was at 455 nm (2.73 eV). The relative intensity of this emission also increased on fluorine doping. This emission might be due to the lattice modification of Zn^{2+} environment in the film because of the incorporation of fluorine atoms [21]. Peak at ~670 nm (1.85 eV), might be corresponding to the transition from the conduction band to the level due to the oxygen interstitial [27]. This was prominent for the sample ZnO:1F and was not seen in undoped and ZnO:0.5F samples. This also gave a strong evidence for the replacement of oxygen by fluorine. This oxygen might be occupying the interstitial position, giving red emission at 670 nm.

5.3.2.5 Temperature Dependent Conductivity Measurements

Temperature dependence on electrical conductivity of the samples was measured in the range 100 – 300 K [Fig. 5.16]. Sample was placed on the cold finger of the liquid helium cryostat, using thermal grease to avoid any thermal gradient along or across the sample. Cryostat was evacuated to a pressure of 10^{-5} mbar. Obtained activation energies, [148 and 65 meV], for the undoped samples

were in good agreement with earlier reported values for intrinsic donor level and octahedral zinc interstitials.
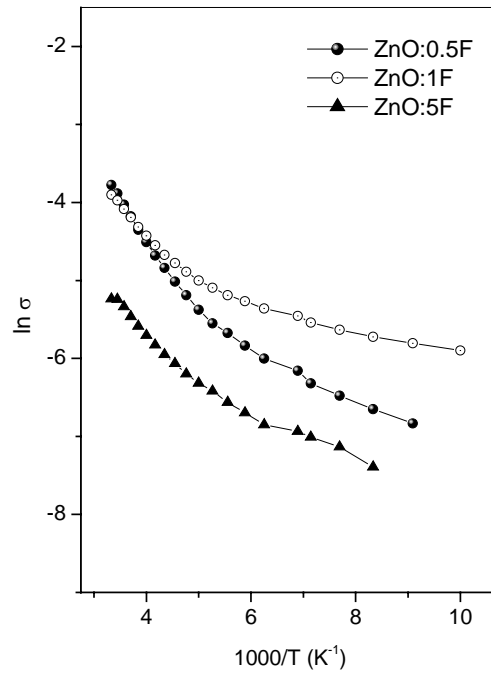

FIG. 5.16 Arrehenius plot of both F-doped and undoped ZnO thin films

When ZnO was doped with fluorine, intrinsic donor level at 148 meV got suppressed. Instead, activation energies 89 and 30 meV were obtained for ZnO:0.5F sample; a slightly different set of values (65 and 22 meV) were obtained for ZnO:1F. Also activation energies, 65 and 33 meV were obtained for ZnO:5F sample. Here one could assume reasonably well that the higher values (89 and 65 meV) were corresponding to octahedral zinc interstitials while the lower values (30 and 22 meV) were corresponding to zinc atoms in tetrahedral positions [13, 28]. The former pair was present in both undoped and doped samples while latter pair became evident only in doped samples. This may be resulting from fluorine doping. As fluorine entered into ZnO lattice, zinc in regular lattice site

was (tetrahedral) also becoming a donor, as only one electron was needed for the bonding.

5.3.3 Effect of vacuum annealing

Two low resistive fluorine doped samples (ZnO:1F and ZnO:2F) were annealed in vacuum for one hour at 673K. Pressure in the chamber was kept at 10^{-5} mbar during the annealing. Heating and cooling rate was fixed at 4 K/min so that no cracks or stress may develop in the film.

5.3.3.1 Structural Analysis

Structural analysis showed that crystallinity slightly increased after annealing [Fig. 5.17]. Grains size also increased to 30.6 nm. Figure depicts the XRD of annealed samples.
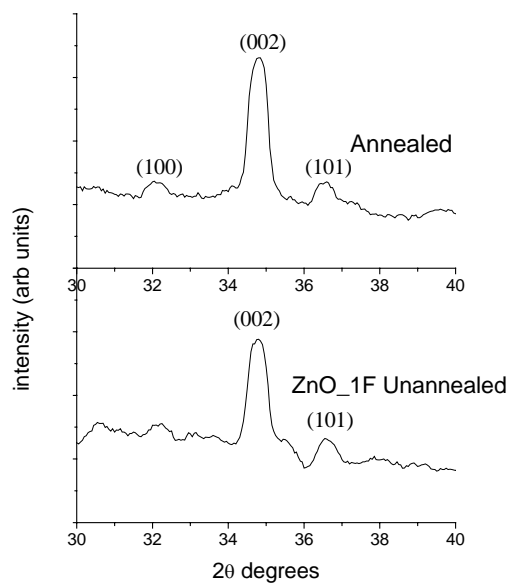

FIG. 5.17 XRD pattern of 1 at % F doped films before and after annealing at 673 K

It was observed that, for both indium doped and fluorine doped samples, annealing improved the crystallinity. In order to see the variation of crystalline quality of undoped samples, these samples were annealed in vacuum at 673 K. Interestingly it was seen that the integrated intensity (area under the curve) of XRD peaks decreased. Hence one could say that, in this case, the crystallinity deteriorated after annealing. Figure depicts the XRD pattern of pristine and annealed samples [Fig 5.18].
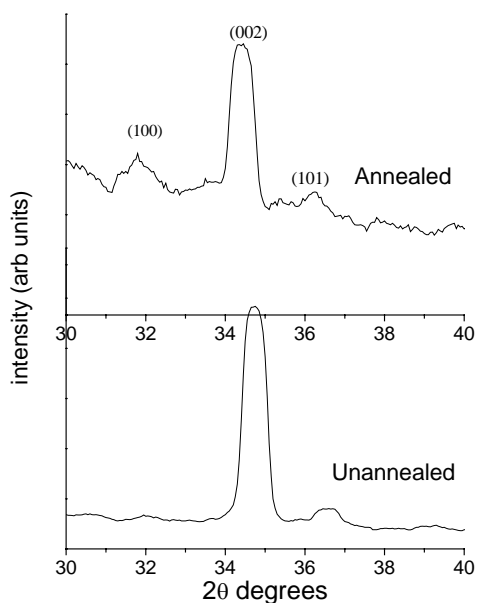

FIG. 5.18 XRD pattern of annealed and pristine ZnO

5.3.3.2 Optical Absorption and Transmission

Optical absorption spectra of annealed F:ZnO, showed that the band edge was unaffected by the annealing. This observation was in good agreement with the results from XRD analysis also. A slight decrease in the percentage of transmission was observed for the annealed samples, which might be due to the formation of metal rich film as result of out diffusion of oxygen from the film.

5.3.3.3 Electrical resistivity Measurements

Electrical resistivity measurements showed a drastic decrease in resistivity after annealing. It was seen that the resistivity of ZnO:1F showed a resistivity of 1.52 Ω cm after the vacuum annealing, while the sample ZnO:2F, showed a resistivity of 1.77 Ω cm after annealing. One of the reasons may be the escape of oxygen, leading to the reduction of acceptor states at the grain boundaries. Another was related to the oxygen replacement by fluorine that resulted in creation of excess electrons.

5.4 Conclusion

Two different elements of halogen family, [viz., Cl and F], were introduced into the ZnO thin films separately. F had comparable ionic radius of Oxygen, while the ionic radius of Cl was much higher than that of oxygen. This difference in ionic radius reflected in the properties of doped films. It was observed that, Cl – doping increased the resistivity of the film, while F – doping decreased it considerably. This difference was attributed to the difference in the *c*ites occupied by these two atoms in ZnO lattice. It was seen that, Cl might have occupied the interstitial or clustered at grain boundaries, while F might have replaced the oxygen at its site. Another important consequence of doping was that, F-doping did not affect the crystallinity to a large extent while Cl-doping affected the crystallinity adversely. Finally it was deduced that, halogen elements, when occupying the oxygen site in ZnO lattice, might enhance the conductivity; but if it is occupying in interstitials or grain boundaries, it will act as electron trap and hence decreases the conductivity.

References

[1] H. L. Hartnagel, A. L. Dawar, A. K. Jain, C. Jagadish, Semiconducting
Transparent Thin Films, IOP Publishing, Bristol and Philadelphia, 1995 p 244.

[2] C. A. Vincent, J. Electrochem. Soc 119 (1972) 515, J. A Aboaf and V. C. Marcotte, J. Electrochem. Soc. **120,** (1973) 701.

[3] D. Jousse, C. Constantino and I. Chambouleyron, J. Appl. Phys. **54,** (1983) 431

[4] D. Jousse, Phys. Rev. B **31,** (1985) 5335.

[5] J. Aranovich, A. Ortiz and R H Bube, J. Vac. Sci. Technol. **16(4),** (1979) 994.

[6] A. Maldonado, M. de la L. Olvera, S. Tirado Guerra, and R. Asomoza, Sol. Energy Mater. Sol. Cells **82,** (2004) 75.

[7] H. C. Ong, A. X. E. Zhu and G. T. Du, Appl. Phys. Lett. **80,** (2002) 941.

[8] Teny Theresa John, S. Bini, Y. Kashiwaba, T. Abe, Y. Yasuhiro, C. Sudha Kartha and K. P. Vijayakumar, Semicond. Sci. Technol. **18,** (2003) 491.

[9] Teny Theresa John K. C. Wilson, P. M. Ratheesh Kumar, C. Sudha Kartha, K. P. Vijayakumar, Y. Kashiwaba, T. Abe and Y. Yasuhiro, Phys. Stat. Sol. (a) **202 (1)**, (2005) 79.

[10] D. Jousse, C. Constantino and I. Chambouleyron, J. Appl. Phys. **54,** (1983) 431.

[11] C. A. Vincent, J. Electrochem. Soc. **119**, (1972) 515.

[12] Teny Theresa John , C. Sudha Kartha, K. P. Vijayakumar,, T. Abe and Y. Kashiwaba, Appl. Surf. Sci. **252,** (2005)1360.

[13] Y. Sun and H. Wang, Physica B **325,** (2003) 157.

[14] A. Guillen-Santiago, M de la L. Olvera, A. Maldonado, R. Asomoza and D. R. Acosta, Phys. Stat (a), Sol. **201,** (2004) 952.

[15] A. Sanchez-Juarez, A. Tiburcio-Silver and A. Ortiz, Sol. Energy Mat. Sol. Cells 52 (1998) 301.

[16] A. Sanchez-Juarez, A. Tiburcio-Silver, A. Ortiz, E. P. Zironi and J. Rickards, Thin Solid Films **333,** (1998) 196.

[17] M de la L. Olvera, A. Maldonado, R. Asomoza and M. Melendez-Lira, Sol. Energy Mat. Sol. Cells **71,** (1998) 301.

[18] M de la L. Olvera, A. Maldonado, R. Asomoza, Sol. Energy Mat. Sol. Cells **73,** (2002) 425.

[19] A. Maldonado, S. Tirado-Guerra, M. Melendez-Lira and M. de la L. Olvera Sol. Energy Mater. Sol. Cells (Article in Press)

225

[20] D. C. Altamirano-Juarez, G. Torres-Delgado, S. Jimenez-Sandoval, O. Jimenez Sandoval and R. Castanedo-Perez, Sol. Energy Mater. Sol. Cells **82,** (2004) 35.

[21] A. El Hichou, A. Bougrine, J. L. Bubendorff, J. Ebothe, M. Addou and M. Troyon, Semicond. Sci. Technol. **17,** (2002) 607.

[22] I. V. Kityk, J. Ebothe, A. El Hichou, M. Addou, A. Bougrine and B. Sahraoui, J. Phys.: Condens. Matter. **14,** (2002) 5407.

[23] S. B. Zhang, S. –H Wei and A. Zunger, J. Appl. Phys. **83,** (1998) 3192.

[24] G. A. Baraff and M. Schluter, Phys. Rev. Lett. **55,** (1985) 1327.

[25] P. M. Ratheesh Kumar et al, J. Appl. Phys. **97,** (2005) 13509.

[26] B. J. Jin, S. Im, S. Y. Lee, Thin Solid Films **366,** (2000) 107.

[27] Y. G. Wang, S. P. Lau, X. H. Zhang, H. W. Lee, H. H. Hng and B. K. Tay, J. Cryst. Growth **252, (**2003) 265.

[28] D. C. Look, J. W. Hemsky and J. R. Sizelove, Phys. Rev. Lett. **82,** (1999) 2552.

EFFECTS 100 KEV O$^+$ ION IMPLANTATION

6.1 Introduction

Even though intensive research works are going on to fully characterize ZnO in thin film as well as crystalline form, still there exists some serious challenges like doping, electrical isolation, type conversion etc that are yet to be overcome for processing ZnO to fabricate good devices. Controlled doping of ZnO is rather challenging, due to the complex behavior of intrinsic lattice defects in this material. In principle, controlled doping in selected area of ZnO can be achieved by ion implantation. This is a precise method for introducing dopants into a semiconductor and can be also used to create high resistance regions for inter-device isolation. But problems exist in such doping and there might be undesirable effects, due to ion beam induced lattice defects and/or the effect of the dopant on the electrical properties of the material. It is highly desirable to have a clear understanding of ion-beam-induced damage in ZnO, through detailed studies, if full potential of this technique, as a device-processing tool, is to be exploited. Such systematic studies of ion-implantation in ZnO are also obviously crucial for understanding the fundamental properties of lattice defects and effects of impurities in this material. Another motivation of doing oxygen ion implantation is to know the possibility of converting n-type ZnO to p-type. It was believed that the n-type conduction in ZnO was due to the presence of oxygen vacancies and zinc interstitials. Hence by making ZnO films O-rich, one can restrain the donor action of Zn-interstitials and O-vacancies, which in turn, might lead to p-type conduction.
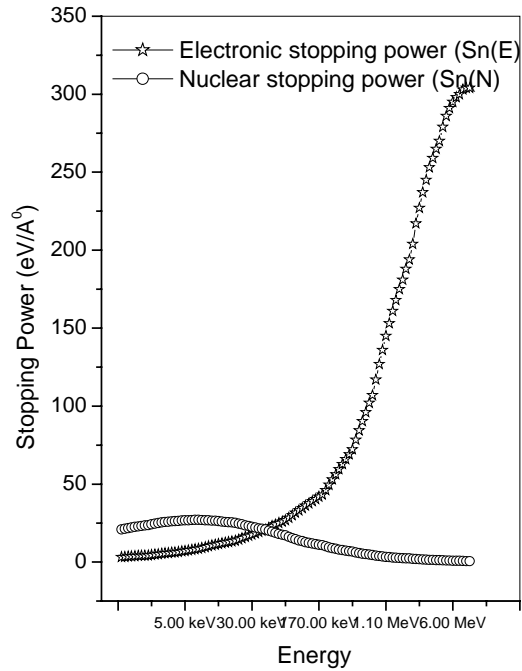
FIG. 6.1 Variation of stopping powers with energy of the ions

In this chapter, the effects of irradiation of ZnO thin films using 100 keV O+ ions are discussed. Several experimental techniques were used for a systematic analysis.

6.2 Experimental Details:

ZnO samples were implanted using mass analysed oxygen ion beam at 100 keV, (Model J-15 Sames, France) with different fluences ($1x10^{14}$ to $2x10^{16}$ ions/cm^2) at room temperature (RT). In this accelerator, ions are extracted from the source by a small accelerating voltage and then injected into the analyzer magnet. Selected ions are injected into the accelerating column, where these ions are accelerated by a static electric field that focuses and shapes the ion beam. Beam size was nearly 9 mm in diameter. Pressure inside the chamber was kept at $1x10^{-6}$ mbar during implantation.

The ion beam was focused onto the samples placed in the high vacuum chamber. Beam current was maintained at 0.5 µA to 0.8 µA to avoid heating effect during implantation. Samples were named as ZnO_F1, ZnO_F2, ZnO_F3, ZnO_F4, ZnO_F5 and ZnO_F6, implying different ion fluences ($1x10^{14}$, $5x10^{14}$, $1x10^{15}$, $5x10^{15}$, $1x10^{16}$ and $2x10^{16}$ respectively). These samples were then analysed with different techniques like XRD, optical absorption and transmission, PL, Thermally stimulated current measurements (TSC) and electrical characterization.

In order to get an idea about the penetration depth of ions and damage concentration in ZnO due to oxygen ions, TRIM (Transport of Ions in Matter) calculations were done. TRIM is the most comprehensive program, which will accept complex targets made of compound materials having even eight layers, of different materials. It will calculate the final 3D distribution of the ions and also all kinetic phenomena associated with the ion's energy loss, target damage, sputtering, ionization, and phonon production.

Variation of electronic and nuclear stopping powers, with the energy of implanted ions, in 540 nm thick ZnO thin films is shown in figure 6.1. It can be clearly seen that, at lower energies, the nuclear stopping power dominates the electronic stopping power. Figure 6.2 shows TRIM calculated path traversed by 100 keV O+ ions in ZnO. The modeling of ion implantation in semiconductors is usually accomplished by approximating the ion distribution using standard mathematical formulae. Pure Gaussian forms were used initially and the expression for ion distribution is given by,

$Y = C \exp [(X-X_0)^2/2\sigma^2]$

Where

X_0 – the initial position of the ion at the surface,

X – the peak position or projected range due to ion distribution into the material and

σ- the straggling or width of the distribution

C – Constant

This was soon found to be inadequate and dual Gaussian forms were introduced such that, one was good for left side and the other for the right side of the distribution. The whole work was to reproduce experimental data. Fig. 6.3 represents the 100 keV O^+ ions distribution in ZnO, calculated using TRIM software.
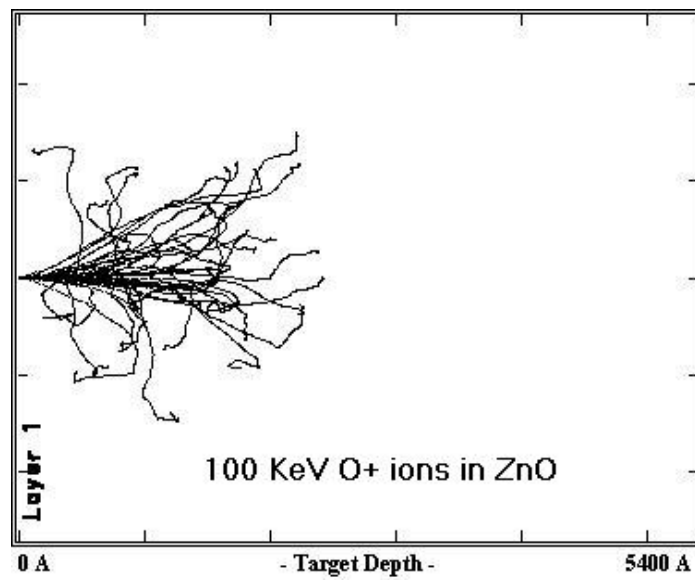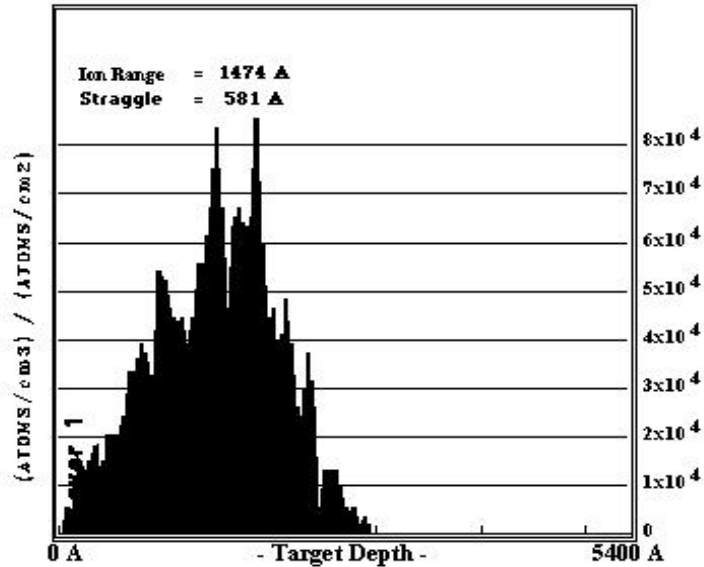

FIG. 6.2 100 keV O^+

FIG. 6.3 100 keV O^+ ions distribution in ZnO thin films

6.3 Results and discussions

6.3.1 Structural   Characterization

XRD patterns of the implanted samples are shown in figure 6.4. All the samples, except ZnO_F6, exhibited two peaks at $2\theta = 34.80°$ and $36.65°$ corresponding to the planes (002) and (101). The intensity ratio of these peaks was 6 for the pristine sample (Table 6.1) and it reduced with increase in ion fluence, up to the sample ZnO_F2. Again, there was an increase in the intensity ratio up to film ZnO_F4 after which it decreased drastically. Figure 6.4, also showed that peak positions, corresponding to the plane (002) and (101), remained almost the same for both implanted and pristine samples, as the lattice constant was the same for all the samples. Grain size was found to be nearly constant (~25 nm) up to the sample ZnO_F3 and further increase in the ion fluence resulted in a drastic decrease of the same. Finally for ZnO_F6, the film became completely amorphous.
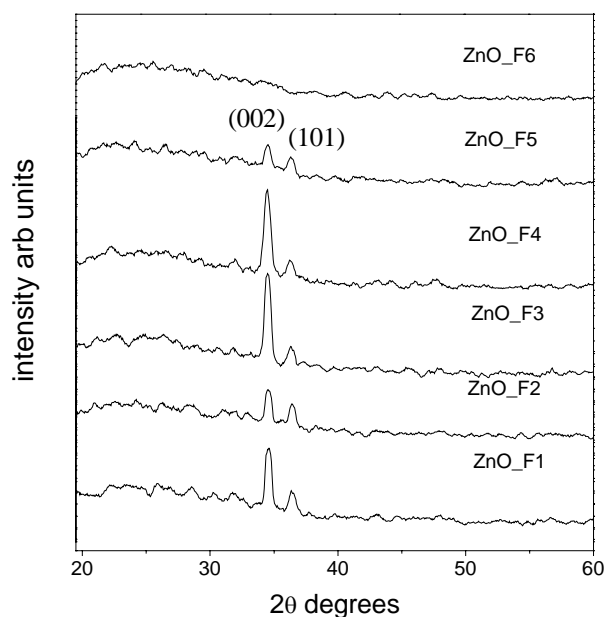
231

FIG. 6.4 Variation in XRD spectrum with ion fluences

It has been shown that ZnO exhibited strong dynamic annealing (i.e., migration and interaction of ion beam generated defects during ion irradiation) and no ion beam induced crystalline - to- amorphous transition was observed, even after bombardment with high fluence of heavy ions [1]. This situation occurred because most Frenkel pairs, ballistically generated in ZnO by the ion beam, experienced annihilation and only a very small portion of such migrating point defects avoided annihilation, to agglomerate into energetically stable defect complexes [2]. In the present case of ZnO, this kind annihilation might be less and hence there was crystalline to amorphous transition. Moreover O^+ ions could induce strong chemical

effects in ZnO. Similar effects were observed in ZnO thin films implanted with Si ions [2].

The phase change of crystalline to amorphous state finds applications in phase change memory devices, where digital information is written or erased in the surrounding crystalline matrix by a heat pulse, achieving local amorphization or crystallization of the material. Such type of experiments with chalcogenide materials (Eg: InSe) was first performed using laser pulse [3]. Very recently it has been suggested that electron beam source could be used for amorphization, in order to create [amorphous] spots of smaller size [4].

Table 6.1 Table showing the variation in the ratio of peak intensity between (002) and (101) planes and grain size with the ion fluence of 100 keV O+ ions

Sample Identity	Intensity ratio $(I_{(002)}/I_{(101)})$	Grain Size (nm)
Pristine	6.0	25.4
ZnO_F1	1.97	25.1
ZnO_F2	1.24	24.4
ZnO_F3	2.5	25.1
ZnO_F4	2.48	21.3
ZnO_F5	1.55	21.9

6.3.2 Optical Absorption

Optical absorption spectra were recorded for all samples in the wavelength region 350 - 900 nm [Fig. 6.5]. There was no absorption in visible region for the pristine sample while the film ZnO_F6 was showing two absorption peaks at 460 nm and 510 nm. The peak at 510 nm might be due to the defect level of antisite oxygen (O_{Zn}) causing the transition to conduction band. The exact origin of the level at 460 nm (2.7 e V) was not clear [5]. The energy level of zinc interstitials is located at 2.9

233

eV above the valence band for the sample with a band gap of 3.36 eV. In the case of oxygen-implanted sample, band gap was 3.2 eV and hence we could suggest that the emission at 460 nm might be due to the zinc interstitial and transition might be from the valence band to the shallow donor level of zinc interstitial.
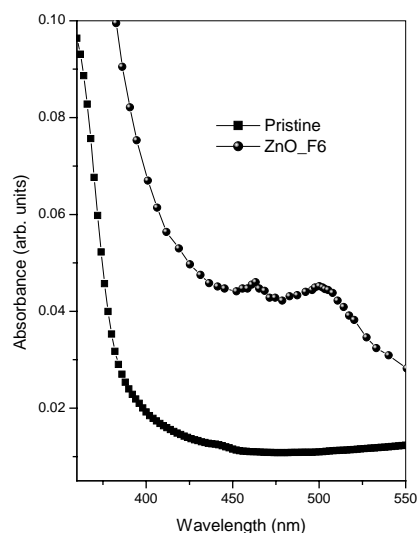

FIG. .6.5 Absorption spectra of pristine and implanted (ZnO_F6) samples

Band gap was determined for all samples [Fig 6.6]and it exhibited a slight decrease from the pristine to the implanted samples [i.e. from 3.3 eV, to ~3.2 eV]. It was interesting to see that band gap was nearly same even for the amorphous samples. In the case of ZnO film deposited using CSP technique, we observed earlier also that the band gap was not at all affected by swift heavy ions irradiation with Au and Ni ions. Hence we could suggest that band edge was much stable for chemically sprayed ZnO thin films. This observation was worth mentioning since we could tune other properties without affecting the absorption edge in the case of samples prepared using CSP technique
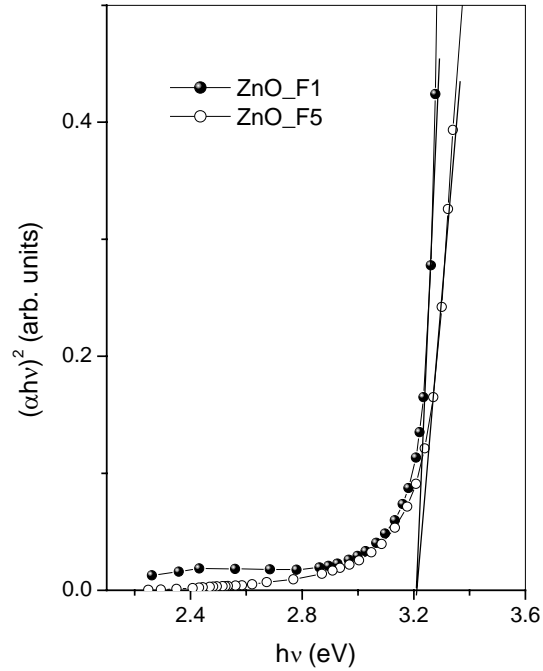
FIG. 6.7 $(\alpha h\nu)^2$ vs. $h\nu$ graph for determining

6.3.3 Photoluminescence (PL) Studies

PL emission of implanted film was giving two peaks at 425 nm and 590 nm [Fig. 6.8 and 6.9]. Surprisingly no emission was detected at 517 nm, which was the only one peak for the pristine. However an absorption peak at 510 nm was observed for the implanted sample. The defects and damages produced in the film during ion implantation might be the reason for this kind of behavior. Emission at 590 nm might be caused by the oxygen vacancy, which formed a deep donor level and this emission might be due to the transition from this level to valence band. TRIM calculation showed that implantation with oxygen ions of energy 100 keV could produce nearly 574 vacancies/ion, in ZnO thin film. According to the earlier calculation, the probability of forming oxygen vacancies was more in ZnO, due to its smaller covalent

radius [6]. Hence one could state that, during the ion implantation process, probability of forming oxygen vacancies was much greater.
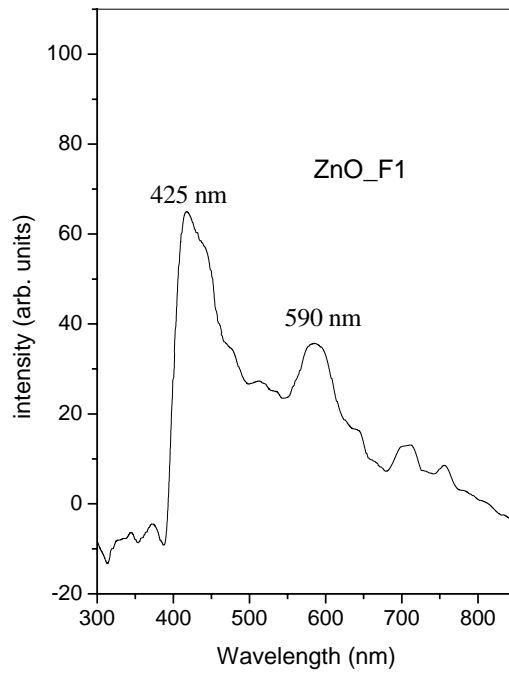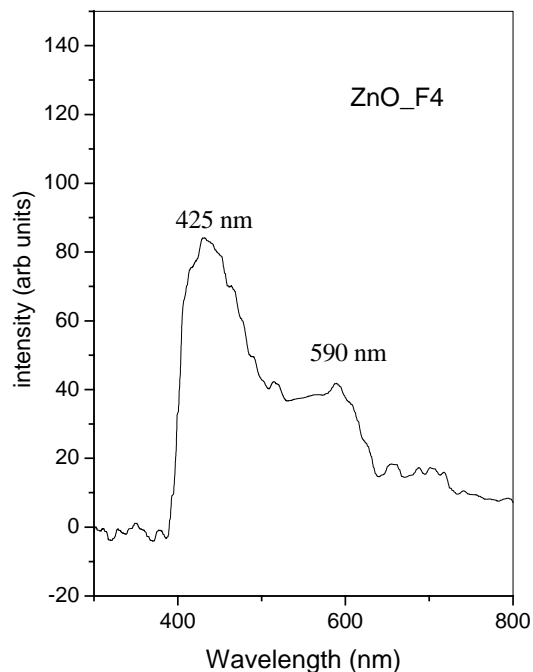

FIG. 6.8 PL spectrum of ZnO_F1

FIG. 6.9 PL spectrum of ZnO_F4

For the violet emission, different authors reported different wavelengths. Violet light luminescence, located at 425 nm, had been reported in Pulsed Laser Deposited ZnO thin films [7]. They suggested that this emission was probably due to radiative defects related to the interface traps, existing at the grain boundaries and emitted from the radiative transition between this level and the valence band. Another suggestion was that this emission might be due to the transition from conduction band tail states to valence band tail states [8]. It was also shown through a calculation based on Linear Muffin-Tin Orbital method, that an acceptor level at ~0.3 e V above the valence band was possible due to zinc vacancy (V_{Zn}) for the sample with a band gap of 3.36 eV [9]. Zinc vacancies were also forming during ion implantation, even though, the probability was small, compared to oxygen vacancies. Energy corresponding to the emission at 425 nm was 2.9 eV and hence we assumed that this

emission was corresponding to the transition from the conduction band to the level due to zinc vacancy.

To verify these emissions, PL spectrum was also recorded [in the wavelength range of 350 nm to 550 nm] using Jobin Yvon spectroflourimeter with the same excitation wavelength of 325 nm [Fig 6.10]. Pristine sample exhibited two emissions at 380 nm and 510 nm while implanted samples were giving emission at 425nm only. The emission at 380 nm was due to the Near Band Edge (NBE) transition. Intensity of the emission at 425 nm decreased slightly with the increase in the ion fluence, probably, because of the loss of emission property of the material, resulting from the damages produced by the ion implantation.
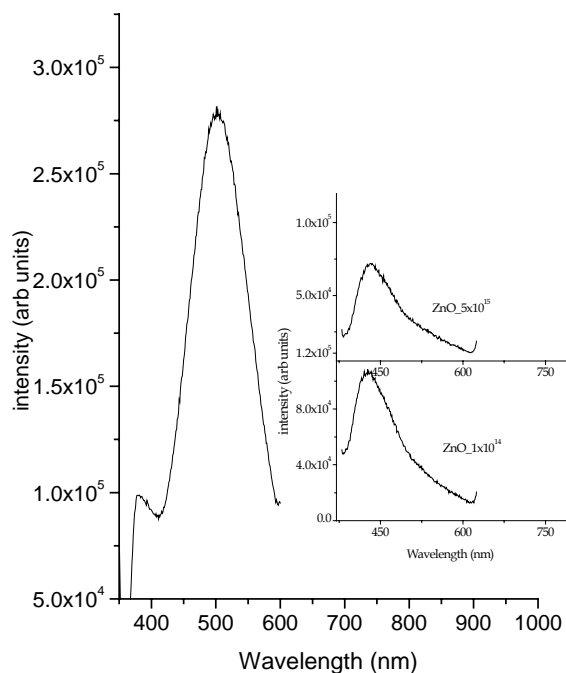

FIG. 6.10: PL spectrum of Pristine ZnO recorded using Jobin Yvon Spectrfluorimeter. Inset shows PL spectra of implanted ZnO

6.3.4 Electrical Resistivity Measurements – Implant Isolation

Electrical resistivity showed an abrupt increase in the values on implantation and the values are tabulated [Table 6.2].

Table 6.2 Electrical parameters of O^+ implanted ZnO thin films. *Hall measurements could not be performed on all the samples, due to the high sheet resistance.

Sample Identity	Resistivity (ohm cm)	Photosensitivity	*Carrier concentration (cm^{-3})	*Mobility (cm^2/Vs)
Pristine	78	200	$1.3x10^{15}$	60
ZnO_F1	$25.2x10^2$	53.1	$1.5x10^{16}$	0.58
ZnO_F2	$20.4x10^2$	29.8		
ZnO_F3	$16.7x10^2$	10.8		
ZnO_F4	$51.9x10^4$	0.17		
ZnO_F5	$36.3x10^4$	0.66		
ZnO_F6	$9.73x10^4$	0.95		

Pristine sample had resistivity of 78 ohm cm. It increased to $25.2x10^2$ ohm cm for the film ZnO_F1 and remained constant up to ZnO_F3. But for the sample ZnO_F4, again the resistivity increased to $\sim10^5$ ohm cm (sheet resistance $\sim10^{10}$ Ω/□). The formation of high resistive ZnO due to the implantation may find application in creating 'inter device isolation' region. In ZnO based future technology, bombardment with energetic ions can be used for electrical isolation of closely spaced devices [2]. It has recently been shown that ion irradiation, under appropriate conditions, could render ZnO highly resistive, with sheet resistance of $\sim10^{10}$ Ω/□ [2]. This was achieved in the present study also and the increase in resistance might be attributed to irradiation-induced degradation of carrier mobility as well as the trapping of free carriers at deep centers, associated with ion beam produced defects. For the sample ZnO_F6, a small reduction in resistivity was again observed even though the film was

amorphous. This could be attributed to the onset of pronounced hopping conduction with the increase of the concentration of ion beam produced defects [10]. The use of ion bombardment for the creation of resistive layers in III – V semiconductors were already been discussed exhaustively [11].

Hall measurements were done in the pristine and in one implanted sample (ZnO:F1). Carrier concentration of 1.3×10^{15} cm^{-3} and a mobility of 60 cm^2 /Vs were obtained for pristine sample while a carrier concentration of 1.5×10^{16} cm^{-3} and a mobility of 0.58 cm^2/Vs were obtained for the oxygen implanted sample. Both these films were n-type. Even though the pristine sample was showing smaller resistance than that of implanted sample, pristine sample was having less carrier concentration than in implanted sample. Implanted films were showing very low carrier mobility and this supported the earlier arguments on higher resistivity. This poor mobility was probably due to the large increase in the damages and/or defects created in the film during ion beam interaction, leading to the increased scattering of carriers. Hall Effect measurements could not be performed on the other implanted samples, due to the very high sheet resistance. It should be noted that all the films were showing n-type conduction, as evident from Hall effect measurements and Hot probe method.

6.3.5 Photosensitivity Measurements

Pristine sample showed a photosensitivity of 200. Photosensitivity of implanted samples decreased with increase in the ion fluence [Table 6.2] and at very high fluences it remained almost constant. Generally, one expects an increase in photosensitivity with increase in electrical resistivity, since the increase in resistivity follows a reduction in majority carriers. Hence the number of surviving minority carriers, created by the illumination, usually increases. But in the case of implanted samples, we observed a decrease in photosensitivity even though the resistivity was high. This might be again due to the creation of large number of ion beam produced

240

defects. The photo-generated carriers also might be trapped/destroyed due to these defects.

6.3.6 TSC Measurements

Thermally Stimulated Current (TSC) measurements were carried out in one irradiated (ZnO_F2) sample [Fig 6.12]. In the case of pristine sample, there was only one peak, corresponding to defect level of activation energy 0.6 eV. This level was identified to be that of 'zinc interstitial'. In the case of irradiated sample (ZnO_F2), there were two peaks corresponding to activation energies 0.5 eV and 1.05 eV. These were due to zinc interstitials and oxygen vacancy.
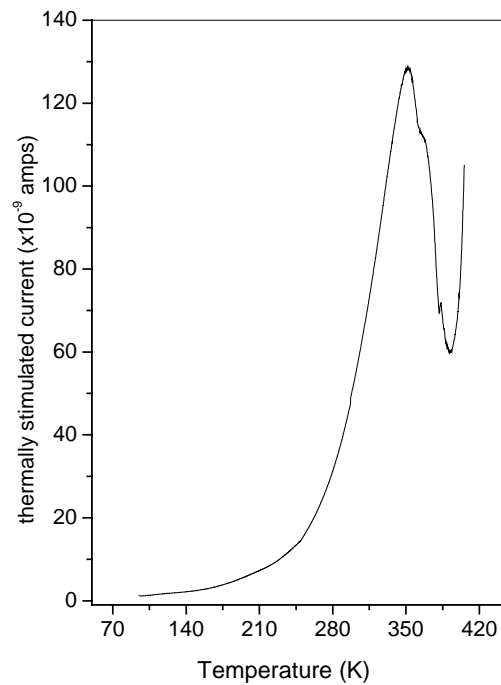

FIG. 6.12 TSC glow curve of ZnO_F2

TSC measurements could not be performed on other implanted samples due to the excessively high resistance. Hence it was clear that zinc interstitial was a common

defect in ZnO thin films and oxygen implantation could create oxygen vacancy. This was the reason for the very low mobility, leading to high resistivity.

6.4 Conclusion

In conclusion, the effects of irradiation, using 100 keV O ions, in ZnO thin films were studied. At very high fluences, crystalline to amorphous phase transition was observed in ZnO, which can be used in 'phase change memory device' applications. Ion beam induced amorphization is more advantageous than the other conventional laser heating induced amorphization, since it allows very small beam spot. Another important observation was the drastic increase in resistivity of the material due to the implantation. This could be further utilized for the device isolation in semiconductor device processing, done on ZnO wafers. Moreover, the optical absorption edge remained the same even after the ion beam irradiation with very high fluence.

References

[1] C. W. White, L. A. Boatner, P. S. Sldad, C. J. McHargue, S. J. Pennycook, M. J. Aziz, G. C. Farlow and J. Rankin, Mater. Res. Soc. Symp. Proc. **540,** (1986) 207.

[2] S. O. Kucheyev, J. S. Williams, C. Jagadish, J. Zou, C. Evans, A. J. Nelson and A. V. Harnza, Phys. Rev. B **67,** (2003) 094115.

[3s] T. Nishida, M. Terao, Y. Miyauchi, S. Horigome, T. Kaku and N. Ohta, Appl. Phys. Lett. **50,** (1987) 667.

[4] G. A. Gibson, A. Chaiken, K. Nauka, C. C. Yang, R. Davidson, A. Holden, R. Bicknell, B. S. Yeh, J. Chen, H. Liao, S. Subramanian, D. Schutt, J. Jasinski and Z. L. Weber, Appl. Phys. Lett. **86**, (2005) 51902.

[5] D. H. Zhang, Z. Y. Xue and Q. P. Wang, J. Phys. D: Appl. Phys. **35,** (2002) 2837.

[6] J. A. Van Vechten, J. Electrochem. Soc. **122,** (1975) 419.

[7] B. J. Jin, S. Im and S. Y. Lee, Thin Solid Films **366,** (2000) 107.

[8] T. Minami, H. Nanto and S. Takata, J. Lumin. **24/25,** (1981) 63.

 [9] B. Lin, Z. Fu and Y. Jia, Appl. Phys. Lett. **79,** (2001) 943.

[10] S. O. Kucheyev, C. Jagadish, J. S. Williams, P. N. K. Deenapanray, M. Yano, K.

 Koike, S. Sasa, M. Innoue and K. Ogata, J. Appl. Phys. **93,** (2003) 2972.

[11] S. J. Pearton, Mater. Sci. Rep. **4,** (1990) 313.

Chapter 8

SUMMARY AND CONCLUSIONS

In the present work, ZnO films were prepared using a cost effective technique, Viz., Chemical Spray Pyrolysis [CSP], and the preparation conditions were optimized [Substrate temperature 400°C, Spray volume of 200 ml, Spray rate at 10 ml/min] so as to get a transparent film of thickness 540 nm. Zinc acetate, dissolved in ethanol and distilled water [mixed in the volume ratio 1:1] was used as the precursor and molarity of the solution was optimized at 0.6 M. These films were showing optical transmittance of about 85 % in the visible region with electrical resistivity of 78 ohm cm.

First, ZnO films were subjected to swift heavy ion irradiation using 120 MeV Au ions and 80 MeV Ni ions, for this experiment. Energy range of each element was selected in such a way that, the maximum effect can be expected in these energy regimes. Moreover, the high-energy beam avoided the effects due to implantation since the range of the ion in the material was quite larger than the film thickness. It was seen that crystalline quality of the film deteriorated after the Au irradiation while Ni irradiation did not modify the structural properties significantly. Optical band gap remained unaffected after the irradiation and optical transmission slightly reduced on Au irradiation. Another important observation from these experiments was that the optical absorption edge remained sharp, even after the swift heavy ion irradiation. Electrical resistivity of ZnO got reduced with the fluence of Au ions due to the out diffusion of oxygen from the film. Ion interaction radius, calculated from the plot of PL intensity versus ion fluence, was 5.6 nm. Ni irradiation also caused a decrease in PL intensity, while it increased the electrical resistivity. In brief, the effects of 120 MeV Au ions were more than that of 80 MeV Ni ions, probably due to the difference in mass of Au and Ni ions and/ or due to the energy difference.

From the results of PL analysis of both pristine and irradiated samples, a satisfactory explanation on the origin of the controversial blue-green emission of ZnO was suggested; this emission was assumed to be due to the transition from the conduction band to the acceptor level of antisite oxygen. In order to support this argument, we performed vacuum annealing of unirradiated films. It was seen that the intensity reduced considerably after the annealing and this reduction might be associated with the depletion of the level due to antisite oxygen. Also, when doped with indium, the blue-green emission was drastically reduced. It was expected that, indium was occupying the Zn lattice and hence the concentration of O at Zn-site might be less, which in turn reduced the intensity of blue-green emission.

In order to make ZnO films low resistive, indium was doped in the film. Initially indium was introduced in the form of indium chloride and the percentage of doping was varied. It was seen that, the resistivity decreased up to 1 at % and then it started to increase. From the XPS analysis, the presence of chlorine was identified at higher doping concentration in elemental form. Hence it was presumed that the increase in resistivity might be due to the chlorine in the film. It was also suggested that, when chlorine segregated or clustered in the grain boundaries, it could act as electron trap. Resistivity can be further reduced by vacuum annealing at higher temperature, say 673 K.

In order to avoid the unintentional doping of chlorine, indium was introduced in the film, by thermal diffusion. For this, a thin layer of indium was thermally deposited over the ZnO film and the bilayer film was annealed at higher temperature; this also resulted in the formation of low resistive films. The lowest resistivity obtained in this case was 8.8×10^{-3} ohm cm. At this temperature, crystallinity of the film increased to a great extent. One of the advantages of this kind of doping was that it did not deteriorate either crystallinity or luminescent properties. Moreover band edge also remained unaffected. To reduce the resistivity further, indium nitrate was used for doping of indium instead of indium chloride, in order to avoid the unintentional

doping of chlorine. Then a thin layer of indium was deposited over this film and annealing of this bilayer at 673 K, resulted the lowest resistvity of 1.4×10^{-3} ohm cm. These films were showing an average visible transmittance of ~85 %. This was one of the lowest values of resistivity reported for the chemically prepared ZnO thin films, deposited using CSP technique.

For understanding the conclusive role of chlorine as electron trap, it was doped separately in the form of ammonium chloride and we found that the electrical resistivity increased with increase in doping concentration. Crystallinity was also affected adversely XPS studies used to identify the presence of Cl in the film.

. Hence our conclusion was that, electron, when occupying the interstitial position and/or the grain boundaries in ZnO films, would act as electron trap. Interestingly it is found to be difficult to have chlorine occupying the position of Oxygen in ZnO films deposited using CSP technique; this may be due to the abundance of Oxygen present in the carrier gas [air]. Generally it is believed that halogen atoms are promoter of electrical conductivity in transparent conducting oxides like SnO_2, ZnO etc, when occupied in O-site. But here we observed a negative result and we believ that there is one more reason for this kind of unusual behavior; the large ionic radius of chlorine [in comparison with that of Oxygen] might be preventing it from occupying the position of Oxygen. To verify this result, fluorine was taken from the halogen family for the further doping studies, since its ionic radius is very close to that of oxygen. Surprisingly it was seen that, when doped with F, resistivity of ZnO reduced to much lower values. Here, when occupied in O-site, F requires only one electron to achieve eight electrons in the outer most orbit, leaving one electron of Zn free and this enhanced the electrical conductivity. It was also interesting to see that, crystallinity of the samples did not modify to a large extent.

Converting n-type ZnO to p-type, is a very interesting topic of research, both in the academic as well as industrial sides. From the existing literature, we could understand that only very few reports are there on the type conversion. Generally it is

246

believed that n-type conduction in ZnO was presumably due to the presence of zinc interstitials (Zn_I) and oxygen vacancies (V_O) and it was very difficult to convert it into p-type due to the self-compensation effect of these donors. Naturally we thought that, if the concentration of oxygen in the film increased, the density of Zn_I and V_O might be less, which might assist the type conversion. Hence oxygen was doped in the film with ion implantation technique, since it offers spatial selectivity and accuracy. 100 keV ions were used for implantation. But unfortunately, the type conversion was not been observed in implanted film. However, another interesting phenomenon, viz., crystalline to amorphous phase transition, was observed in ZnO at very high ion fluence. Another attractive result was the possibility of making electrical isolation in ZnO with ion implantation.

Different defect analysis like Photoluminescence, Thermally stimulated current measurements, Temperature dependent conductivity measurements were performed on different ZnO samples. On the basis of these studies, an electronic level diagram was derived for undoped ZnO films. Figure 8.1 shows the proposed electronic level diagram from the present studies.
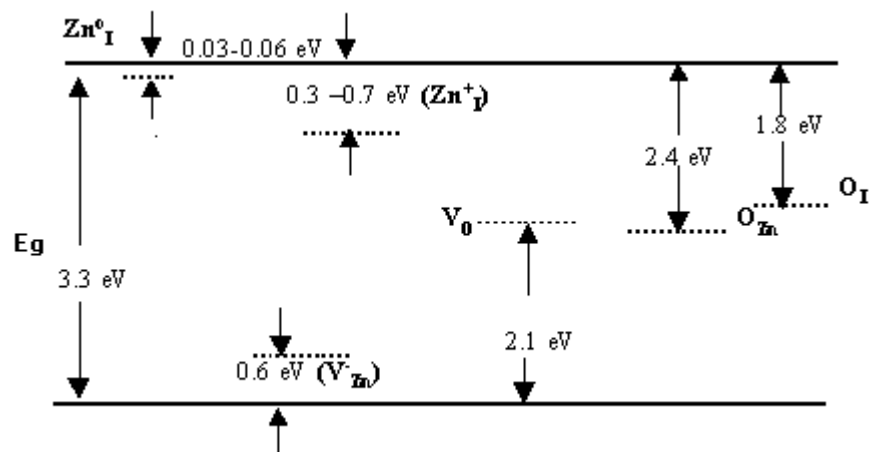
FUTURE SCOPES

Major advances have been made by many groups around the world recently in demonstrating p-type ZnO, fabricating improved ohmic contacts, developing high resolution dry etch pattern transfer process and implant isolation process and in realizing room temperature ferromagnetism in ZnO, there are still many areas that need intensive research work;some of these are listed below.

1. Higher p-type doping levels, for better control of the background n-type conductivity in the material that arises from native defects and impurities such as hydrogen.

2. Realization of high quality p-n junction, with good breakdown characteristics. These are building blocks for devices such as UV LEDs or lasers

3. P-type ohmic contacts with lower specific contact resistance for ZnO based light emitters so that self heating in the contact region does not degrade their reliability

4. Development of implant doping processes, to realize both n and p-type layers. This will require a better understanding of defects created by the implant step and their thermal stability; also a better understanding of the stability of the ZnO surface during activation annealing is required.